INFORMATION TO USERS

This manuscript has been reproduced from the microfilm master. UMI films the text directly from the original or copy submitted. Thus, some thesis and dissertation copies are in typewriter face, while others may be from any type of computer printer.

The quality of this reproduction is dependent upon the quality of the copy submitted. Broken or indistinct print, colored or poor quality illustrations and photographs, print bleedthrough, substandard margins, and improper alignment can adversely affect reproduction.

In the unlikely event that the author did not send UMI a complete manuscript and there are missing pages, these will be noted. Also, if unauthorized copyright material had to be removed, a note will indicate the deletion.

Oversize materials (e.g., maps, drawings, charts) are reproduced by sectioning the original, beginning at the upper left-hand corner and continuing from left to right in equal sections with small overlaps. Each original is also photographed in one exposure and is included in reduced form at the back of the book.

Photographs included in the original manuscript have been reproduced xerographically in this copy. Higher quality 6" x 9" black and white photographic prints are available for any photographs or illustrations appearing in this copy for an additional charge. Contact UMI directly to order.

U·M·I

University Microfilms International
A Bell & Howell Information Company
300 North Zeeb Road, Ann Arbor, MI 48106-1346 USA
313·761-4700 800·521-0600

Reproduced with permission of the copyright owner. Further reproduction prohibited without permission.

Reproduced with permission of the copyright owner. Further reproduction prohibited without permission.

Order Number 9315470

Electrochemistry in liquid microphase and simulation analysis of *EC* mechanism for vitamin B_{12} analogs

Huang, Qingdong, Ph.D.

City University of New York, 1993

Copyright ©1993 by Huang, Qingdong. All rights reserved.

U·M·I
300 N. Zeeb Rd.
Ann Arbor, MI 48106

Reproduced with permission of the copyright owner. Further reproduction prohibited without permission.

Reproduced with permission of the copyright owner. Further reproduction prohibited without permission.

Electrochemistry in Liquid Microphase and Simulation Analysis of *EC* Mechanism for Vitamin B_{12} Analogs

by

Qingdong Huang

A dissertation submitted to the Graduate Faculty in Chemistry
in partial fulfillment of the requirement for the degree of Doctor of Philosophy
The City University of New York
1993

Reproduced with permission of the copyright owner. Further reproduction prohibited without permission.

Copyright 1993

Qingdong Huang

All Rights Reserved

Reproduced with permission of the copyright owner. Further reproduction prohibited without permission.

This manuscript has been read and accepted for the Graduate Faculty in Chemistry in satisfaction of the dissertation requirement for the degree of Doctor of Philosophy.

1/21/93
Date

Chairman of Examining Committee

1/21/93
Date

Executive Officer

David C. Lozier

Supervisory Committee

The City University of New York

Reproduced with permission of the copyright owner. Further reproduction prohibited without permission.

Electrochemistry in Liquid Microphase and Simulation Analysis of *EC* Mechanism for Vitamin B_{12} Analogs

by

Qingdong Huang

Thesis Advisors: Professor David K. Gosser and Ronald L. Birke

The thesis includes three parts of work related to electrochemistry. Part 1 describes the instrument and set-up, where one PC worked as waveform generator and another PC worked as oscilloscope interfaced with a home-built potentiostat. With this system, fast k_{chem} in *EC* mechanism was measured. Part 2 describes electrochemical properties of solvent-electrolyte system with DMSO at low temperature below the freezing point. Based on electrochemical and ESR results, a theoretical model was developed to explain these phenomena as the existence of a liquid microphase. These electrochemical methods may open a new window to search for and optimize the components of cryopreservation systems with much better efficiency. Part 3 describes the electrochemical study of vitamin B_{12}. The electrochemical parameters of methylcobalamin were precisely measured by digital simulation - simplex curve fitting method. The solvent and temperature effects on k_{chem} of methylcobalamin were investigated. The application region of simulation-fitting method in Butler-Volmer approach with fast k_{chem} in *EC* mechanism was discussed. Electrochemical experiments of alkylcobalamin indicate that the spherical effect is the major effect on the $E^{o'}$ and k_{chem}, which favor the postulated mechanism of the innnr spherical single electron transfer in biological processes.

Reproduced with permission of the copyright owner. Further reproduction prohibited without permission.

To My Grandmother

Reproduced with permission of the copyright owner. Further reproduction prohibited without permission.

Acknowledgement

I wish to extend my appreciation to my thesis advisors Professor David K. Gosser and Professor Ronald L. Birke for their excellent direction, accessibility, encouragement, understanding and friendship throughout this work. I would like to thank Professor David C. Locke, my thesis committee member, for his advice and finding time in his busy schedule to serve on my thesis committee. I am also grateful to Professor Michael E. Green, Chairman of the Chemistry Department, and Professor Evan T. Williams, my former thesis advisor, for their aid and advice. I am indebted to my laboratory fellows Feng Zhang, Zuopeng Huang, Jianzhong Qi, Hanru Zhu, Vimal T. Kumar and others for their friendship and assistance during my years at City College. I would also like to thank my wife Helen, my parents Zuyi and Hongbi, my uncle Zusheng and my sister Qinglin, without their love, patience and support this work could have never been done.

Reproduced with permission of the copyright owner. Further reproduction prohibited without permission.

Table of Contents

Copyright ii
Approval iii
Abstract iv
Dedication v
Acknowledgement vi
Table of Contents vii
List of Tables xii
List of Figures xiv
List of Schemes xxiii

Part 1 Instrument Improvement and Set-up 1

Chapter 1 Coupling BAS-100A Electrochemical Analyzer with External Computer 1

1.1 The Communication between BAS-100A Electrochemical Analyzer and External Computer 2
1.2 Data Conversion 3
1.2.1 Memory Maps in Random Access Memory 3
1.2.2 The Data Storage Format 4
1.2.3 Data Conversion Programs 5
1.3 The Operation Procedure 8
1.3.1 Data Transfer from BAS-100A to External Computer 8
1.3.2 Data File Conversion 9

Chapter 2 The Set-up of New Electrochemical Analysis System 10

2.1 The Personal Computer Based Waveform Generator 11

Reproduced with permission of the copyright owner. Further reproduction prohibited without permission.

2.1.1 The Operation Theory of Waveform Generator 12
2.1.2 The Hardware of WSB-10 Board and the Controlling Software 14
2.1.3 The Cyclic Staircase (Cyclic Voltammetry) Waveform Generator Program 15
2.1.4 The Potential Step Chronoamperometry Waveform Generator Program 18
2.2 The Oscilloscope and Data Processing 19
2.2.1 The Waveform Analysis System 19
2.2.2 Data Processing and the Application Program 20
2.3 The Potentiostat and the Application of the System 22
2.3.1 The Background of the Circuit 22
2.3.2 The Influence of High Frequency and the Noise Problem 26
2.3.3 Circuit Test and the Application of the System 28

Part 2 Electrochemical Properties of Solvent-Electrolyte System with DMSO at Low Temperature below the Freezing Point 30

Chapter 3 The New Observation in the Electrochemical System with DMSO below the Freezing Point 30
3.1 The Electrochemical Experiments of the DMSO-Electrolyte Freezing System 35
3.2 Discussion of Experimental Results 37
3.2.1 Electrochemical Experiments with Conventional Electrodes 37
3.2.2 Electrochemical Experiments with Microelectrode 40

Chapter 4 Electron Spin Resonance Experiments of the Freezing System 43
4.1 The Principle of ESR Experiments in Freezing System 43
4.1.1 Electron Spin Resonance Spectroscopy 43

Reproduced with permission of the copyright owner. Further reproduction prohibited without permission.

4.1.2 The Application of ESR in Freezing System 47
4.1.3 The Nitroxide Spin Labels and Their Applications in ESR 49
4.2 The ESR Experiments 50
4.3 The Discussion of ESR Results 50

Chapter 5 The Theoretical Model of the DMSO-Electrolyte Freezing Systems and the Application in Cryopreservation 52
5.1 The Physical Significance of the Electrochemical Model in DMSO-Electrolyte System below the Freezing Point 52
5.2 The Model for Electrochemical Reaction in DMSO-Electrolyte System at Temperature below the Freezing Point 54
5.3 The Application of the DMSO-Electrolyte System in Cryopreservation 60

Part 3 The Electrochemical Study of Vitamin B_{12} -- The Electron Transfer and the Ligand Effects in the B_{12} Electrochemical Process 65

Chapter 6 Introduction: The Development of Vitamin B_{12} Research 65
6.1 The Development of Vitamin B_{12} in Research and Application 65
6.1.1 The History of Vitamin B_{12} 65
6.1.2 The Function of Vitamin B_{12} to Human Being 68
6.1.3 The Chemistry and Electrochemistry of Vitamin B_{12} 70
6.2 The Electrochemistry of Alkylcobalamin 73

Chapter 7 Simulation and Simplex Curve Fitting Analysis of *EC* Mechanism of Methylcobalamin 78
7.1 Introduction 78
7.2 Experimental Section 82

Reproduced with permission of the copyright owner. Further reproduction prohibited without permission.

7.3 Results and Discussion 85

Chapter 8 The Solvent and Temperature Effects on the Rate Constant of the Following Chemical Reaction of Methylcobalamin 93

8.1 Introduction 93

8.2 Experimental Section 94

8.3 Results and Discussion 95

Chapter 9 The Electrochemical Study of B_{12} Derivatives 99

9.1 Introduction 99

9.2 The Preparation of Alkylcobalamin 101

9.2.1 The Principle Consideration in Synthesizing Alkylcobalamin 101

9.2.2 The Synthesis Procedure 104

9.2.3 The Characterization of Alkylcobalamin 106

9.3 Electrochemical Experiment Section 109

9.4 Results and Discussion 110

9.4.1 Experiments in Nonaqueous Media 110

9.4.2 Experiments in Aqueous Media 120

9.4.3 Conclusion 122

Tables 127

Figures 137

Schemes 193

Appendix 195

Appendix 1.1 Data Communication Program 195

Appendix 1.2 BAS-100A Data Conversion Program 196

Appendix 2.1 The Cyclic Staircase (Cyclic Voltammetry) Waveform Generator Program 198

Reproduced with permission of the copyright owner. Further reproduction prohibited without permission.

Appendix 2.2 The Potential Step Chronoamperometry Waveform Generator Program 208

Appendix 2.3 Data Conversion Program for Waveform Analysis System 214

Reference Cited in Part 1 216

Reference Cited in Part 2 218

Reference Cited in Part 3 221

Reproduced with permission of the copyright owner. Further reproduction prohibited without permission.

List of Tables

Table 2-1 The F factor and its representative values of IS-2010 waveform analysis system.....127

Table 2-2 The relationship of the sample time interval and the sweep time division in IS-2010 waveform analysis system.....127

Table 2-3 The major features of 353 operational amplifier 128

Table 2-4 The noise sources and their representations. In these equations, k_B is Boltzmann constant (1.73×10^{-23}V/K), T is the temperature in K, R_f is the current convertor feedback resistance (Ω), B is the bandwidth (Hz) of potentiostat, e_n is the manufacturer-specified amplifier voltage noise ($V/(Hz)^{1/2}$), i_n is the specified amplifier current noise ($A/(Hz)^{1/2}$), R_u is cell resistance, Z_{in} is cell impedance, and e_{pc} is the rms sum of noise from potential control amplifiers.....129

Table 3-1 The wave width ($E_{3/4}$ - $E_{1/4}$) of cyclic voltammetry on microelectrode in DMSO-electrolyte system at various temperatures. Cyclic voltammetry were performed with 5.0 mM ferrocene and 0.10 M TBAP in DMSO. Glassy carbon microelectrode (33 μm in diameter) with a scan rate 10 mv/sec. The system was frozen at 15°C 129

Table 4-1 The relationship of the rotational correlation time and temperature. Temperature changes from 20°C down to -100°C for the system with 0.4 mM TEMPO and 0.10 M TBAP in DMSO. The system was frozen at 15°C 130

Reproduced with permission of the copyright owner. Further reproduction prohibited without permission.

Table 5-1 The peak separation of ferricyanide in DMSO-H_2O-NaCl system at different temperatures. Ferricyanide of 5.0×10^{-4} M in DMSO (31.50 g)-H_2O(65.00 g)-NaCl(3.50 g). The system was frozen at -26°C 131

Table 7-1 Simulation-fitting results of methylcobalamin electrochemical parameters at -30°C. The iteration indicates the simplex iteration times. The resistance measured and used in CVFIT program was 1650 Ω 132

Table 7-2 The various measurements of α. The values of α_{app} are measured from experimental results through equation (7-9). The values of $\alpha_{app,corr}$ are the experimental results measured through equation (7-9) and corrected through equation (7-10). The values of α_{fit} are measured from simulation-fitting of the corresponding cyclic voltammograms..... 133

Table 9-1 The second-order rate constants for the reaction of B_{12s} with alkyl halides (RX). Data cited from reference 83 in reactions Co(I) + RX → Co-R + X^- 134

Table 9-2 Paper chromatographic results of the alkylcobalamins. The data in parentheses were cited from the experimental results of Johnson et al[80] 135

Table 9-3 Simulation-fitting results for methylcobalamin electrochemical parameters at 20°C 135

Table 9-4 Simulation results of alkylcobalamin electrochemical parameters at 20°C 136

Reproduced with permission of the copyright owner. Further reproduction prohibited without permission.

List of Figures

Fig. 1-1 The communication between BAS-100A and external computer 137

Fig. 1-2 The data image in the RAM of BAS-100A 138

Fig. 2-1 The arrangement of electroanalytical system with separated waveform generator, oscilloscope and interfaced potentiostat 139

Fig. 2-2 The appearance of the screen for cyclic staircase (cyclic voltammetry) waveform generator program 140

Fig. 2-3 The appearance of the screen for potential step waveform generator program 141

Fig. 2-4 (a) A simple potentiostat; (b) the view of an electrochemical cell as an impedance network 142

Fig. 2-5 The home-built potentiostatic system 143

Fig. 2-6 The double potential step chronoamperometry experiments by home-built electrochemical analyzer (solid line) and BAS-100A (solid dot). The dash line on the same plot is the theoretical calculation result. Ferrocene = 5.0 mM, TBAF = 0.2 M. CH_3CN solvent was dried by 3A molecular sieves. The working electrode was a carbon microelectrode in diameter 33 μm and the

Reproduced with permission of the copyright owner. Further reproduction prohibited without permission.

reference was an Ag/AgCl electrode with ethanol solvent saturated by LiCl. The period time was 1 mSec with initial potential 380 mV, step potential 850 mV and final potential 380 mV 144

Fig. 3-1 Cyclic voltammetry of *p*-benzoquinone in DMSO with TBAP at different temperatures. Scan rate 75 mV/sec, resolution 1 mV/point with 4.0×10^{-4} M *p*-benzoquinone and 0.10 M TBAP. (a) at 26°C, resistance 969 Ω and uncompensated resistance 290 Ω ; (b) at -20°C, resistance 138 kΩ and uncompensated resistance 69 kΩ 145

Fig. 3-2 Changes in solution (uncompensated) resistance of DMSO-TBAP-*p*-benzoquinone system *vs.* temperature. Similar experimental conditions as Fig. 3-1. Triangles represent the measurements made while decreasing the temperature and circles represent the measurements made while increasing the temperature 146

Fig. 3-3 Cyclic voltammetric peak currents of *p*-benzoquinone *vs.* temperature. Similar experimental conditions as Fig. 3-1. Triangles represent the measurements made while decreasing the temperature and circles represent the measurements made while increasing the temperature 147

Fig. 3-4 Changes in solution (uncompensated) resistance of DMSO-TBAP-ferrocene *vs.* temperature with 0.10 M TBAP and 5.0×10^{-4} M ferrocene in DMSO. Triangles represent the measurements made while decreasing the temperature and circles represent the measurements made while increasing the temperature 148

Reproduced with permission of the copyright owner. Further reproduction prohibited without permission.

Fig. 3-5 Cyclic voltammetric peak currents of ferrocene *vs.* temperature. Similar experimental conditions as Fig. 3-4 with scan rate 50 mV/sec. Triangles represent the measurements made while decreasing the temperature and circles represent the measurements made while increasing the temperature 149

Fig. 3-6 Peak currents *vs.* square root of scan rates in logarithmic scales. 5.0×10^{-4} M ferrocene and 0.10 M TBAP in DMSO. The scan rate is in the unit volt /sec. Solid circles represent experiments at 20°C with the fitted straight line in slope 0.96 and dependency 0.937. Hollow circles represent experiments at 0°C with the fitted straight line in slope 1.2 and dependency 0.969..... 150

Fig. 3-7 Peak current *vs.* TBAP concentration at various temperatures. 5.0×10^{-4} M ferrocene with scan rate 50 mV/sec. Circles represent experiments at 20°C, diamonds represent experiments at 10°C and squares represent experiments at 0°C 151

Fig. 3-8 Cyclic voltammograms with microelectrode. 5.0 mM ferrocene and 0.10 M TBAP in DMSO at glassy carbon microelectrode (33 μm in diameter). Scan rate 10 mV/sec. (a) 30°C (liquid), (b) 20°C (liquid), (c) 10°C (frozen), (d) 0°C (frozen), (e) -10°C (frozen) and (f) -20°C (frozen) 152

Fig. 4-1 ESR spectra of TEMPO in DMSO-TBAP system at various temperatures. 4.0×10^{-4} M TEMPO and 0.10 M TBAP in DMSO. Temperature was changed from 20°C

Reproduced with permission of the copyright owner. Further reproduction prohibited without permission.

down to -100°C. The system was frozen at 15°C..... 155

Fig. 4-2 The relationship of temperature and related viscosity in DMSO-TBAP system. The (τ_{cor} • T) is proportional to the related viscosity of the liquid microphase, which follows the Arrhenius behavior..... 156

Fig. 5-1 Normalized peak currents *vs.* temperature. 5.0×10^{-4} M ferrocene and 0.10 M TBAP in DMSO. Scan rate 50 mV/sec. According to ESR spectra, T_o was estimated as 233 K. The dots represent experimental data. The curve represents theoretical data from equation (5-11) with $\phi(T,C'_{elec}) = 0.088$ and B' = 54 K. Reference temperature was 15°C, where the eutectic environment was initially formed..... 157

Fig. 5-2 Normalized peak currents *vs.* temperature. Similar experiment as Fig. 5-1 except the TBAP was 0.20 M. The dots represent experimental data. The curve represents theoretical data from equation (5-11) with $\phi(T,C'_{elec}) = 0.12$ and B' = 74 K. The reference temperature was 14°C 158

Fig. 5-3 The salt effect on the DMSO-TBAP system below the freezing point. Scan rate 50 mV/sec with 5.0×10^{-4} M ferrocene at 0°C 159

Fig. 5-4 Cyclic voltammetry of ferricyanide in DMSO-H_2O-NaCl system. Scan rate 50 mV/sec with resolution 1 mV/point. 5×10^{-4} M potassium ferricyanide in a mixture of DMSO 31.50 g, H_2O 65.00 g and NaCl 3.50 g. The system was

Reproduced with permission of the copyright owner. Further reproduction prohibited without permission.

frozen at -26°C. (a) at 10°C in liquid state, resistance 671Ω and uncompensated resistance 570 Ω. (b) at -40°C in frozen state, resistance 4449Ω, uncompensated resistance 444 Ω 160

Fig. 5-5 Peak current *vs.* square root of scan rate (volt/sec) in logarithmic scale. Similar experiment as Fig. 5-4 at -40°C. The slope of the fitted straight line is 0.92 and the dependency is 0.962 162

Fig. 6-1 The structure of vitamin B_{12} derivatives. *R* represents various substitutes for the corresponding derivatives 163

Fig. 7-1 Double potential step chronoamperometry experimental and fitting results of methylcobalamin in solvent mixture DMF (40%) and methanol (60%) at -30°C. Silver amalgam electrode in diameter 0.25 mm, methylcobalamin = 2 mM, TBAF = 0.30 M. (a) results fitted by k_{chem} = 590 sec^{-1}, the solid dots are experimental results. (b) detail of the fitting with an error range, where the data close to noise background (at the end of the time period) are ignored. The hollow dots are experimental results. Curves a with k_{chem} = 590 sec^{-1}, b with 690 sec^{-1} and c with 490 sec^{-1} 164

Fig. 7-2 Cyclic voltammograms of 2.0 mM methylcobalamin in a solvent mixture of DMF (40%) and methanol (60%) at -30°C. The supporting electrolyte is TBAF in 0.30 M and the working electrode is a silver amalgam electrode in diameter 1.6 mm. The simulation-fitting results of parameter are shown in Table 7-1. Solid lines are experimental data

Reproduced with permission of the copyright owner. Further reproduction prohibited without permission.

and solid dots are the simulation-fitting results. Scan rates: (a) 50 mV/sec; (b) 100 mV/sec and (c) 300 mV/sec..... 166

Fig. 7-3 The relationship of the reversibility factor f_r and the heterogeneous charge transfer constant k^o. The concentrations of the electroactive species in the electrode surface were evaluated at the peaks of cyclic voltammogram by digital simulation with $E^{o'}$ = -1.529 volt, α = 0.78, k^o = 1.8×10^{-6} cm^2/sec at -30°C. The reversibility factor f_r was calculated through equation (7-8). (a) 300 mV/sec and k_{chem} = 590 sec^{-1}, (b) 50 mV/sec and k_{chem} = 590 sec^{-1}, (c) 300 mV/sec and k_{chem} = 0 sec^{-1}, (d) 50 mV/sec and k_{chem} = 0 sec^{-1} 169

Fig. 7-4 The relationship of the reversibility factor f_r and the apparent transfer coefficient α_{app}. The solid point represents the simulation-fitting result of Fig. 7-2 (a) and estimated through equation (7-9) 170

Fig. 8-1 DPSC experimental data and the fitting result of methylcobalamin in the solvent mixture of DMF (50%) and methanol (50%) at -40°C. Silver amalgam working electrode in diameter 0.50 mm. Methylcobalamin = 2.0 mM, TBAF = 0.20 M. The initial potential was -1300 mV, the potential step -1600 mV and the final potential back to -1300 mV. The theoretical curve with the rate constant of the following chemical reaction 90 sec^{-1}. The solid dots represent the experimental data 171

Fig. 8-2 The plot of $it^{1/2}$ *vs.* time for DPSC with the same

Reproduced with permission of the copyright owner. Further reproduction prohibited without permission.

experimental data as Fig. 8-1 illustrating the "time window"..... 172

Fig. 8-3 (a) The rate constants of the following chemical reaction of methylcobalamin in two different solvent mixtures as temperature decreasing. The solvent components in ratio of DMF and methanol were 40:60 (hollow circles) and 50:50 (solid circles) with methylcobalamin 2.0 mM and TBAF 2.0 mM. (b) same experimental data as (a) but with the natural logarithm in vertical scale 173

Fig. 8-4 Plot of $\frac{1}{T}$ *vs.* $ln(k_{chem} / T)$ in the "normal" behavior temperature range. The solvent components in ratio of DMF and methanol were 40:60 (hollow circles) and 50:50 (solid circles). The corresponding activation energies calculated were 5.5 kcal/mol and 7.8 kcal/mol..... 175

Fig. 8-5 Dimerization of DMF at low temperature. The dimerization form minimizes the steric interaction and enhances the charge delocation and stability by forming a chair like six-member ring 176

Fig. 9-1 The UV/VIS spectra of alkylcobalamins. (a) methylcobalamin, (b) ethylcobalamin, (c) *n*-propylcobalamin, (d) *n*-butylcobalamin, (e) *iso*-butylcobalamin. The solid curves represent the spectra in H_2O, and the dash curves represent the spectra in 0.05 M HCl 177

Fig. 9-2 The UV/VIS spectra of hydroxocobalamin. The solid curve represents the spectrum in H_2O, and the dash curve represents the spectrum in 0.05 M HCl..... 182

Fig. 9-3 The UV/VIS spectra of photolyzed alkylcobalamins.

Reproduced with permission of the copyright owner. Further reproduction prohibited without permission.

Experiments were performed after both solutions were exposure in daylight for 5 min. (a) *n*-butylcobalamin, (b) *iso*-butylcobalamin. The solid curves represent the spectra in H_2O, and the dash curves represent the spectra in 0.05 M HCl 183

Fig. 9-4 The cyclic voltammograms of B_{12} derivatives in 2.0 mM with 0.20 M TBAF at 20°C. Experiments were performed with silver amalgam working electrode at scan rate 300 mV/sec in a solvent mixture of DMF (40%) and methanol (60%). (a) methylcobalamin, (b) ethylcobalamin, (c) *n*-propylcobalamin, (d) *n*-butylcobalamin, (e) *iso*-butylcobalamin and (f) adenosylcobalamin 185

Fig. 9-5 Cyclic voltammograms of methylcobalamin and simulation-fitting results in DMF-Methanol (40:60) solvent mixture at 20°C with k_{chem} 5,550 sec^{-1}. Experiment was performed with scan rate 300 mV/sec. Methylcobalamin 2.0 mM and TBAF 0.20 M with mercury amalgam electrode in diameter 1.6 mm. The solution resistance 660 Ω and diffusion coefficient 4.1×10^{-6} cm^2/sec were used in simulation. The simulation-fitting results are shown in Table 9-3. The curve represents experimental data and the dots represent the simulation-fitting results 186

Fig. 9-6 The application region of simulation-fitting method in Butler-Volmer approach with the fast rate constant of following chemical reaction in *EC* mechanism. The input data in simulation are k_{chem}= 5,500 sec^{-1}, α = 0.78, $D_o = 4.1 \times 10^{-6}$ cm^2/sec and scan rate 300 mV/sec at 20°C 187

Reproduced with permission of the copyright owner. Further reproduction prohibited without permission.

Fig. 9-7 CV simulation with various rate constants of following chemical reaction (k_{chem}). The electrochemical parameters of methylcobalamin at 20°C were used in simulation ($E^{o'}$ = -1.464 volt, k^o = 0.016 cm/sec, $D_o = 4.1X10^{-6}$ cm^2/sec, α = 0.77, A = 0.020 cm^2, C_o^* = 2.0 mM and scan rate 300 mV/sec). The values of k_{chem} are (a) 10 sec^{-1}, (b) 100 sec^{-1}, (c) 1,000 sec^{-1}, (d) 10,000 sec^{-1} and (e) 100,000 sec^{-1}. The CV curve shift tendency indicates that once k_{chem} is larger than 10,000 sec^{-1}, the cyclic voltammograms will almost not be influenced by k_{chem} 188

Fig. 9-8 *Iso*-butylcobalamin experimental and simulation results. CV simulation at 20°C with electrochemical parameters $E^{o'}$=-1.320 volt, α = 0.61, k^o = 0.016 cm /sec, k_{chem} = 10,000 sec^{-1}, scan rate 300 mV/see and R = 400 Ω. Dots represent experimental results..... 189

Fig. 9-9 Cyclic voltammograms of 1.0 mM methylcobalamin in aqueous media at 20°C. The system has *pH* 13.0 with the supporting electrolyte NaCl 0.20 M. Triton *X*-100 was used in concentration about 0.002%. Scan rate 1 volt /sec. Resistance 704 Ω. Dots represent the simulation results 190

Fig. 9-10 The logarithm relation of peak current (μA) *vs.* scan rate (volt/sec) of methylcobalamin in aqueous basic media. Same experimental condition as Fig. 9-9. The slope of the straight line fitted is 0.56 191

Fig. 9-11 Ethylcobalamin DPSC experimental (solid curve) and simulation results (dash curve) with microelectrode (10 μm indiameter)..... 192

Reproduced with permission of the copyright owner. Further reproduction prohibited without permission.

List of Schemes

Scheme 6-1 The general catalytic scheme for the cobalamin-dependent methionine synthesis reaction 193

Scheme 7-1 Electrochemical reaction of methylcobalamin 194

Reproduced with permission of the copyright owner. Further reproduction prohibited without permission.

Part 1 Instrument Improvement and Set-up

Chapter 1 Coupling BAS-100A Electrochemical Analyzer with External Computer

The power of the computer and microprocessor has been applied in many areas where control of an electrochemical system and a measurement process is required. This control has allowed automation of certain routine procedures and has improved the precision and speed of the measurement. Power in an electrochemical laboratory arises from an ability to bring a variety of techniques to bear on the electrochemical measurements. BAS-100A electrochemical analyzer is an instrument that has a wide range of options on a single set. It has a simple style for selecting and setting up the experiments, and it is very easy to be controlled and used[1-2]. The data of electrochemical experiments can be stored in the BAS-100A for a short period of time and they then can be transferred to an external computer with disk storage for further manipulation. The BAS-100A/IBM PC Service System provides a means for storing these data in the disk of the external computer. Unfortunately these working files only work in 100% IBM machines, not in any other kind of compatible machines. The reason is that as in the memory address space of F-block used to hold the computer's built-in ROM-BIOS program, only the members of family made by IBM have the built-in ROM-BASIC program located at the segmented memory address F600:0000[3]. Since there are so many compatible machines used in various laboratories, it is meaningful to develop a set of

Reproduced with permission of the copyright owner. Further reproduction prohibited without permission.

new programs for compatible machines.

1.1 The Communication between BAS-100A Electrochemical Analyzer and External Computer

The communication between BAS-100A electrochemical analyzer and external computer through an RS-232 serial port can pass and receive information at baud rates from 110 to 9600. In our system, the BAS-100A default rate 2400 is used[2]. There is a 25 pin D-type connector on the rear of the BAS-100A with pin 1 for shield ground, pin 2 for transmitted data (TXD), pin 3 for received data (RXD) and pin 7 for signal ground. The signal ground serves as a common reference point from which the polarity and voltage of the other lines can be determined. In this communication the BAS-100A is a Data Terminal Equipment (DTE) and external computer is a Data Communication Equipment (DCE). They are connected through a cable by pins 1 to 1, 2 to 2, 3 to 3 and 7 to 7 as shown in Fig. 1-1.

As the communication progressing, it is necessary for the BAS-100A to know whether the external computer is ready to receive information. If the speed of communication is faster than the speed of the external computer to receive, the computer have to be able to stop the BAS-100A by sending a special signal until it has processed all the data received. In this case information must be sent back from the receiving device to the transmitting device to show whether it is ready or not. This information is known as flow control or handshaking. There are two types of handshaking: hardware and software. Both types involve signals coming back from the receiving device to the

Reproduced with permission of the copyright owner. Further reproduction prohibited without permission.

transmitting device. With hardware handshaking, the receiving device sends a positive voltage along a dedicated handshaking circuit as long as it is ready to receive. Once the transmitting computer receive a negative voltage, it knows to stop sending data. With software handshaking, the handshaking signals are sent as data along the data wire instead of along the dedicated handshaking circuits[4]. In our system, the software handshaking is serviced by program. The XOFF signal will sent to the BAS-100A when the computer buffer is almost full, and the XON signal will be sent when the computer buffer is almost empty. The source code of the communication program BASCOM24.BAS, written in Portland QuickBASIC 4.5, is listed in Appendix 1.1.

1.2 Data Conversion

In order to minimize the time required to transmit data between the BAS-100A and the external computer, and to limit the disk space required for storing data record, a hexadecimal image of the BAS-100A's random access memory (RAM) is chosen as a format for the stored files. The drawback of this choice is that the stored files can not be converted to decimal values without an intricate knowledge of the memory map in RAM and the storage standards employed in the BAS-100A. Data conversion programs for various electrochemical experiments were developed.

1.2.1 Memory Maps in Random Access Memory

There are seven distinct zones of memory space in the BAS-100A. First there is a primary zone from 0000H to 2FFFH, that exits in an unswitched configuration. Then

Reproduced with permission of the copyright owner. Further reproduction prohibited without permission.

there are three zones (8000H to 9FFFH, A000H to BFFFH, and C000H to DFFFH) that are individually bank-switchable between a main memory chip and a secondary chip. All the operating software for the BAS-100A is contained in this read only memory (ROM) space. Since these addresses will never exist in the data files stored, they are not of concern to us in data communication and conversion. The last part of memory addresses in three zones exit as RAM space. The first zone in RAM is a long contiguous block from 3000H to 7FFFH. The low part of this zone is used to store experimental data extended upward, and the high part of the zone, over these data from 7E00H, is used for storage of pointers and operating parameters. The second zone in RAM, from E000H to F7FFH, is used for storage of the information that appears on the video display. The last zone in RAM, from F800H to FFFFH, contains additional parameters, pointers and other operating information[2]. They are also not of concern in dealing with externally stored files.

1.2.2 The Data Storage Format

The BAS-100A stores information in RAM with ASCII strings as shown in Fig. 1-2. The first thirteen lines are related to the experiment parameters, time and labels. The final line is composed of zero which is recognized by the BAS-100A software as a file terminator when reloaded. The lines after thirteen and before the final terminator are the data concerned. The standard string has the following structure:

:aabbccddeeeeee.....eeeeff

Each string begins with a colon, which serves as a delimiter. Following the colon is a

Reproduced with permission of the copyright owner. Further reproduction prohibited without permission.

group of hexadecimal digits interpreted as byte values in pairs. The first pair "aa" is the number of bytes of data represented in the string. This number is usually 10H, *i.e.* 16_{10}. It might be some smaller number but it is never larger than 10H. The next four hexadecimal digits "bbcc" represent the RAM address for the first group of data in the string. The high order byte of the address is "bb" and the low order byte of the address is "cc". "dd" exists as the data type specifier and is always "00". The string "eeeeee...eeee" represents the experimental results stored in back-word format. Each data point is defined by two-byte pairs and is a 16-bit hexadecimal value. The low-order part is stored in the lower address of the pair and the high-order part in the higher address. The first byte in the string is assigned to memory address indicated by "bbcc" and subsequent bytes are assigned to subsequent addresses. These hexadecimal values represent experimental results. The final byte "ff" is a checksum, which value will be adjusted so that the sum of all bytes in the string will be zero of module 256. Within these conventions, each ASCII string, called data record, can store 16 bytes of information in RAM space. A typical stored file ordinarily contains hundreds to thousands of bytes of information, so there will be many such records in a single data file.

1.2.3 Data Conversion Programs

The conversion from hexadecimal digit block to decimal data follows similar rules in all experiments carried by the BAS-100A. In cyclic voltammetry, linear sweep voltammetry *etc.*, the first data point in buffer is assigned to the initial potential of the

Reproduced with permission of the copyright owner. Further reproduction prohibited without permission.

scan, and successive points are spaced a constant distance apart on the potential scale. The assignment of the successive current values to actual potentials is determined by the initial scan direction and the scan range. Successive currents are associated with potentials progressing by steps and the direction of initial scan until the first switching potential. Then the sign of potential increment is reversed, so that the potential progresses toward the opposite direction until the second switching potential or the final potential. If there are second or more cycles, the program will do the same way until the end of data buffer. The increment of step is dependent on the scan rate of the BAS-100A. For other experiments as a function of time, *e.g.*, potential step chronoamperometry and chronocoulometry, similar rules are applied except that the time scales instead of the potential scales are used.

Since the method of storage has been optimized for three different modes in correspondence with three different ranges of scan rate or time scales, the hexadecimal values stored in buffer should be interrupted by several conversion methods. The storage involves (a) single reading of the twelve-bit analog-to-digit converter (ADC), (b) sums of 16 successive readings of the ADC, or (c) sums of 256 successive readings of the ADC[5]. For example, experiments on a short time scale, such as fast cyclic voltammetry ($\geq$500 mV/sec), involve single reading. The full scale range of the ADC is -10 volts to +10 volts, so the middle of the hexadecimal scale represents 0 volt. The BAS-100A takes 7FFFFH, 7FFFH, and 07FFH as the converted representation of zero volt input in three different scan ranges respectively. They are defined as ADC offset in the program. All techniques involve a constant sensitivity for entire experiments, and whole

Reproduced with permission of the copyright owner. Further reproduction prohibited without permission.

data points are stored in two-byte, 16-bit form. Actually some techniques only use parts of these three modes. For example, cyclic voltammetry only uses two modes (a) and (b), and they are ultimately represented in one mode (b) even though they are not all acquired in that way. Because there is not enough time to allow aggregation of 16 reading of the ADC in the faster scan rate, the data are acquired in single reading. At the end of running, each point is then multiplied by 16 in order to convert it artificially to the original mode. The ADC offset is then set as 7FFFH and the full scale value is set as FFFFH. Chronoamperometry and chronocoulometry are in the similar situations and they also only use one mode[5].

In the data image of the BAS-100A RAM as shown in Fig. 1-2, there are eight groups of data in each standard string. The last string may be less than eight groups depending on the situation. Each group includes four hexadecimal numbers in two-byte form. Because it is in the back-word format, the program reads the second hexadecimal number then the first hexadecimal one in the first byte. They are the first (the lowest order) and second (next to the lowest order) hexadecimal numbers in the two-byte group. The program then reads the second and the first hexadecimal numbers in the second byte. They are the third (next to the highest) and fourth (highest order) hexadecimal number in the same two-byte group. These hexadecimal numbers are converted to the corresponding decimal values and summarized immediately after each reading. The decimal value of current in correspondence with an individual data point can be straightforwardly calculated from the relationship:

Reproduced with permission of the copyright owner. Further reproduction prohibited without permission.

$$current = \frac{(sensitivity) \times (data\ point - ADC\ offset) \times (20\ volt)}{(full\ scale\ value)} \qquad (1\text{-}1)$$

where the sensitivity is an amplifying ratio in the current/potential conversion and the data point is the numerical value of one group in decimal form. The cyclic voltammetry data conversion program is listed in Appendix 1.2. These programs were also written in QuickBASIC 4.5 because of its features for string manipulation.

1.3 The Operation Procedure

1.3.1 Data Transfer from BAS-100A to External Computer

First, set the experimental condition in the BAS-100A and run the desired experiment. Run the communication program BASGW240.EXE in external computer and give the file name to be saved, so that the coupling computer is ready to communicate. Then going back to the BAS-100A type TERM at the star prompt and hit the carriage return, the terminal emulation will be invoked. Hit *Ctrl*-U then carriage return, the communication is triggered and you will observe an image of meaningful RAM contents as they are transmitted to the external computer *via* cable and saved under the named file. Once the communication is achieved, you will hear a beep and see a string of "000000...0000" which indicates all the RAM image is successfully transferred. Then hit *Esc* key in the keyboard of external computer to close the file stored on the disk. On the BAS-100A side, hit *Ctrl*-W to make the BAS-100A leave the emulation and return to ready mode. The communication is completed.

Reproduced with permission of the copyright owner. Further reproduction prohibited without permission.

1.3.2 Data File Conversion

As running the data conversion program CVCONVT.EXE of cyclic voltammetry (similar programs CACONVT.EXE for chronoamperometry and CCCONVT.EXE for chronocoulometry *etc.*), type the hexadecimal file name, the file name to be saved in decimal format, the scanning potential range, the resolution in the increment of step and the sensitivity index (answering similar questions in chronoamperometry and chronocoulometry data conversion programs except that the ranges and resolution are in time scale instead of the potential). The first thirteen lines containing experimental condition information in the original hexadecimal file should be canceled before running the program. The program then will convert all data from hexadecimal format to decimal format in voltage (mV) and current (A) and saved them on the disk (chronoamperometry in time (msec) and current (A), chronocoulometry in time (msec) and charge (coulomb) *etc.*). These new data files in decimal format will be easily read and used for further data processing and analyzing.

Reproduced with permission of the copyright owner. Further reproduction prohibited without permission.

Chapter 2 The Set-up of New Electrochemical Analysis System

The present commercial electroanalytical system and the capacitive nature of the regular electrochemical cell preclude rapid changes in potential. The electrochemical measurements with commercial instrument and conventional electrodes have generally been restricted to the millisecond or even longer time scale[1-2,6-7]. However the ability to make fast electrochemical measurements is desirable especially in potential step chronoamperometry and cyclic voltammetry, so that rapid heterogeneous or homogeneous reaction rate constants can be measured. Because of the small surface areas of microelectrode, the double layer capacitance and the current magnitude can be reduced tremendously when compared with conventional electrodes. These reductions in scale yield small cell time constants and bring about an improved instrumental ability to meet the power requirements of an electrochemical system on short time scales. Thus, microsecond level potential step chronoamperometry and fast scanning voltammetry become possible. The small current magnitudes can also dramatically reduce experimental distortions caused by *iR* drop. The technique of the fast electrochemical measurement with microelectrode is particularly useful to outrun chemical reactions that consume electro-generated products[7-9].

In general, the waveform generation, data acquisition and signal processing for an electrochemical instrument can all be put under the control of a computer. However, difficulties may be encountered for fast experiments because the processor may not have sufficient time to execute all tasks on demand. When the scan rate is high or within very

Reproduced with permission of the copyright owner. Further reproduction prohibited without permission.

short time scale, it is difficult for the processor to generate the waveform directly, to acquire data and to make changes as needed all at the same time. In order to overcome this difficulty, a separated settlement was designed where one computer was set-up as a waveform generator, and another computer was set-up as an oscilloscope interfaced with a home-built potentiostat as shown in Fig. 2-1.

2.1 The Personal Computer Based Waveform Generator

The waveform generator for electrochemistry was built based on the Qua Tech WSB-10 waveform generator (Akron, Ohio) controlled by user defined programs. The output signal from the WSB-10 can be programmed to any value from -5.12 volts to +5.12 volts with a resolution of 2.50 mV. The rate at which data points are generated can be program selected from 200 nSec/point (5 MHz) to 6.55 msec/point (153 Hz) in steps of 100 nsec. For slower data rates, a secondary programmable clock divider will be used with the primary divider and the data rate can be programmed to a rate as slow as 429 sec/point. The rate clock also can be controlled by the program selected external clock input[10]. The WSB-10 can be programmed to either continuously repeat the same waveform, or to produce a single occurrence of a waveform. In the repeat mode, there is an optional delay factor which determines the length of time interval between the end of one waveform cycle and the beginning of the next cycle. The delay factor can be programmed to a value between 2 to 65535 clock period with the time unit being the same as the intervals between the data points in active waveform, or disabled by setting the value to 0. The envelope of the analog waveform is programmable with an amplitude

Reproduced with permission of the copyright owner. Further reproduction prohibited without permission.

resolution of 12 bits and the number of points in a waveform is programmable from 1 to 2048. The WSB-10 has an externally available TTL strobe output at BNC connector 2 on the board, which is pulsed at the beginning of each waveform cycle. This strobe is an 1 microsecond positive pulse and provides a convenient method to synchronize an oscilloscope or other equipment at the beginning of a waveform cycle. Because of the complexity of the waveform generator, the system places an extra layer between the high level language program and the waveform generator board. Two general-used programs, STEP.BAS for potential step chronoamperometry and CV.BAS for staircase waveform or cyclic voltammetry, were developed. These programs send programmed signal to WSB-10 board and communicate with the board through its low level hardware interface. The programs enable the users to set and adjust the waveform parameters in very easy and reliable ways. For example, users can select scan rate in cyclic voltammetry experiments rather than consider the frequency related to the logic of digitizing module itself.

2.1.1 The Operation Theory of Waveform Generator

The WSB-10 waveform generator can reproduce any arbitrary waveform by a stair-step approximation. The period of the desired waveform is divided into a set of equal length time intervals. The value of each interval is calculated and used as the data points for creating waveform. The length of time interval T can be calculated as:

Reproduced with permission of the copyright owner. Further reproduction prohibited without permission.

$$T = \frac{P}{N} \qquad (2\text{-}1)$$

where P is the period of waveform and N is the number of points used to describe the waveform. The following equation indicates the relationship of data values and the desired output voltages:

$$Data\ Value = \frac{Desired\ Output\ Voltage}{Conversion\ Factor} \qquad (2\text{-}2)$$

where the conversion factor of 2.5 mV/count is used in present system situation[10]. Thus the first value in the array should be the first point in the waveform and each successive value should correspond to the following successive point. These values of data point must be integer values from -2047 to 2047. A digital value of 2047 produces the most positive output of 5.118 volts and a digital value of -2047 produces the most negative output of -5.118 volts.

The WSB-10 has an onboard 10 MHz crystal oscillator. It is divided by two 16-bit programmable dividers to produce the data rate clock. These two dividers must be programmed to set the rate at which the data points are to be reproduced. Once the time between data points is calculated by relation 2-1, the data rate R is decided by following equation:

$$R = \frac{1}{T} = \frac{10\ MHz}{RATE0 \times RATE1} \qquad (2\text{-}3)$$

Since RATE0 and RATE1 are unsigned 16-bit integers, they must be rounded to get the actual values. The rate ranges for them are $1 < RATE0 < 65536$ and $1 < RATE1 <$

Reproduced with permission of the copyright owner. Further reproduction prohibited without permission.

65536. After all of these values have been determined, they will be sent to the WSB-10 board where the WSB-10 will generate the waveform started under program control or external trigger. The WSB-10 will then continuously generate the waveform until it is commanded to stop or reset to a single mode.

2.1.2 The Hardware of WSB-10 Board and the Controlling Software

The WSB-10 board is installed in a free slot of personal computer. Header H1 in WSB-10 provides a 16-bit buffered digital output for each data point which is synchronized with the data for digit-to-analog (D/A) converter. Only the lower twelve bits are used for the D/A conversion, leaving the other four bits for various trigger and control functions or as a 16-bit input to an external D/A converter. The strobe and clock output signals as well as the external clock/trigger input are available on the header. There are three BNC connectors in the board. BNC 1 is the output connector for the generated analog signal with output impedance 50 Ohms. BNC 2 is used for two functions depending on the jumper configuration of the board. It can provide the output strobe pulse with a one microsecond positive pulse occurring at the beginning of each waveform cycle or provide the internal data rate clock. BNC 3 is the input for external clock or external trigger normally terminated by 110 Ohms. The external clock or trigger should be a TTL level signal[10].

In order to generate a waveform, the WSB-10 board must be programmed with waveform parameters such as the number of data points, data rate, delay between waveform cycles, mode of operation (repeat or single modes) and data array itself. To

Reproduced with permission of the copyright owner. Further reproduction prohibited without permission.

simplify the writing of application programs for waveform generator, a hardware driver program named WSB1B.EXE was supplied by Qua Tech. The drivers must be installed in system memory before the WSB-10 can be used by BASIC application programs. It is not available to write the application programs in QuickBASIC because some parameters of WSB-10 are the reserve words of QuickBASIC. The installation program WSB1B.EXE will leave its entry address in a special memory location called a hook, write its sign-on message and return to the operating system. Then the BASIC application program will read the driver's segment addresses and use them in calling the drivers. The drivers will remain installed in memory until the system has been rebooted. All parameters passed to the drivers must be 16-bit integers. Failure to do so will cause the stack to become corrupted, and the drivers will not correctly return control to the BASIC application program[10]. The location used to hold the segment number of drivers is the location normally reserved for interrupt 96, 0:180H. The BASIC application should read the word stored at 0:180H and set BASIC's data segment to this value before calling any of the drivers in WSB1B.

2.1.3 The Cyclic Staircase (Cyclic Voltammetry) Waveform Generator Program

The cyclic staircase waveform generator program (CV.BAS) is designed for the cyclic staircase and cyclic voltammetry (if the vertical potential increment is set small enough) experiments. The vertical potential increment in this program can be set as small as 2.5 mV. The program CV.BAS, written in Microsoft GWBASIC, is listed in Appendix 2.1.

Reproduced with permission of the copyright owner. Further reproduction prohibited without permission.

In this program, lines 240 to 430 are used for WSB-10 board preset, where the program defines the offsets of all the drivers, gets the segment addresses of WSB1B.EXE, checks if the drivers have been installed and sets I/O port address. Lines 630 to 760 initialize the waveform generator board and set all the default parameters. The clock rate is determined by RATE0% and RATE1% in equation 2-3. The NPOINTS1% is the number of data and NPOINTSP% is the preset number of data in the waveform. They are 16-bit integer in the range between 1 and 2048. The preset data set a number of data points with initial potential for a defined time PRESETM before the first data point. This function is used for precondition experiments. If PRESETM is one, the preset time equals the time of the first cycle; and if it is two, the preset time is as long as the twice time of the first cycle and so on. DELAY% is a 16-bit integer variable that determines the delay between waveform cycles. To disable the delay, set DELAY% to zero. To enable the delay, set delay% to the number of delaying clock cycles. CALL SETDLY(DELAY%) resets the WSB-10's internal data point counter back to the beginning of waveform. Thus whenever the WSB-10 is restarted after a delay, it will restart from the beginning of the waveform. The RATE0%, RATE1% and DELAY% are all considered to be 16-bit unsigned integer variables in the WSB1B. However BASIC program considers them as two's complement variables. As long as the value is between 0 and 32767, the two's representations are the same as regular valuables. To set them to a value out of this range would require hexadecimal notation, *e.g.*, these two representations would be converted to an unsigned integer by 65536 minus this two's complement number. MODE$ equaling "R" indicates the repetitive mode of operation

Reproduced with permission of the copyright owner. Further reproduction prohibited without permission.

is selected. When the WSB-10 is started in REPEAT mode, it will repeatedly generate the programmed waveform until commanded to stop, or the SINGLE cycle mode is selected, or the delay parameter is used *via* CALL SETDLY command, or it is reset by CALL RESET. Command CALL WINIT resets the WSB-10 to its power-up condition. The data point generation and board programming are executed *via* a subroutine call from line 720. Line 730 calls a subroutine program to initialize the screen message, display all default parameters and activate whole function keys (F1 to F10). Line 740 calls a subroutine program to calculate and display the clock rates and frequency. Command CALL WSTART in line 750 calls the board to start generating waveform. Line 760 presets a status parameter, which will be used in line 870 by CALL STATUS(T%) where T% is a 16-bit integer variable. Upon return from the function, T% will equal 1 if the generator is running or T% will equal 0 if the generator is not running.

Lines 850 to 890 check status and update display. Lines 980 to 1300 are the subroutine section in which the waveform data points are calculated and converted to the value of data points for the WSB-10 board. The whole waveform period depends on the initial, switching and final potentials together with the scan rate. The resolution of potential increment is related to the number of points in this particular time period. If the point interval is larger than 6.55 mSec, RATE1%=1 is automatically preset by the program, otherwise both RATE0% and RATE1% are adjusted. Command CALL INTCLK selects the internal clock in the rate decided by equation 2-3. WDATA%(n) is an array of 16-bit 2's complement integers containing the data points. The program presets the initial experimental condition in desired time period through lines 1170 to

Reproduced with permission of the copyright owner. Further reproduction prohibited without permission.

1190. WDATA(0) contains the first data point and the value of each point decided by WDATA%(n) must be within the range: -2048 < WDATA%(n) < 2048. There are six different situations for the waveform types through subroutines from lines 1400 to 1920. The program then updates the status. The command CALL DEFWAV is executed to define the number of points in the waveform generated and return to main program.

Lines 2690 to 4020 set function keys F1 to F10. These function keys are used to reset the waveform generator parameters. Ten parameters and functions including initial potential, switching potential, final potential, scan rate, data point number in the first cycle, function mode for single or repeated waveforms, preset time before the experiment, quit from generating the waveform, exit from the waveform generating program, start and stop functions, can be controlled through the corresponding function keys. F9 key starts generator which is particular useful to run a single waveform. F10 key stops generator by CALL WRESET, which also resets the internal data point counter to the beginning of the waveform. If the WSB-10 is restarted, it will not start from where it was stopped in the waveform cycle, but from the beginning of the waveform. Fig. 2-2 shows the appearance of the screen for this cyclic staircase (cyclic voltammetry) waveform generator program.

2.1.4 The Potential Step Chronoamperometry Waveform Generator Program

This program is similar to the cyclic staircase (cyclic voltammetry) waveform generator program in structure. The only difference is the waveform function where a potential step is applied instead of the staircase. The program is listed in Appendix 2.2

Reproduced with permission of the copyright owner. Further reproduction prohibited without permission.

and the appearance of the screen is shown in Fig. 2-3.

2.2 The Oscilloscope and Data Processing

2.2.1 The Waveform Analysis System

The digital oscilloscope used as a data collector is a IS-2010 waveform analysis system (Integrated Systems Products, Inc., Camarillo, California) assembled on a personal computer. The IS-2010 system consists of an IM-50 waveform acquisition module and an IS-2010 system software. The IM-50 module can fit into any of the expansion slots of IBM and its compatible computers[11].

The IS-2010 module provides a high speed digitization function for personal computer with the capability to store up to 2048, 7-bit (128 levels) samples of an incoming waveform. The digitization is controlled by an on-board micro-sequencer, which is programmed by host computer to carry out a number of functions concerned with digitization process. The rise time of oscilloscope system is 35 nSec and the full scale range is 40 mV to 40 volts in 10 steps. An important function of the module is to determine the correct trigger event and decide the time interval within the beginning and the end of sample captured period. The control functions executed by on-board micro-sequencer are the selections of gain and offset settings, the selections of correct sample rate and trigger level. The digitizer can operate at sample rates ranging from 250 Hz to 25 MHz in 16 steps. At any instant, the sample memory will contain the most recent 2048 samples of the incoming waveform. This process begins when capture is turned on and continues at the selected sample rate until capture is turned off. The clock generator

Reproduced with permission of the copyright owner. Further reproduction prohibited without permission.

provides two clock functions within the IM-50 module, the capture clock and the search clock. The capture clock is used to clock the digitizer and is selectable by the on-board micro-sequencer to provide digitizer clocking from 250 Hz to 25 MHz. The search clock is used to detect valid trigger patterns and also to provide controllable delays during the capture sequence. The source of both clocks is a 50 MHz crystal controlled oscillator. A precision offset is added to the selected trigger signal in trigger amplifier to provide control of the trigger level. This offset voltage is derived from a digital to analog converter and can be selected from 64 alternative values. The output from the trigger amplifier is applied to a comparator which compares it to a fixed voltage and provides a high output when the trigger amplifier output is above the trigger level.

2.2.2 Data Processing and the Application Program

The IS-2010 waveform analysis system can save the trace file that containing incoming signal information. These files are accessed by IS-2010 software when a trace is loaded to display on the screen. One trace file contains 33 records, each record being 64 bytes long. The first record contains the attributes of oscilloscope, which are these selected parameters relating to the sample set saved along with the waveform. The other 32 records contain binary sample information for the trace. A total of 2048 samples are included, 64 to each record. The samples are arranged sequentially in the order that they are captured, so that if they are read sequentially from the file, they will be in the correct order. Each byte represents 7-bit integer value of the sample obtained form analog to digital converter. They can be converted into voltage values with scaling constants. These

Reproduced with permission of the copyright owner. Further reproduction prohibited without permission.

constants are related to the calibration factors that are contained in the calibration file and were individually adjusted before leaving factory for the IM-50 module[11]. The trace attribute record consists of 19 attributes with 16-bit followed by 18 attributes with 8-bit and then by 8 undefined attributes with 8-bit. The program reads all of these into arrays and subsequently accesses the attributes of interest. The equation to be used for calculation is:

$$Voltage(mV) = Y \times \left\{ 82 - \left[\frac{D \times X + C}{256} + (G-8) \times 20 \right] \right\} \qquad (2\text{-}4)$$

where X is the sample value, Y is a gain setting dependent factor, D, C, and G are scaling constants. The program gets words[14] value in the first record of trace file then converts it to represent Y value in equation 2-4. These 16-bit binary values of gain setting and scaling constants are stored in the trace files with the low byte first in 2's complement format. The integer values of 16-bit number are read from the trace file by statement:

$$\text{words[i]} = \text{getc(in)} + 256 * \text{getc(in)} \qquad (2\text{-}5)$$

where words[i] must be a single precision real variable since otherwise an overflow error may occur in the case that the 16-bit number in file is negative. This is because the compiler will not know that the expression on the right of the statement is really a 2's complement representation of an integer and will assume that it is a positive integer outside the range of the integer variable between -32768 and +32767. Following this statement a further conditional statement must be used to take account of the case where the 16-bit integer being read from the file is negative:

Reproduced with permission of the copyright owner. Further reproduction prohibited without permission.

if (words[i] > 32767) words[i] = word[i] - 65536 (2-6)

After reading the word attributes in 16-bit integer with 19 repetitions, the program reads the byte attributes in 8-bit integers with 18 repetitions. Since all of these attributes are positive integers rather than 2's complement, there is no negative case to be considered. Then the program skips the spare 8 bytes. Finally the sample data are read into the array by treating each sample as an 8-bit integer. The complex assignment statements within the loop are actually a straightforward translation of equation 2-4, where Y is the GAINFACT array contained the values of Y in Table 2-1 by the sequence of assignment, C is the value in words[9], D is the value in words[12] and G is the value in words[15]. The time interval of sample is dependent on the sweep rate so that the suitable time scale will be assigned for the converted data file to each data point. Their relationship is listed in Table 2-2. The data conversion program for oscilloscope was written in Turbo C++ and one of the application program is listed in Appendix 2.3.

2.3 The Potentiostat and the Application of the System

2.3.1 The Background of the Circuit

In most electrochemical experiments, the aim is to relate the voltage across the electrode double layer to the current flowing across it. The current is easily measured but the voltage is always subject to an error. The error is due to the fact that the potential-measuring probe in the electrolyte can not measure at a point directly on the solution side of double layer. The non-zero distance from this point results in the current flowing through the resistance of the electrochemical system between the ideal and the actual

Reproduced with permission of the copyright owner. Further reproduction prohibited without permission.

measuring points. This will cause a small voltage drop that disorders the measuring voltage. In many cell configurations there are additional resistances that can not easily be eliminated. The sum of the voltage drops across all these resistances is the *iR* drop all electrochemists have to contend with. Fig. 2-4(a) shows the cell arrangement usually employed with three-electrode configuration. The cell current passes from counter electrode (*ctr*) to working electrode (*wk*) and the potential of the working electrode is measured with respect to reference electrode (*ref*). From the electronic standpoint, an electrochemical cell can be regarded as a network of impedances like those equivalent circuit of cell shown in Fig. 2-4(b). R_s is the resistance of the electrolyte solution between the counter and reference electrodes, which will be compensated in the system. R_u is the uncompensated or residual resistance between the reference and working electrodes. R_u represents the error resistance across these two electrodes where the error *iR* drop takes place. Z_d is the impedance of the interface between working electrode and electrolyte. This is grossly simplified, ignoring, for example, the impedance of the interface between counter electrode and electrolyte *etc.* If the current, R_u and Z_d are constants, the problem is simply a constant error. Then the error can easily be eliminated arithmetically. One measures the current as a function of applied potential, and obtains the real potential for each current by subtracting iR_u from the applied potential. If any of the experimental parameters, such as R_u, Z_d or the desired electrode potential vary with time, then other effects may occur. The error may not be allowed for simple correction. In cyclic voltammetry, the current will vary in a non-linear way with applied potential, so that, even for a constant value of R_u, the actual electrode potential will be

Reproduced with permission of the copyright owner. Further reproduction prohibited without permission.

a non-linear function of time because of the varying *iR* drop. You may be able to calculate the true potential-time curve for the potential applied but this may not help you if you wish to use linear-sweep theory. Potential step techniques share this problem where the potential will reach the electrode double layer in a distorted form. In the system we developed, a three-electrode potentiostat was constructed in order to greatly reduce the *iR* problem especially the iR_s drop effect[12-13].

Considering Fig. 2-4(a), since the currents into the summing point *S* must add to zero, we have

$$-i_{ref} = i_{input} \qquad (2\text{-}7)$$

Because *S* is a virtual ground, we have the relationship:

$$-e_{ref} = e_{in}\ (R_{ref}/R_{in}) \qquad (2\text{-}8)$$

where e_{in} is the input potential and e_{ref} is the potential on reference electrode. The current through the cell is controlled by amplifier so that the potential of reference electrode is $-e_{in}$ *vs.* ground if R_{ref} equals R_{in}. Since the working electrode is grounded, we have

$$e_{wk}\ (vs.\ e_{ref}) = e_{in} \qquad (2\text{-}9)$$

regardless of fluctuations in R_s, R_u and Z_d. The amplifier will adjust its output to control the currents through the resistors. The current through R_u and Z_d is dependent on both of them and e_{in}. It passes through R_s too and independent of the value of R_s or fluctuations in it. This kind of circuit has a means for controlling the voltage at a fixed point in a network of resistance, even if the compensated resistances or more generally the impedances fluctuate during the experiment. The controlled voltage, e_{ref} *vs.* ground, contains a portion iR_u of the total voltage drop in the solution. The presence of this

Reproduced with permission of the copyright owner. Further reproduction prohibited without permission.

uncompensated resistance makes the circuit give inaccurate control over the true potential, but in many cases iR_u can be made negligibly small by careful placement of the reference electrode.

A home-built potentiostat with three-electrode configuration is shown in Fig. 2-5. The central part of circuit is the widely used DeFord-type potentiostat[14]. Its advantages are concerned in the input requirements where one of the input terminals is at ground, hence the function generator supplying the waveform for potential control would not have to possess a differential floating output. Most waveform sources would meet this demand. Another advantage is the circuit with basic adder function. If it is desired to add more input sources, one can add another input resistance at the inverting point of the amplifier. The operational amplifiers were selected as a compromise between the simultaneous requirements of wide bandwidth, low bias current, high slew rate, and low noises of current and voltage. The 353 operational amplifiers, the dual JFET input operational amplifier (Radio Shack catalog number 276-1715), were used in this circuit. It requires low supply current yet maintains large gain bandwidth product and high slew rate. The device also exhibits low noise and offset voltage drift. Its major features[15] are listed in Table 2-3. Practically a voltage follower will be inserted into the feedback loop, so that the reference electrode is not loaded by the current fed into the summing point. The follower's output is also available externally for the use with a recording device (switch S3 in position b). It is a convenient continuous monitor of $-e_{wk}$ (*vs. ref*).

Reproduced with permission of the copyright owner. Further reproduction prohibited without permission.

2.3.2 The Influence of High Frequency and the Noise Problem

The critical part of the circuit is the current transducer. The feedback configuration is employed because it is advantageous when a rapid time response is required[16-22]. If there is no feedback in the circuit, the gain reduction with *ac* input as frequency increases will be caused by distributed capacitance and some complex characteristics of active devices such as propagation delay and switching time on the integrated circuit chip. The gain of the operational amplifier without feedback is known as open-loop gain (A_{ol}). Once the open-loop gain in *dc* is known, the gain at any frequency of operation can be found by following equation:

$$A = \frac{A_{ol}}{\sqrt{[1+(\frac{f}{f_c})^2]}} \qquad (2\text{-}10)$$

where f is the frequency of operation and f_c is the cutoff frequency. As the frequency increases, gain drops steadily. In the feedback network, the gain is reduced, but the bandwidth is increased and the gain is kept constant as frequency changes. The current transducer also allows the working electrode to remain at virtual ground, which is an essential condition for the operation of the system. For any given current, the feedback resistance (R_f) must not be so large that iR_f exceeds the possible maximum output voltage of the optional amplifier, which is ± 10 volts the power supply provides. In addition, the current may not exceed the current capability of the power dissipation (500 mW) of the operational amplifier either. Considering the phase response, we expect that a typical inverting amplifier's output is 180° out of phase with its input. This is true only at low and medium frequencies when the feedback signal cancels part of input signal, so that

Reproduced with permission of the copyright owner. Further reproduction prohibited without permission.

both gain and the output impedance are reduced, and input impedance is increased. However at higher frequencies, internal capacitance, circuit delays and semiconductor characteristics start increasing more delay or phase shift effects, so that the feedback signal might not be in the phase with 180° out of the input signal. Then a small capacitor connected across the feedback resistance was used for this frequency compensation[16,21-22].

In the situation that the results from background subtraction are not disordered by chemical phenomena, the ultimate limitation will depend on electronic noise. Since all electrical signals are an ordered drift of electrons superimposed on a basic random fluctuation, the Johnson noise or resistor noise from R_f and the amplifier current noise must accompany with the circuit[19]. The noise also arises from the potential control portion of the potentiostat and the cell resistance because of the uncompensated resistance R_u and the double layer capacitor C_{dl}. Shot noise is negligible for the conditions used according to Weber's similar analysis for amperometric detectors[16,22]. The noise sources and their related equations are listed in Table 2-4. Under these conditions, an increment in R_f increases the maximal noise sources, the Johnson noise, by $R_f^{1/2}$ but the faradaic signal is increased by R_f. Thus, the maximum signal-to-noise ratio, within these constraints, is obtained with as large a value of R_f as possible. The bandpass and power dissipation requirements, however, limit the upper value of R_f so that R_f = 100 kΩ was selected. In order to reduce the noise from amplifying circuit, the number of amplifiers in this part of the circuit should be minimized so that a two step amplifying configuration is preferable.

When the potentiostat was connected to the electrochemical cell, a slight ringing

Reproduced with permission of the copyright owner. Further reproduction prohibited without permission.

could be observed on the rising and falling edge of a square wave at the potential monitor output. This was not present when the counter and reference electrode leads were shorted together, indicating the instability is caused by the reference electrode impedance. This was alleviated by the use of a small capacitor between the counter and reference electrodes suggested by Howell *etc.*[16] Actually in the application, the switch (S2) was not used in the current measurement section of the potentiostat. The gain was varied by the interchange of resistors in plug-in sockets at the feedback of the second voltage amplifier. To minimize the noise coupling through the power system, a decoupling network was connected to each power terminal. For avoiding the crisis from power problems, a protecting system was designed and used for this potentiostat. A trigger adjusted circuit was used to reduce the trigger peak potential by nearly half and protect the oscilloscope. The circuit diagram of the potentiostat is shown in Fig. 2-5.

2.3.3 Circuit Test and the Application of the System

The circuit of the potentiostat was tested by direct potential signals and some typical waveforms on the equivalent circuit of the cell. Then several typical electrochemical compounds were tested and their results were compared with the ones from the BAS-100A and theoretical model in same potentials applied and time scale. The results were satisfied. Fig. 2-6 shows one of these results where the double potential step chronoamperometry experiments with ferrocene were performed by the home-built electrochemical analyzer, BAS-100A and calculated from the theoretical model. All experiments were performed in a faraday cage to minimize the 60 *Hz* interference. This

Reproduced with permission of the copyright owner. Further reproduction prohibited without permission.

home-built electrochemical analyzer will be used to measure the rate of the fast following chemical reaction of ethylcobalamin in aqueous media at *pH* 13.0, which will be discussed in chapter 9.

Reproduced with permission of the copyright owner. Further reproduction prohibited without permission.

Part 2 Electrochemical Properties of Solvent-Electrolyte System with DMSO at Low Temperature below the Freezing Point

Chapter 3 The New Observation in the Electrochemical System with DMSO below the Freezing Point

Electrochemical studies at low temperatures have been of interest for many years as a means of studying the mechanisms of electrode processes, activation parameters, identification of reaction intermediates and the temperature effect on transfer coefficients[1-3]. At low temperatures, unstable species associated with electrode processes may be stabilized and the characteristic lifetimes associated with these reactions can be put on a time scale amenable to be studied by transient electrochemical techniques such as cyclic voltammetry (*CV*). The kinetics of their reactions has been studied and the quantum effects on electron transfer kinetics have been predicted in these low temperature environments[4]. Initially, studies were confined to the liquid phase using low freezing point solvents. This is because of the requirement that the solution is a conductor and allows the electroactive species to diffuse to and from the surface of the electrode. It was found that a number of common nonaqueous solvent-electrolyte systems were suitable for low temperature work in terms of potential window and conductance. It is usually assumed that a natural limit of a solvent usefulness in electrochemical experiments is the solvent freezing point, although the possibility of supercooling was noted in several cases[1]. Recently, electrochemical studies in frozen solutions of perchloric

Reproduced with permission of the copyright owner. Further reproduction prohibited without permission.

acid ($HClO_4 \cdot 5H_2O$) over the temperature range 4.2 to 300K have been described[5]. The impedance studies at gold electrodes characterized important properties such as conductivity and dielectric constant over a wide temperature range and extended data available on the frozen electrolyte media[6-11]. In the frozen perchloric acid and frozen sulfuric acid electrolyte media, the studies at gold microelectrode have noted the existence of a change in the mass transport mechanism from diffusion control to a surface confined pathway as the temperature is lowered[11]. The most recent work was reported by Bond and Pfund on cyclic voltammetric research with gold, platinum and glassy carbon microelectrodes in ice without added supporting electrolyte[12]. The use of three different electrode materials was employed to distinguish frozen solvent effects from phenomena resulting from the electrode materials. The influence of the anion was tested through the ferric ion added as the nitrate, chloride and sulphate salts. Electrochemical data have also been reported in frozen acetonitrile containing electrolyte where a steady-state response was observed with microelectrode[13]. Analogous results in chemical reactions have been observed in multicomponent frozen systems, and a simple model has been proposed to account for these results that supposes the existence of a liquid microphase which concentrates solutes and then accelerates chemical reactions[14]. All these works opened up a new approach in electrochemistry by showing that conventional electrochemical experiments could be performed in solid media where Faradaic processes have been examined by cyclic voltammetry with both conventional size electrodes and microelectrodes.

In the course of the study of low temperature electrochemistry, we have also

Reproduced with permission of the copyright owner. Further reproduction prohibited without permission.

encountered some unusual phenomena. High quality electrochemical results were obtained in dimethylsulfoxide (DMSO) solvent with tetrabutylammonium peroxide (TBAP) as low as 40°C below the freezing point of DMSO (18.5°C). DMSO is known as an excellent solvent for inorganic and organic materials. It is resistant to oxidation and reduction, and has a high dielectric constant. Electrochemistry of DMSO has in fact been extensively reviewed[15]. However its physical properties provide no immediate explanation for our results. These unusual features such as an increase in current at temperatures below the freezing point and at low electrolyte concentrations are explained by us on the basis of the presence of a liquid microphase. This liquid microphase coexisting with the predominantly solid material accelerates electrochemical and chemical reactions by concentrating components in the liquid microphase[14,16-18]. The experimental results confirm that the natural limit of solvent usefulness with respect to voltammetric techniques may be extended well below the freezing point of the solvent-electrolyte combination provided sufficient conductivity is available so that the ohmic drop (iR) is not so severe as to prevent meaningful measurements. Several approaches have been applied including the use of microelectrode and electron spin resonance (ESR). It is believed that similar results might be obtained in other solvent-electrolyte systems[12,14]. There is also some evidence, for instance, from NMR experiments, that a tetrahydrofuran (THF)-solute system shows similar properties as the DMSO-solute system. In these experiments, narrow lineshapes of typical liquid NMR spectra were observed in THF well below the freezing point[19].

Low temperature technologies have long been used to slow down reactions and

Reproduced with permission of the copyright owner. Further reproduction prohibited without permission.

to preserve food for extended periods of time. Recently an increased interest in the long-term storage and preservation of simple and complex biological materials and living organisms has been seen. This interest has been stimulated by the needs of medicine, notably in the wake of advances in hypothermia and cryothermal mechanisms. At present, international banks have been set up for organs and biological preparations such as organ and tissue transplantations. If the biological materials are to be preserved for a long time, *e.g.*, months or even years, they must be completely frozen and cooled down to the low temperature of liquid carbon dioxide or liquid nitrogen, which are beyond the capabilities of conventional refrigerator and freezer. The biological material can be destroyed by simply freezing. Cells subjected to direct freezing can be killed either on rapid or slow cooling. Rapidly cooled cells appear to be killed by the formation of intracellular ice[20-22]. Slowly cooled cells are believed to be killed as result of changes in extracellular solution composition accompanying extracellular freezing[23-24]. The type of injury leading to damage or death of biological materials during slow cooling has been termed solution effects[25]. The effects of cooling on the viability of different human tissues have been defined as avoiding intracellular ice formation or avoiding the injury by solution effects[26-27]. These difficulties can be circumvented through the use of cryoprotectants such as DMSO, glycerin and ethylene glycol. With the aid of cryoprotectants, it is possible to accomplish the prolonged reversible preservation of biological materials such as leucocyte, sperm, cartilage, pancreatic islets and bone marrow cells. These biological materials have been safely utilized in clinical practice[28]. Because of the incredible speed of DMSO penetration ability in nearly all biological

Reproduced with permission of the copyright owner. Further reproduction prohibited without permission.

membranes, DMSO has been universally used as cryoprotectant[14-15]. A human neuronal cell freezing technique has been developed, in which the human fetal neuronal cells can be deeply frozen with DMSO as cryoprotectant. The survival of these isolated thawed cells was evaluated in culture where the cells were frozen at -196°C for 370 days without loss of viability. The average recovery rate of frozen cells was 62% of the recovery rate of cultured unfrozen controls. Morphological integrity of cryopreserved neurons has been confirmed at the ultrastructural level[29]. Recently the successful banking of pancreatic endocrine cells for transplantation was also achieved with DMSO as cryoprotectant[30]. An empirical equation was developed for the DMSO-H_2O-NaCl and glycerin-DMSO-H_2O ternary systems where the area of the liquid surface, described by the ternary phase diagram equations, was explained as the water-rich region bounded by the pseudobinary eutectic troughs[31]. Work is under way on methods of reversible preservation for more complex biological systems and even organs.

Since the importance of DMSO mixtures in cryopreservation of biological and medical fields, a through understanding of the mechanism will help us to optimize the system components and develop new systems. In investigations concerned with the mechanism of low-temperature biochemical reactions, it is important to know how the physical and chemical properties of the system change with decreasing temperature. Electrochemical experiments can be easily used to find the ion diffusion and other movements of the testing system although they look like "frozen". Besides the electrochemical experiments, the data obtained in DMSO-electrolyte media, in terms of the existence of a liquid microphase at temperatures well below the freezing point of

Reproduced with permission of the copyright owner. Further reproduction prohibited without permission.

solvent, were further confirmed by electron spin resonance experiments. Based on these results, a theoretical model was developed. Because traditionally understanding the effect of cryopreservation system for biological and medical samples needs a long time period, the theoretical model and electrochemical results are expected to be applied to optimize the system components of cryopreservation with better efficiency.

3.1 The Electrochemical Experiments of the DMSO-Electrolyte Freezing System

In order to investigate the electrochemical properties of the DMSO-electrolyte freezing system, the electrochemical experiments of *p*-benzoquinone and ferrocene were carried out. All experiments were performed using a conventional three electrode configuration. The working electrodes were 1.6 mm diameter platinum, 3.0 mm carbon and 33 μm glassy carbon. The reference electrode was an Ag/AgCl electrode with ethanol solvent saturated by LiCl (ultrapure grade, Alfa) at -85°C. The connection between the reference compartment and the test solution was through a glass-frit liquid junction. The counter electrode was a 0.5 mm diameter platinum wire. The distances between the working, reference and counter electrode were kept to a minimum in order to minimize the uncompensated resistance. Prior to the commencement of each experiment, electrodes were polished with an aqueous slurry of 0.05 μm Al_2O_3 on a polishing cloth. After rinsing the electrode with water, polishing was repeated without Al_2O_3 on a clean, wet cloth. The electrode was then again washed thoroughly with deionized-distilled water and followed by DMSO, and was immediately used in electrochemical experiments.

Reproduced with permission of the copyright owner. Further reproduction prohibited without permission.

The experiments were performed with a BAS-100A electrochemical analyzer. The experimental data were transferred to a coupling personal computer where data were converted and further processed. The entire cell was immersed into the Multicool chamber which was filled with ethanol. The cell temperature was monitored with an Omega temperature probe near the working electrode and was controlled by the temperature bath controller (FTS Systems). The measurements were taken only when the system had reached a steady state temperature, and the temperature indicated in bath controller coincided with the temperature probe. A good check on temperature was by measuring the resistance of the cell. The resistance and temperature would reach steady state in a period of minutes while changing the temperature in a small increments (about 5°C). In the case of 0.10 M TBAP system a supercooling effect of 4 to 6 degrees could be observed. The supercooled solutions might be induced to crystallize by vibration of the electrochemical cell. The metal chamber of the temperature bath controller was grounded as a Faraday cage. DMSO (Burdick and Jackson Laboratories, Inc.) was dried over 3Å molecular sieves. It has been mentioned that purification of the best commercial grades of DMSO is not normally necessary for electrochemical studies except for water removal, because the residual currents observed in commercial C.P. grade DMSO were 20 times smaller than that in acetonitrile of the best commercial purity that had been further purified by distillation from P_2O_5 and CaH_2[15,32]. Water analysis by Karl Fisher method established that the water content in DMSO was less than 0.03%. The *p*-benzoquinone and TBAP were used as received from Kodak, and the ferrocene as received from Sigma. Up to 90% *iR* drop correction was utilized. At lower temperature

Reproduced with permission of the copyright owner. Further reproduction prohibited without permission.

(below 15°C) the electrodes were imbedded in a solid matrix, so that it is clear that supercooling did not occur. The solution was purged with high purity nitrogen saturated with DMSO for 15 min. Then a flow of nitrogen was maintained over the solution or solid during the course of electrochemical experiments. Results reported are the average of three or more measurements with reproducibility error of $\pm 5\%$ or better (reproducibility varied somewhat with temperature).

3.2 Discussion of Experimental Results

3.2.1 Electrochemical Experiments with Conventional Electrodes

Cyclic voltammograms of *p*-benzoquinone are shown in Figs. 3-1 (a) and (b) for temperatures above (26°C) and below (-20°C) the freezing point. Both experiments were in the scan rate 75 mV/sec with *p*-benzoquinone 4.0×10^{-4} M and TBAP 0.10 M. The reversibility of the system was examined and the results are shown in Figs. 3-2 and 3-3 for the behaviors of resistance and peak current. These experiments were performed as the temperature was gradually lowered from room temperature to -20°C and subsequently raised back. Several details are worth noting. Nearly complete reversibility was observed in the measurements of (uncompensated) solution resistance, peak current and the peak potential difference of cathodic and anodic waves (ΔE_p). The solution resistance does not change dramatically in passing through the freezing point, although it does increase more rapidly once the solid is formed. The supercooling state was observed as low as 11°C, however the transition from liquid to frozen states was easily observed and the freezing point was determined in the range of 15 to 17°C. Only at temperatures below -20°C does

Reproduced with permission of the copyright owner. Further reproduction prohibited without permission.

the resistance increase to the point where reproducible measurement becomes difficult (although some results were obtained as low as -32°C, these were more difficult to obtain with reproducibility). As the temperature was lowered the peak current first decreased, then increased by about 50% and finally decreased as the temperature was lowered further. The current observed at -20°C was still above the current at room temperature. The change in ΔE_p, from 60 mV just below the freezing point to about 40 mV at -20°C, is somewhat larger than the decrease predicted from the temperature effect alone. The digital simulation showed ΔE_p only decreased 8 mV as the temperature was lowered from 20°C (ΔE_p=60mV) to -20°C (ΔE_p=52mV) (simulation inputs k^o=0.050 cm/sec, α=0.50, $D_o=3.0\times10^{-6}$ cm^2/sec, scan rate 75 mV/sec and electroactive species 4.0×10^{-4}M). In addition, the low temperature voltammograms exhibit narrower peaks than their counterparts at room temperature, which matched the computer simulation results made by Duyne and Reilley for the reversible electroactive species in liquid system at low temperature[1] and confirmed by our own computer simulation.

Ferrocene was also examined in a series of low temperature experiments. Compared to the *p*-benzoquinone system the results are qualitatively similar. The peak currents at frozen situation could reach as high as three times the values in liquid solution at room temperature. Trends in uncompensated resistance shown in Fig. 3-4 are the same as the system with *p*-benzoquinone. A plot of peak current *vs.* temperature in Fig. 3-5 shows a tripling of the current as the temperature was lowered. A plot of peak currents of ferrocene *vs.* the square root of the scan rates in logarithmic scales shown in Fig. 3-6 confirms a diffusion-controlled process with the linearity and the slope of the best-fit

Reproduced with permission of the copyright owner. Further reproduction prohibited without permission.

straight line in this system below the freezing point. Finally, the peak currents at temperatures of 0°C (frozen state), 10°C (frozen state) and 20°C (liquid state) were measured for different concentrations of electrolyte TBAP shown in Fig. 3-7. There is an increase of peak current with the decrease in electrolyte concentration at temperatures below the freezing point. At 0°C, the peak current increases with decreasing electrolyte concentration and with the highest value measured being about four times the peak current at 20°C in liquid state. At 10°C, this effect of electrolyte is smaller but it still exists. Since DMSO is in the liquid state at 20°C, there is no influence on changing the concentration of electrolyte.

Comparing the results obtained here with these in solvents other than DMSO described by Stimming[5-7] and Bond[10-13], the reproducibility of this system is better. The "frozen" electrochemistry was performed in DMSO system repeatedly over several hours and no significant degradation of electrode response was found. This markedly different nature of voltammograms indicates a fundamentally different phenomena in the system properties.

The same experiments for a similar system, except the solvent was dimethyl formamide (DMF) instead of DMSO, were performed. The results showed that there was immediately no diffusion current when the solvent approached the freezing point, even though the dimerization property of DMF at low temperature was mentioned (for example, more than 97% DMF in the dimer form in supercooling at -78°C) which may be the reason for the substantial supercooling behavior of DMF[1].

These unusual electrochemical properties were also observed in several DMSO-

Reproduced with permission of the copyright owner. Further reproduction prohibited without permission.

H_2O-NaCl systems used for cryopreservation (details will be presented in chapter 5). Based on these results, we have reason to believe that this is not a general phenomenon but only for some special solvent systems, especially the systems involving DMSO.

3.2.2 Electrochemical Experiments with Microelectrode

Cyclic voltammetry with a glassy carbon microelectrode in diameter 33 μm was studied. Fig. 3-8 shows a series of curves obtained in DMSO with 5.0 mM ferrocene and 0.10 M TBAP over the temperature range 30°C to -20°C. The values of wave width $E_{3/4}$-$E_{1/4}$, experimental and theoretical, which were developed for diffusion controlled process with the reversible electrode, are listed in Table 3-1. When the temperature was well below the freezing point but not lower than zero degree, the sigmoidal shaped curves were still observed. Above the freezing point of DMSO in this system (15-17°C), nearly superimposed sigmoidal shaped curves were obtained as shown in Fig. 3-8(a) and (b). The $E_{3/4}$-$E_{1/4}$ value of 56$\pm$1 mV obtained at 30°C is very close to the theoretical value of 57.4 mV through the relation $E_{3/4}$-$E_{1/4}$=Ln(9)(RT/nF) expected for the reversible steady state response where radial or edge diffusion terms are dominant[33]. At 20°C, the $E_{3/4}$-$E_{1/4}$ value of 51$\pm$1 mV obtained is also close to the theoretical value of 55.5 mV. The limiting currents for ferrocene oxidation decrease significantly over this temperature range due to the diffusion coefficient decreasing with temperature change (Fig. 3-8(b)). In experiments at 10°C and 0°C, which are below the freezing point of DMSO, the faradaic currents are still always negative (oxidation) and the limiting currents decrease as the temperature is lowered (Fig. 3-8 (c) and (d)).

Reproduced with permission of the copyright owner. Further reproduction prohibited without permission.

As the temperature was decreased below 0°C, remarkable changes were observed. These voltammograms are closely related to those results observed in H_2O-$HClO_4$-$Fe_2(SO_4)_3$ system below the freezing point with a platinum microelectrode of 25 μm in diameter[12]. At -10°C (Fig. 3-8(e)), the diffusion component of mass transfer is confined and positive (reduction) faradaic current is present on the reverse scan of cyclic voltammogram. The sigmoidal shaped response is replaced by a peak shaped response. The waveform has the characteristics of a surface confined process in which ferrocene is oxidized but the oxidation form is trapped at the surface and can not escape by diffusion. The areas under the peaks for both oxidation and reduction are nearly equivalent. At -20°C, similar characteristic as -10°C was observed (Fig. 3-8(f)) but with distortion which might be attributed to the high value of *iR* drop and the dominant of solid matrix. Unlike the case above 0°C, the current no longer decreases with decreasing temperature as expected if the change is solely due to a decreased diffusion coefficient. The slight increase of the peak current with lowering temperature over the range -10°C to -20°C indicates that the concentration increase effect has more influence than that of diffusion coefficient decrease effect. The observation from Figs.3-8 (a) to (f) is consistent with a gradual change from one mass transport mechanism to another in the eutectic state. Because of the more dominant solid matrix at low temperature, there is not enough space for spherical diffusion on the surface of microelectrode. The diffusion layer is then confined to the distance similar to or smaller than the size of microelectrode. The electroactive species become trapped at or near to the electrode surface, giving rise to the thin layer type electrolysis in a confined or restricted volume where no diffusion of

Reproduced with permission of the copyright owner. Further reproduction prohibited without permission.

electroactive species away from the electrode surface may take place within the time scale of the voltammetric experiment. For this circumstance, the sigmoidal shape curve can not be observed. Instead, the surface-confined waveform is formed. These results with the microelectrode indicate that a eutectic system is formed as the system freezes and the solid matrix in the eutectic system dominates more and more space as the temperature is lowered. The formation of liquid microphase is the reason for all these unusual electrochemical behaviors in both conventional and microsize electrodes.

Reproduced with permission of the copyright owner. Further reproduction prohibited without permission.

Chapter 4 Electron Spin Resonance Experiments of the Freezing System

Analogous results in multicomponent freezing system as we observed in DMSO-electrolyte system have previously been noticed in chemical reactions[14,34], and a simple model has been proposed to account for these results. This model supposes the existence of a liquid microphase that concentrates solutes and accelerates chemical reactions. Based on the electrochemical experiments described in chapter 3, the DMSO-electrolyte system could also be understood on the basis of the formation of a liquid microphase, which formed as a consequence of freezing out of pure solvent and remaining the concentrated solutes in the liquid solvent. Since the phase state of frozen solution can conveniently be investigated by the ESR technique, it was expected that ESR spectra of spin label in DMSO-electrolyte system should give further information about the phase state and the mobility in freezing solution. If there does exist a liquid microphase, the ESR experimental data should support the electrochemical results.

4.1 The Principle of ESR Experiments in Freezing System

4.1.1 Electron Spin Resonance Spectroscopy

The electron spin resonance (ESR) technique, also called electron paramagnetic resonance (EPR), is based on the fact that atoms, ions, molecules or molecular fragments that have an odd number of electrons exhibit characteristic magnetic properties. These magnetic properties arise from either the orbiting action or the spinning action, or both, of unpaired electrons about the nucleus. Unpaired electrons, although they are relatively

Reproduced with permission of the copyright owner. Further reproduction prohibited without permission.

unusual in occurrence, are present in free radicals, transition element ions, *etc.* If an electron possesses a spin or is associated with the spin, there is a magnetic moment. This magnetic moment can be detected by its interaction with a magnetic field. In zero field, the magnetic moments of unpaired electrons in a sample are randomly oriented. When a strong and constant magnetic field H is applied to the unpaired spins of an electron, there is a torque acting to make the electron dipoles line up either parallel or antiparallel to the direction of the magnetic field. This torque precesses about the field axis at a frequency which is proportional to both the applied magnetic field and the electron magnetic moment[35]. The energy of an electron moment in a magnetic field is given by

$$E = -\mu_e H \qquad (4\text{-}1)$$

where μ_e is a magnetic moment in the units of $h/2\pi$ (h is Planck constant). The magnetic moment is given by

$$\mu_e = -g\beta m_s \qquad (4\text{-}2)$$

In this relation g is a dimensionless constant called g-factor and its value equals 2.0023 for the free electron, but when strong coupling occurs the value differs significantly. ß is a constant called the Bohn magneton. m_s is the magnetic spin quantum number, which can take the values $+S$, $+(S\text{-}1)$,..., $-(S\text{-}1)$, $-S$. The equation (4-1) can be represented as

$$E = m_s g\beta H \qquad (4\text{-}3)$$

When S=½, there are two energy levels

$$E_{+½} = +½g\beta H \qquad (4\text{-}4)$$

and

$$E_{+½} = -½g\beta H \qquad (4\text{-}5)$$

Reproduced with permission of the copyright owner. Further reproduction prohibited without permission.

whose energy is linearly dependent on the strength of magnetic field H. The separation between these energy levels at a particular value of the magnetic field H_R is

$$\Delta E = +\frac{1}{2}g\beta H_R - (-\frac{1}{2}g\beta H_R) = g\beta H_R \qquad (4\text{-}6)$$

In an ESR experiment, an oscillating magnetic field perpendicular to H_R induces transitions between the $m_s=-\frac{1}{2}$ and $m_s=+\frac{1}{2}$ levels, provided the frequency ν is satisfied the resonance condition:

$$\Delta E = h\nu = g\beta H_R \qquad (4\text{-}7)$$

Actually in the ESR instrument, the frequency is held constant and the magnetic field is varied. At a particular value of the magnetic field, H_R, resonance absorption of energy occurs, resulting in a peak in spectrum. The frequencies commonly employed in ESR experiments are in the microwave region.

The nuclear spin also interacts with the electron spin and with the external magnetic field as well. For an ion with a nonzero nuclear moment I, $2I+1$ lines can be expected. In the ESR spectra, the A_0 value is taken as the separation between the two central ESR lines, and g_0 value is calculated from the magnetic field halfway between those lines. The isotropic electron-spin-nuclear-spin hyperfine coupling constant A_0 can be qualitatively related to the amount of time the unpaired electron spins in an s-orbital on nucleus. The larger A_0 value, the greater the probability of finding the electron at the nucleus. If the free radicals in solution exhibit hyperfine coupling with several nuclei and these nuclei are chemically equivalent, the number of lines is given by $2nI+1$, where n is the number of equivalent nuclei having nuclear spin I. The selection rules for ESR spectroscopy are $\Delta m_s = \pm 1$ and $\Delta m_I = 0$.

Reproduced with permission of the copyright owner. Further reproduction prohibited without permission.

The theory of ESR spectroscopy shares much in common with that of nuclear magnetic resonance spectroscopy. However, the magnetic moment of an electron is about 1000 times as large as the nuclear moment and the constants employed in NMR theory are frequently different in magnitude and sign.

ESR spectroscopy is also concerned with a particular electronic state, the ground state. Other electronic states of a system are important only insofar as they become "mixed in" the electronic state being studied *via* perturbations or structural dynamics of the ground state.

As in most other types of spectroscopy, the instrumentation employed in ESR spectroscopy consists of a source of electromagnetic radiation, a magnetic field provided by an electromagnet, a sample holder and appropriate detection equipment for monitoring the amount of radiation absorbed by the sample. Monochromatic radiation of various frequencies employed in ESR is obtained from a klystron, which is an electronic oscillator producing microwave energy. Spectrometers operating at X-band (3 cm wavelength) are the one most commonly employed. The microwave radiation is transmitted along hollow rectangular metal pipes called waveguides because it can not be directed by the usual optical devices. The sample is placed at the center of the sample cavity where the magnetic vector is at a maximum. Pyrex tubes in 3 mm i.d. are generally employed to contain solution and frozen samples. Usually a sweep generator with constant frequency provides modulation of DC magnetic field at the sample position. This magnetic field is slowly and linearly increased by varying the current in a pair of sweep coils until the resonance condition is satisfied, where the power is absorbed by the

Reproduced with permission of the copyright owner. Further reproduction prohibited without permission.

sample and a change in the crystal detector is monitored. At resonance the absorption of energy causes the spins of electrons to flip from the lower energy level to the higher level. The signal detected by the phase-sensitive detection system is proportional to the slope of ESR absorption as the magnetic field passes through resonance. The recorder system then presents the first-derivative spectrum against magnetic field. It is also important to monitor the microwave frequency at which the spectrometer operates and the magnetic field sweeps during the experiment. Since its discovery by Zavoisky in 1944, ESR has become an essential tool for the study of the structure and dynamics of molecular systems containing one or more unpaired electrons.

4.1.2 The Application of ESR in Freezing System

With ESR spectroscopy, the phase state and mobility in frozen solutions are usually investigated using stable radicals as a paramagnetic probe. ESR technique can yield valuable data about the phase state and structure of frozen solution and has a high sensitivity[14]. The use of stable radicals for the study of molecular mobility is based on the relation that exists between the line width of ESR spectra and the rotational and transitional mobility of these radicals. It is known from ESR theory that the anisotropic hyperfine electron-nuclear and spin-orbital interactions in a radical depend on the relative orientation of the external magnetic field and the orbital of the unpaired electron. The rotation of the radical modulates these interactions, thereby bringing about fluctuations in the local magnetic fields and broadening ESR spectroscopic lines. This broadening in turn depends on the characteristics of the unpaired electron orbital and is determined by

Reproduced with permission of the copyright owner. Further reproduction prohibited without permission.

the correlation time, τ_{cor}, which characterizes the intensity of the rotational motion of the radical. The magnitude of correlation time corresponds to the time required for the radical to change its orientation by an angle of one radian.

At $\tau_{cor} \leq 10^{-11}$ sec, the rotation of the radical averages the anisotropic interaction and the ESR spectrum consists of three lines of equal intensity when spin label TEMPO (2,2,6,6-tetramethyl-1-piperidinyloxy radical) is used. In the interval $5\times10^{-11} < \tau_{cor} < 10^{-9}$ sec, the width and, as a consequence, the intensity of the spectral lines change, which is the interesting range for our DMSO-electrolyte system. The increase in τ_{cor} from 10^{-9} to 1×10^{-7} sec leads to a change not only in the width, but also in the position and shape of the spectral lines. No further changes are observed in the spectrum at longer correlation times because the rotation of the radical fails to average the anisotropic intermolecular interactions completely[14].

The correlation times can be conveniently calculated by the theory developed by Stone[36], Freed[37] and Goldman[38] *et al.* when the motion is slow and/or anisotropic[39]:

$$\tau_{cor} = 5.47\times10^{-10}\,\Delta H_0\left(\sqrt{\frac{h_0}{h_{-1}}} + \sqrt{\frac{h_0}{h_{+1}}} - 2\right) \qquad (4\text{-}8)$$

where h_{+1}, h_0 and h_{-1} are the peak heights of three peaks (h_0 for central peak) in arbitrary units, ΔH_0 is the peak-to-peak separation of the center peak in Gauss and the correlation time is in the unit of second. This equation does not hold in the region of slow motion and is valid for correlation times shorter than approximately 5×10^{-9} sec.

Reproduced with permission of the copyright owner. Further reproduction prohibited without permission.

4.1.3 The Nitroxide Spin Labels and Their Applications in ESR

Spin labeling is a spectroscopic technique which employs stable organic free radicals (spin labels) as structure probes or reporter groups to investigate systems of biological and chemical importance[40]. The organic free radicals normally employed in spin labelling experiments are "protected" nitroxide free radicals, *i.e.* nitroxide radicals bearing no α-hydrogens[41]. Since such systems are essentially paramagnetic, an ESR sensitive probe possesses a distinct physical property that is readily detectable and, furthermore, sensitive to its environment. In other words, ESR spectral appearance is critically dependent on the mobility of spin label[42-43]. These labels can be obtained in pure form and they are stable to storage and compatible with a variety of reagents.

When the nitroxide radical is present with low concentration in a nonviscous solvent its ESR spectrum consists of three equally spaced lines of about the same height. These are characterized by parameters such as the position of center line (g-factor) and the peak-to-peak line width[35]. The spectrum is sensitive to changes in the molecular motion of the label, the polarity of the label environment and the orientation of the label with respect to the applied magnetic field. The most interested point to us is that ESR spectrum can provide useful information regarding the mobility of a nitroxide spin label. An increase in solvent viscosity causes broadening of the ESR lines with concomitant loss of spectral symmetry. The limiting in the shape of spectrum usually results when the molecular motion of the label is absent or very slow on the ESR time scale[14].

Reproduced with permission of the copyright owner. Further reproduction prohibited without permission.

4.2 The ESR Experiments

ESR experiments were performed in DMSO solution with 0.4 mM spin label TEMPO and 0.10 M TBAP. The TEMPO (Aldrich) and TBAP (Sterm) were used as received. DMSO (Burdick and Jackson) was dried over 3Å molecular sieves, and water analyzed by the Karl Fisher method established that the water content of DMSO was less than 0.03%. The temperature was controlled by a liquid nitrogen cooling system to ±2°C. For each measurement, the designated temperature was set for 5 min after the temperature was reached in order to thermally balance the system. Experiments began in 20°C, then temperature was lowered and the ESR spectra were measured at 10°C, 5°C *etc.* until as low as -100°C.

4.3 The Discussion of ESR Results

The ESR spectra of TEMPO with TBAP in DMSO at various temperatures are shown in Fig. 4-1. Within the temperature range from 20°C down to -20°C, the ESR spectra of liquid (20°C) and frozen solutions (0°C, -10°C and -20°C) are triplets. Qualitatively, the spectra in frozen solution show narrow lines similar in appearance to the spectrum in liquid solution at 20°C. The frozen solution could be verified by visual inspection and by the fact that large dielectric changes upon freezing were noted in turning the ESR spectrometer. The spectra confirm the existence of a liquid environment for the solute at temperature down to 40 degree below the freezing point, similar as the temperature range in which the unusual electrochemical results with both conventional electrode and microelectrode were observed.

Reproduced with permission of the copyright owner. Further reproduction prohibited without permission.

The rotational correlation time τ_{cor} for TEMPO can be calculated by equation (4-8). Table 4-1 lists τ_{cor} calculated for various temperatures from 20°C down to -40°C. The τ_{cor} values indicate that TEMPO radical in frozen solution at temperature down to -20°C, where reproducible electrochemical results were still observed, possesses the mobility comparable with them in liquid phase. Even at -30°C, τ_{cor} is still smaller than 10^{-9} sec.

The results obtained thus show that frozen solutions are inhomogeneous as regards structure and phase setup. They are complex two-phase systems consisting of a solid matrix and a liquid microphase whose molecular mobility is completely frozen only at the freezing point of entire system. In the case of eutectic environment, practically nearly all solutes are concentrated in the liquid microphase, and the matrix is the solid solvent.

The rotational correlation time is also related to the viscosity (η) of the system by[44]

$$\eta = \frac{\tau_{cor}\, k_B\, T}{V} \qquad (4-9)$$

where k_B is Boltzmann's constant, T is absolute temperature and V is the hydrodynamic volume of the TEMPO molecule. Since k_B and V are constants, the viscosity is proportional to the product of the correlation time and the related absolute temperature. A plot of the relative viscosities in logarithmic scale *vs.* T^{-1} is shown in Fig. 4-2. This plot indicates that the viscosity of liquid microphase follows Arrhenius behavior. These ESR experimental results of DMSO-TBAP system clearly show the existence of a liquid microphase and give a strong support to the explanation with electrochemical method.

Reproduced with permission of the copyright owner. Further reproduction prohibited without permission.

Chapter 5 The Theoretical Model of the DMSO-Electrolyte Freezing Systems and the Application in Cryopreservation

5.1 The Physical Significance of the Electrochemical Model in DMSO-Electrolyte System below the Freezing Point

In the electrochemical and ESR experiments, the unusual characteristics of DMSO-electrolyte system below the freezing point has been described. The cyclic voltammograms of various electroactive species in this system could be obtained at temperature down to 40 degree below the freezing point, and the system appeared to be diffusion controlled in frozen solution. The particularly interesting aspects of these results below the freezing point are the increase in the peak current with lowering of temperature and/or with decrease in electrolyte concentration. As the temperature was lowered further, an extreme was reached then the peak current began to decrease. In the experiments with the microelectrode, it was found that the nature of mass transport changed from steady-state diffusion (sigmoidal shaped curves) at the temperature as low as 20 degree below the freezing point to a surface-confined process (peak shaped curves) at further lower temperatures. Meanwhile in this further low temperature range with microelectrode, a small increase in peak current, rather than a decrease expected if mass transport occurred solely by diffusion, was observed. The diffusion component was gradually replaced by a surface confined redox pathway consistent with electrolysis in a thin layer electrochemical configuration. Experimental results suggest that the change in mass transport mechanism is a function of the DMSO-electrolyte properties rather than

Reproduced with permission of the copyright owner. Further reproduction prohibited without permission.

the properties of electrode materials and electrochemical active species.

These unusual results could be understood on the basis of the formation of a liquid microphase constructed with an increasingly concentrated solution and a pure solid matrix[16-18]. ESR experiments have clearly shown there is a liquid phase existing even at the temperature about 40 degree below the freezing point. An NMR study of DMSO also concluded the unusual mobility of solvent occurred in the solid[45]. As a first approximation, the phase diagram of such a system is predicted from the cryoscopic constant of DMSO, and an overall increase in peak currents is predicted to be due to the concentration effect of the liquid microphase. The diffusion coefficient decreases as the temperature decreases in all temperature ranges. At temperatures higher than the freezing point of the DMSO-electrolyte system, the peak currents decrease as the temperature decreases. Once the DMSO-electrolyte system is frozen, the peak currents begin to increase because of the concentration effects in liquid microphase over the influence of diffusion coefficient decreasing. At the temperature about 20°C below the freezing point, a sigmoidal shape curve of experiments, with closing value of $E_{3/4}$-$E_{1/4}$ to the theoretical model, was still obtained. These data further support the diffusion control effect in the frozen DMSO-electrolyte system and the existence of a liquid microphase. Finally a decreasing trend of the peak current occurs since the temperature effect on the diffusion coefficient overtakes the concentration effect. The eutectic system is assumed to contact the electrode with sandwiching of the liquid microphase. This assumption is based on the experiments with the microelectrode, where the spherical diffusion is gradually changed to a surface confined process as the temperature decreases since there is not enough space

Reproduced with permission of the copyright owner. Further reproduction prohibited without permission.

for a complete spherical diffusion layer so that the diffusion layer is compressed. As the temperature is decreased further, the liquid microphase begins to disappear and solid matrix begins to contact the electrode surface and dominate the whole system. Within these temperatures, the electrochemical results are difficult to reproduce. The former model of electrochemistry for this system qualitatively describes the tendency, but the model can not make good fitting for the experimental results because it is based on the assumption that frozen phase has the same probability to contact the electrode as the liquid microphase does with one third power of the liquid microphase volume[17-18]. In the present electrochemical model, based on the extended experiments, it is assumed that there is a surface confined process on the electrode where the eutectic system contacts the electrode sandwiching a thin layer liquid microphase. The surface area of electrode which the thin layer contacts is roughly a constant until the liquid microphase begins to vanish at a further lower temperature.

5.2 The Model for Electrochemical Reaction in DMSO-Electrolyte System at Temperature below the Freezing Point

The expression of the peak current in cyclic voltammetry is described as[46]:

$$i_p = 0.4463 nFAC_o^* \left(\frac{nF}{RT}\right)^{1/2} (\nu D_o)^{1/2} \qquad (5\text{-}1)$$

where i_p is peak current, n is the number of electron transfer, F is Faraday constant, A is the surface area of working electrode, C_o^* is bulk concentration of electroactive species, R is gas constant, T is absolute temperature, υ is scan rate and D_o is diffusion

Reproduced with permission of the copyright owner. Further reproduction prohibited without permission.

coefficient. As the temperature is lowered and the liquid microphase forms in the eutectic environment, we assume that[14] any motion of a reactive species is independent of its history. This implies that a reactive species attains a state of thermal equilibrium with the surroundings immediately after each movement. Based on general electrochemical theory and the assumption of the eutectic state formed in the temperature below the freezing point, we have

$$i_p' = 0.4463 nFA' C_o^{*'} \left(\frac{nF}{RT}\right)^{1/2} (\nu D_o')^{1/2} \qquad (5\text{-}2)$$

The apostrophes on these representatives indicate the eutectic environment. If the peak current is normalized to the current of the first observed eutectic at temperature T_{ref}, the representation will be simplified. The normalized peak current then can be expressed as:

$$I = \frac{i_p'}{i_{p,ref}'} = \frac{A'}{A_{ref}'} \frac{C_o^{*'}}{C_{o,ref}^{*'}} \left(\frac{T_{ref}}{T}\right)^{1/2} \left(\frac{D_o'}{D_{o,ref}'}\right)^{1/2} \qquad (5\text{-}3)$$

According to Stokes Einstein equation:

$$D_o = \frac{k_b T}{6\pi\eta R} \qquad (5\text{-}4)$$

The ratio I in equation (5-3) can then be rearranged as:

$$I = \frac{A'}{A_{ref}'} \frac{C_o^{*'}}{C_{o,ref}^{*'}} \left(\frac{\eta_{ref}'}{\eta'}\right)^{1/2} \qquad (5\text{-}5)$$

In the liquid microphase, there are two situations which will affect the area of working electrode and the concentration of electroactive species besides the temperature effect. One is the surface area of working electrode in contact with the liquid microphase in

Reproduced with permission of the copyright owner. Further reproduction prohibited without permission.

eutectic system, which changes in different microphase environments. Another is the distribution of electroactive species and electrolytes between liquid microphase and really frozen solid matrix. With the experimental results of microelectrode, we can assume that the liquid microphase is in direct contact with the surface of working electrode, and the solid matrix is mainly in contact with the electrode surface *via* a sandwich of liquid microphase. Only when the temperature is low enough (about 40 degrees below the freezing point in this DMSO-electrolyte system) where the reduced volume of liquid microphase is not enough to cover the electrode or make a sandwich between the electrode and the solid matrix, then cyclic voltammetry appears abnormal and the reproducibility of measurement is difficult. The area effect of the electrode surface in the eutectic situation can be summarized as an area coefficient $\phi(T,C'_{elec})$ multiplied the electrode surface area A'_{ref} observed at the temperature initial eutectic noticed. This area coefficient is a function of the support electrolyte concentration (because it is much more concentrated than that of electroactive species) in the liquid microphase and the corresponding temperature. The ratio of A'/A'_{ref} then can be simplified as:

$$\frac{A'}{A'_{ref}} = \frac{\varphi(T, C'_{elec}) \cdot A'_{ref}}{A'_{ref}} = \varphi(T, C'_{elec}) \qquad (5\text{-}6)$$

At the temperature just below the freezing point, the eutectic system forms with the components of liquid microphase and solid matrix. Based on the experimental results with the microelectrode, the surface of electrode is in contact with the liquid microphase and a typical sigmoidal curve of cyclic voltammetry is observed. As the temperature is further lowered, *e.g.*, within the temperature range 0°C to -20°C in this DMSO-

Reproduced with permission of the copyright owner. Further reproduction prohibited without permission.

electrolyte system, electrochemical experiments with the microelectrode indicate the surface confined process on the working electrode. The volume of liquid microphase certainly decreases so that the system can not maintain a spherical diffusion process on the microelectrode. But even in this temperature range, the majority of the surface area is still in contact with the liquid microphase. In both circumstances with spherical and surface confined diffusion processes on microelectrode, we have reason to believe that the area coefficient $\phi(T,C'_{elec})$ will not change dramatically and is roughly a constant. Only in the circumstances that the liquid microphase is going to vanish, the area coefficient then begins apparently to decrease.

For the liquid in microphase, there must exist a temperature range where the viscosity rises steeply with a decrease in temperature. The Fulcher equation[47] describes the relationship of system viscosity and temperature:

$$\eta = A \exp\left(\frac{B}{T - T_o}\right) \qquad (5-7)$$

where A, B are the constants related to the material system. T_0 is the temperature in which the solution is completely frozen so that there is no liquid microphase anymore at or below this temperature. The concentration of electrolyte in liquid microphase below the freezing point, mainly the concentration of TBAP in liquid DMSO, can be estimated by the cryoscopic constant and the temperature difference between the freezing point of DMSO and the one experiments taken. The relationship is described as:

Reproduced with permission of the copyright owner. Further reproduction prohibited without permission.

$$C^{*\prime}_{elec} = \frac{T_f - T}{k_f} \qquad (5\text{-}8)$$

where k_f is the cryoscopic constant. The k_f depends solely on the physical properties of solvent and is given by

$$k_f = \frac{R(T_f)^2}{1000\ \Delta H_f} \qquad (5\text{-}9)$$

where ΔH_f is the latent heat of fusion. Equation (5-8) describes that the freezing point depression of a solution containing 1 mol of solute in 1000 grams of solvent is k_f degrees and it is independent of the solute nature. The cryoscopic constant of DMSO is 3.96°C/M (or 4.36°C/m)[15]. Since the derivation of equation (5-9) is based on a number of simplifying assumptions, it is expected to be useful only in dilute solution. A better approximation is provided by the use of mole fraction units of concentration and a much more complicated expression[47]. In general electrochemical experiment, *e.g.*, the cyclic voltammetry, the concentration of electrolyte is in great excess over electroactive species. These strong electrolytes normally dissociate in solvent. For example hydrogen chloride is in a full dissociated state in methanol-H_2O mixtures containing up to 70% (by weight) of methanol to the temperature as low as their complete freezing point[48]. Sodium chloride at a concentration of 1×10^{-2} M is fully dissociated down to -80°C in a solution containing 44% (by weight) of methanol, whereas at concentration of 0.1 M this is so down to -50°C[49]. Sodium and potassium iodides dissolve more readily in mixed solvents than sodium chloride does, and they can be utilized to secure the desired ionic strength over a broad temperature range[14]. Based on these experimental results, TBAP can be

Reproduced with permission of the copyright owner. Further reproduction prohibited without permission.

considered to be in a dissociated state in the liquid microphase. It is also assumed that most of the electrolyte and electroactive species are concentrated in liquid microphase or have the similar distribution between the liquid microphase and the solid matrix:

$$\frac{C_o^{*\prime}}{C_{o,ref}^{*\prime}} \approx \frac{C_{elec}^{*\prime}}{C_{elec,ref}^{*\prime}} \qquad (5\text{-}10)$$

Combining equations (5-5) through (5-10), we have

$$I = \varphi\,(T, C'_{elec})\,\frac{T_f - T}{k_f\, C_{elec,ref}^{*\prime}}\exp\left[B'\left(\frac{1}{T_{ref} - T_o} - \frac{1}{T - T_o}\right)\right] \qquad (5\text{-}11)$$

where B' represents $(1/2)B$. Since we know that the area coefficient $\phi(T, C'_{elec})$ will not change dramatically at the temperature range where the liquid microphase is not extremely reduced, the temperature effect only changes the thickness of the liquid microphase between the solid matrix and the electrode, we can approximate the area coefficient as constant. Because we observed the peak current did not change dramatically as the eutectic system formed initially (Figs. 3-3, 3-5 and 3-7), we have reason to believe the concentration of electroactive species and electrolyte did not change dramatically. Then we can approximately use the concentration of the electrolyte before frozen as the concentration of electrolyte in the initial eutectic system. Based on these assumptions, the plot of the normalized peak current *vs.* temperature for both theoretical and experimental data are shown in Figs. 5-1 and 5-2. The curves of the theoretical model have good fitting with the experimental data in both systems. In these experiments, ferrocene was dissolved in DMSO with 0.10 M and 0.20 M TBAP. The experimental conditions were described previously. The different values of constant B' used in Fig. 5-1 and Fig. 5-2

Reproduced with permission of the copyright owner. Further reproduction prohibited without permission.

may be due to the different structures of liquid microphase because of their electrolyte concentrations. The different values of $\phi(T,C'_{elec})$ may be due to the different distribution of the electrolyte and electroactive species between liquid microphase and solid matrix, and due to the different volume of liquid microspace on the surface of the electrode. Fig. 5-3 shows the experimental and predicted salt effects on the peak current for TBAP concentrations of 0.25 M to 0.01 M at 0°C. The model described here predicts the current behavior very well at a constant temperature in the TBAP concentration range of 0.10 M to 0.25 M. Below the TBAP concentration of 0.10 M, system resistance is very high which causes the electrochemical measurement to show poor reproducibility and large error. The corresponding normalized peak currents then deviate from the theoretical model. The reason for the deviation may be also due to that coefficient $\phi(T,C'_{elec})$ and parameter B' may not be kept in constant for various low electrolyte concentrations and T_o may not be in a same value for different eutectic environments in the model.

5.3 The Application of the DMSO-Electrolyte System in Cryopreservation

The DMSO-electrolyte system can be applied in biological and medical fields. It can be a good cryoprotectant system to prevent solution effect injury at low temperature when cryopreserving blood plasma, marrow, human cell and tissues *etc.* Blood and marrow can now be cryopreserved for years and then used successfully for medical purposes[14]. The basic effect of DMSO is the reduction of water content in specimen to be preserved and the permeability to cell membrane. Solvents with different contents of

Reproduced with permission of the copyright owner. Further reproduction prohibited without permission.

DMSO mixed with water have been successfully used in cryopreservation. Several DMSO-H_2O-electrolyte systems used in cryopreservation were tested by electrochemical experiments in our laboratory. Their results show the similar electrochemical responses in frozen solution as the systems discussed above at the temperature below the freezing point. Figs. 5-4 (a) and (b) show the cyclic voltammograms of ferricyanide in DMSO-H_2O-NaCl system with liquid and frozen situations. Table 5-1 lists the peak potential differences at various temperatures and the states observed. There is no significant change in $\Delta P_{c,a}$ as the system state undergoes a phase change from liquid to solid. When temperature is lower than -50°C, $\Delta P_{a,c}$ increases very fast, which may be due to the resistance effect where liquid microphase begin to vanish. This change indicates that the system with this DMSO-H_2O-NaCl components, if used in cryopreservation, should not be too far below these temperatures. Similar situations were observed in peak current and formal reduction potential as the system state undergoing a phase change as observed in DMSO-electrolyte system. Fig. 5-5 shows a plot of peak current of ferricyanide *vs.* the square root of the scan rate in logarithmic scales at -40°C in frozen solution. The linearity of the corresponding peak currents with good dependency coefficient (0.962) and nearly unity of slope (0.92) for fitted straight line indicates a diffusion controlled precess in this DMSO-H_2O-NaCl frozen system. All these electrochemical results show us that the liquid microphase does exist in these DMSO mixtures, which may be the major reason that liquid effect injury to biological and medical samples is greatly reduced.

DMSO is of low toxicity. It is transported through human skin and incorporated

Reproduced with permission of the copyright owner. Further reproduction prohibited without permission.

into blood stream with incredible speed. Minutes after touching a drop of DMSO to the palm in the hand, its sweetish taste can be detected in the mouth[50]. DMSO appears to penetrate nearly all membranes, and, largely for this reason and liquid microphase as we indicated, has been established as the universal cryoprotectant. It is certainly important that enzymes should not be denatured in storage and their activity should change reversibly on cooling/rewarming. Some organic compounds can control the activity of enzymes at normal and reduced temperatures, and DMSO mixture system is one of them[14]. The penetration of DMSO can avoid large temperature gradients in cooling and rewarming processes. Research has shown that if enzyme activity is to be preserved at low temperature the dielectric constant of the medium should be close to its value in water under normal conditions so that the enzyme molecule will be in a conformation characteristic of its native state[51]. The various combinations of DMSO-H_2O-NaCl system control the dielectric constant, viscosity and ionic strength of solutions. On the other side, methods which have been developed for the preservation of single cells and small cell clusters have invariably proved unsuccessful when applied to mature organs. Patient methodological research has isolated some of the problems, but has not yet produced solutions. The geometry of organs and the different permeabilities associated with the various membrane systems set limits to the fluxes of cryoprotectant substances, thus leading to additional temperature gradients during cooling and rewarming, making it almost impossible to achieve uniform cooling rates throughout the organ. Another problem concerns the ratio of actual volume occupied by cells to extracellular space. This ratio is very high in organs, and there is evidence that the injury in slow freezing process

Reproduced with permission of the copyright owner. Further reproduction prohibited without permission.

may be related to increasingly higher fractions of the volume being occupied by cells[52]. The vascular system, the proper functioning of which is a prerequisite for successful preservation, is particularly susceptible to freezing damage. In cell suspensions the growth of extracellular ice is not usually a damaging factor, but it may be so in vascular tissue. The amount of such damage may be limited if it is possible to control the location, amount and morphology of extracellular ice in the tissue. Novel approaches include attempts to prevent, or at least reduce the injury as freezing with the aid of rapid cooling protocols in combination with high levels of cryoprotectant or hydrostatic pressure[53]. These are several useful systems in aqueous media, but these systems require high concentrations of additives, high pressures and high cooling rates. In order to minimize the toxic effects produced by some cryoadditives, experiments are in progress with cryoprotectant mixtures. One of the outstanding successes in preservation technology to date is the development of freeze-thaw protocols for mammalian embryos. Survival rates of up to 80% have been reported and have led to the applications of embryo storage as a viable technique in mammalian genetics and in animal breeding programs[54]. The basic principles of these development do not differ from those described for single cells with DMSO. Electrochemical experiments clearly describe these system behaviors at low temperatures. Using electrochemistry methods, we may optimize the system components and avoid carrying out the time-wasting biological and medical experiments. The theoretical model, which based on the electrochemical and ESR results below the freezing point, can be used as a guide to simplify the procedure in optimization. This model offers a tool to qualitatively explain the kinetics of the electrochemical reactions in frozen

Reproduced with permission of the copyright owner. Further reproduction prohibited without permission.

solutions and also to predict other factors. Since the solute is concentrated in eutectic system, some chemical reactions especially some reactions with unstable intermediates can be accelerated. The principle of these DMSO mixture systems in biological and medical fields at low temperature also may be applied in other fields. There are some unresolved questions including the questions of the unusually high conductivity of the DMSO-electrolyte system at temperatures well below the freezing point as well as the nature of the results at lower electrolyte concentration. At the lowest electrolyte concentration and at the lowest temperature, reproducible results are more difficult to be obtained. The mechanisms of various chemical reactions in similar systems are among the most challenging problems of chemical kinetics. It is challenging from both theoretical and practical stand-points, and its knowledge can go a long way towards enhancing the efficiency of chemical synthesis[14]. Studies on the behavior of biochemical systems at low temperatures will provide better insight for their functioning. Work in this direction will help to solve problems of long-term cryopreservation of biological material in the future.

Reproduced with permission of the copyright owner. Further reproduction prohibited without permission.

Part 3 The Electrochemical Study of Vitamin B_{12} - The Electron Transfer and the Ligand Effects in the B_{12} Electrochemical Process

Chapter 6 Introduction: The Development of Vitamin B_{12} Research

6.1 The Development of Vitamin B_{12} in Research and Application

Vitamin B_{12}, the antipernicious-anemia factor, is a group of organometallic compounds which are among the most complex of the naturally occurring compound[1]. Vitamin B_{12} is unique and it differs from other vitamins even those of the *B*-complex in many ways. It has a chemical structure much more complex than that of any other vitamins. It is the only vitamin to contain an inorganic element as an integral part of its makeup. Microorganisms or bacteria can synthesize vitamin B_{12}, but plants and animals can not[2].

6.1.1 The History of Vitamin B_{12}

The early history of vitamin B_{12} belongs entirely to medicine. The disease, now known as pernicious anemia, was first described in 1821[3]. The next hundred years a slow but steady increase in human knowledge of the signs for the disease and the methods for the diagnosis went on but with a total absence of an advance in the treatment of the disease, which remained incurable and was usually fatal. Then in 1920, Whipple in California showed that the regeneration of red blood cells in dogs, which made anemia by bleeding, was stimulated by a diet containing liver, and in 1926 Minot and Murphy

Reproduced with permission of the copyright owner. Further reproduction prohibited without permission.

in Boston reported a remarkable improvement in patients fed a diet almost a pound of raw liver per day. Investigators did not know why but speculated that liver must contain some substance that prevents or cures the disorder. The clue started the search for the "liver factor" or "anti-pernicious anemia factor", which lasted more than twenty years. Whipple, Minot and Murphy were awarded the Nobel Prize in Physiology and Medicine in 1934[3]. The research was time-consuming since experimental animals were not suitable for the test required. Instead, testing had to be performed over long periods of time on human subjects. For these experiments, scientist prepared extracts of liver and separated them into different fractions. Then, each fraction was given to someone with pernicious anemia, and the researchers had to wait for a change to see which fraction, if any, contained the effective factor. Progress was slow until 1948, when an "experimental animal" was found that could be used for testing - the microorganism Lactobacillus Lactus Dorner (*LLD*)[2]. Instead of testing liver extracts on people, researchers tested them on *LLD*. Since *LLD* reproduces so quickly, many generations could be tested in a short period of time. In less than one year still in 1948, the isolation of crystalline vitamin B_{12} (cyanocobalamin) was reported independently by two teams. The race to isolate the factor was very close, first by Folkers and his colleagues at Merck Laboratories[4] and then by Smith and Parker at Glaxo Laboratories in England[5-6], and in the following year by Ellis, Petrow and Snook at British Drug Houses[7]. As a matter of fact, they extracted about 20 mg of the vitamin B_{12} from a ton of liver. It turned out that vitamin B_{12} was the antipernicious anemia factor. The year of 1948 can be considered as the date which marked the beginning of the study of vitamin B_{12} chemistry. From the chemists' point

Reproduced with permission of the copyright owner. Further reproduction prohibited without permission.

of view, the most interesting developments in this area would be the elucidation of the exact role played by vitamin B_{12} in metabolism in man and other animals. It soon became clear that B_{12} was the only one of the family of closely-related compounds called corrinoids occurring in nature[3]. Following the discovery and development, the isolation of coenzyme, 5'-deoxyadenosylcobalamin, another member of B_{12} family, was completed by Barker and his associates in California in 1958[8].

The task of elucidating the vitamin B_{12} structure was taken up by both X-ray crystallographers and organic chemists. The two approaches were complementary. The X-ray diffraction located the atoms near the cobalt atom in the center, while the classical degradative techniques used by organic chemists provided evidence for the periphery structure of the molecule. The structure of the corrin ring was announced by X-ray crystallographers in 1954[9] and the complete structures of several corrinoids in the next few years. X-ray analysis by Hodgkin *et al.* at Oxford played an important role in the development of vitamin B_{12} chemistry. Their work revealed the presence of two structures unknown in nature[10], namely the corrin ring which is present in all corrinoids and the cobalt-carbon bond which is present in the coenzyme form of B_{12} and its derivatives. Therefore they found the first naturally occurring organo-metallic compound and their work in applying X-ray diffraction techniques was rewarded with Nobel Prize for chemistry in 1964[3]. Hodgkin's discovery led to an immediate outburst of activity among organic chemists in synthesizing both the coenzyme itself and a wide range of other organo-corrinoids. This provided co-ordination chemists with a wealth of different organo-ligands, whose properties and reactions could be investigated. It also became

Reproduced with permission of the copyright owner. Further reproduction prohibited without permission.

clear that corrinoids which contained an organo-ligand showed properties in spectra, formation constants and photochemical reactions very different from those of corrinoids containing the ligands more commonly studied such as H_2O, CN^- *etc.*[3] Contributions to the co-ordination chemistry of corrinoids have come from many laboratories throughout the world, and much of the work has been done by organic chemists who have been interested primarily in the organometallic aspects. The very beginning research in organic chemistry of B_{12} was the determination of the structure, chiefly by classical degradative methods after the isolation of B_{12} in 1948. Most of this work was carried out in the pharmaceutical companies by teams led by Folkers at Merck, Smith at Glaxo, England, Petrow at British Drug Houses and by Todd with his colleagues at Cambridge[3,11-13]. Their research came to an end shortly after the structure of B_{12} was finally established by X-ray analysis. The isolation of the coenzyme in 1958 again led to work on structural elucidation, which lasted until X-ray analysis in 1961 showed the coenzyme to be an organometallic complex with a cobalt-carbon bond. This in turn led to a great deal of work on the synthesis of organocorrinoids and on the properties and reactions of these compounds. Based on the B_{12} research results in the early 1960's, organic chemists began to focus on the synthesis of the corrinoid structure with the correct substituents and stereochemistry found in the naturally occurring compounds[3].

6.1.2 The Function of Vitamin B_{12} to Human Being

Vitamin B_{12}, like other vitamins, is required by human being and other animals in small amounts to perform some catalytic roles. It is the only vitamin which contains

Reproduced with permission of the copyright owner. Further reproduction prohibited without permission.

a metal and has the most complex structure in the vitamin family. It is also apparently the only one which requires a special mechanism for absorption into the body from the gut. Vitamin B_{12} can not be absorbed from the intestinal tract without the help of a substance made in stomach - the intrinsic factor. The intrinsic factor combines with the vitamin B_{12} released from food during digestion and carries the vitamin to the lower part of the small intestine, where it attaches itself to special receptor cells. The vitamin B_{12} is then released from its carrier and enters these cells where it is absorbed into the body. Without the intrinsic factor, vitamin B_{12} will miss its connection with the receptor cells and will pass out of the body. Some people have a condition known as pernicious anemia and can not make the intrinsic factor. They can not absorb vitamin B_{12} even if there is plenty of the vitamin B_{12} in their diets. Eventually, they show symptoms of a vitamin B_{12} deficiency. Vitamin B_{12} is essential to cells because it is needed for the synthesis of DNA (deoxyribonucleic acid) and RNA (ribonucleic acid). It also helps human being to maintain normal bone marrow and functions in the production of a material called myelin, which covers and protects nerve fibers[2].

The reported B_{12} requirement for human being is amazing low, about 1 μg per day or less than 1 mg per year[3]. The Recommended Dietary Allowance (*RDA*) for vitamin B_{12} is 3 μg daily for adults and 4 μg for women who are pregnant or breast-feeding. It is estimated that the average diet eaten by Americans provides 7 to 30 μg of the vitamin - more than enough to meet the daily need[2]. Vitamin B_{12} is found largely in animal foods like liver, meat, clams, oysters, sardines and salmon. It is also added to some cereals. Bacteria in the intestine make some of the vitamin, but far less than the

Reproduced with permission of the copyright owner. Further reproduction prohibited without permission.

amount needed to be absorbed. Pernicious anemia is treated with an injection of 50 to 100 μg of vitamin B_{12} three times a week until symptoms subside. On the other hand, vitamin B_{12} can be stored in human liver that may last five years or longer. There are no reports of vitamin B_{12} causing any toxicity or adverse effects even then taken in large amounts. Taking the vitamin orally, however, will not help those people with undiagnosed pernicious anemia as they will not be able to absorb it.

The B_{12} in animal tissues is almost exclusively in the form of 5'-deoxyadenosyl-cobalamin and the overwhelming majority of natural occurring corrinoids contain the organo-ligand 5'-deoxyadenosyl, which in fact was the first naturally occurring organometallic complex to be discovered. Certain corrinoids containing a methyl ligand have been found both in animals and in microorganisms[14-15] and there is some evidence for the occurrence of a carboxymethyl B_{12}(Co-CH_2COOH)[3,16]. It was mentioned that all known organocorrinoids can be regarded as cobalt(III) complexes.

6.1.3 The Chemistry and Electrochemistry of Vitamin B_{12}

A considerable number of B_{12}-dependent reactions have been identified and studied in microorganisms. The reactions can be classified into two groups: (a) reactions which involve the transfer of a methyl group to give methionine (Met), acetic acid, *etc.*; and (b) reactions which involve a hydride transfer and which depend on the presence of a 5'-deoxyadenosylcorrinoid. In each case the catalyst is the complex formed from a corrinoid acting as the coenzyme together with the protein[3].

Various derivatives of vitamin B_{12} are the series of cobalamins having the

Reproduced with permission of the copyright owner. Further reproduction prohibited without permission.

structures shown in Fig. 6-1. The central cobalt atom is coordinatively bound to the four nitrogen atoms of the corrin ring, one of these bearing a negative charge[17]. Attached to a carbon of the corrin ring is a nucleotide side chain terminated by 5,6-dimethyl-benzimidazole group (*Bzm*), which may act as an axial ligand toward the cobalt atom. The side chain bears an additional negative charge on the phosphate group down to *pH* 1. Cobalamin complexes in which the *Bzm* is bound to the cobalt atom are usually called base-on forms, whereas if such a coordination is absent or replaced by an exogenous ligand the designation base-off is used. Cobinamides are named for the complexes in which the nucleotide side chain is cleaved at the phosphate group. The side chain then loses its potential liganding ability toward the cobalt atom. Complexes that still have the side chain but are not terminated by *Bzm*, which may be replaced by other imidazolic structures, are named cobamides. The side chains of the corrin ring do not appear to undergo any reactions of interest, but play a very important role in, for example, determining the solubility properties of the corrinoids and in the binding of other molecules such as proteins[3]. The various cobalamins, cobinamides and cobamides differ one from the other with the nature of the axial ligands in α (lower) and ß (upper) positions by H_2O, OH^-, CN^-, alkyl carbanions *etc.* giving the names respectively aquo-, hydroxo-, cyano- and alkylcobalamins.

The cobalt atom in corrinoids can exist in three formal oxidation states, Co(III), Co(II) and Co(I), which are usually named as B_{12a}, B_{12r} and B_{12s} and display quite different chemical properties. In general Co(III) appears as an electrophile, Co(II) as a radical and Co(I) as a nucleophile. Redox conversion among three oxidation states is thus

Reproduced with permission of the copyright owner. Further reproduction prohibited without permission.

of key importance in the chemistry of vitamin B_{12}. Being able to produce these conversions under controlled conditions, electrochemistry appears as a particularly valuable source of information for investigating the redox chemistry of vitamin B_{12} derivatives.

Early work for vitamin B_{12} in electrochemistry mostly used polarography and concerned mainly cyano- and aquocobalamins[18-20]. Hogenkamp and Holmes gave a survey of the polarographic characteristics of a broad series of cobalamins and cobinamides[20]. Later cyclic voltammetry (*CV*) was used to describe the electrochemical behavior of various B_{12} derivatives[21-23]. Controlled potential electrolysis and coulometry were applied to prepare and characterize the reduced states of cyano- and aquocobalamin[24-28]. The contribution by Lexa and Saveant on the electrochemistry was an attempt to unravel the complexities deriving from the interplay between electron transfer and changes in axial ligandation in the electrochemical reactions of the major vitamin B_{12} derivatives. Besides thermodynamic characterizations, the kinetics of the electrochemical reactions was investigated systematically with the aim of determining the reaction mechanisms and estimating the rate constants of the key steps[17,29-40]. This also helped to understand the exact meaning of the thermodynamic data. From a more chemical point of view, the redox patterns of most B_{12} derivatives are very well understood with the exception of alkylcobalamins[17].

As a redox reaction occurs in a molecule of the vitamin B_{12} complexes, for example, the formal oxidation state of the cobalt atom decreases and its coordination number tends to decrease accordingly. In the thermodynamically predominating forms,

Reproduced with permission of the copyright owner. Further reproduction prohibited without permission.

the coordination number is generally six (two axial ligands) for Co(III), five (one axial ligand) for Co(II) and four (no axial ligands) for Co(I). In B_{12} electrochemistry, electron transfer is therefore expected not to be a simple outer-sphere process. It is generally accompanied by the expulsion of one ligand when going to a lower oxidation state and by the formation of a coordination bond upon increasing the oxidation state. The electrochemistry of B_{12} derivatives under both thermodynamic and kinetic aspects is thus anticipated to depend heavily upon trans-ligandation factors. Since most of the above cited previous results was carried out with mercury working electrode, specific adsorption may then interfere with and influence the electrochemical characteristics. This has been shown to be the case in water with alkali-metal salts as supporting electrolyte[29,41-43]. The reductions of alkylcobalamins on mercury in the presence of ethanol may lead to the formation of the corresponding alkylmercury compounds[44]. Particular attention was devoted to minimizing reactant adsorption at the electrode surface for the purpose of obtaining data characterizing intrinsically the molecules under study. As we expected, to minimize adsorption, extend the range of the working window, find and obtain better reproducibility and longer working life time, the development of new working electrode is essential. Comparison between the responses obtained with different electrode materials has been made in a number of cases in order to check if the observed behaviors depend upon the nature of the electrodes or not.

6.2 The Electrochemistry of Alkylcobalamin

Alkylcobalamins are of particular interest since the two main series of B_{12}

Reproduced with permission of the copyright owner. Further reproduction prohibited without permission.

enzymes belong to this class of compounds. The 5'-deoxyadenosylcobalamin, the B_{12} coenzyme, catalyzes a series of rearrangement reactions involving the transfer of a hydrogen atom from one carbon atom to the adjacent carbon atom in exchange for another group that migrates in the opposite direction[17]. Methylcobalamin is involved in enzymatic catalysis of methyl-transfer reactions and yields methionine. The catalysis occurs with three compounds (methylcobalamin, CH_3-H_4folate and homocysteine (HCy)) shown in scheme 6-1. The enzyme-bound cobalamin cycles between Cob(I)alamin and methylcobalamin forms, alternately being methylated by CH_3-H_4folate and demethylated by homocysteine. Since cob(I)alamin does react with alkyl halides through a S_N2 mechanism, H_4folate would be a reasonable leaving group of CH_3-H_4folate because cob(I)alamin will function as a nucleophile. Occasional interception of the reactive cob(I)alamin by electron acceptors results in oxidation to form enzyme-bound cob(II)alamin, which is inactive in catalysis. To return the inactive enzyme to the catalytic cycle requires a reductive methylation with adenosylmethionine (AdoMet) serving as the methyl donor[45-47]. Methylcobalamin is also involved in acetate biosynthesis starting form carbon dioxide. These reactions of the B_{12} derivatives are of particular interest in view of their roles in biological reactions occurring under reducing conditions. In spite of intensive research efforts in many laboratories, the detailed mechanisms of action of B_{12}-dependent enzymes in biology are still the subject of lively controversy. However, it is generally believed that the enzymatic reactions involve a mechanism in which the Co-C bond is regenerated after completion of the catalytic cycle. Investigating electrochemical parameters for the series of alkylcobalamins will help us

Reproduced with permission of the copyright owner. Further reproduction prohibited without permission.

to understand the details of B_{12} electrochemistry. Upon reduction process, the C-Co bond of alkylcobalamins is broken. Methane has been detected as one of the reduction products of controlled potential electrolysis, and more careful experiments indicate the quantitative formation of ethane in water on a mercury electrode[17,48]. The reduction on the electrodes of mercury, glassy carbon, platinum and gold involves the consumption of one electron per molecule. These observations have been described by Lexa and Saveant[17,49], which involving a cleavage of the C-Co bond and the formation of an alkyl radical and the Co(I) complex. The further reduction of the alkyl radical generated, in apparently rather slow rate, results in dimerization or the reaction with mercury.

The electrochemical reactions of the alkylcobalamins are completely different from those of cyanocobalamin, hydroxocobalamin and other cobalamins[17,30,47]. The formation of the Co(I) complex upon reduction of alkylcobalamins has been used for devising a catalytic cycle for the electrochemical reduction of alkyl halides[42,50]. The rate-determining step is then the nucleophilic attack of Co(I) on the alkyl halide. The catalytic system appears much more stable than that with the related cobalt tetraphenylprophyrin in which the degradation of the catalyst occurs after a few cycles.

In the methylcobalamin and methylcobinamide reduction processes, the intermediate complexes were formed upon attachment of one electron and were detected by using high sweep rate cyclic voltammetry on mercury electrode in 1:1 DMF to 1-propanol[49]. Its half-life of methylcobinamide varies from 0.1 to 4×10^{-4} sec in the temperature range between -20°C and 19°C. The standard potential is -1.45 volt *vs. SCE*. The one-electron intermediate formed upon reduction of methylcobalamin in the same

Reproduced with permission of the copyright owner. Further reproduction prohibited without permission.

medium appears as more unstable. It gives rise to the base-on one electron reduced intermediate that is reoxidized as in the case of methylcobinamide[49]. The standard potential, about -1.6 volt *vs. SEC*, appears as more negative than that with methylcobinamide as expected from the electron-donating character of *Bzm* being stronger than that of a solvent molecule. Similar results were obtained with DMSO at room temperature. It was shown, however, that the cleavage of the Co-C bonding is slower in DMSO than in DMF-propanol mixture at the same temperature. Lexa and Saveant emphasized that alkylcobalamins behave differently from other B_{12} compounds bearing strong axial ligands such as OH^- and CN^- and their reduction potentials are quite negative[17].

The goals of this research are the study of the redox chemistry of vitamin B_{12} species especially alkylcobalamins using electrochemical techniques in order to understand in detail the reductive cleavage mechanism where the carbon-cobalt bond is cleaved by an electron transfer reaction. It is necessary to precisely measure some important electrochemical parameters because electrochemical processes play an important role in the catalytic cycle of biochemistry. The accurate formal reduction potential provides a measurement of the driving force for redox reaction and it is related to the charge donated into the corrin ring. Therefore precise measurement of $E^{o'}$ and other parameters can be applied to better explain the mechanism. The measurement of the transfer coefficient α may further elucidate the suggested mechanism of the electrochemical process. Experiments to investigate the solvent effect and temperature dependence of the following chemical reaction are necessary for a better explanation of

Reproduced with permission of the copyright owner. Further reproduction prohibited without permission.

the mechanism. It is expected to get the information on how substituent group structure affects the reduction potentials of alkylcobalamin species, the electron transfer coefficients (α), the rate constants of electron transfer (k^o) and for Co-C bond fission rate constant (k_{chem}). It is also expected to further understand the vitamin B_{12} involvement in biochemical processes through this electrochemical study. The method developed here can certainly be applied to other similar *EC* mechanisms.

Reproduced with permission of the copyright owner. Further reproduction prohibited without permission.

Chapter 7 Simulation and Simplex Curve Fitting Analysis of *EC* Mechanism of Methylcobalamin

7.1 Introduction

Methylcobalamin is an important member in B_{12} family and is involved in the methyl group transfer reaction as a coenzyme[20]. In general, the involvement of vitamin B_{12} compounds in a variety of metabolic and neurological diseases is a major reason for the through understanding of their chemistry and biochemistry, particularly of their redox chemistry. The nature of the cobalt-carbon bond is a fundamental concern, both from the point of view of basic chemistry and as an aid in understanding the function of the coenzyme in protein substrates. The electrochemistry of vitamin B_{12} species has been reviewed by Lexa and Saveant[17]. Since it is a cobalt coordination compound where the cobalt ion can have three different formal oxidation states, redox chemistry is expected to play an important role in their enzymatic reactions.

The reduction of methylcobalamin is typical of many electrochemical reactions in that the electron transfer is followed by a fast and irreversible chemical reaction. In such systems the determination of the formal reduction potential $E^{o'}$ by cyclic voltammetry is problematical. No reverse wave is obtained at slow scan rates. At fast scan rate[32], data are distorted by *iR* drop, which is the error in potential control due to the uncompensated solution resistance and capacitive current that prevents a precise analysis of the *CV* wave shape. Also for the case of slow electron transfer, the range of scan rate will be limited. This chapter presents a detailed cyclic voltammetric study in

Reproduced with permission of the copyright owner. Further reproduction prohibited without permission.

the slow scan rate regime. Analysis by *CV* simulation and simplex curve fitting, combined with double potential step chronoamperometry (*DPSC*), allows the study for the combination of sluggish charge transfer and fast following chemical reaction for this mechanism in apparently irreversible cyclic voltammograms. It has been shown that the thermodynamic and kinetic parameters of *EC* mechanism (electrode reaction - chemical reaction) can be determined by careful data analysis. The analysis method applied here is an example using the electrochemical *EC* mechanism for the study of unstable radical ions. The frequent occurrence of the *EC* mechanism in organometallic reactions and their possible relevance to biochemical mechanisms show the importance of having accurate methodologies for this mechanism.

The mechanism of the reductive electrochemistry of methylcobalamin was suggested by Lexa and Saveant using rapid sweep *CV* in 50%:50% ratio of DMF and 1-propanol[32]. They were able to show the existence of a one electron adduct and estimated the rate constant for the following chemical reaction k_{chem} as 1200 sec^{-1} at -30°C and the formal reduction potential to be $E^{o'}$ = -1.6 volt. Spectroelectrochemical experiments have confirmed that the product formed by exhaustive reduction is [Co(I)]cobalamin[30,48,51], the vitamin B_{12s}. The electrode process has been shown to be one electron overall because of the results of controlled potential coulometry. Gas chromatography - mass spectroscopy experiments have indicated that ethane is greater than 97% of the cleavage product of the methylcobalamin reduction[48]. Based on these results, the mechanism in scheme 7-1 was put forward. Such *EC* mechanism was further studied through a combination of *CV* and potential step experiments by Kim and

Reproduced with permission of the copyright owner. Further reproduction prohibited without permission.

Birke[52]. It is apparent that this mechanism might actually be understood as a sequence of steps more complicated than that shown in scheme 7-1. For instance, the timing of the base-on to the base-off transition is not resolved. However, experiments indicated that nearly all of the methylcobalamin exist in used media (solvent mixtures of DMF and methanol) are in the form of base-on, by comparing the formal reduction potential of methylcobalamin and methylcobinamide in which the later loses its potential liganding ability toward the cobalt atom[32].

While the effective electrochemical techniques, mainly *CV* and *DPSC*, are applied to study *EC* mechanism, the information obtained is usually restricted to one or two electrochemical parameters. Part of the reason for this limitation is the fact that only a small part of the experimental data is utilized. Due to the fast development of digital computers, it is now possible to analyze more complicated data sets and to extract useful information from them. The goal in pursuing this work was to fully characterize this *EC* mechanism by *CV* simulation and simplex curve fitting with program *CVFIT* [53]. A complete characterization of the *EC* mechanism requires the determination of $E^{o'}$, k^o, α and k_{chem}, where $E^{o'}$, k^o and α are the kinetic parameters of the Butler-Volmer equation and k_{chem} influences the concentration of the reduced products in the same equation[54] so that k_{chem} could shift the potential of the peak current in cyclic voltammograms.

Usually the exact differential equations, which describe the transformations and movements of material according to the situations and the general rules of electrochemistry, can be written but usually they are solved in closed forms with difficulty or not at all. Recently such problems have been attacked by variants of the

Reproduced with permission of the copyright owner. Further reproduction prohibited without permission.

method of finite differences[54-55]. In one approach, a numerical model of the electrochemical system is set up with a digital computer, and the model is allowed to evolve simulation by a set of algebraic laws derived from the differential equations defining material flow. In effect, one carries out a digital simulation of the experimental data to extract the numerical representations of current functions, concentration profiles and other useful electrochemical parameters. In order to get optimum parameters in the simulation, the simulation and curve fitting procedures are combined, because the variables do interact with each other and each variable can not be optimized independently of the others. In general, one-factor-at-a-time approach will not always result in an optimum set of conditions. The modified simplex method developed by Nelder and Mead was used to fit the model, which can especially accelerate the progress of the simplex and reduce the chance of failure on the ridge[56]. With this method, it fits the experimental data to a known mathematical model, variables in the theoretical model are adjusted until the calculated values are closely in agreement with the experimental results.

In order to characterize the electrochemical properties of a system by simulation and curve fitting analysis, a working electrode that gives facile charge transfer is essential. Methylcobalamin usually shows adsorption on common electrode materials. When a mercury electrode was used in DMF with ethanol or 1-propanol solvent mixture, some interfacial adsorption was noticeable even though the results were better than that obtained with a gold or vitreous carbon disk electrode[32]. Reduction of alkylcobalamins on mercury in the presence of ethanol leads to the formation of the corresponding

Reproduced with permission of the copyright owner. Further reproduction prohibited without permission.

alkylmercury compounds[44], so that the electrode responses of methylcobalamin were examined at a number of electrodes in order to find a system which would be amenable to a rigorous simulation analysis. Platinum and silver electrodes had poor characteristics. Glassy carbon was better, but the performance deteriorated quickly with time. A silver amalgam electrode was found to have the best electrode response. It is very stable and its surface does not need to be repolished during the experimental period. Cyclic voltammetry indicates the diffusion control in the electrode kinetic process and *CV* simulation and fitting shows no adsorption on the surface. This electrode is suitable for the present experiments with methylcobalamin and other alkylcobalamins utilizing a low temperature cell where frequent electrode treatment is inconvenient[57].

7.2 Experimental Section

The reference electrode was an Ag/AgCl electrode with ethanol solvent saturated by LiCl (ultrapure grade, Alfa) at -85°C, the lowest temperature the temperature control system could reach. The cell temperature was controlled by a Multicool temperature bath controller (FTS systems). The temperature was monitored near the working electrode with an Omege temperature probe. The solvent was a mixture of DMF (Burdick Jackson Laboratories, Inc.) and methanol (Fisher Scientific) in the ratio 40%:60%. The DMF was dried over 3Å molecular sieves (Alfa). The supporting electrolyte was TBAF (tetrabutylammonium fluoroborate, Fisher Scientific) in 0.30 M and the concentration of methylcobalamin (Sigma) was 2.0 mM for both *CV* and *DPSC*. The solutions were prepared in room temperature at 24°C, so that the molar concentrations pertain to that

Reproduced with permission of the copyright owner. Further reproduction prohibited without permission.

temperature. Experiments were performed by a BAS-100A electrochemical analyzer. The experimental results were transferred to a PC-XT computer in the hexadecimal form through cable, then converted to the corresponding decimal digits. The *DPSC* fitting for following chemical reaction rate k_{chem} and *CV* simulation-fitting for the formal reduction potential $E^{o'}$, the standard heterogeneous rete constant k^o, the transfer coefficient α and the surface area of the working electrode were performed in a Gateway 2000 IBM compatible 386 machine (20 MHz) with math co-processor.

The working electrodes were silver amalgam electrodes. They were made from silver electrodes with diameters 1.6 mm (Bioanalytical System) and 0.25 mm (home made). The original silver electrode was polished by fine aluminum oxide powder (0.05 μm), put into an electrochemical cell in which there was a drop of liquid mercury on the bottom immersed in nitric acid solution at *pH* 1.5. Using an aqueous Ag/AgCl electrode as reference electrode and a platinum wire as counter electrode, a potential of -1.0 volt was applied. This potential reduced hydrogen ions in solution and produced hydrogen gas at the silver working electrode where the surface was activated. After 3 min, the silver electrode was put in contact with the mercury in the cell while still maintaining the potential constant. A film of mercury formed on the surface of the silver electrode. This electrode was rinsed by deionized-distilled water several times and then was immersed in the same type of water for 50 to 70 min to form a silver amalgam layer on the electrode surface with thickness about 3 μm[58]. The electrode was polished with aluminum oxide powder (0.05 μm) again and finally was washed with deionized-distilled water followed by DMF-methanol solvent.

Reproduced with permission of the copyright owner. Further reproduction prohibited without permission.

Several solvent mixtures with different ratios of DMF and methanol were tested. Since DMF has a higher freezing point compared with methanol and it has limited solubility for methylcobalamin, a high ratio of DMF was avoided. On the other hand, methanol has lower dielectric constant compared with DMF, which causes higher resistance particularly at low temperatures. Experiments showed no significant difference in *CV* for the reduction of methylcobalamin for ratios varying from 25%:75% to 75%:25% for DMF with methanol, ethanol, 1-propanol and other alcohol, except that the rate of the following chemical reaction was sensitive to the exact solvent mixture[a]. These solvent mixtures were not frozen at temperatures as low as -85°C. Nitrogen, which was saturated with the same ratio of components and pre-cooled through a *U*-type tube immersed in the cooling system, was used to purge the solvent until the initial background current was minimized. The *CV* results for methylcobalamin, with a silver amalgam electrode (diameter 1.6 mm), were subjected to background subtracting with the data taken under same experimental condition but only with solvent and electrolyte. The *DPSC* experiments for the following chemical reaction rate k_{chem} were carried out with time resolution 100 μsec with a silver amalgam electrode (diameter 0.25 mm).

The *CVFIT* program includes the correction of *iR* drop in *CV*. For this *iR* correction, the uncompensated resistance was analyzed by potential step chronoamperometry. The initial potential was set as same as the initial potential in *CV* experiments, and then a step of -50 mV to the initial potential was applied. This step potential was applied for 1 or 2 msec. Since the procedure did not involve faradaic

---

[a] Detail will be discussed in chapter 8.

Reproduced with permission of the copyright owner. Further reproduction prohibited without permission.

current, the current response follows the relationship:

$$i_t = \frac{\Delta E}{R} \exp\left(\frac{-t}{RC_{dl}}\right) \qquad (7-1)$$

where i_t is the response current, ΔE is the potential step applied, R is resistant, C_{dl} is the capacitance of the double layer and t is the time. A plot of time *vs.* $ln(i_t)$ extrapolated to the zero time was used to find the resistance from the intercept[59].

7.3 Results and Discussion

The rate constant of the following chemical reaction was determined by *DPSC* and then used as a fixed parameter in the simulation and fitting analysis. *DPSC* offered a convenient access to the decay kinetics of electrochemically generated short-lived species. The potential was stepped from the region where the species was not electroactive to the plateau of the *i-E* curve and then back to the initial potential. Stepping the potential well beyond the reduction potential avoided the tedious correction of solution ohmic drop and electrode electron transfer kinetics. The *DPSC* results were fitted to the theoretical curve developed by Schwarz and Shain[60]. The first few points of data were ignored because of double layer charging current. The usable time window as confirmed by the Cottrell equation[54] where constancy of $it^{1/2}$ was observed. The cathodic current was fitted first within time $0 < t \leq \tau$, where τ is the period of pulse applied. The current follows the Cottrell relation:

Reproduced with permission of the copyright owner. Further reproduction prohibited without permission.

$$i_c = nFAC_o^*\sqrt{\frac{D_o}{\pi t}} \qquad (7\text{-}2)$$

where n is the number of electrons involved in the charge transfer, F is the Faraday constant, A is the area of the electrode, C_o^* is the bulk concentration of methylcobalamin and D_o is the diffusion coefficient. Then k_{chem} was adjusted when the same parameters (n, A, C_o^* and D_o) were maintained within time $\tau < t \leq 2\tau$ until the anodic current was fitted to the relation[60]:

$$i_a = nFAC_o^* D_o^{1/2}\left[\frac{\phi}{\sqrt{\pi(t-\tau)}} - \frac{1}{\sqrt{\pi t}}\right] \qquad (7\text{-}3)$$

where

$$\phi = e^{-\frac{k_{chem}\tau}{2}} I_0\left(\frac{k_{chem}\tau}{2}\right) + 2e^{-\frac{k_{chem}\tau}{2}} e^{-k_{chem}(t-\tau)} \times \sum_{n=1}^{\infty} I_n\left(\frac{k_{chem}\tau}{2}\right) \frac{\int_0^{k_{chem}(t-\tau)} \int_0^{\lambda_2} \cdots \int \lambda_1^n e^{\lambda_1} d\lambda_1 \cdots d\lambda_n}{[k_{chem}(t-\tau)]^n} \qquad (7\text{-}4)$$

and $I_n(k_{chem}\tau/2)$ represents the modified Bessel functions. Based on the theory and confirmed by the theoretical data analysis with reasonable error range, three terms of the infinite series were used. The experimental and fitted results are shown in Figs. 7-1(a) and (b). Fig. 7-1(a) is a general experimental and the fitted result, and Fig. 7-1(b) is a detail with the error range indicated. The k_{chem} results were also checked by the measured current ratios $-i_a/i_c$ with the working curve data[60]. All results fall within 5-15% of an average value.

Cyclic voltammetry with a resolution of 1 mV per point was carried out at -30°C with the silver amalgam working electrode. The cyclic voltammograms at scan rates 50

Reproduced with permission of the copyright owner. Further reproduction prohibited without permission.

mV/sec, 100 mV/sec and 300 mV/sec are shown in Figs. 7-2 (a) to (c). These voltammograms are characterized by a cathodic wave showing a well-defined current maximum but no anodic wave on the reserve scan. The digital simulation and fitted results from *CVFIT* program are also shown on the same voltammograms. The input parameters of the program included the diffusion coefficient D_o, the rate of the following chemical reaction k_{chem}, the resistance R and the experimental condition including scan range and scan rate. The initial guess parameters were provided for the formal reduction potential $E^{o'}$, the standard heterogeneous charge transfer constant k^o, the transfer coefficient α, and a proportionality constant including small errors in concentration of methylcobalamin and the electrode area. The program *CVFIT* utilized Nelder and Mead's modified simplex minimizing procedure to find the best fit between the experimental and simulation results by adjusting these guesses in the simulation process[53,55-56]. Before running *CVFIT*, the diffusion coefficient used at -30°C was measured by *DPSC* in the time window of constancy $it^{1/2}$ and checked by *CV*. The *iR* drop was corrected by adding each experimental point of current multiplied with the measured solution resistance to the applied potential, then the calibrated potential (E) was used through equation 7-5 in order to employ the actual scan rate as input to simulation program, where the reduction currents are considered positive[61]:

$$E = E_{applied} + iR \qquad (7-5)$$

The calculation errors are estimated by summation of the square of the difference between experiment and simulation-fitting currents for the corresponding potentials:

Reproduced with permission of the copyright owner. Further reproduction prohibited without permission.

$$\chi^2 = \sum_{j=1}^{n} W_j \left[current_j(measured) - current_j(theory)\right]^2 \quad (7\text{-}6)$$

where the weighting factor W_j is set to 1 in the present case of constant variance.

The formal reduction potentials, the heterogeneous rate constants and the transfer coefficients obtained through simulation-fitting are listed in Table 7-1. The constancy of the reduction potential and other fitted parameters for repeated experiments and the experiments at three different scan rates provides strong evidence that the values obtained are not spurious or the result of the location of fortuitous local minimum in the fitting procedure. In addition, the $E^{o'}$ value is in agreement with the less precise value (-1.6 volt *vs. SCE*) obtained by Saveant *et al* in the similar experimental condition with fast scan rate[32].

In order to estimate the error of the $E^{o'}$ measurement which is caused by the error in the measurement of the following chemical reaction k_{chem}, a series of *CV* simulations with different scan rates and k_{chem} were performed. It was found that the deviation in k_{chem} would not affect $E^{o'}$ measurement in our electrochemical system. At scan rate 300 mV/sec, the peak potential shift is less than 1 mV as k_{chem} changing from 490 sec^{-1} to 690 sec^{-1}; and the shift is 1 mV in the same k_{chem} change range at the scan rate 50 mV/sec.

It has been suggested that the reduction potential can be estimated at slow scan rates by assuming electron transfer reversibility and applying the formula for the kinetic shift due to the following chemical reaction under such circumstances[54,62]:

Reproduced with permission of the copyright owner. Further reproduction prohibited without permission.

$$E^{o'} = E_p + 0.780\frac{RT}{nF} - \frac{RT}{2nF}\ln(\frac{RT}{nF}\frac{k_{chem}}{\nu}) \qquad (7\text{-}7)$$

where E_p is the peak potential in *CV* and ν is the scan rate. Application of this formula to our system even at the slowest scan rate (50 mV/sec) leads to an error in the reduction potential of 30 mV compared to that obtained by the more rigorous method presented here (±4 mV).

From the simulation and fitting results, α was found to be 0.78, which is significantly larger than 0.5. A value of $\alpha > 0.5$ indicates that the structure of the transition state for reduction is close to that of the reactant[54]. Our results ($\alpha = 0.78$) supports the mechanism in Scheme 7-1 where the compound of the transition state $[B^{\bullet}_{12a}]^-$ is expected to have the similar structure of the reactant B_{12a}.

Although the cyclic voltammograms appear irreversible, analysis of the data showed this is not entirely the case (otherwise we can not expect to obtain a reliable $E^{o'}$)[b]. In order to understand this more fully we carried out a study of the system reversibility. The electrochemical current corresponds to the difference between the rate of the forward electron transfer $k_f[B_{12a}]$ and its rate $k_b[B^{\bullet}_{12a}]^-$ for reverse process. However, under conditions there is a following chemical reaction, the reversibility of the system will be influenced. If the following chemical reaction rate is much faster than the rate of the reverse electron transfer, the rate of the forward electron transfer will become rate limiting. Under these circumstances, the electrochemical process is totally

---

[b] An examination of the Butler-Volmer equation suggests that both forward and reverse processes must be occurring in order to separate the three terms $E^{o'}$, k^o, and α.

Reproduced with permission of the copyright owner. Further reproduction prohibited without permission.

irreversible. If the rate of the forward electron transfer is not completely rate limiting, the system is described as quasi-reversible. In general the reversibility of an *EC* mechanism depends on the heterogeneous kinetics, the homogeneous kinetics and the scan rate. The reversibility factor f_r, introduced by Klingler and Kochi[63], describes the reversibility of the system. It is a continuous function of the electrode kinetics varying smoothly from $f_r = 1$ for Nernstian behavior to $f_r = 0$ for the total irreversibility. It also can be applied to estimate the error range for the transfer coefficient α. The reversibility factor f_r for methylcobalamin system is described as:

$$f_r \frac{[B_{12a}]_o}{[B^{\bullet}_{12a}]_o^-} = \exp\left[\frac{nF}{RT}(E - E^{o'})\right] \qquad (7\text{-}8)$$

where $[B_{12a}]_o$ and $[B^{\bullet}_{12a}]_o^-$ are the corresponding concentrations on the electrode surface in Scheme 7-1. These concentrations can be obtained from the digital simulation by extrapolating the concentrations in the first few spatial grid points of the simulation to the electrode surface. The variation of the reversibility factor f_r as the function of the heterogeneous charge transfer constant is shown in Fig. 7-3. The reversibility factors f_r were evaluated at the corresponding peak potential. The results demonstrate that electrode reversibility is actually a continuum with total irreversibility merely being one limiting extreme. For the value of the chemical rate constant in the system ($k_{chem} = 590$ sec^{-1}) we are concerning, the reversibility factors have a maximum value of $f_r = 0.73$ as the heterogenous rate increases. We are particularly interested in the reversibility under the conditions of our experiments. The *CV* simulations for methylcobalamin at -30°C result in reversibility factors $f_r = 0.18$ at scan rate 300 mV/sec and $f_r = 0.21$ at 50 mV/sec.

Reproduced with permission of the copyright owner. Further reproduction prohibited without permission.

Both of them are close to the root of the curve, but they are not completely irreversible even though the cyclic voltammograms appear "irreversible".

The charge transfer coefficient α is an important electrochemical parameter. For a totally irreversible system, α is given by[54,63]

$$\alpha = \frac{1.857RT}{nF}\frac{1}{|E_p - E_{p/2}|} \qquad (7\text{-}9)$$

where $E_{p/2}$ is the potential of half wave height peak current. It is expected that α_{app} obtained in this manner will be a reasonable value even though the system is not totally irreversible. Klingler and Kochi's results[63] and our digital simulation data also show the influence of f_r to α_{app} values by using relation (7-9) that the larger α_{app} value will have the smaller error if a system has the similar irreversibility. Since $\alpha = 0.78$ in this system, it is expected a small error for estimating α_{app} through relation (7-9) if f_r is in the foot region of the curves *a* and *b* in Fig. 7-3. The small error in potentials used in equation (7-9) due to *iR* drop also results in errors of α_{app} values. It is introduced *iR* correction into equation (7-9) in the following means:

$$\begin{aligned} E_p - E_{p/2} &= (E_p + i_p R)_{exp} - (E_{p/2} + i_{p/2} R)_{exp} \\ &= (E_p - E_{p/2} + \frac{1}{2} i_p R)_{exp} \end{aligned} \qquad (7\text{-}10)$$

where i_p is the peak current and $i_{p/2}$ is the half wave height peak current. The values of $\alpha_{app,corr}$ from measurements after *iR* correction through equation (7-10) in cyclic voltammogram are listed in Table 7-2. These results are consistent with the α values obtained by simulation. Fig. 7-4 shows the influence of f_r to α values by estimation

Reproduced with permission of the copyright owner. Further reproduction prohibited without permission.

calculated from simulation and through equation (7-10). The error caused by estimation method is also consistent with the experimental measurements where the values of the transfer coefficient are larger than the more precise values from simulation and fitting. The reason for slight larger values in $\alpha_{app,corr}$ than that in α_{fit} is the system is not completely irreversible or f_r is not small enough.

Reproduced with permission of the copyright owner. Further reproduction prohibited without permission.

Chapter 8 The Solvent and Temperature Effects on the Rate Constant of the Following Chemical Reaction of Methylcobalamin

8.1 Introduction

Since methylcobalamin is a cobalt coordination compound and one of the two biological alkylcobalamins, a better understanding of the biological role of methylcobalamin is its characterization of the key Co-C bond properties and its behavior in various environments. The mechanism of methylcobalamin in electrochemical system has been discussed in chapter 7. By rapid sweep *CV*, Lexa and Saveant estimated the following chemical rate as 1200 sec^{-1} in a solvent mixture of DMF and 1-propanol (50:50) at -30°C[32]. In the aqueous media, Kim and Birke's results showed the rate constant 0.37 sec^{-1} at room temperature[52]. They also mentioned this large difference in the rate constant with different solvent media as that the leaving group methyl radical would require much less solvation energy in nonaqueous media than in aqueous media. In the study of methylcobalamin electrochemical behavior at low temperature with nonaqueous solvent mixtures (DMF and methanol), similar phenomenon was observed. It was confirmed that the rate constant determined for the following chemical reaction will have obviously different values in different media of dielectric constants, as do the corresponding activation free energies. The larger the value of the dielectric constant, the lower the rate constant and the higher the activation free energy were observed. Since $\cdot CH_3$ radical is an organic group, the solvent effect will allow it more easily to leave the bonding cobalt if the solvent dielectric constant is lowered, which makes the rate constant

Reproduced with permission of the copyright owner. Further reproduction prohibited without permission.

of the following chemical reaction to be increased. Opposite effects will be found if the solvent dielectric constant is higher. It was also observed the rate constants of the following chemical reaction decreased as the temperature was lowered, but this change of the rate constant leveled off around -40°C. Continuing to lower the temperature, the rate constant decreased again. This unusual phenomenon was concluded to be the result of the changes in the dielectric constant of solvent. As the temperature is decreased, DMF will dimerize so that it reduces the solvent dielectric constant and makes the rate constant of following chemical reaction faster. Once the dimerization is close to complete, the temperature effect resumes "normal" behavior and redominates the change of rate constant of the following chemical reaction.

8.2 Experimental Section

Similar experimental set-up described in chapter 7 was applied. The solvent mixtures were not frozen at temperatures as low as -85°C in the experiment. Cyclic voltammetry was carried out as a general diagnostic technique using a working electrode of mercury amalgam in diameter 1.6 mm. The mercury amalgam electrodes in the diameters 0.25 and 0.50 mm were used for *DPSC* measurement to measure the rate constants of the following chemical reaction. The selected time period τ was controlled as the same order as the estimated half life time of the methylcobalamin in the reduced form.

Reproduced with permission of the copyright owner. Further reproduction prohibited without permission.

8.3 Results and Discussion

The rate constants of the following chemical reaction were measured by fitting the *DPSC* experimental data with the theoretical model through equations (7-2) to (7-4). The data points at the very beginning time due to the double layer charging current were ignored. The data used to fit the theoretical model are only within the time window where the constancy of $it^{1/2}$ was observed. Fig. 8-1 shows one of the k_{chem} fitted at -40°C in the solvent mixtures of DMF and methanol (50%:50%). Fig. 8-2 indicates the time window used for fitting was confirmed by the Cottrell equation. According to the chemical kinetic theory, k_{chem} will follow the Arrhenius relationship so that k_{chem} changes exponentially with temperature, if other electrochemical parameters such as k^o and α do not change dramatically. Fig. 8-3(a) shows the relationship of temperature and k_{chem} in two different solvent mixtures as temperature is decreased. Comparing k_{chem} of the methylcobalamin in two media, it was found that the rate constant is faster in the less polar media at the same corresponding temperature. This is because the methyl radical needs less solvation energy in the less polar or low dielectric constant media. The k_{chem} is reduced as the temperature is decreased, but the change in rate constant levels off around -40°C for solvent mixture of 50:50 of DMF and methanol, and around -50°C for solvent mixture of 40:60. Continuing to decrease the temperature, the rate constants resumed decreasing. Fig. 8-3(b) shows their relationship in natural logarithm scale. The k_{chem} followed the Arrhenius relationship as the temperature was decreased but was still higher than -40°C for solvent mixture of 50:50 of DMF and methanol. Similar change was observed as the temperature was higher than -50°C for solvent mixture of 40:60 of

Reproduced with permission of the copyright owner. Further reproduction prohibited without permission.

DMF and methanol.

The relationship between the rate constant of the following chemical reaction and temperature was expressed in the form[54,61]:

$$k_{chem} = \kappa \frac{k_B T}{h} \exp(-\frac{\Delta G^{\neq}}{RT}) \qquad (8\text{-}1)$$

where κ is transmission coefficient, k_B is Boltzmann constant, h is Planck constant and $\Delta G^{\neq}$ is the activation free energy. The activation free energies of the following chemical reaction for two different solvent mixtures are calculated by measuring the slope of experimental data in logarithmic scale and comparing it with equation (8-1) in their "normal" behavior temperature range. Fig. 8-4 shows the relationship of (1/T) *vs.* $\ln(k_{chem}/T)$. The activation free energies are 7.8 kcal/mol with dependency coefficient 0.997 in solvent mixture of 50:50 of DMF and methanol, and 5.5 kcal/mol with dependency coefficient 0.998 in 40:60 of DMF and methanol[c]. Experimental results have shown that the methyl radical may require less solvation energy in low dielectric constant media than that in high dielectric constant media[52]. Comparing Lexa and Saveant's results[32] of the activation free energy for methylcobalamin (10.7 kcal/mol), where methylcobalamin was dissolved in a solvent mixture DMF and 1-propanol with ratio 50:50, the results we have here are in the reasonable range because methanol is more polar than 1-propanol.

DMF was observed to have a substantial increase in the available potential window at low temperature due to the formation of cyclic DMF dimer[64-65]. The

---

[c] In this estimation, κ was assumed as one[61].

Reproduced with permission of the copyright owner. Further reproduction prohibited without permission.

dimeric species would have to be both more difficult to oxidize and reduce than the monomer. This dimerization has been confirmed by NMR experiments[65]. A structure shown in Fig. 8-5 of DMF dimerization has minimum steric interaction and could undoubtedly enhance charge delocation and stability of the complex through the formation of a chair-like six-member ring. The leveling effects for k_{chem}, as the temperature was decreased around -40°C and -50°C for the corresponding solvent mixtures, are postulated to be the result of DMF dimerization. Obviously the solvent dielectric constant decreases as DMF dimerizes because the dimerized form reduces the polarity and delocalizes the charge as it exists in a single molecule. This makes it easier for the methyl radical bonded with cobalt in methylcobalamin to leave because the process requires less solvation energy in the medium with low polarity or low dielectric constant. The methylcobalamin in less polar media (40:60) has smaller activation energy (5.5 kcal/mol) than that (7.8 kcal/mol) in more polar media (50:50). In these two solvent mixtures, the high polarity or dielectric constant media (50:50 of DMF and methanol) causes the leveling effects beginning at temperature just below -40°C while the low polarity or dielectric constant media (40:60 DMF and methanol) causes the same effect beginning at temperature below -50°C. It may be that at a high percentage of DMF, which is more polar, there will be larger dimerization effects and dimerization will occur at high temperature.

In the enzymatic reactions requiring methylcobalamin as a cofactor such as homocysteine methyl transfer and the methane biosynthesis processes, the Co-C bond cleavage may be the rate determining step if the system is in a high dielectric constant

Reproduced with permission of the copyright owner. Further reproduction prohibited without permission.

or an aqueous environment; whereas, the Co-C bond cleavage is less likely to be involved in rate determine step if the system is in a nonaqueous environment with low dielectric constant. The sensitivity to the environment in the rate constant of the following chemical reaction suggests a nonaqueous dielectric media for proteins in the enzymatic methyl group transfer reaction if the methyl radical mechanism is involved. The experimental results here may give useful suggestion of explanation for some important biological processes.

Reproduced with permission of the copyright owner. Further reproduction prohibited without permission.

Chapter 9 The Electrochemical Study of B_{12} Derivatives

9.1 Introduction

The quantitative understanding of the electrochemistry and axial ligand effects of alkylcobalamins is less complete than that when the ß-axial ligand is an inorganic species[17,66]. It still attracts considerable interest because of the mechanism of adenosylcobalamin and methylcobalamin dependent enzymatic reactions. Alkylcobalamins are nearly ideal for electrochemical investigation because their LUMO orbitals are antibonding with respect to the key Co-C bond and the approximately square planar corrin system minimizing any other structural distortions following one-electron reduction[67]. The homolysis in adenosylcobalamin proceeds 10 orders of magnitude faster in the enzymatic reaction than that in an enzyme-free environment[68-70]. Conformational changes of the coenzyme, induced by the interactions within the protein-substrate complex that lower the bond-dissociation energy, have been invoked to rationalize the rate enhancement. This hypothesis is supported by increased homolysis rates observed for organocobalamins under nonenzymatic conditions but exhibiting steric hindrance between the organic group and the corrin macrocycle[71-73]. The rate enhancement of the Co-C bond homolysis in methylcobalamin achieved by one-electron reduction is even of the same magnitude order as the acceleration of bond homolysis introduced by enzyme in the case of adenosylcobalamin[74]. On the other hand, a reductively triggered Co-C bond homolysis in an enzymatic reaction seemed so far unrealistic because the reduction potentials of isolated methylcobalamin,

Reproduced with permission of the copyright owner. Further reproduction prohibited without permission.

adenosylcobalamin and other alkylcobalamins are generally too negative to be accessible to biological reductants. Nothing is known on the influence of the interactions between the enzyme and the alkyl ligand of an alkylcobalamin on the reduction potential in biological processes. If the conformational restrictions in the coenzyme-substrate-enzyme complex could shift the reduction potential positively enough, the generation of an adenosyl or methyl radical reductions in the Co-C bond cleavage could become biochemically feasible.

The *CV* approach in the solvent mixture of DMF and methanol (40:60) determined the effects of steric and electronic factors on reduction potentials, heterogeneous electron transfer rate constants, electron transfer coefficients and the homogeneous bond fission rate constants, as well as on the pathway of reductive cleavage mechanism itself. With the simple alkyl groups, a series of substituted cobalamins, which have increasing steric substitution on their ß position from methyl to ethyl, *n*-propyl, *n*-butyl and *iso*-butyl, were tested. The behaviors of 5'-deoxyadenosylcobalamin was also investigated to see where it fits in the above series of compounds. Electrochemical experiments of *t*-butylcobalamin and *iso*-propylcobalamin were not performed because *t*-butylcobalamin can not be prepared and *iso*-propylcobalamin has a very short lifetime which is only stable on a scale of minutes[66]. On the other side as in aqueous media, reduction on mercury electrode is complicated by adsorption effects. However, in the presence of a surfactant, the electrochemical parameters of methylcobalamin for the reductive cleavage reaction can be successfully investigated[52]. The essential issue here is the exactly right amount of the surfactant to be used.

Reproduced with permission of the copyright owner. Further reproduction prohibited without permission.

Since the microelectrode has low ohmic potential drop and small charging currents at shorter times, the use of microelectrode (10 μm in diameter) in experiments allows the measurement of the fast following chemical reaction for ethylcobalamin in aqueous media at room temperature. The electrochemical behavior and the rate constant of the following chemical reaction will be used to describe the role alkylcobalamin may play in biochemical processes.

All these experiments were performed in a dark environment and in the electrochemical cell shielded by aluminum foil, because all alkylcobalamins should be protected from light since the Co-R bond is easily cleaved by photolysis. Since there are no commercial available alkylcobalamins (except methylcobalamin) due to their instability and sensitivity to the light and temperature, they have to be synthesized and characterized in the laboratory.

9.2 The Preparation of Alkylcobalamin

9.2.1 The Principle Consideration in Synthesizing Alkylcobalamin

Generally, B_{12} derivatives are synthesized through the chemical or electrochemical reduction of hydroxocobalamin followed by the addition of the indicated alkyl iodide[75-77], which is based on the reaction of B_{12s} with suitable electrophiles. The limiting factor in this synthesis through nucleophilic displacement reactions is steric. The synthesis also involves follow-up purification and characterization procedures.

The reduction of the hydroxocobalamin, which contains trivalent cobalt, is a key procedure with two distinct steps. The first one-electron reduction product ($E_1^{o'} = 0$ volt

Reproduced with permission of the copyright owner. Further reproduction prohibited without permission.

vs. SCE) is vitamin B_{12r} then undergoes a further one-electron reduction ($E_2^{\circ'}$ = -0.7 volt *vs.* SCE) to B_{12s}. The later may be considered as either containing monovalent cobalt or being a trivalent cobalt hydride[78]:

$$\begin{matrix} H^+ & & H^- \\ Co(I) & \rightleftarrows & Co(III) \end{matrix}$$

Since B_{12s} is one of the most nucleophilic species known to exist in aqueous solution[79], its high nucleophilicity results in the ease of preparation of the B_{12} derivatives. The B_{12s} undergoes both rapid substitution and addition reactions with a variety of electrophiles[80].

Generally speaking, there are two methods to reduce B_{12a} to B_{12s} and then substitute B_{12s} with suitable alkyl groups to synthesize the B_{12} derivatives. One method is controlled potential reduction and the other one is chemical reduction. The advantage of the first method is that no excess of reducing agent is present, but a special apparatus must be built and the experiments take longer. In our experiments, the second method was used because it is simpler and experiments can be completed in shorter time.

The most convenient chemical reduction is that brought about by sodium borohydride, $NaBH_4$. Although such reductions are usually completed with a few minutes, they occasionally stop at the brown B_{12r} stage. The further reduction to B_{12s} then requires both a large excess of sodium borohydride and an extended reaction time, which usually results in some irreversible reduction of the corrin chromophore. It has been reported[75] that addition of copper to the system catalyzes the reduction, but the reducing system also reduces the alkylcobalamins which are normally stable toward sodium borohydride. Thus, the copper-catalyzed reduction is unsuitable for the preparation of B_{12s} as a precursor of the alkylcobalamins. If, however, cobaltous ions are added to a

Reproduced with permission of the copyright owner. Further reproduction prohibited without permission.

cobalamin borohydride solution, the reduction is catalyzed without further reduction of alkylcobalamins. Thus, this reduction is suitable for the syntheses of the vitamin B_{12} derivatives[75].

The limiting factors in the synthesis of B_{12} derivatives by nucleophilic displacement reactions are primarily steric[75,80-81], and the steric effect may either limit the rate of the reaction or affect the stability of the derivatives once they have been formed. Thus, no reaction is observed between B_{12s} and *t*-butyl halides or *neo*-pentyl chloride. While the reaction between B_{12s} secondary halides, such as α-chloropropionic acid and 2-bromobutane, is fast, the resulting derivatives are not sufficiently stable to survive the purification procedures. Although steric considerations are of primary importance in determining stability, certain derivatives that are sterically feasible still require considerable care during their isolation. Hine[82] and Schrauzer *etc.*[79,83] indicated that the relative reaction rates of vitamin B_{12s} with methyl, ethyl, *n*-propyl and *n*-butyl chlorides as 180:11.7:1.3:1.0 in methanol at 25°C, and vitamin B_{12s} is obviously the one of the most powerful nucleophiles. Steric effects play an important role in the synthesis process because they dominate the process over the alkyl electron-donor effects. Schrauzer's conclusion is listed in Table 9-1. From the observation and the effects of *R* and *X* on the rate constants, they concluded that the B_{12s} alkylation occurred by a classical S_N2 mechanism. For these slow reaction rates between B_{12s} and some alkyl halides, excess amount of alkyl iodide is necessary.

The low solubility of the cobalamins in most solvents, coupled with the need for solvents that are stable toward reducing agents, restricts the choice for the preparation

Reproduced with permission of the copyright owner. Further reproduction prohibited without permission.

of the B_{12} derivatives to water, methanol, ethanol and aqueous acetic acid[75]. These derivatives are light sensitive, especially in solution.

Following the synthesis, the extraction procedure by phenol removes water-soluble salts from cobalamins. The *UV* spectra are obtained in order to characterize synthesized alkylcobalamins. Thin-layer chromatography on cellulose is useful for the rapid analysis of cobalamins, but the close similarity in relative mobilities for many cobalamins makes paper chromatography more reliable. It is advisable to use several different solvent systems in paper chromatography when determining the composition or purity of alkylcobalamins with the mobilities quoted relative to cyanocobalamin[80].

9.2.2 The Synthesis Procedure[d]

A solution of hydroxocobalamin[e] (Sigma, in the form of chloride salt crystalline, 100 mg) and cobalt nitrate (Aldrich, 1 mg) in deionized-distilled water (10 ml) was placed in a 20-ml weighing bottle, stoppered with a cap and deoxygenated with a gentle stream of nitrogen[f]. After 10 minutes, a deoxygenated solution of sodium borohydride (Aldrich, 20 mg) in water (0.5 ml) was added. The solution immediately turned brown and then purple (if it was viewed in daylight, the color finally looked like blue-green).

---

[d] Here is given the example of synthesizing ethylcobalamin, other B_{12} derivatives use a similar procedure.

[e] When B_{12s} is prepared from cyanocobalamin, cyanide ion is present at the end of the reduction.

[f] Either nitrogen or argon are suitable for the deoxygenation, but argon is less readily displaced by air, because of its higher density than nitrogen; it is, therefore, more useful if we do not consider the purchase price.

Reproduced with permission of the copyright owner. Further reproduction prohibited without permission.

After a further 5 minutes, ethyl iodide (Aldrich, 200 mg) was added whereupon the solution turned yellow-orange. For synthesizing *n*-propyl- or *n*-butylcobalamin, the same mole amounts of *n*-propyl or *n*-butyl iodides as ethyl iodide were added. While synthesizing *iso*-butylcobalamin the mole number of *iso*-butyl iodide was doubled because of the relatively slow reaction rate indicated in Table 9-1 and the low yield. The extra amount of *iso*-butyl iodide could be easily sucked away before the extraction procedure because it has higher density.

The aqueous cobalamin solution was extracted with one-fifth of its volume of a solution of phenol in methylene chloride. The stock solution of phenol (Aldrich) was prepared by dissolving 100 grams of phenol in 100 ml methylene chloride (Fisher Scientific). The organic layer was separated, and the aqueous layer was reextracted with successive aliquots of phenol-methylene chloride until no further color was extracted. The combined organic extracts were washed with water in one-fifth volume of the organic layer two times. After washing, the organic layer was diluted with methylene chloride to ten times its original volume. The cobalamin was reextracted from the organic layer with aliquots of water in one-twentieth volume of the organic layer until no color remained in the organic layer. The combined aqueous extract was then washed with methylene chloride in three times the volume of the combined aqueous layer to remove trace phenol. The methylene chloride remaining in the aqueous phase was removed in the procedure of reduced pressure evaporation or by passing a stream of nitrogen through the solution.

The resulting solution purified by phenol extraction was reduced to 5 ml on a

Reproduced with permission of the copyright owner. Further reproduction prohibited without permission.

rotary evaporator with a mechanical vacuum system, where the bath was kept in 20°C with water. This solution was placed on a column (30×2 cm) of 30 to 60 mesh silica gel. The silica gel column had been pre-washed with 0.1 M hydrochloric acid and then deionized-distilled water until the washing was neutral. The alkylcobalamin was eluted from the column with water. The eluate was reduced in volume to 1 ml and treated with acetone until the solution showed a faint turbidity. On standing overnight, bright red crystals of ethylcobalamin (or other alkylcobalamins) were deposited. They were collected by filtration, washed with acetone, air dried and then stored in refrigerator.

9.2.3 The Characterization of Alkylcobalamin

Because the infrared spectra (*IR*) of alkylcobalamins, coenzyme B_{12}, cyano- and hydroxocobalamin are very similar[84], one of the most useful methods characterizing alkylcobalamins is ultraviolet and visible (*UV/VIS*) spectra. The *UV/VIS* experiments mentioned below were performed on a Perkin-Elmer Lambda 3B *UV/VIS* spectrophotometer with 1 cm cell, scanning from 650 nm to 200 nm at room temperature.

The most important property of the axial ligand which determined by the influence of alkylcobalamins is the amount of negative charge donated *via* the σ-bond to the cobalt. In contrast to the effects of changes in the axial ligands or substituents of the conjugated ring, changes in the side-chains or even in the outer ring of carbon atoms have very little effect on the spectrum. When the hydroxy ligand of vitamin B_{12} is replaced by other ligands such as H_2O or CN^-, only small changes occur in the spectra. However, when

Reproduced with permission of the copyright owner. Further reproduction prohibited without permission.

the hydroxy ligand is replaced by an alkyl ligand such as methyl or ethyl, there is a considerable change in the spectrum. Since the extent of the conjugated chromophore in the corrin ring and the valency of the cobalt are the same in these vitamin B_{12} derivatives, the differences in the observed spectra are due to the influence of the ligand change in ß position. All alkylcobalamins and coenzyme used in experiments change from red to yellow on acidification. Ladd *et al* [85] assumed the red-yellow shift to be due to the breaking of the cobalt-nucleotide nitrogen bond, whereas Williams[86], though agreeing with this, regarded the change as more fundamental and involving protonation of the chromophore, possibly at position 10. Alkylcobalamins are uncharged in neutral aqueous solution although the *Bzm* is protonated in the yellow form in acid[84,87]. Dolphin[78] also indicated that in the protonated species the 5,6-dimethylbenzimidazole is protonated and no longer coordinated to the cobalt. Alkylcobalamins are generally more stable in acidic media, in which the axial base is protonated, while in neutral or basic solution axial coordination of this base causes a conformational change of the corrin ligand which may accelerate the Co-C bond cleavage by orders of magnitude[72]. Electrophoresis of such protonated species has shown that only one proton is involved, indicating that water is coordinated in place of the previously coordinating benzimidazole. This results in a change in electron density on the cobalt and a general shift of the absorption bands to shorter wavelengths[3]. In the protonated species the differences in the spectra, particularly below 400 nm, suggest that changes in the inductive character of the alkyl group cause profound changes in the electronic nature of the corrin ring[84]. The absorption bands at wavelengths longer 300 nm are due almost entirely to π-π^* transitions

Reproduced with permission of the copyright owner. Further reproduction prohibited without permission.

within the corrin ring. Their energies and intensities are very sensitive to changes in the axial ligands[3]. The spectrum is only slightly affected by changes in the temperature except where temperature causes a change in the nature of the axial ligands. Changes involving the conjugated chain itself such as chlorination at C_{10} affect the spectrum[3], but these need not concern us here. The *Bzm* also has absorption below 300 nm. These cobalt corrinoids, in fact, provide us an important sample whose electronic structure can be profoundly altered by the nature of the ligands attached to the metal. All corrinoids are highly colored. Their wide variation in spectra with the high extinction coefficients makes different corrinoids readily distinguishable and enables the *UV/VIS* experiments to be carried out with very small amounts of material. These provide the main reasons why *UV/VIS* absorption spectroscopy has played such an important role in the chemistry of B_{12}. The spectra of methylcobalamin (Sigma) and synthesized ethyl-, *n*-propyl-, *n*-butyl- and *iso*-butylcobalamins are shown in Fig. 9-1 (a) to (e) in both water and acidic media of 0.05 M HCl. These spectra are very similar to the results in the published papers[75-76,80]. There is a peak intensity increasing around 300 nm in acidic media as the alkyl group increasing in volume from methyl- to *n*-butylcobalamins, which could be rationalized as increasing the charge intensity on the cobalt. This peak increase is not observed in the spectrum of *iso*-butylcobalamin, which may be due to the much larger steric effect in this crowed molecules[3] because the spectrum is very similar to the spectrum of 5'-deoxyadenosylcobalamin at the same wavelength. The spectra of alkylcobalamins are significantly different from the spectra of hydroxocobalamin (Fig. 9-2), the original compound they are synthesized from in both neutral and acidic

Reproduced with permission of the copyright owner. Further reproduction prohibited without permission.

media. All these alkylcobalamins are very sensitive to light. *UV/VIS* spectra indicate that they will be easily photo-decomposed with the cleavage of Co-C bond and replacement of the alkyl groups by hydroxyl. Figs. 9-3 (a) and (b) show the spectra of *n*-butyl-cobalamin and *iso*-butylcobalamin after both were exposure to daylight for 5 min. The nearly similar spectra as hydroxocobalamin shown in Fig. 9-2 are a support for this photo-decomposing postulation.

In order to further confirm the quality of the synthesized alkylcobalamins, paper chromatography was performed for *n*-butylcobalamin by the descending technique on Whatman No. 1 paper. The results were shown in Table 9-2, where R_f values were quoted for the alkylcobalamins relative to cyanocobalamin at room temperature. Solvent 1 is *n*-butan-1-ol/propan-2-ol/H_2O with the ratio of 10:7:10 in volume. Solvent 2 is the saturated H_2O in butan-2-ol. The reference R_f values were cited from the experimental results of Johnson *et al*[80]. The methylcobalamin and 5'-deoxyadenosyl-cobalamin from a commercial source (Sigma) were tested in parallel for confirmation. The results of paper chromatography indicated the success of the synthesis.

9.3 Electrochemical Experiment Section

Electrochemical experiments were performed with the set-up described in chapter 7. The solvent mixture of DMF and methanol in ratio 40:60 was used. Cyclic voltammetry was carried out using a working electrode of mercury amalgam in diameter 1.6 mm. The concentrations of B_{12} derivatives in 2.0 mM and TBAF in 0.20 M were used through all experiments. Corresponding potentials were referred to Ag/AgCl

Reproduced with permission of the copyright owner. Further reproduction prohibited without permission.

nonaqueous reference electrode with ethanol saturated LiCl at -85°C.

TBAF (Fisher Scientific) was purified by recrystallization. It was first dissolved in ethyl acetate (Fisher Scientific) and filtered through Whatman No. 1 filter paper. Pentane (Fisher Scientific) was added to recrystallize the TBAF. The crystal form of TBAF was washed by pentane two times and then redissolved in ethyl acetate to repeat above purifying procedure. Finally, the crystallized TBAF was dried under vacuum at room temperature for 64 hours.

DMF (Fisher Scientific) was redistilled two times in vacuum distilling apparatus at 30°C under reduced pressure. The DMF solvent was filtered with Whatman No. 1 paper before each distillation. Methanol (Fisher Scientific) was redistilled two times at 64°C under regular pressure. Before each distillation, the methanol solvent was filtered with Whatman No.1 paper. In order to drive away trace water from methanol, I_2 and metal Mg were added to the evaporating beaker.

9.4 Results and Discussion

9.4.1 Experiments in Nonaqueous Media

Cyclic voltammetries of B_{12} derivatives, including methyl-, ethyl-, *n*-propyl-, *n*-butyl-, *iso*-butyl and adenosylcobalamins, were carried out at 20°C. The voltammograms with a scan rate of 300 mV/sec are shown in Fig. 9-4. As methylcobalamin *CV* results discussed in chapter 7, all these voltammograms are characterized by a cathodic wave showing a well-defined current maximum but no anodic wave on the reverse scan. The peak potentials for same series of B_{12} derivative are

Reproduced with permission of the copyright owner. Further reproduction prohibited without permission.

-1.472 volt (methylcobalamin), -1.355 volt (ethylcobalamin), -1.352 volt (*n*-propylcobalamin), -1.357 volt (*n*-butylcobalamin), -1.317 volt (*iso*-butylcobalamin) and -1.306 volt (adenosylcobalamin). It is obviously that the peak potentials of ethyl-, *n*-propyl- and *n*-butylcobalamins are very close, and they are with the peak potentials between methylcobalamin and the group of *iso*-butylcobalamin and adenosylcobalamin. From the series of ethyl-, *n*-propyl-, *n*-butyl-, *iso*-butyl- and adenosylcobalamins, they gradually increase the steric effect with corrin ring and certainly all have much larger steric effects than that in methylcobalamin. The hydrogen and methyl on corrin ring could make these alkyl groups leave easily so that they would have more positive reduction potentials and faster rate constants of the following chemical reaction. The unusually large values, found for C_1-C_{19}-C_{18} bond angle of a formally tetrahedral carbon atom in different corrinoids from 120° to even 129°, are also caused by the need to reduce repulsion between these corresponding neighbor groups[88-92]. The absence of free rotation of the methyl groups about the Co-C bond, revealed by neutron diffraction of methylcobalamin, is probably another indication of extensive overcrowding in the corrinoid molecule[93]. Since the steric effects mainly come from the ß carbon and the hydrogens connecting to the ß carbon in alkyl groups, the ethylcobalamin, *n*-propylcobalamin and *n*-butylcobalamin are expected to show the similar steric effects between the alkyl group and the corrin ring, so that they have the close reduction potentials and the close rate constants of the following chemical reactions. For the same reason, *iso*-butylcobalamin and adenosylcobalamin, which have the biggest steric effects from the alkyl groups, should certainly have the lowest reduction potentials and faster rate constants of the following

Reproduced with permission of the copyright owner. Further reproduction prohibited without permission.

chemical reactions.

According to the estimation of the following chemical reaction rates of alkylcobalamins through *DPSC* at various temperatures especially at low temperatures, methylcobalamin has the slowest rate. Hogenkamp and his coworker's polarographic experimental results indicated that an increase in the nucleophilic character of the corresponding ligand causes a shift of the polarographic wave to a more negative potential; and the formal reduction potential is lowered if the leaving group contains an electron-withdrawing function[20]. Since ethyl and other alkyl groups used in the experiments are better electron donors, their formal reduction potentials should move to the potentials more difficult to be reduced in theory, which is just opposite to what we observed in the experiments. This shift of the formal reduction potentials in cyclic voltammetry can only be explained as the steric effects especially the steric effects between the corrin ring and the ß carbon or the hydrogen connecting to the ß carbon in the alkyl groups. Cobalamins with ethyl, *n*-propyl and *n*-butyl groups have very close formal reduction potentials because they have similar steric effects of ß carbon or the hydrogens on the ß carbon.

Based on the *DPSC* results of methylcobalamin in various temperatures in chapter 8 (Fig. 8-4), a plot of Arrhenius relationship is extrapolated from low temperatures to room temperature. The following chemical reaction rate of methylcobalamin in the solvent mixture of DMF and methanol (40:60) is estimated as 5,500 sec^{-1} at 20°C. Ethylcobalamin and other alkylcobalamins, due to the stronger steric effects, have much faster rate constants of the following chemical reaction and estimation

Reproduced with permission of the copyright owner. Further reproduction prohibited without permission.

for them is beyond the scope of the presently available experimental facilities. Comparing this rate constant with others measured in DMSO (1.5×10^{3} sec^{-1})[94] and in H_2O (0.37 sec^{-1})[52] for methylcobalamin at similar room temperature, it is consistent with the solvation effect of the methyl radical leaving group on the rate of the chemical step. The lower the dielectric constant the faster the bond breaking rate was observed. The rate constant for the following chemical reaction in the solvent mixture of DMF and methanal (40:60) is about 1.5×10^{4} fold faster than the similar process in aqueous media.

Comparing the peak potential of methylcobalamin in same solvent mixture at -30°C (see chapter 7), it was shifted about 65 mV toward positive at 20°C. There are several reasons for this. In the quasi-reversible or irreversible systems, the peak potential will be shifted toward positive if the temperature increased[64]. The rate constant of the following chemical reaction will increase as the temperature increased, which will make the peak potential shift positively according to the Nernstian relationship decided by the surface concentrations of electroactive species. The temperature effects on the reference electrode may also be one of the reason for the potential shifting.

According to the Butler-Volmer equation, the electrochemical behavior of a system can be described as:

$$i(t) = nFAk^{o}[C_O(0,t)e^{\frac{-\alpha nF}{RT}(E-E^{o'})} - C_R(0,t)e^{\frac{(1-\alpha)nF}{RT}(E-E^{o'})}] \qquad (9\text{-}1)$$

where $C_O(0,t)$ and $C_R(0,t)$ represent the concentrations of electroactive species *O* and *R* at the electrode surface. If the electrochemical system is completely irreversible, the second term in the equation for $C_R(0,t)$ can be ignored, and the current is only dependent

Reproduced with permission of the copyright owner. Further reproduction prohibited without permission.

on the electrochemical behavior related to $C_O(0,t)$. In this circumstance, the electrochemical parameters (k^o, α and $E^{o'}$) in the first term can not be calculated through the simulation-fitting procedure because we can not separate them. Since the rate constants of the following chemical reaction are very fast for all alkylcobalamins in the solvent mixture of DMF and methanol at room temperature, we must estimate the available application region for simulation-fitting before further discussion. If we try different sets of electrochemical parameters (k^o, α and $E^{o'}$) and ignore the second term of Butler-Volmer equation related to $C_R(0,t)$ in simulation but always satisfy the following condition:

$$\ln k^o - \frac{\alpha n F}{RT}(E - E^{o'}) = constant \qquad (9\text{-}2)$$

we can get unlimited sets of parameters but still have the exact simulation results in the region where the electrochemical system is completely irreversible. The useful region of the simulation-fitting can be estimated, where we only change the rate constant of electron transfer, meanwhile satisfy the condition as equation (9-2) by adjusting $E^{o'}$. The peak potentials of cyclic voltammetry are used as criterion for estimation. In the region k^o is small enough so that the system is completely irreversible, exactly the same cyclic voltammograms will be obtained even k^o can be changed by several orders within the suitable range of irreversibility. While the electrochemical system is not completely irreversible, the second term in Butler-Volmer equation begins to influence the whole equation, the cyclic voltammograms, including the peak potentials of course, will certainly change even the equation (9-2) is satisfied. The useful simulation-fitting region

Reproduced with permission of the copyright owner. Further reproduction prohibited without permission.

is the quasi-reversible area where the peak potential changes as k^o changing. Simulation-fitting for methylcobalamin at room temperature (20°C) was performed, where the rate constant of the following chemical reaction, 5,500 sec^{-1}, was inputted into the digital program as a constant parameter, and the results were shown in Table 9-3 and Fig. 9-5. The useful region of simulation-fitting for this electrochemical system can be estimated through Fig. 9-6. Since the simulation-fitting result of methylcobalamin (k^o=0.016 cm/sec) is in the k^o-dependent region in Fig. 9-6, we have reason to believe this result is still in the quasi-reversible region. It is also noted the k^o measured is close to the flat area of the curve, so that the simulation-fitting method is close to its useful region limit for this electrochemical system.

The rate constant of electron transfer of methylcobalamin at 20°C was measured through simulation-fitting as 0.016 cm/sec, which is 33% larger than the value measured at -30°C in the same solvent mixture. From the Marcus' quantum mechanical theory of electron transfer at an electrode, we have[64,95]:

$$k^o = \kappa \rho \left[\frac{k_B T}{2\pi m}\right]^{1/2} e^{-\frac{\lambda_{el}}{4RT}} \qquad (9\text{-}3)$$

where κ is the velocity-weighted average of the transition probability and typically a value of $\kappa \approx 1$ is assumed[64]. For an indicated electrochemical system, ρ and m could be considered as constants[g] and k_B is a Boltzmann constant. The reorganization free energy parameter λ_{el} is calculated from a suitable model which describes the energies of solvent

---

[g] The detail for treatment of electron transfer by Marcus is given in reference 95.

Reproduced with permission of the copyright owner. Further reproduction prohibited without permission.

reorganization and bond length distortion accompanying charge transfer, generally is taken as 1/2 of the value for the corresponding homogeneous electron exchange process. If we take the corresponding Co-C bond activation energy, 5.5 kCal/mol, measured from methylcobalamin, the normalized rate constant of electron transfer k^o_n can be expressed as:

$$k_n^o = \left(\frac{T_2}{T_1}\right)^{1/2} \exp\left[\frac{\lambda_{el}}{4R}\left(\frac{1}{T_1} - \frac{1}{T_2}\right)\right] \qquad (9\text{-}4)$$

The k^o_n corresponding to 20°C and -30°C is calculated as 1.4. Since we know k^o=0.012 cm/sec at -30°C, the expected k^o at 20°C will be 0.017 cm/sec. The simulation-fitting result k^o=0.016 cm/sec is close to the calculation result.

The measured electron transfer coefficient (α=0.77) for methylcobalamin is nearly same as the value measured at -30°C (α=0.78). It also matched the value ($\alpha_{app,corr}$=0.76) calculated through equations (7-9) and (7-10) at the corresponding temperatures. The result indicates that the temperature effect will not change methylcobalamin *EC* mechanism in the solvent mixture of DMF and methanol.

Since the other alkylcobalamins (ethyl-, *n*-propyl-, *n*-butyl-, *iso*-butyl- and adenosylcobalamins) have faster rate constants of following chemical reaction, their *EC* processes are certainly more irreversible than methylcobalamin in electrochemical experiments. Because methylcobalamin is in the marginal area for simulation-fitting, it is not realistic to analyze the electrochemical behavior of these alkylcobalamins with the simulation-fitting method. On the other hand, when the rate constants of the following chemical reaction at 20°C are faster than the rate constant of methylcobalamin, *e.g.*,

Reproduced with permission of the copyright owner. Further reproduction prohibited without permission.

5.5×10^3 sec^{-1}, the electrochemical system will be in or very close to the irreversible region where k_{chem} will not affect the shape of the cyclic voltammogram. Fig. 9-7 illustrates the effects of k_{chem} change to the cyclic voltammograms. It is clear that k_{chem} will not influence much of the cyclic voltammogram if k_{chem} is larger than 1×10^4 sec^{-1} in the electrochemical system where methylcobalamin's electrochemical parameters are applied. The simulation shows if k_{chem} is changed from 10,000 sec^{-1} to 100,000 sec^{-1}, the peak potential is only shifted 2 mV positively. The region of the quasi-reversible usefulness for simulation-fitting in Fig. 9-7 is consistent with the analysis in Fig. 9-6 as the electrochemical system is in the margin of quasi-reversibility.

The heterogeneous electron transfer coefficient is related to the energy barrier for electron transfer. If electron transfer at the electrode is an outer sphere reaction then less of a steric effect on k^o will be expected, *i.e.* the alkyl substitute group will not show much change in k^o. On the other hand, the rate constant for the bond fission reaction would be expected to be very sensitive to steric effects as it is the decomposition reactions of the alkylcobalamins. It has been suggested[74] that the heterogeneous electron transfer in alkylcobalamin *EC* mechanism is accelerated by a stepwise process and the electron is initially accepted by a rather delocalized orbital. This electron-accepting orbital has not much Co-C antibonding σ^* character and is delocalized *via* a corrin localized π^* orbital. The decay of the intermediate in Scheme 7-1 is then due to an intramolecular dissociative redox reaction involving a thermal electronic transition from the corrin π^* orbital to the Co-C σ^* orbital. This two-step electron transfer mechanism was classified as intramolecular electron transfer catalysis[74]. On the other hand, the rate

Reproduced with permission of the copyright owner. Further reproduction prohibited without permission.

constant for the bond fission reaction would be expected to be very sensitive to steric effects, which was just what we observed in electrochemical experiments for these alkylcobalamin derivatives. Based on these postulates and the *CV* results that the root regions of the alkylcobalamin cyclic voltammograms are very similar in the shape and slope, the electron can be expected to add to the corrin ring or the ring conjugated system initially, then we have reason to believe that these alkylcobalamins may have the similar values of k^o. We can input methylcobalamin's k^o value and $k_{chem}=1\times10^4$ sec^{-1}, in which k_{chem} is much larger than the k_{chem} value of methylcobalamin, into the digital simulation program to simulate other alkylcobalamin derivatives' cyclic voltammograms. The simulation results for these alkylcobalamins are listed in Table 9-4. One of these simulated cyclic voltammograms, the *CV* experimental and simulation results for *iso*-butylcobalamin, is shown in Fig. 9-8.

All electron transfer coefficients calculated through simulation for alkylcobalamin derivatives are significantly larger than 0.5. This indicates that the mechanisms in reduction process for these B_{12} derivatives are similar as mentioned in Scheme 7-1. The structures of the transition state are close to their reactants and the electrochemical process on the electrode at 20°C is the same *EC* mechanism as in the low temperature. The experimental results indicate that temperature does not affect the corresponding *EC* mechanism.

The formal reduction potentials of alkylcobalamin reflect the energy of the LUMO orbital into which electron transfer occurs and would be expected to be related to charge donated into the corrin ring. The one-electron reduction to form a radical anion in which

Reproduced with permission of the copyright owner. Further reproduction prohibited without permission.

the Co-C σ^* antibonding orbital has been populated, thereby forming a three-electron or a net one-bonding-electron σ bond[96]. The formal reduction potentials of alkylcobalamin from simulation results are greatly different. Methylcobalamin has the most negative formal reduction potential; ethylcobalamin, *n*-propylcobalamin and *n*-butylcobalamin have more positive but similar formal reduction potentials. The $E^{o'}$ positive shift of 114 mV from methylcobalamin to ethylcobalamin is a little larger than the expected value for a single base-on/base-off form if we compare the same observation with other group's results. It was shown the similar shift of 60 mV by linear scan voltammetry in DMF solvent[74] and of 20 mV by polarography in aqueous solvent[20]. Since Lexa and Saveant have confirmed that methylcobalamin in similar solvent mixture is in base-on form by comparing the electrochemical behavior with methylcobinamid[49], combined with the fact that ethyl has both stronger electron-donor and steric effects, we postulate the ethylcobalamin reduction peak is in base-off form. To the same reason, *n*-propyl, *n*-butyl, *iso*-butyl and adenosylcobalamins should also be in the base-off form. The more positive shift for *iso*-butylcobalamin and adenosylcobalamin may be due to stronger steric effect between ligand group and the corrin ring than that in ethyl, *n*-propyl and *n*-butyl-cobalamins. This result is consistent with the observation by single scan voltammetry of hydroxocobalamin in presence of the corresponding alkyl halides in DMF solvent[74]. According to the polarographic experiments, the electron-donor group shifts the formal reduction potential negatively; whereas the steric hindrance tends to shift the reduction potentials to more positive probably *via* a lengthening of the Co-C bond that also translates into a ^{59}Co-NMR chemical shift[97]. From methyl to ethyl, *n*-propyl, *n*-butyl

Reproduced with permission of the copyright owner. Further reproduction prohibited without permission.

and *iso*-butyl, the alkyl electron-donor property is increased which makes the $E^{o'}$ shift negatively in theory; meanwhile the steric effect should make the $E^{o'}$ shift positively. Since the $E^{o'}$ is shifted positively in the experiments, we have reason to believe the steric effect dominates the formal reduction potentials of alkylcobalamin.

9.4.2 Experiments in Aqueous Media

Methylcobalamin electrochemical behavior in aqueous basic media was investigated through digital simulation. In order to avoid the strong adsorption on the electrode, surfactant Triton *X*-100 was used. The adsorption can be greatly depressed by exactly right amount of surfactant. Stationary mercury electrodes were used where the mercury was stuck on the silver or gold electrodes. All potentials in aqueous media were referred to AgCl/Ag aqueous reference electrode (Bioanalytical Systems). The procedure depositing mercury on silver electrode of normal size (1.6 mm in diameter) was described previously (Chapter 7). The *CV* simulation results of methylcobalamin in aqueous media at *pH* 13.0 are shown in Fig.9-9. The simulation electrochemical parameters are: $E^{o'}$=-1.200 Volt, k^o=0.020 cm/sec, α=0.88 and k_{chem}=0.20 sec^{-1}. To confirm the diffusion control in the electrode process, the experiments of scan rate *vs.* peak current were performed. The linear relationship and the slope in Fig.9-10 indicates the diffusion control mostly in this system. A comparison shows that the electron transfer rate constant is slightly higher in aqueous media than that in nonaqueous media at similar temperature. This result is to be expected because the electron transfer step involves the formation of a charged species which should be stabilized in more polar solvent[94].

Reproduced with permission of the copyright owner. Further reproduction prohibited without permission.

The rate constant of the following chemical reaction for ethylcobalamin in aqueous media was measured through *DPSC* with microelectrode as 3100 sec^{-1} at 20°C shown in Fig. 9-11. The measured k_{chem} for ethylcobalamin is much larger than that of methylcobalamin in the same aqueous media, but it is in the same order of adenosylcobalamin reported[52]. The steric effect, especially the ß carbon and the hydrogens connecting to the ß carbon, must play an important role here. The experiment was carried out by the home-built electrochemical system (Chapter 2) and was made in a Faraday cage to reduce the noise pick-up. Because of the small size of microelectrode, the double layer capacitance is greatly reduced. This allows the electrode potential to be changed rapidly and permits *DPSC* measurements to be made on microsecond time scale for much faster fission rate constant of ethylcobalamin. Chronoamperometric response on the microelectrode in the potential step process has following *i-t* relationship[98]:

$$i_c = \frac{4nFC_o r_o}{1+\xi}\left[\left(\frac{\pi}{4\tau}\right)^{\frac{1}{2}} + \frac{\pi}{4} + 0.094\tau^{\frac{1}{2}}\right] \qquad (9\text{-}5)$$

where r_o is the radius of the microelectrode, $\xi = \exp[nF(E-E^{o'})/RT]$ and $\tau = (4D_o t)/r_o^2$. If t is in a short time scale and ξ is ignored when the applied potential well beyond the formal reduction potential, then equation (9-5) will tend toward equation (7-2). On this circumstance, the electrode radius is larger than the thickness of diffusion layer so that relationship of (7-2) to (7-4) for planar diffusion control can be applied. The way depositing mercury by activating electrode surface (Chapter 6) can not be used here because microelectrode is easily pitted in the process. Then electrochemical deposit method was applied. It is important to ensure the smooth spreading of the mercury

Reproduced with permission of the copyright owner. Further reproduction prohibited without permission.

during the electrodeposition. The choice of electrode material influences the fabrication of a well-covered electrode[99]. On platinum electrode, the wetting process is slow and the mercury electrodeposition process may form one or more isolated drops which do not cover the entire surface[100]. For mercury deposition on a carbon disk electrode, the deposition process is very non-reproducible and usually results in failure of the drop to adhere to the carbon[101]. Gold and silver are more easily wetted by mercury than platinum because they can form Au-Hg or Ag-Hg amalgam. However, to enhance the rate of wetting for a silver microelectrode, it is necessary to apply an oxidizing pre-pulse to form silver cation[102]. Gold wetting process is fast and quite simple. After the electrode is polished, it can be directly wetted without any other pretreatment[99]. For all these reasons, the choice in this experiment was gold microelectrode (10 μm in diameter, Bioanalytical Systems). A deoxygenated solution of 0.25 M $HClO_4$ containing 5.0 mM $Hg_2(ClO_4)_2$ was used for the mercury deposition by application of a constant potential of -50 mV *vs.* Ag/AgCl reference electrode for 50 sec. This applied potential ensures Hg(I) reduction but it is too low for the reduction of most other metal ions if they are present in trace amount. The *i-t* curve was monitored to ensure proper coverage of the mercury on the gold microelectrode. This mercury deposited microelectrode is relatively durable and rugged. It can normally be washed repeatedly with deionized-distilled water or left in solution while being deoxygenated with a nitrogen stream without loss of the mercury.

9.4.3 Conclusion

The reductive electrochemistry of methylcobalamin and other B_{12} derivatives in

Reproduced with permission of the copyright owner. Further reproduction prohibited without permission.

non-aqueous solution is typical of many electrochemical mechanisms. The methods developed here (cyclic voltammetry, double potential step chronoamperometry and data analysis) can be used in many similar systems. The results are satisfactory with small error especially in the measurement of formal reduction potential when the electrochemical system is quasi-reversible. Even if the electrochemical system is irreversible, careful data analysis still can give some useful information. The simulation method also confirms the curve measurement method for electron transfer coefficient and the precise data of α support the B_{12} *EC* mechanism proposed. The results of various B_{12} derivatives indicate that the steric effects play an important role in their *EC* process. The similar slope and shape near the *CV* curve root region suggest that these B_{12} derivatives may have similar k^o values and so that a two-step electron transfer mechanism[74] is reasonably postulated to explain the electron transfer process. These results may be used to better explain the mechanism for the B_{12}-dependent methionine synthesis in biochemistry.

Recently there have been carried out experiments concerning the relevance of the reductive cleavage mechanism of electron transfer with Co-CH_3 for methylcobalamin dependent enzymatic reactions[67,96,103]. A comparison of the chemical rate constant measured for the *EC* mechanism with the rate constant for homolytic solution cleavage shows an enormous enhancement about 10^{15} after one electron addition, *i.e.* in the process of the reductive cleavage of the Co-C bond. The lowest unoccupied molecular orbital (LUMO) of alkylcobalamins is the σ^* orbital lying along the C-Co bond perpendicular to the corrin system; it and the highest occupied molecular orbital (HOMO)

Reproduced with permission of the copyright owner. Further reproduction prohibited without permission.

are formed from interaction of the alkyl sp^3 orbital with the cobalt d orbital. It is noted that interaction with the nitrogen frontier orbital of the corrin ring and the axial base does not change the relative order of the HOMO and LUMO. Electrochemical reduction of alkylcobalamin promotes the rate of dissociation of Co-C bond through the bond-weakening effect as the electron entering the Co-C antibonding σ^* LUMO. A comparison of activation parameters available for $(\sigma)^2$ and reduced $(\sigma)^2(\sigma^*)^1$ of methylcobalamin reveals that an antibonding electron greatly lowers the Co-C bond strength[96] because non-axial structural distortions and electronic rearrangements are minimized by the approximately square-planar corrin ligand[104]. This antibonding effect of an extra electron in the σ^* LUMO along the C-Co bond facilitates methyl radical dissociation from the cobalt and promotes the key Co-C homolysis rate. Enzymes also greatly enhance the rate of Co-C bond breaking. In principle, the electron-transfer process could explain the rapidity of cobalamin-dependent enzyme processes if one could find a biological electron source at a sufficiently reducing potential. However, it is not likely postulated for four major reasons by Martin and Finke[96]. Because the reduction potentials of various alkylcobalamins are so negative (-1.2 to -1.5 volt *vs.* Ag/AgCl non-aqueous reference electrode), it has been concluded that alkylcobalamins are not reducible by biological reductants so that the biological electron transfer can not be the activating mechanism for alkylcobalamin bond cleavage[67,94,96,105]. On the other hand, it is to be expected that holoenzyme binding lowers the reduction potential by displacement of the dimethylbenzimidazole axial base and other structural changes so that the LUMO energy of the σ^* antibonding orbital is lowered[94]. The methyl transfer reactions were also found

Reproduced with permission of the copyright owner. Further reproduction prohibited without permission.

to occur rapidly between cob(III)inamides and cob(II)inamides as well as cob(I)inamides in aqueous solution. These methyl transfer reactions were found to occur without formation of free methyl radicals and were classified as methyl bridged electron transfer reactions[106-107]. The intrinsic binding energy of the alkylcobalamin-enzyme-substrate complex is then invoked to explain catalytic Co-C activation[105,108]. It has been found that the homolysis in adenosylcobalamin proceeds 10 orders of magnitude faster in the enzymatic reaction than that in an enzyme-free environment[68-69,109]. Although the methylcobalamin-enzyme may be probably not reduced in an outer sphere step of electron transfer, it is certainly possible that the enzymatic transfer of a methyl group to homocysteine to form methionine goes by an inner sphere single electron transfer mechanism[94,110]. Such a mechanism involves an electron transfer from the mercapto group of homocysteine to enzyme bound methylcobalamin followed by radical coupling to form methionine and vitamin B_{12s}:

$$R\text{-}S:^- + CH_3\text{-}B_{12}\text{-}enzyme \rightarrow [R\text{-}S^{\cdot}(^{\cdot}CH_3\text{-}B_{12}\text{-}enzyme)^-]$$
$$\rightarrow R\text{-}S\text{-}CH_3 + B_{12s}^- + enzyme \qquad (9\text{-}6)$$

where $R\text{-}S:^-$ represents homocysteine and $R\text{-}S\text{-}CH_3$ represents methionine. In the conventional view, reaction (9-6) is represented as an S_N2 nucleophilic displacement reaction involving a carbonium ion transfer[103]. According to Pross and Shaik, the S_N2 mechanism can always be viewed as single electron transfer pathway[110]. The main difference between the single electron transfer and conventional mechanism is whether radical intermediates are formed after the single electron shift[110], *i.e.* the radical intermediates $R\text{-}S\cdot$ and $\cdot CH_3$. The large increase in the rate constant of the following

Reproduced with permission of the copyright owner. Further reproduction prohibited without permission.

chemical reaction in nonaqueous solvents observed in solvent mixture of DMF and methanol suggests a nonaqueous protein dielectric environment for the enzymatic methyl group transfer reaction if a radical mechanism is involved. The postulation needs to be further investigated through structural and kinetic studies of enzyme-methylcobalamin complex with thiols to see if the validity of a radical mechanism can be established[94].

Reproduced with permission of the copyright owner. Further reproduction prohibited without permission.

Words[14]	Y
0	0.25
1	0.50
2	1.00
3	2.50
4	5.00
5	10.0
6	25.0
7	50.0
8	100.0
9	250.0

Table 2-1 The F factor and its representative values

Words[13]	Sample Interval	Sweep Time
7	40 ns	5.0 μs/Div
8	80 ns	10.0 μs/Div
9	160 ns	20.0 μs/Div
10	400 ns	50.0 μs/Div
11	800 ns	0.1 ms/Div
12	1.6 μs	0.2 ms/Div
13	4.0 μs	0.5 ms/Div
14	8.0 μs	1.0 ms/Div
15	16.0 μs	2.0 ms/Div
16	40.0 μs	5.0 ms/Div
17	80.0 μs	10.0 ms/Div
18	160.0 μs	20.0 ms/Div
19	400.0 μs	50.0 ms/Div
20	800.0 μs	0.1 s/Div
21	1.6 ms	0.2 s/Div
22	4.0 ms	0.5 s/Div

Table 2-2 The relationship of the sample interval and the sweep time

Reproduced with permission of the copyright owner. Further reproduction prohibited without permission.

Input bias current	50 pA
Input noise voltage	16 nV/(Hz)$^{1/2}$
Input noise current	0.01 pA/(Hz)$^{1/2}$
Gain bandwidth	4 MHz
Slew rate	13 V/μsec
Input impedance	10^{12} Ω
Supply voltage	$\pm$ 18 V
Power dissipation	500 mW
Input voltage range	$\pm$ 15 V
$T_{j(MAX)}$	115 °C
Operating temperature range	0 to 70 °C

Table 2-3 The major features of 353 operational amplifier

Reproduced with permission of the copyright owner. Further reproduction prohibited without permission.

Noise Source	Representation
Johnson noise from R_f	$e_{n1} = (4k_BTR_f B)^{1/2}$
Amplifier current noise	$e_{n2} = i_n R_f B^{1/2}$
Johnson noise from R_u	$e_{n3} = (4k_BTR_uB)^{1/2}(Z_f/Z_i)$
Amplifier voltage noise	$e_{n4} = e_n(1+Z_f/Z_i)B^{1/2}$
Noise from potential control circuit	$e_{n5} = e_{pc}(Z_f/Z_i)B^{1/2}$

Table 2-4 The noise sources and their representations

Temp (°C)	$E_{3/4}$-$E_{1/4}$(exp)	$E_{3/4}$-$E_{1/4}$(theory)	State Observed
30	56 ± 1 mv	57.4 mv	liquid
20	51 ± 1 mv	55.5 mv	liquid
10	50 ± 2 mv	53.6 mv	frozen
0	50 ± 5 mv	51.7 mv	frozen

Table 3-1 CV wave width ($E_{3/4}$-$E_{1/4}$) on microelectrode in DMSO-electrolyte system at various temperatures

Reproduced with permission of the copyright owner. Further reproduction prohibited without permission.

Temperature (°C)	τ_{cor} (sec x 10^{10})	DMSO State Observed
20	0.158	liquid
15	0.334	frozen
5	0.797	frozen
0	1.35	frozen
-5	1.14	frozen
-10	1.35	frozen
-15	2.00	frozen
-20	3.14	frozen
-30	9.29	frozen
-40	69.9	frozen

Table 4-1 The relationship of the rotational correlation time and temperature

Reproduced with permission of the copyright owner. Further reproduction prohibited without permission.

Temperature (°C)	$\Delta P_{a,c}$ (mv)	DMSO State Observed
10	67	liquid
0	68	liquid
-10	63	liquid
-20	62	liquid
-27	61	frozen
-30	61	frozen
-35	62	frozen
-40	62	frozen
-45	62	frozen
-50	68	frozen
-55	76	frozen
-60	94	frozen

Table 5-1 The peak separation of ferricyanide in DMSO-H_2O-NaCl system at different temperatures

Reproduced with permission of the copyright owner. Further reproduction prohibited without permission.

Rate (mV/s)	$E^{o'}$ (V)	k^o (cm/s)	α	A 10^{-2} cm^2	χ^2 10^{-13} $ampere^2$	Iteration
50	-1.529	0.012	0.79	1.9	1.0	125
50	-1.533	0.014	0.75	1.9	1.1	72
100	-1.524	0.010	0.80	2.0	2.2	102
100	-1.523	0.010	0.80	2.0	2.1	95
300	-1.530	0.012	0.77	1.9	7.9	100
300	-1.532	0.013	0.75	1.9	7.0	120
	-1.529 ± 0.004	0.012 ± 0.002	0.78 ± 0.02	1.9 ± 0.006		

Table 7-1 Simulation-fitting results of methylcobalamin

Reproduced with permission of the copyright owner. Further reproduction prohibited without permission.

Rate (mv/sec)	α_{app}	$\alpha_{app,corr}$	α_{fit}	f_r
300	0.72	0.80	0.76	0.18
	0.71	0.80		
	0.71	0.80		
	0.71	0.80		
100	0.76	0.83	0.80	0.20
	0.78	0.84		
	0.78	0.84		
	0.78	0.84		
50	0.81	0.85	0.77	0.21
	0.81	0.86		
	0.81	0.86		
	0.81	0.86		

Table 7-2 The various measurements of α

Reproduced with permission of the copyright owner. Further reproduction prohibited without permission.

RX	k ($mol^{-1}sec^{-1}$)
CH_3Cl	5.0
CH_3CH_2Cl	4.7×10^{-2}
$CH_3(CH_2)_2Cl$	3.7×10^{-2}
$CH_3(CH_2)_3Cl$	2.8×10^{-2}
$CH_3(CH_2)_4Cl$	2.5×10^{-2}
$CH_3(CH_2)_5Cl$	2.6×10^{-2}
$(CH_3)_2CHCH_2Cl$	4.1×10^{-3}
CH_3Br	1.6×10^{3}
CH_3CH_2Br	3.1×10^{1}
$CH_3(CH_2)_2Br$	1.4×10^{1}
$(CH_3)_2CHBr$	1.8
$(CH_3)_2CHCH_2Br$	2.1
$(CH_3)_3CCH_2Br$	9.6×10^{-2}
$(CH_3)_2CH(CH_2)_2Br$	5.2
CH_3I	3.4×10^{4}
$(CH_3)_2CHI$	2.3×10^{2}

Table 9-1 The second-order rate constants for the reaction of B_{12s} with alkyl halides

Reproduced with permission of the copyright owner. Further reproduction prohibited without permission.

Compounds	R_f (solvent 1)	R_f (solvent 2)
cynolcobalamin	1.0	1.0
coenzyme-B_{12}	0.74 (0.75)	0.74 (0.73)
methylcobalamin	1.2 (1.25)	1.3 (1.6)
n-butylcobalamin	1.4 (1.5)	2.2 (2.4)

Table 9-2 Paper chromatographic results of alkylcobalamins

Rate (mV/s)	$E^{o'}$ (V)	k^o (cm/s)	α	A 10^{-2} cm^2	χ^2 10^{-13} ampere^2	Iteration
300	-1.466	0.017	0.76	2.0	2.6	227
300	-1.461	0.015	0.77	2.0	2.4	274
Average	-1.464	0.016	0.77	2.0		

Table 9-3 Simulation-fitting results for methylcobalamin at 20°C

Reproduced with permission of the copyright owner. Further reproduction prohibited without permission.

Compounds	$E^{o'}$ (Volt)	α_{sim}
Methyl-B_{12}	-1.464	0.77
Ethyl-B_{12}	-1.350	0.84
n-Propyl-B_{12}	-1.351	0.79
n-Butyl-B_{12}	-1.366	0.68
iso-Butyl-B_{12}	-1.320	0.61
Adenosyl-B_{12}	-1.308	0.63

Table 9-4 Simulation results of alkylcobalamins at 20°C

Reproduced with permission of the copyright owner. Further reproduction prohibited without permission.

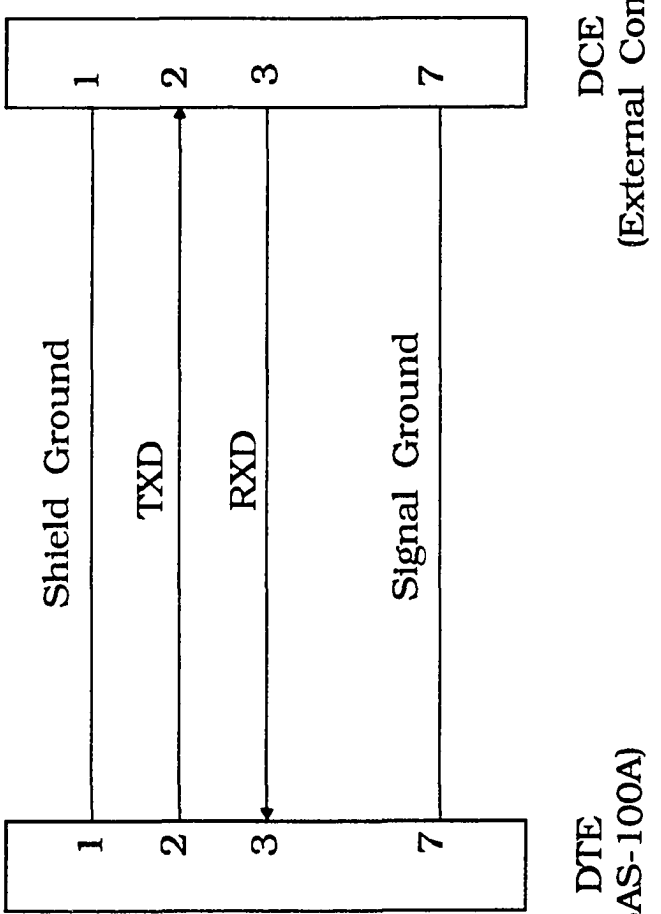

Fig. 1-1

Reproduced with permission of the copyright owner. Further reproduction prohibited without permission.

```
◄:10F80000E80300000100E803DC050101F401003019
◄:10F81000D0372C01020000000A0001000500100191
◄:10F82000EE58EE586645FE7F4F00E87C0100000070
◄:10F8300000000000000008110000DA000000640A67
◄:10F8400002000000080180030000A00A24850F8B2
◄:10F850000000000000000000000000000000000A8
◄:10F860000000000000000E803E803744D563B70
◄:10F8700000452D374D2048454D494E2B314D4D20EB
◄:10F88000233633342C452F545249532C47432C31C3
◄:10F890004D4D000306000204020102010600020 9A8
◄:10F8A0000101B201000300010101000000100009C
◄:10F8B000000001020100001092146400140001 3CD9
◄:10F8C000000000000000020030832806272825E1
◄◄:103000004B7D4C7D4D7D4D7D4D7D4E7D4E7D4E7D70
◄:103010004E7D4E7D4E7D4E7D4E7D4E7D4E7D4E7D58
◄:103020004D7D4D7D4D7D4D7D4C7D4C7D4B7D4B7D56
◄:103030004B7D4B7D4B7D4B7D4B7D4A7D4A7D497D54
◄:10304000497D487D487D487D487D477D477D477D5A
◄:10305000477D467D467D467D467D457D457D447D5B
◄:10306000447D437D437D427D427D417D417D407D68
◄:10307000407D3F7D3F7D3F7D3E7D3E7D3D7D3D7D75
◄:103080003C7D3C7D3B7D3B7D3B7D3A7D3A7D397D82
◄:10309000397D397D397D397D397D397D387D81
◄:1030A000387D377D377D367D367D357D347D347D89
◄:1030B000347D347D347D347D337D337D337D327D8D
◄:1030C000327D317D317D317D317D317D307D90
◄:1030D000307D307D307D2F7D2F7D2F7D2F7D8C
◄:1030E0002F7D2F7D2F7D2F7D2F7D2F7D2F7D2F7D80
◄:1030F0002F7D2F7D2E7D2E7D2E7D2D7D2D7D2C7D7A
◄:103100002C7D2B7D2B7D2B7D2A7D2A7D297D297D84
◄:10311000297D297D297D287D287D287D287D287D84
◄:10312000287D277D277D267D267D257D247D247D88
◄:10313000237D237D227D227D217D207D1F7D1F7D9E
◄:103140001E7D1E7D1E7D1E7D1E7D1D7D1D7D1D7DAA
◄:103150001D7D1D7D1D7D1D7D1D7D1D7D1D7D1C7DA0
◄:103160001C7D1B7D1B7D1A7D1A7D197D197D197DA6
◄:10317000187D187D177D177D177D167D167D157DB1
◄:10318000157D157D147D147D137D137D127D127DBB
◄:10319000117D117D117D117D117D117D107DC0
◄:1031A000107D107D107D107D107D107D107D107DB7
◄:103210000A7D0A7D097D087D087D087D077D
◄:000000000000
```

Fig. 1-2

Reproduced with permission of the copyright owner. Further reproduction prohibited without permission.

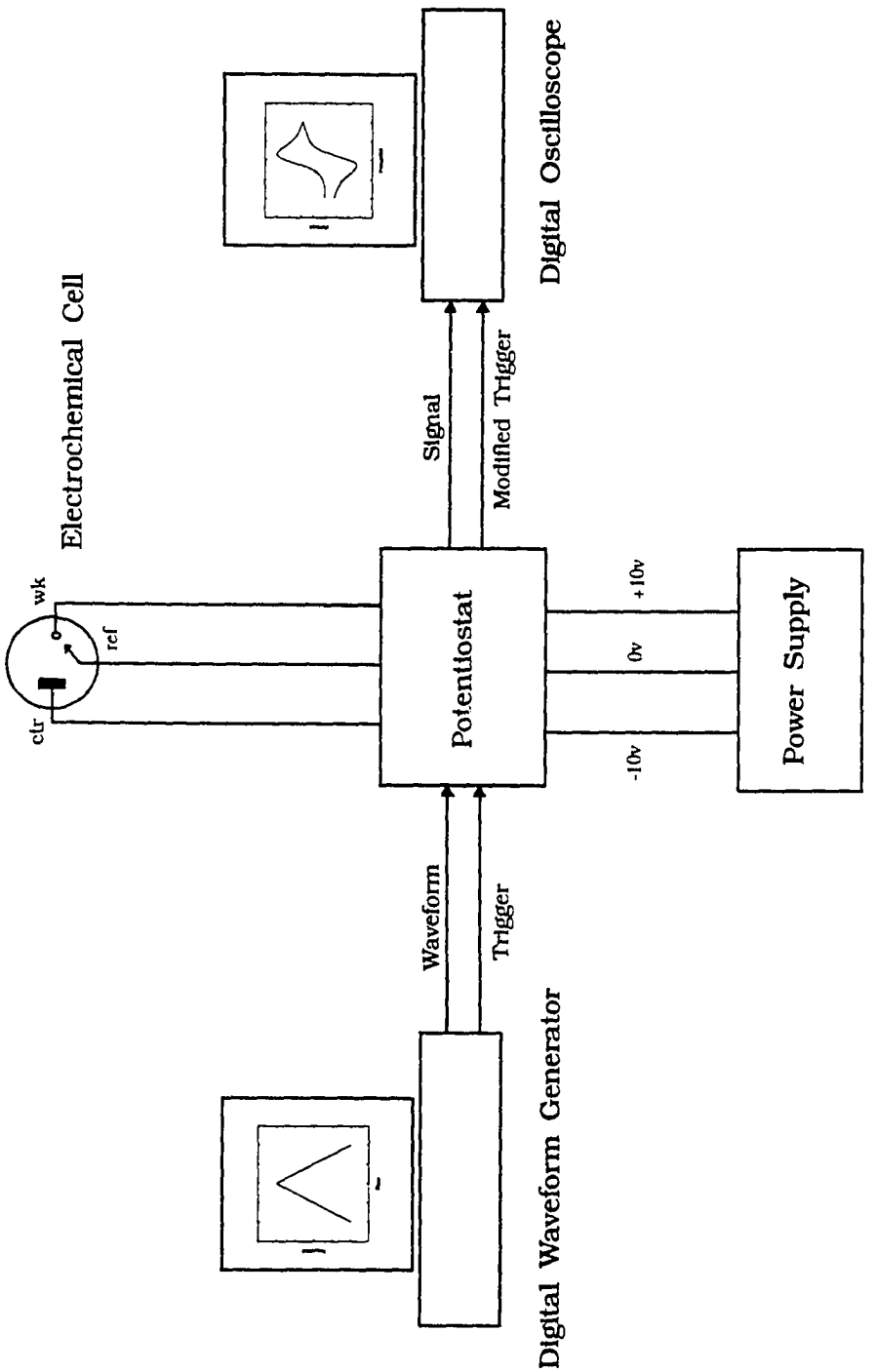

Fig. 2-1

Reproduced with permission of the copyright owner. Further reproduction prohibited without permission.

Reproduced with permission of the copyright owner. Further reproduction prohibited without permission.

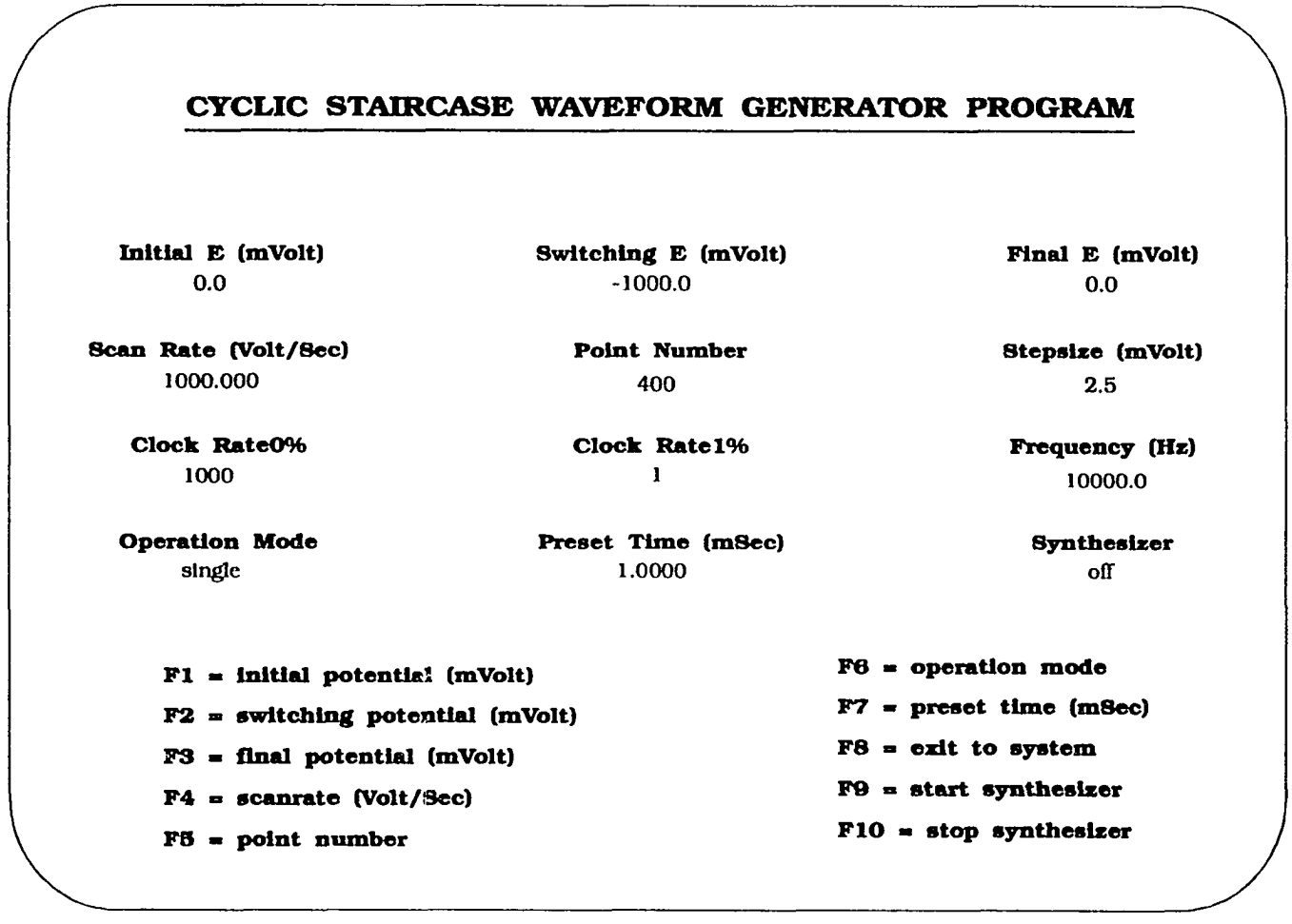

Fig. 2-2

Reproduced with permission of the copyright owner. Further reproduction prohibited without permission.

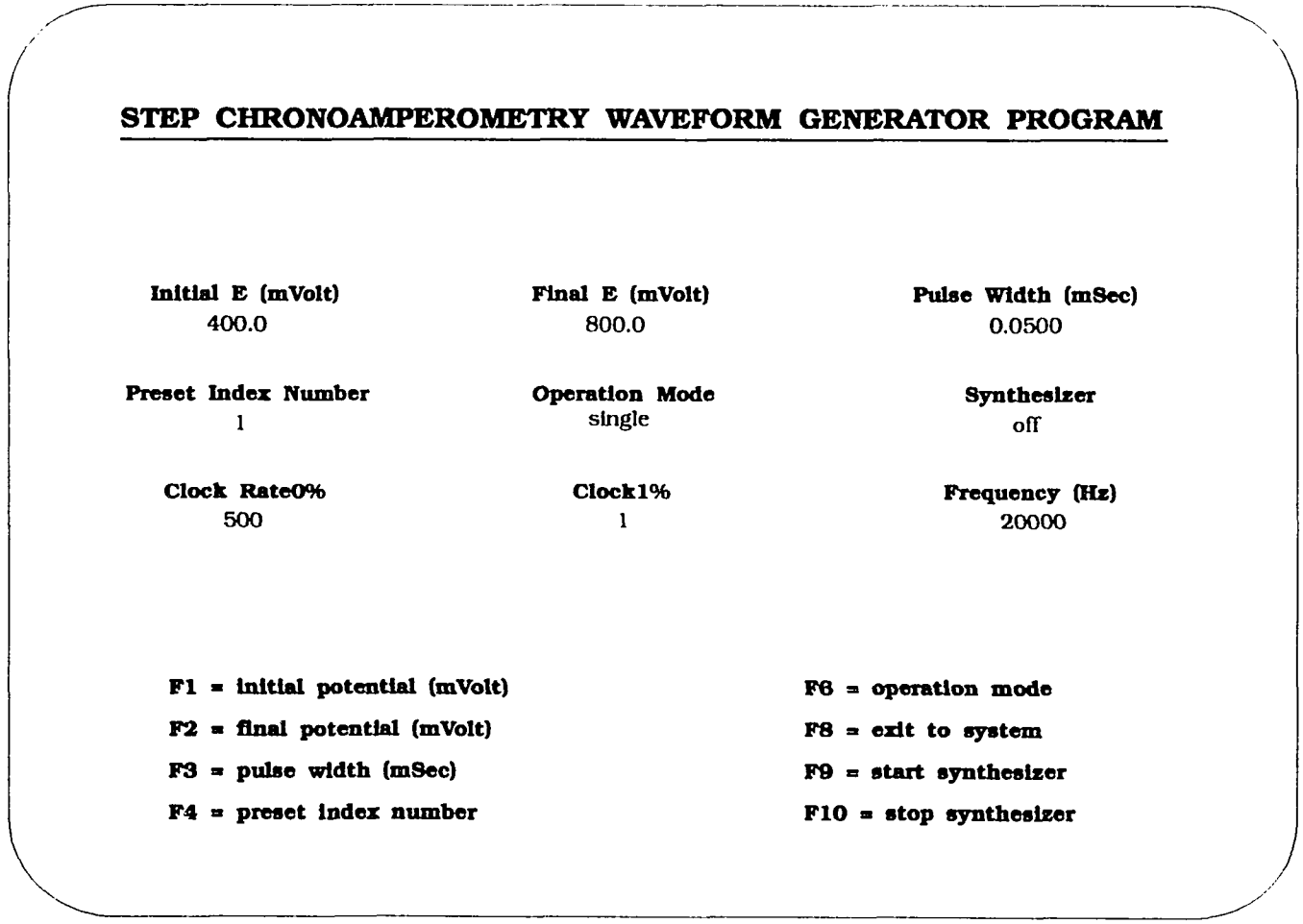

Fig. 2-3

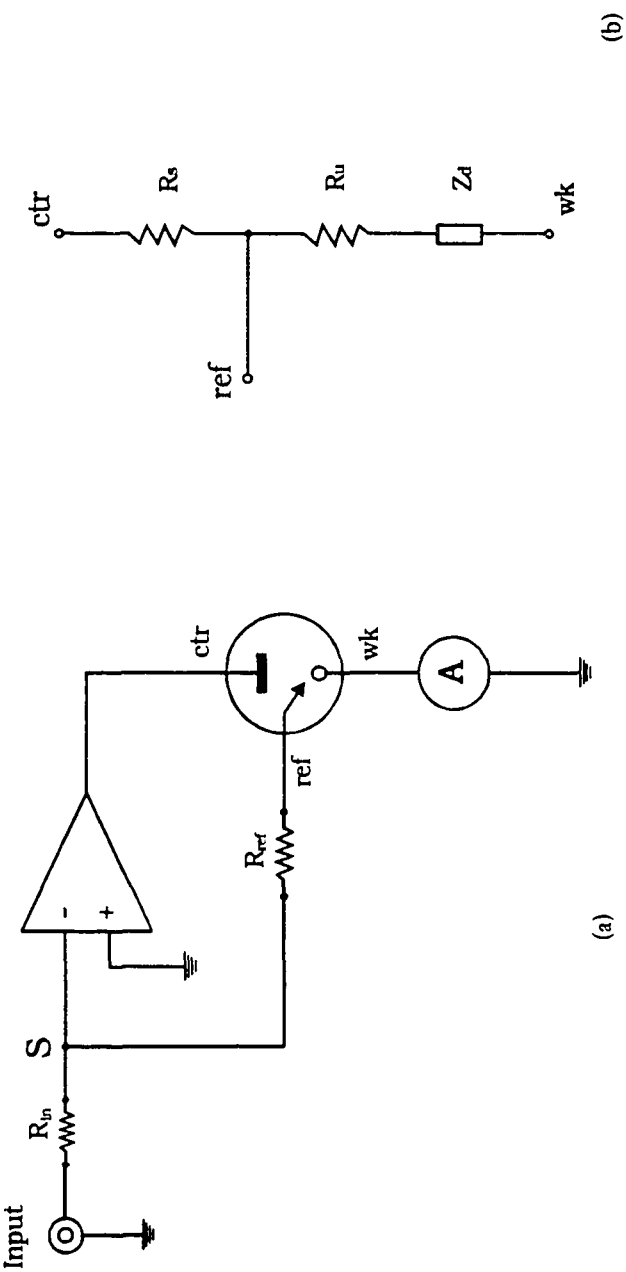

Fig. 2-4

Reproduced with permission of the copyright owner. Further reproduction prohibited without permission.

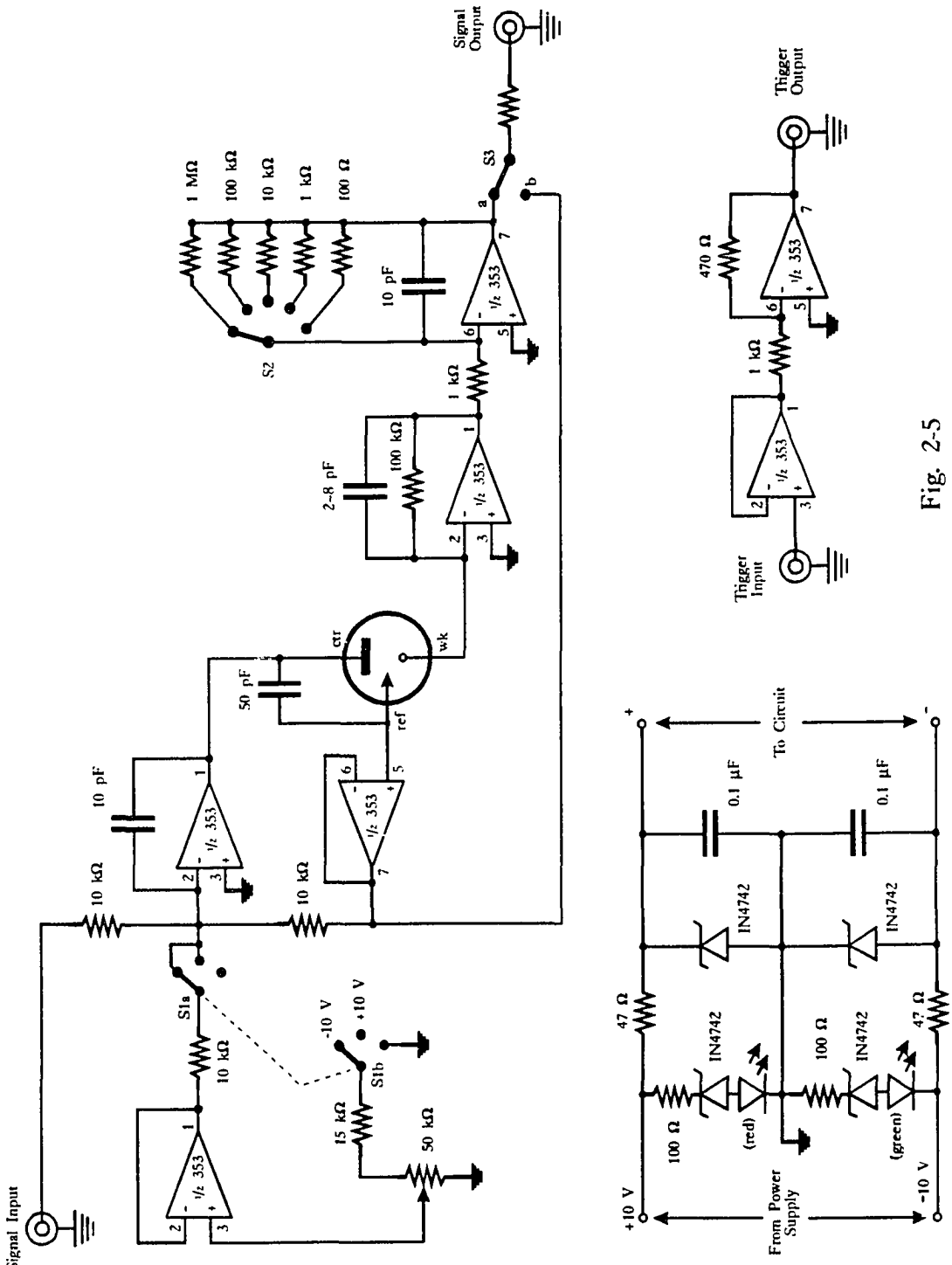

Fig. 2-5

Reproduced with permission of the copyright owner. Further reproduction prohibited without permission.

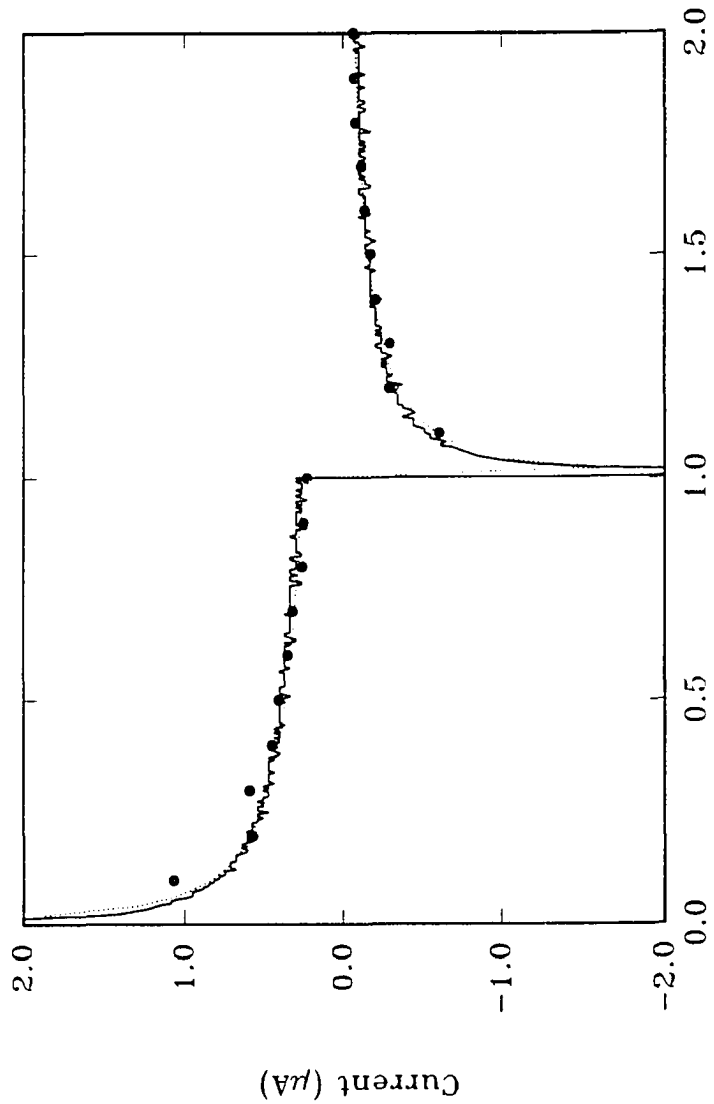

Fig. 2-6

Reproduced with permission of the copyright owner. Further reproduction prohibited without permission.

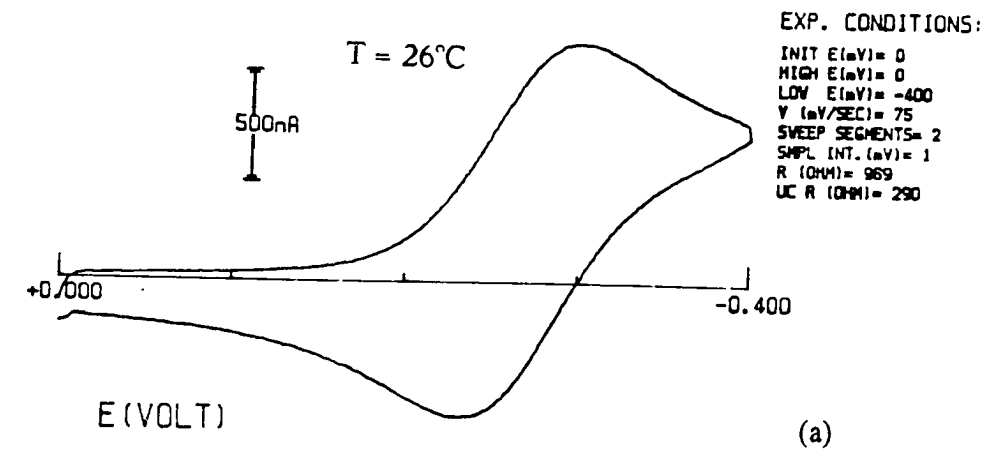

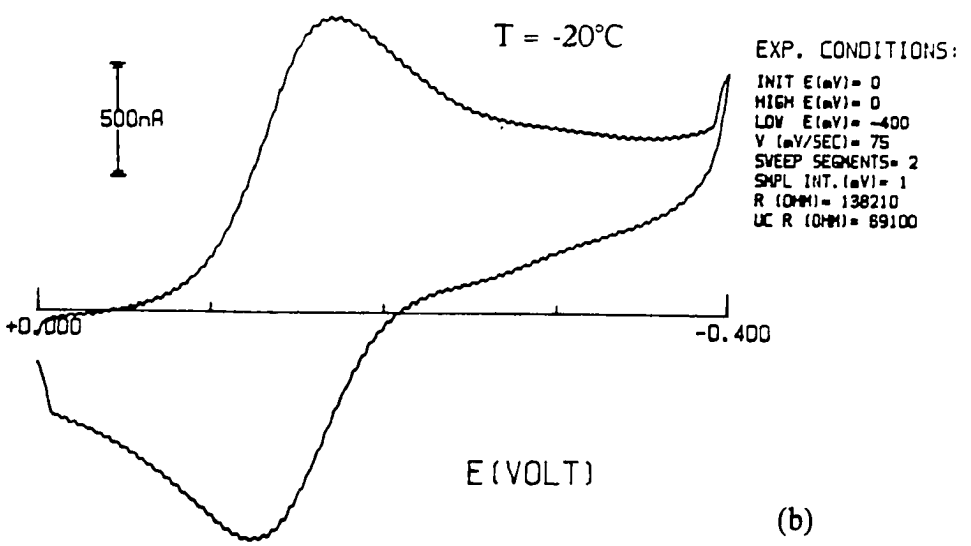

Fig. 3-1

Reproduced with permission of the copyright owner. Further reproduction prohibited without permission.

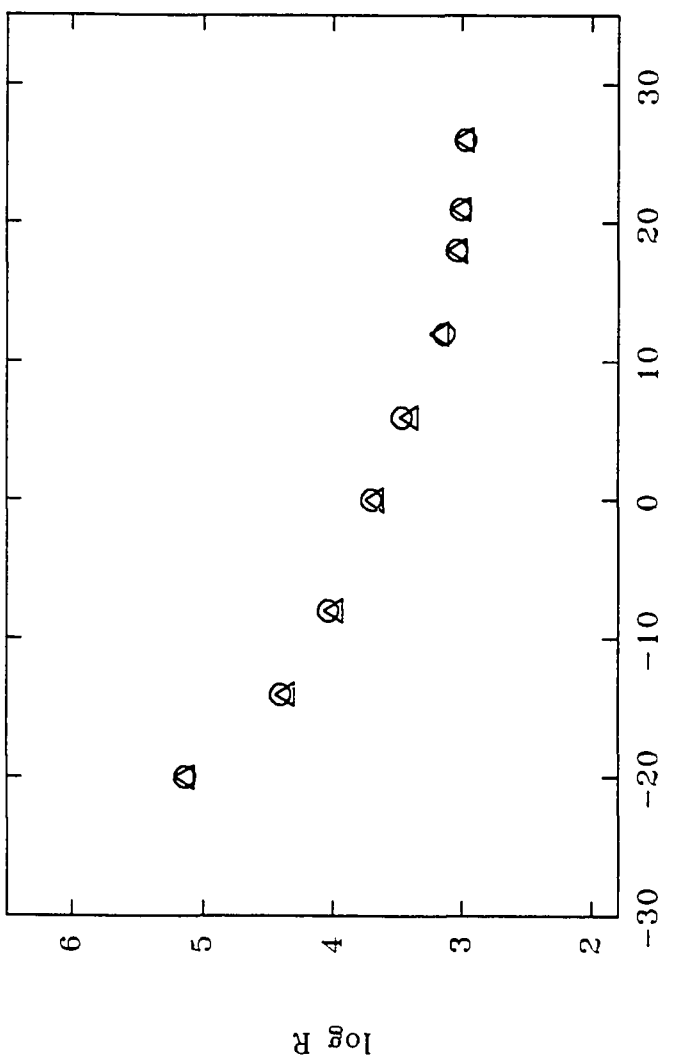

Fig. 3-2

Reproduced with permission of the copyright owner. Further reproduction prohibited without permission.

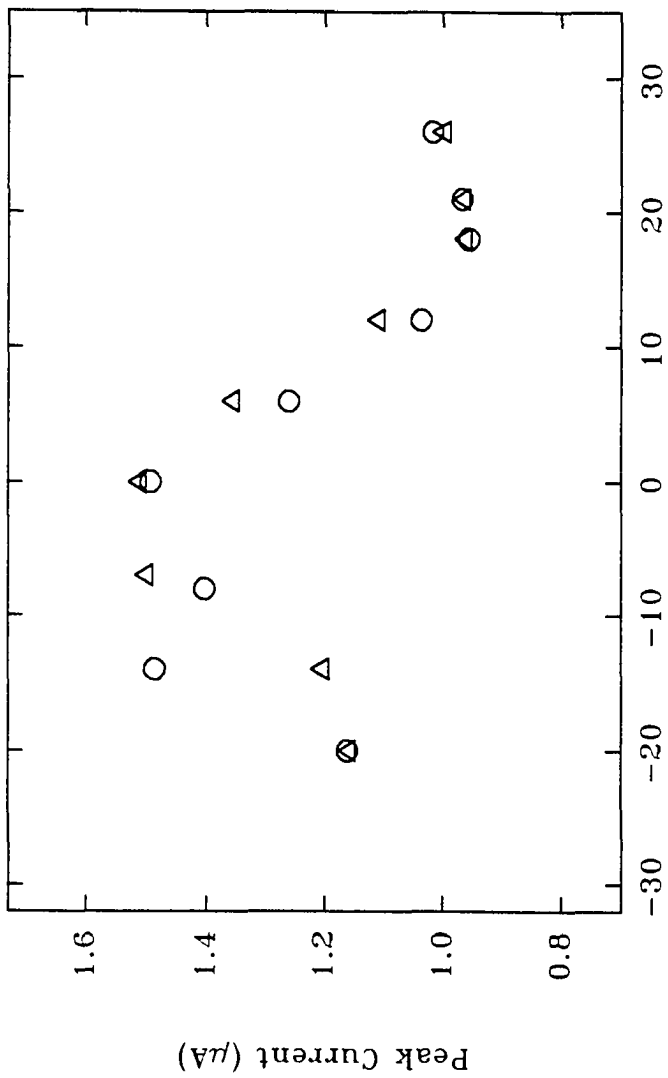

Fig. 3-3

Reproduced with permission of the copyright owner. Further reproduction prohibited without permission.

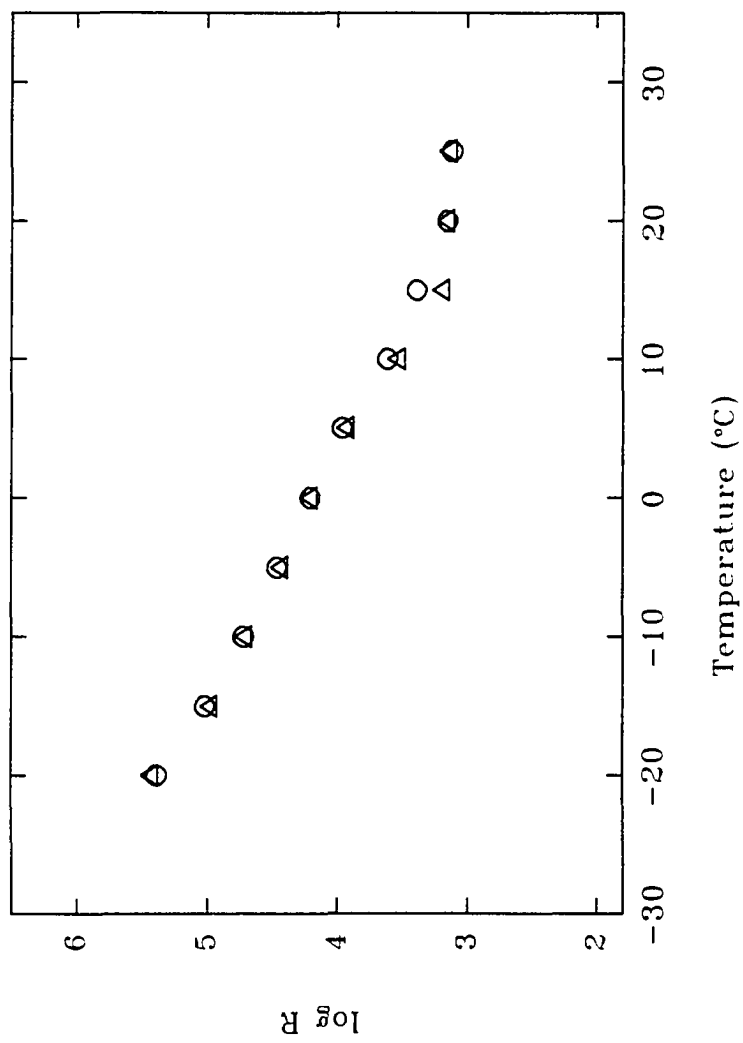

Fig. 3-4

Reproduced with permission of the copyright owner. Further reproduction prohibited without permission.

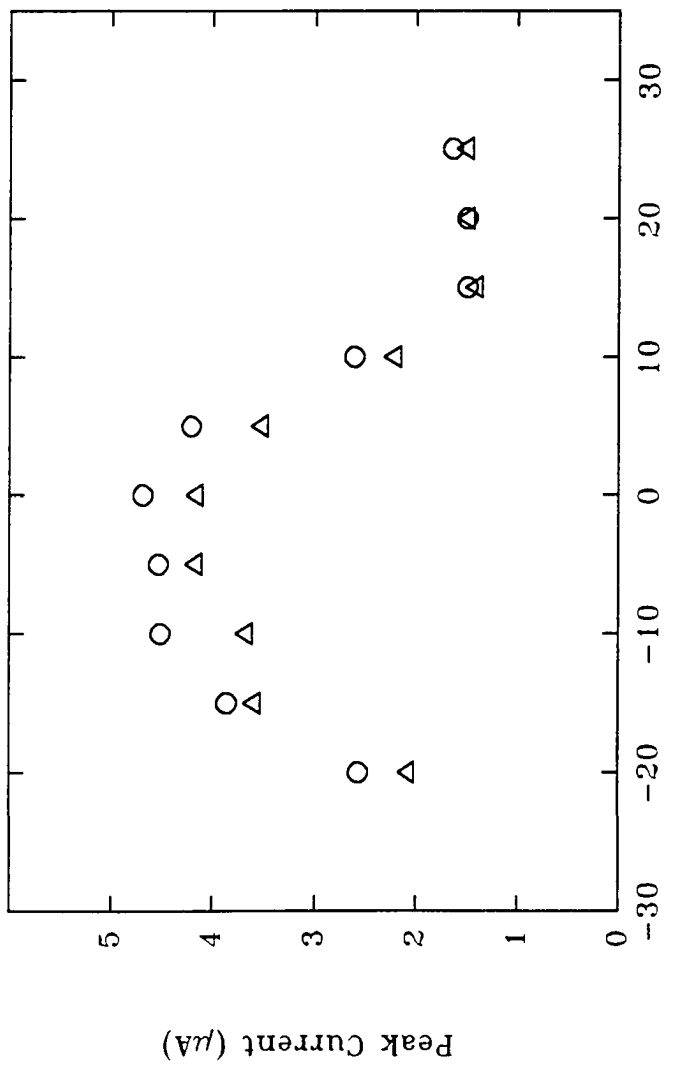

Fig. 3-5

Reproduced with permission of the copyright owner. Further reproduction prohibited without permission.

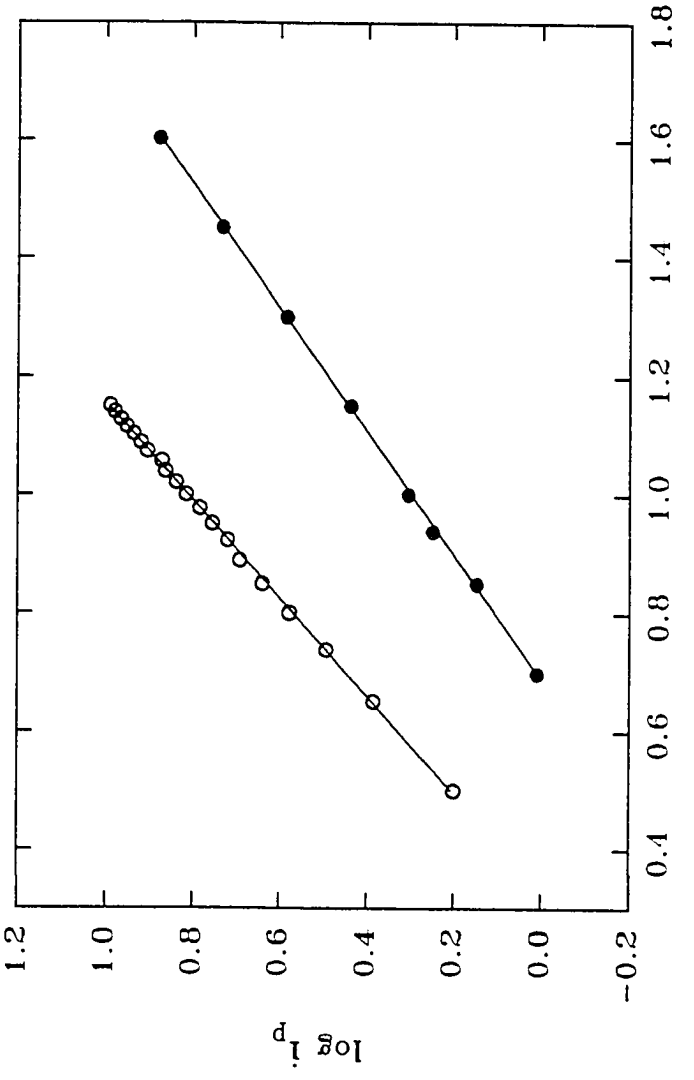

Fig. 3-6

Reproduced with permission of the copyright owner. Further reproduction prohibited without permission.

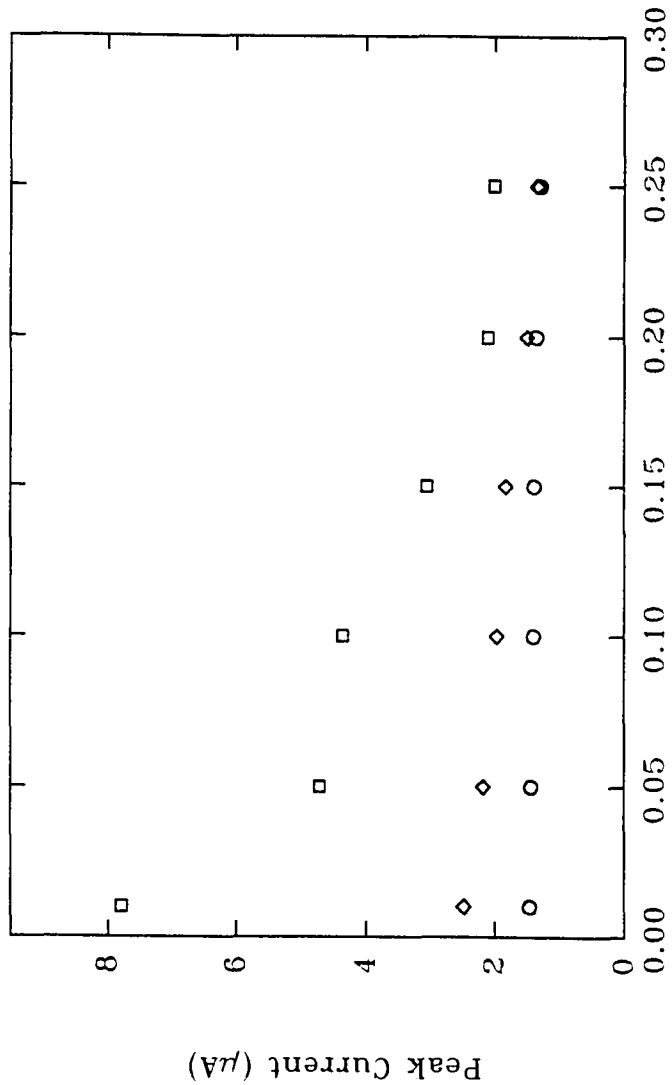

Fig. 3-7

Reproduced with permission of the copyright owner. Further reproduction prohibited without permission.

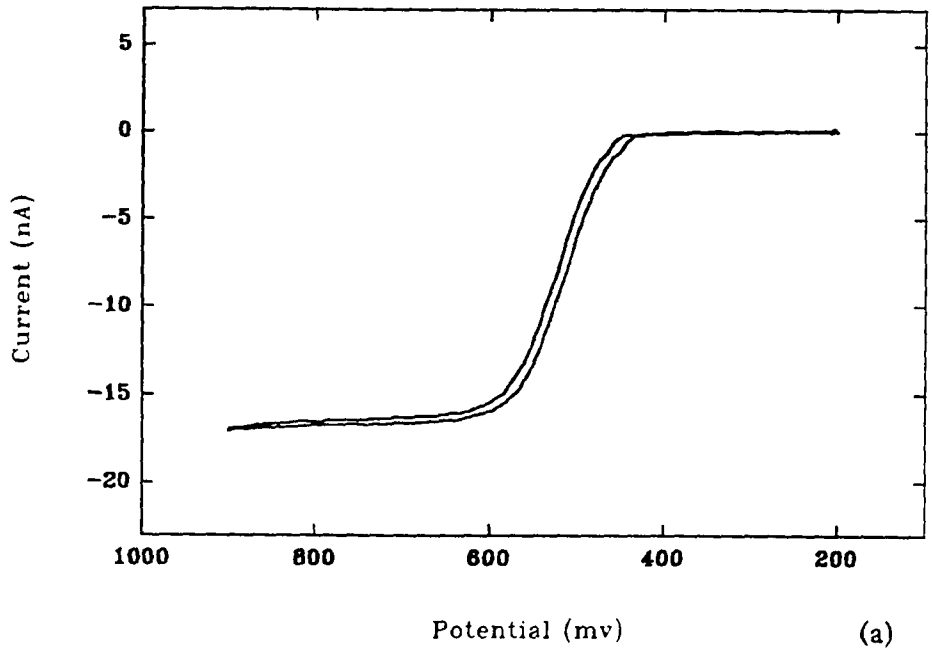

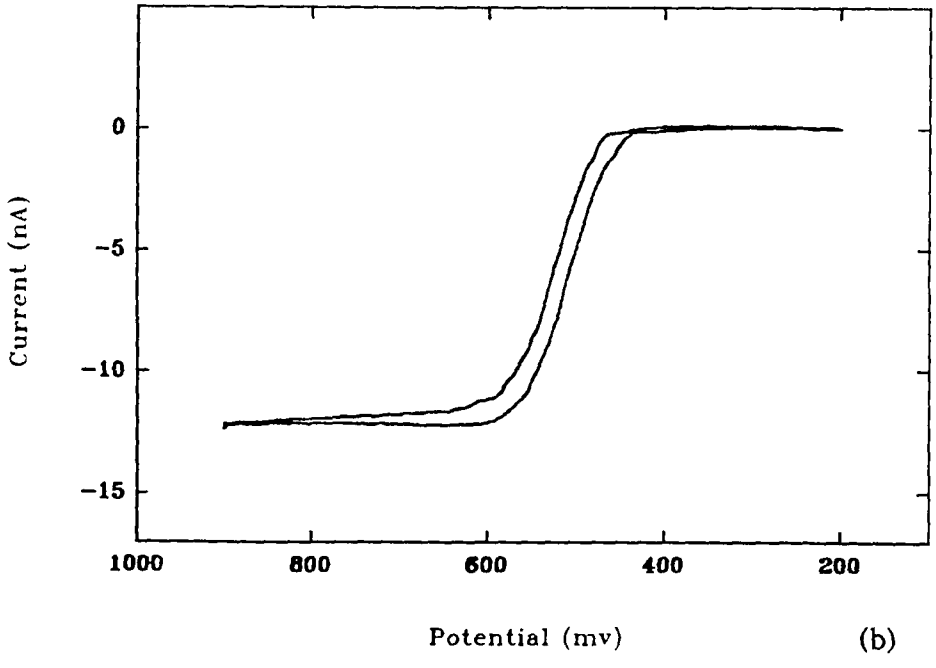

Fig. 3-8 (a) & (b)

Reproduced with permission of the copyright owner. Further reproduction prohibited without permission.

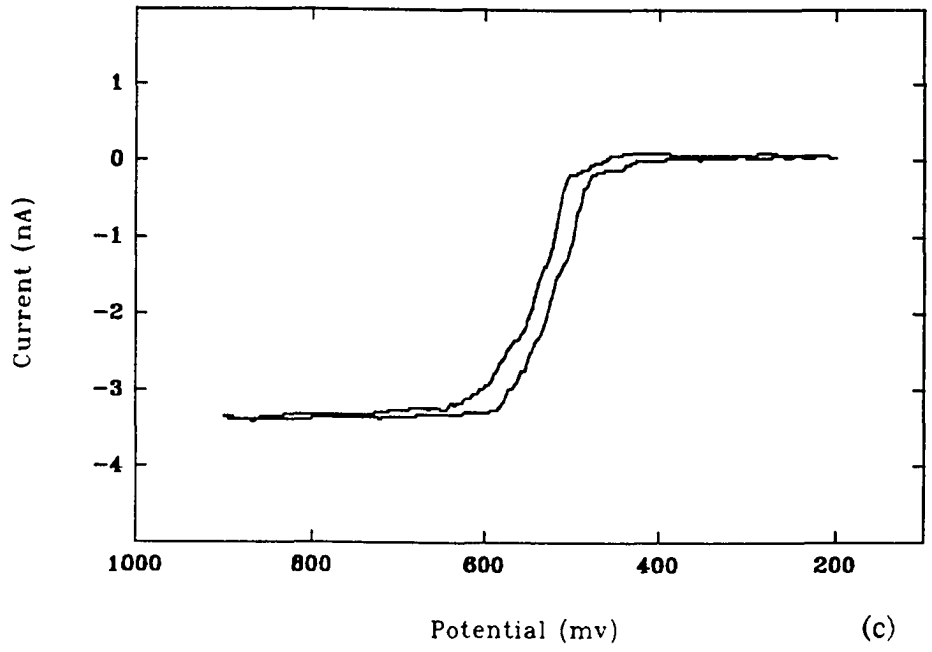

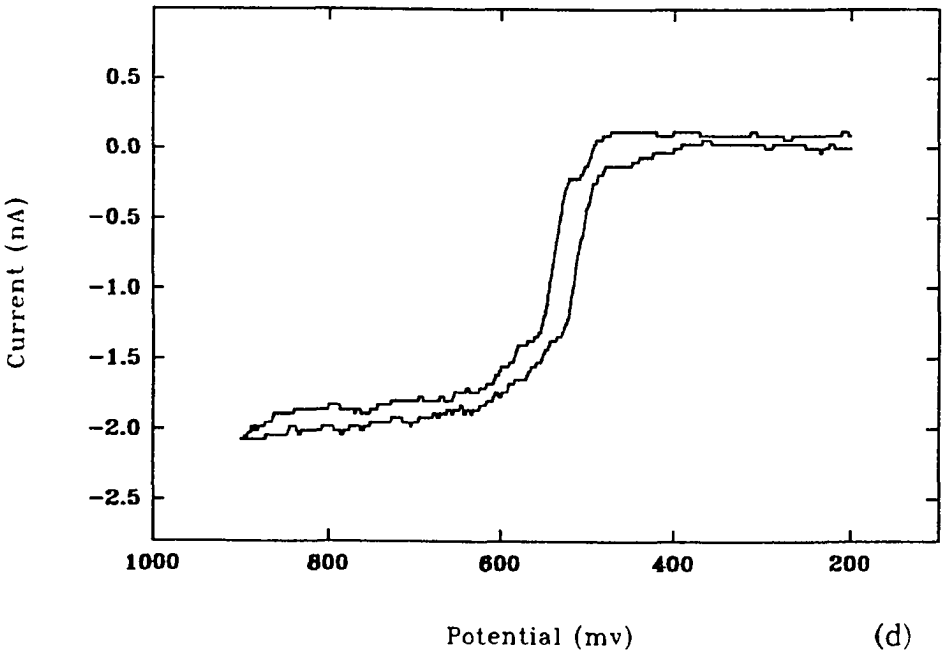

Fig. 3-8 (c) & (d)

Reproduced with permission of the copyright owner. Further reproduction prohibited without permission.

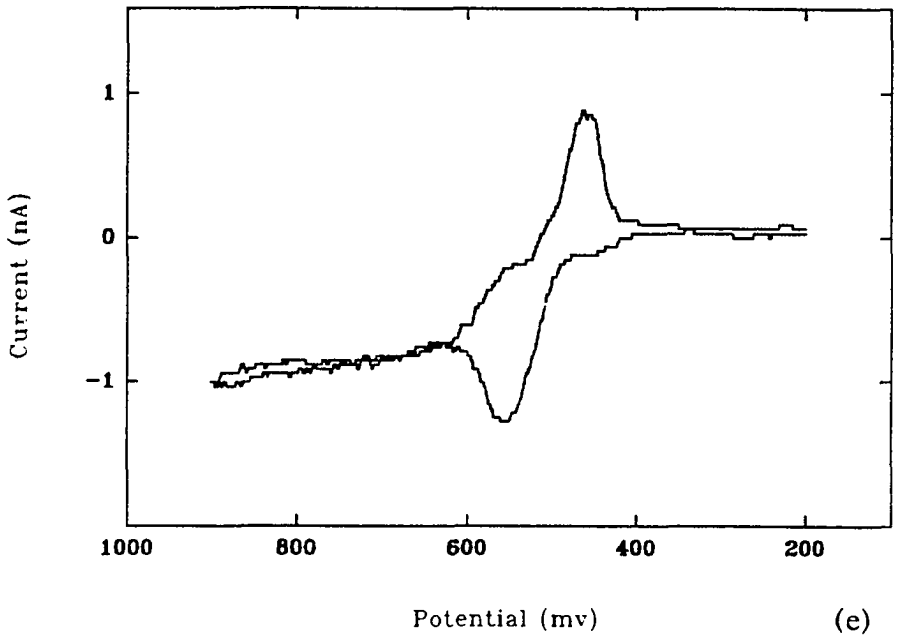

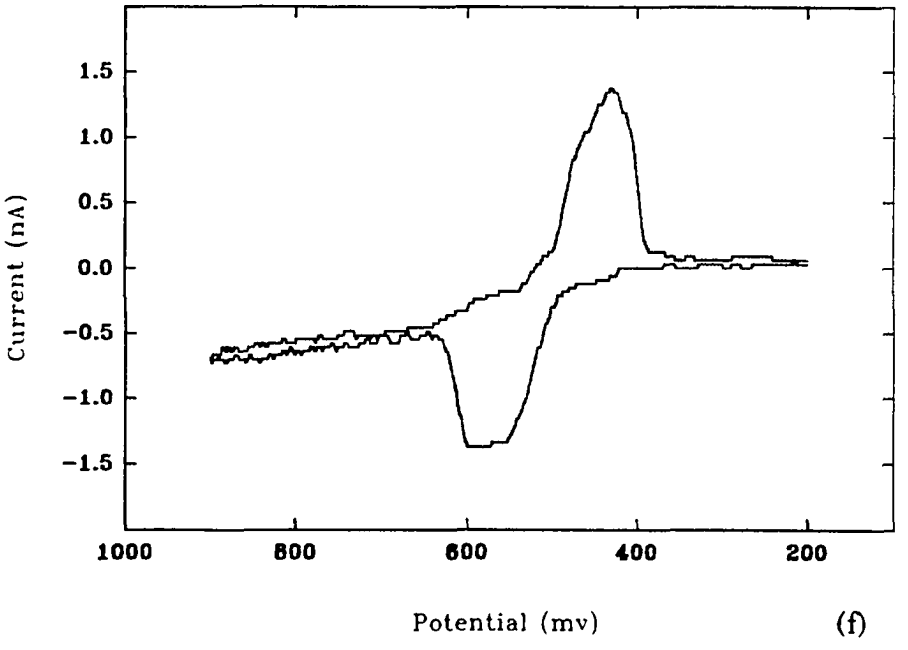

Fig. 3-8 (e) & (f)

Reproduced with permission of the copyright owner. Further reproduction prohibited without permission.

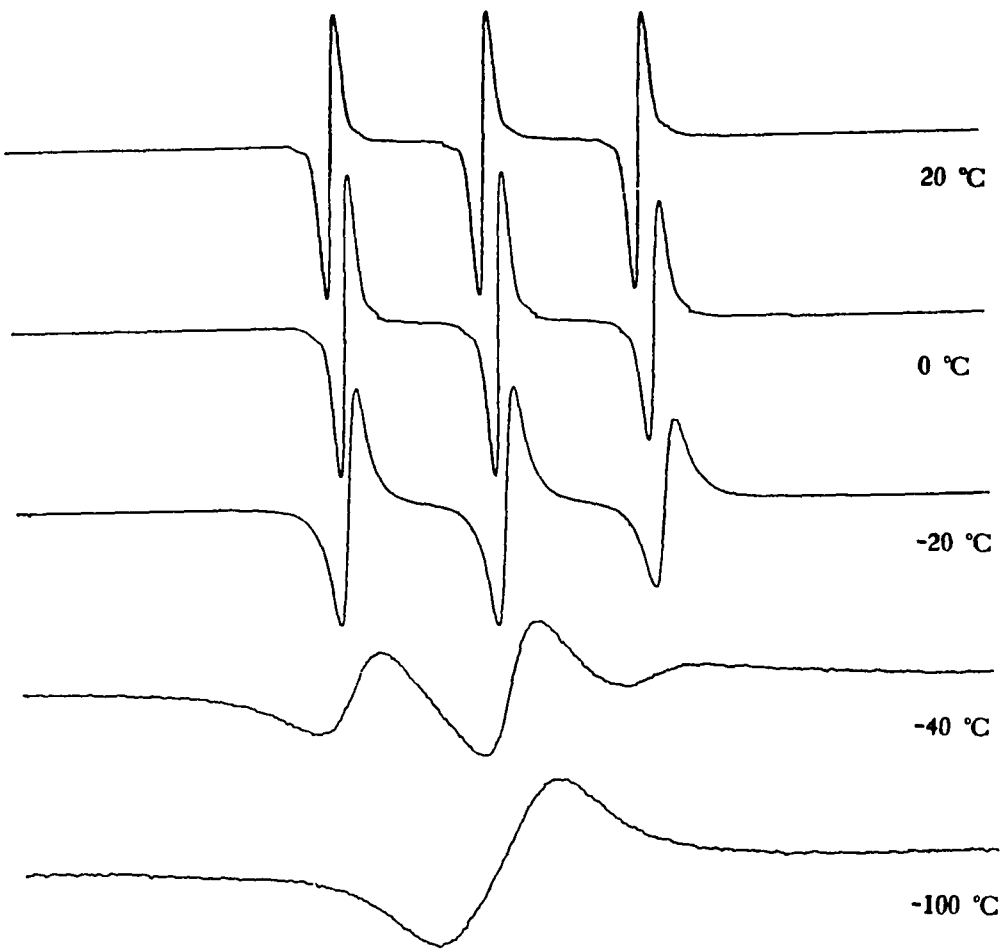

Fig. 4-1

Reproduced with permission of the copyright owner. Further reproduction prohibited without permission.

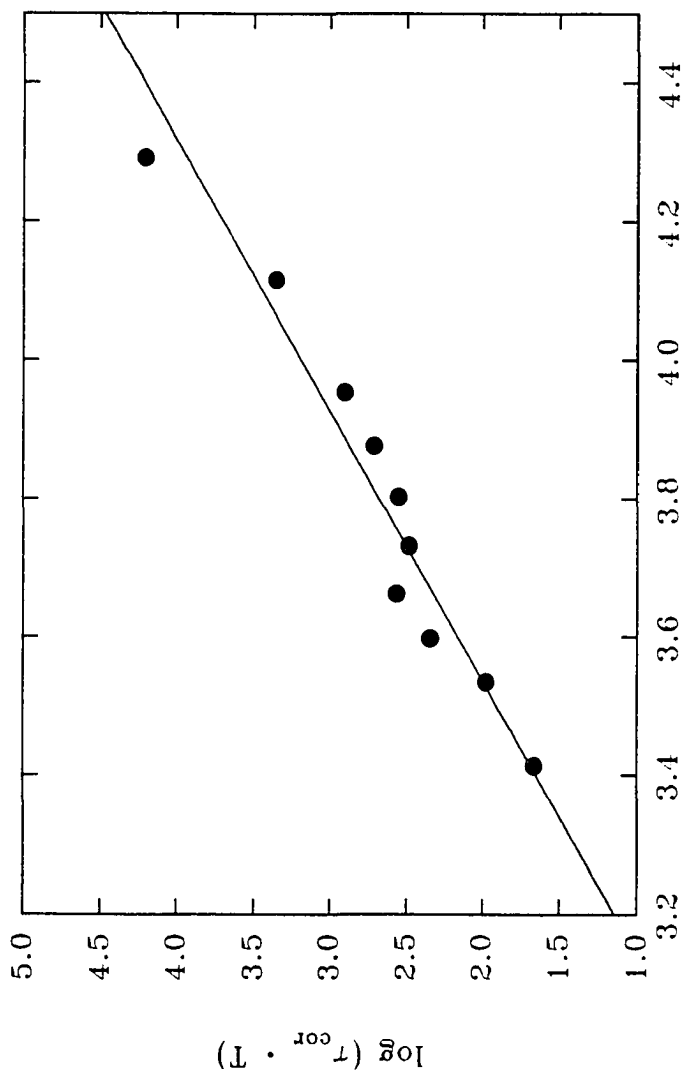

Fig. 4-2

Reproduced with permission of the copyright owner. Further reproduction prohibited without permission.

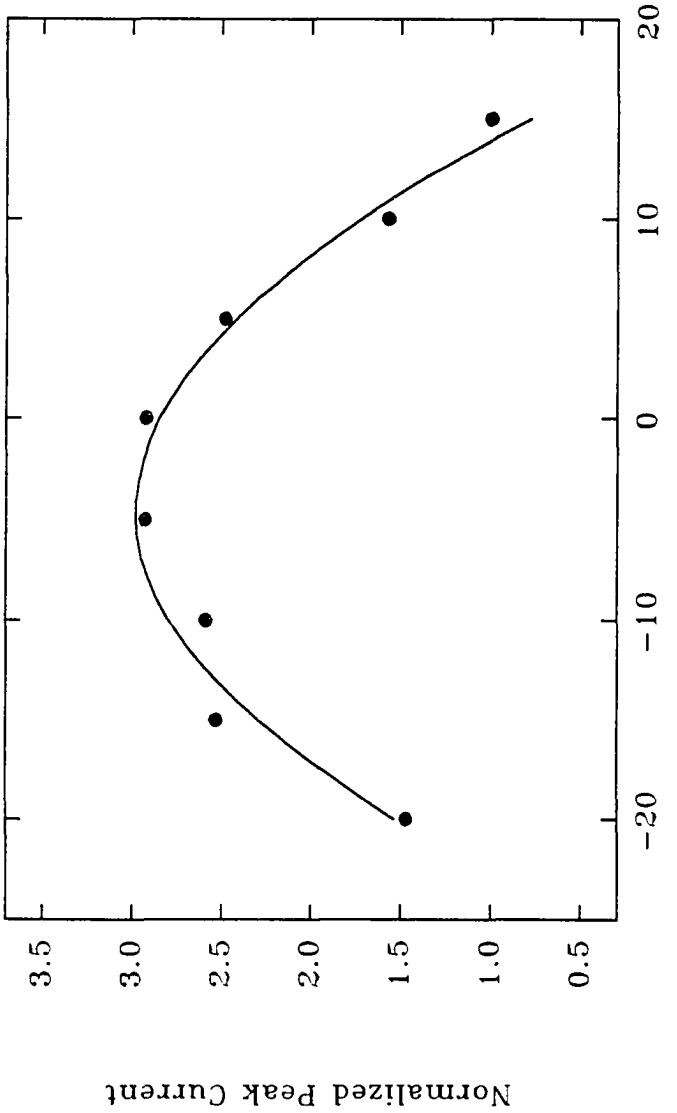

Fig. 5-1

Reproduced with permission of the copyright owner. Further reproduction prohibited without permission.

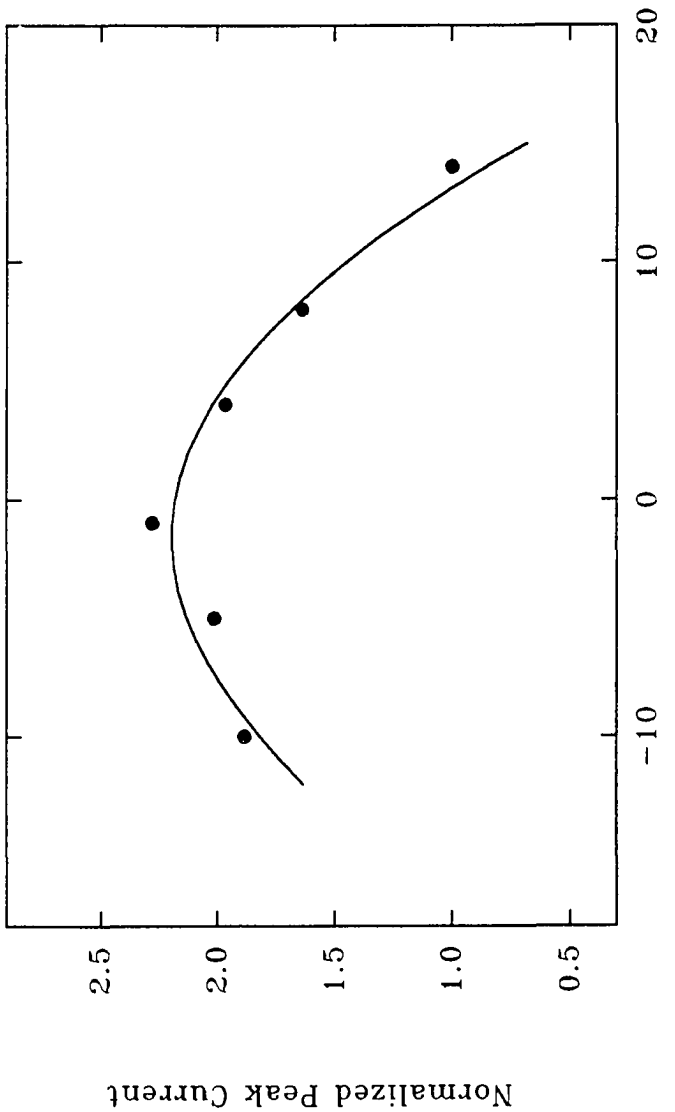

Fig. 5-2

Reproduced with permission of the copyright owner. Further reproduction prohibited without permission.

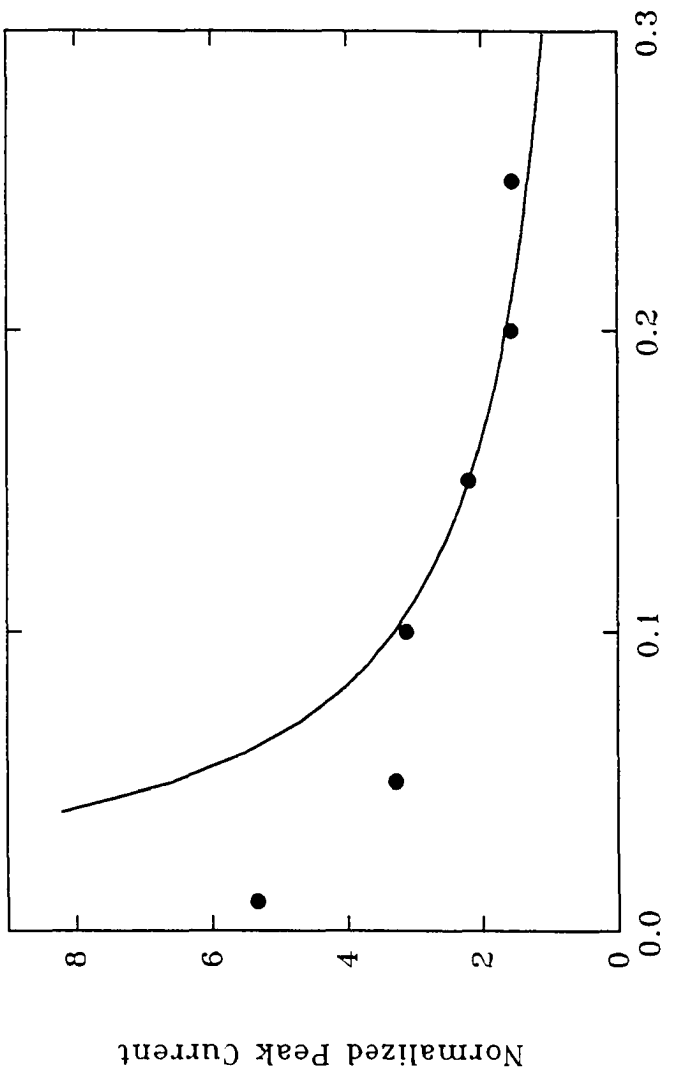

Fig. 5-3

Reproduced with permission of the copyright owner. Further reproduction prohibited without permission.

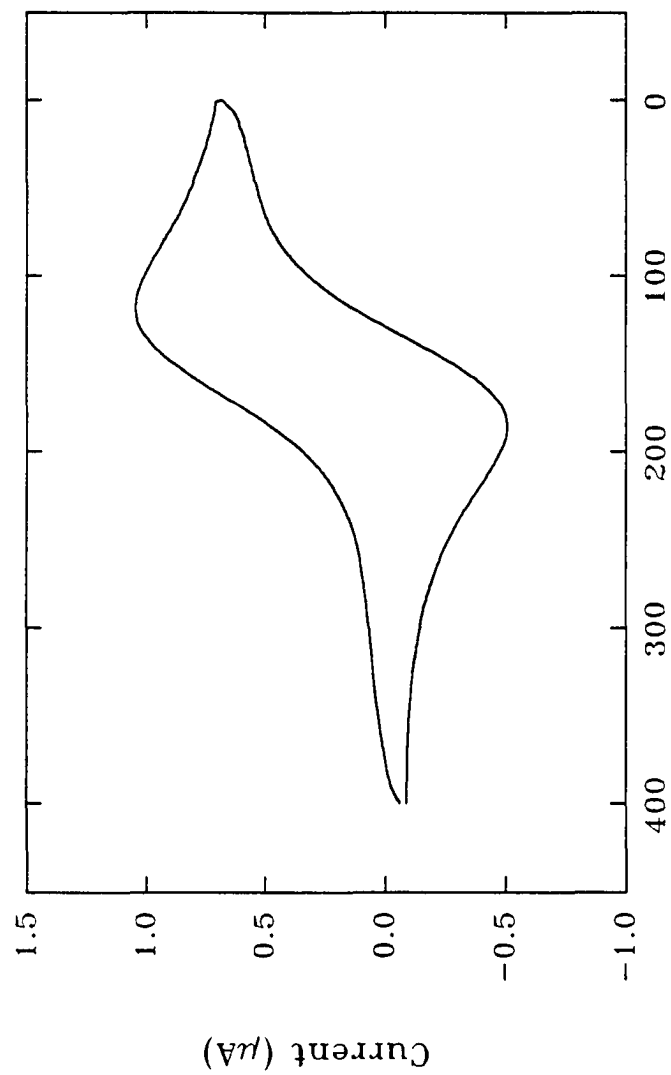

Fig. 5-4 (a)

Reproduced with permission of the copyright owner. Further reproduction prohibited without permission.

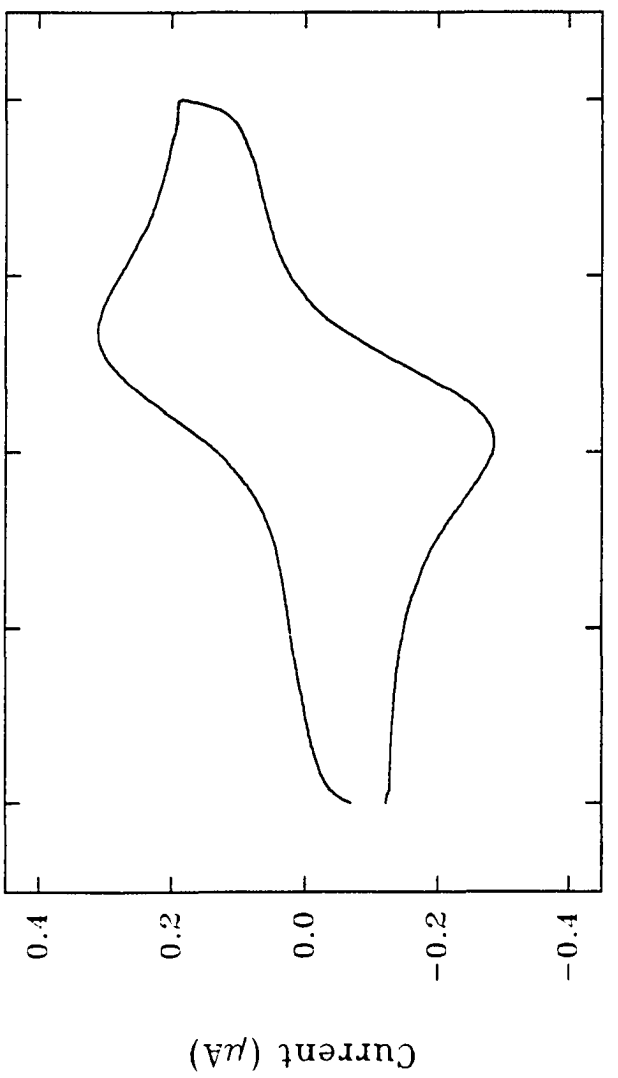

Fig. 5-4 (b)

Reproduced with permission of the copyright owner. Further reproduction prohibited without permission.

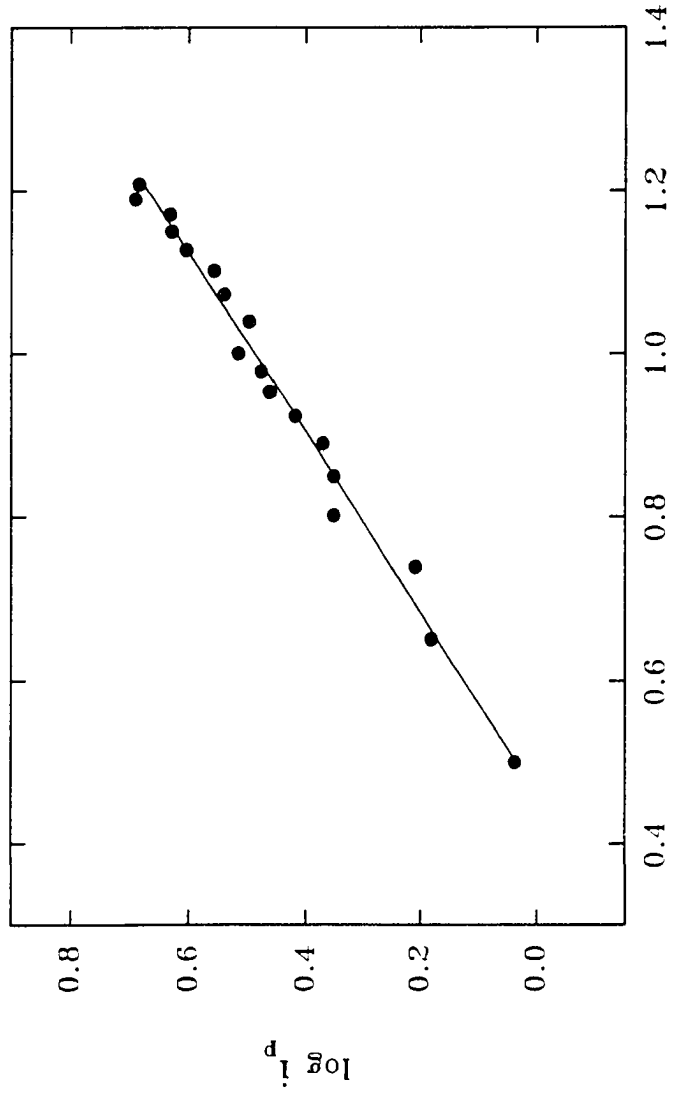

Fig. 5-5

Reproduced with permission of the copyright owner. Further reproduction prohibited without permission.

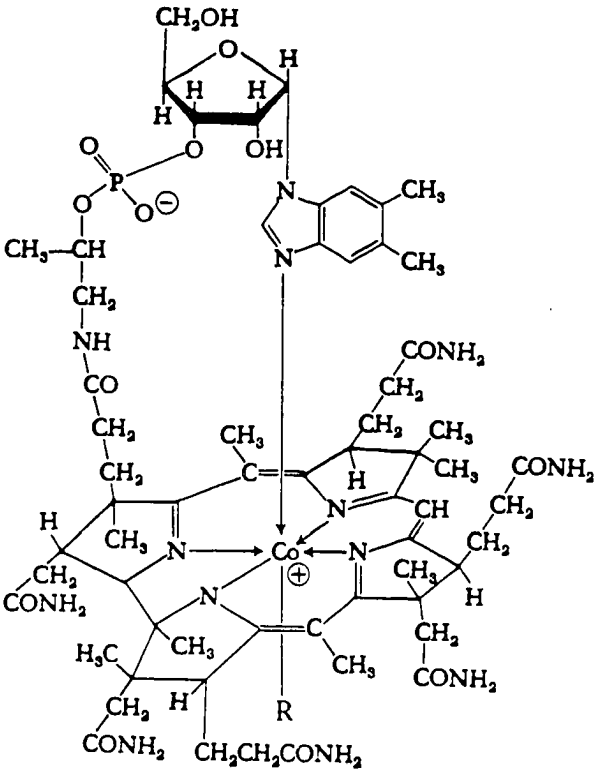

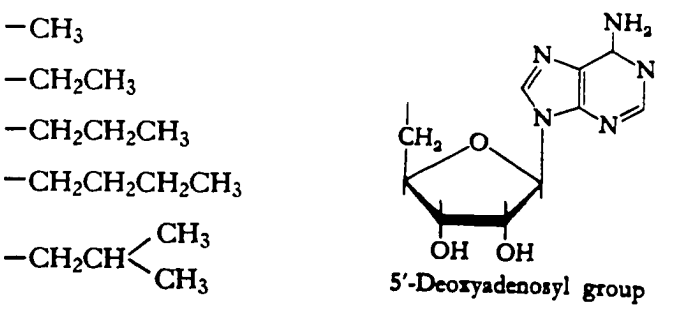

Fig. 6-1

Reproduced with permission of the copyright owner. Further reproduction prohibited without permission.

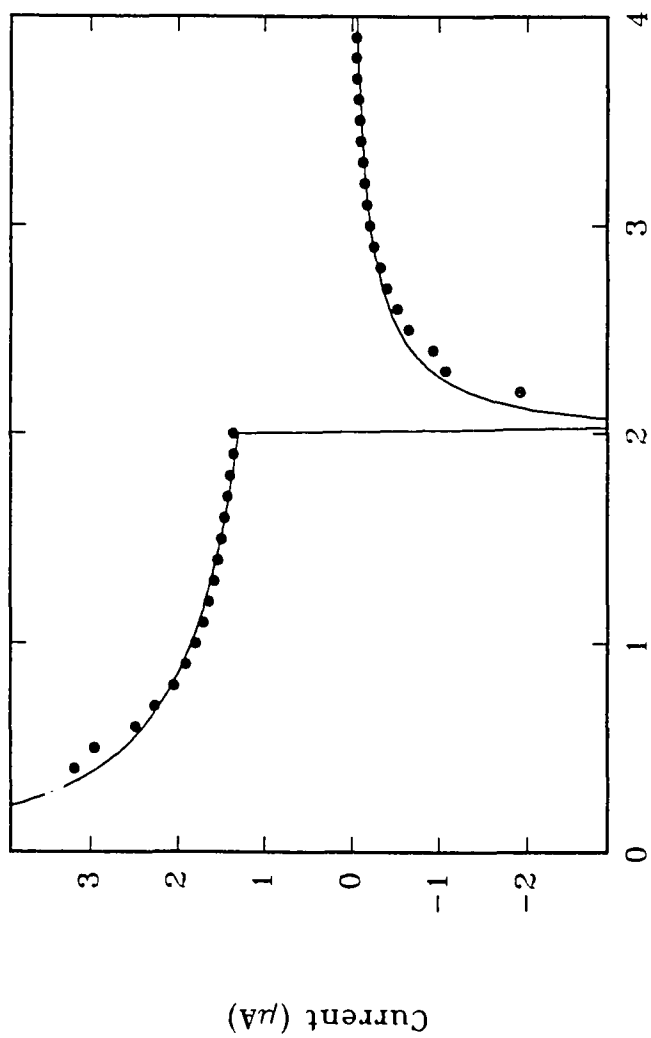

Fig. 7-1 (a)

Reproduced with permission of the copyright owner. Further reproduction prohibited without permission.

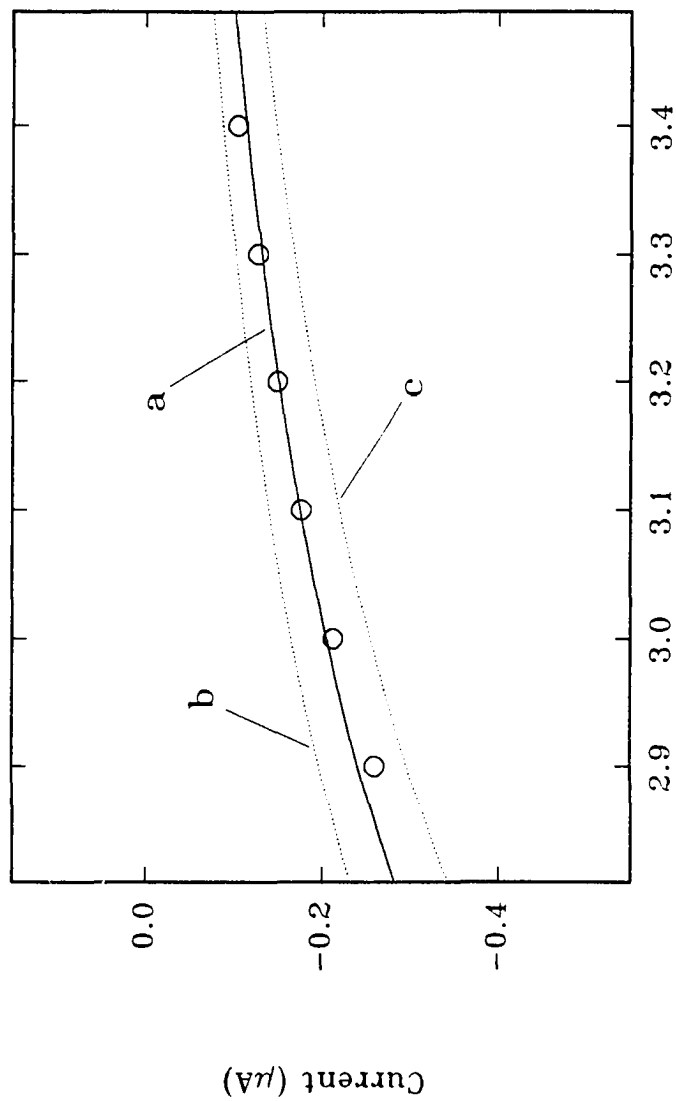

Fig. 7-1 (b)

Reproduced with permission of the copyright owner. Further reproduction prohibited without permission.

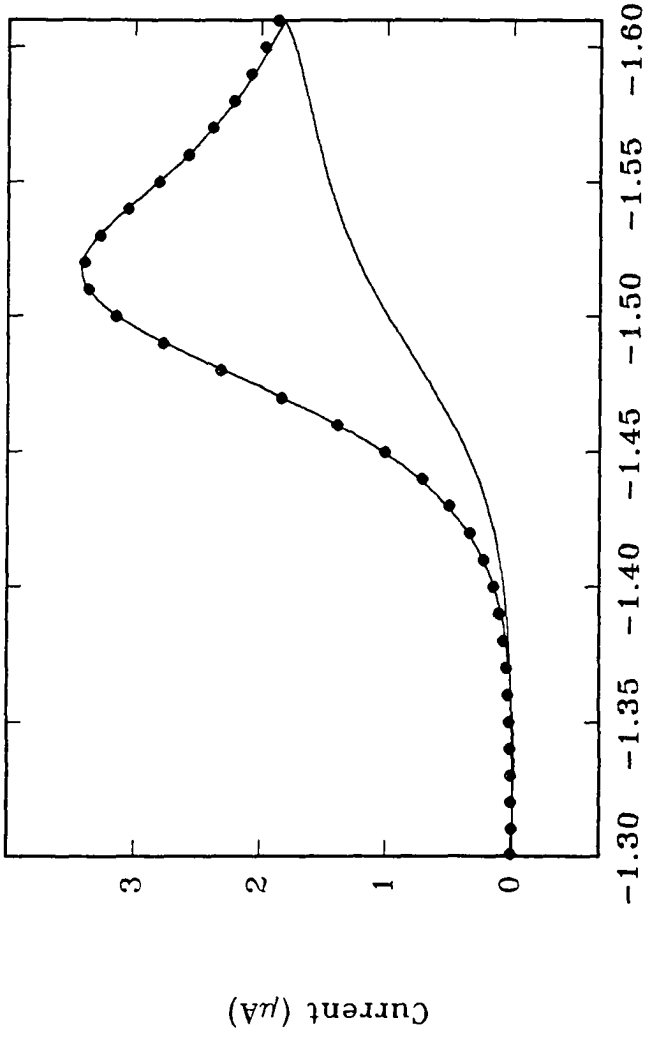

Fig. 7-2 (a)

Reproduced with permission of the copyright owner. Further reproduction prohibited without permission.

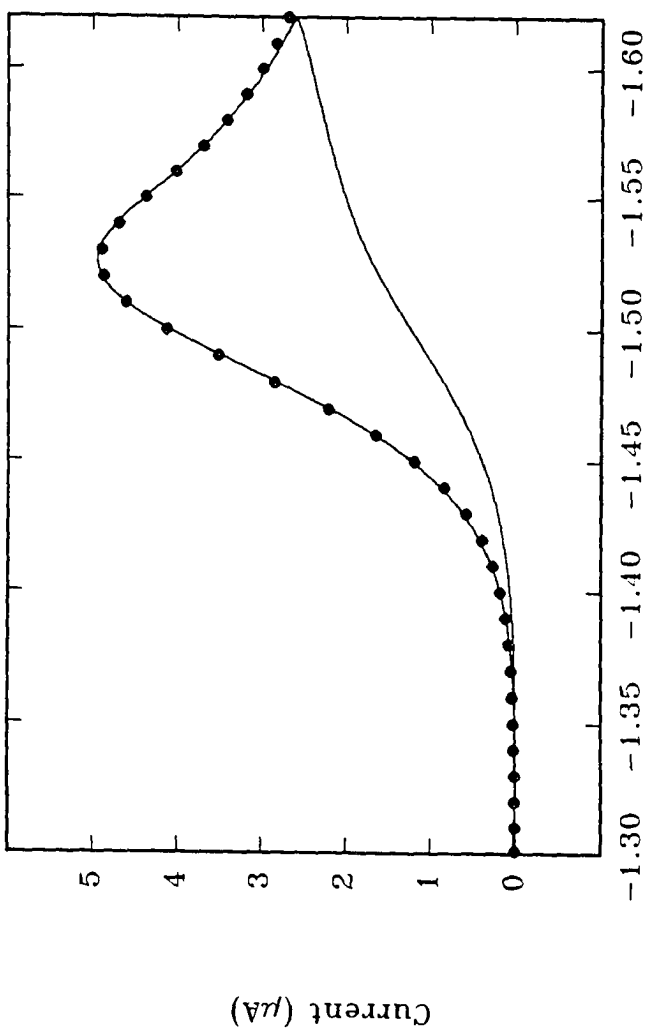

Fig. 7-2 (b)

Reproduced with permission of the copyright owner. Further reproduction prohibited without permission.

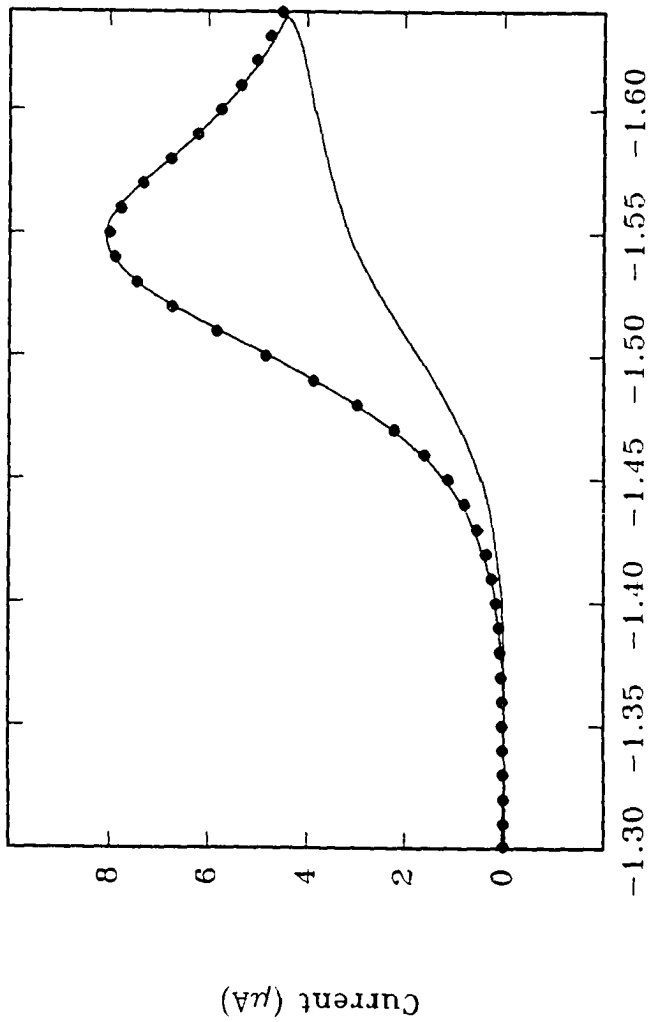

Fig. 7-2 (c)

Reproduced with permission of the copyright owner. Further reproduction prohibited without permission.

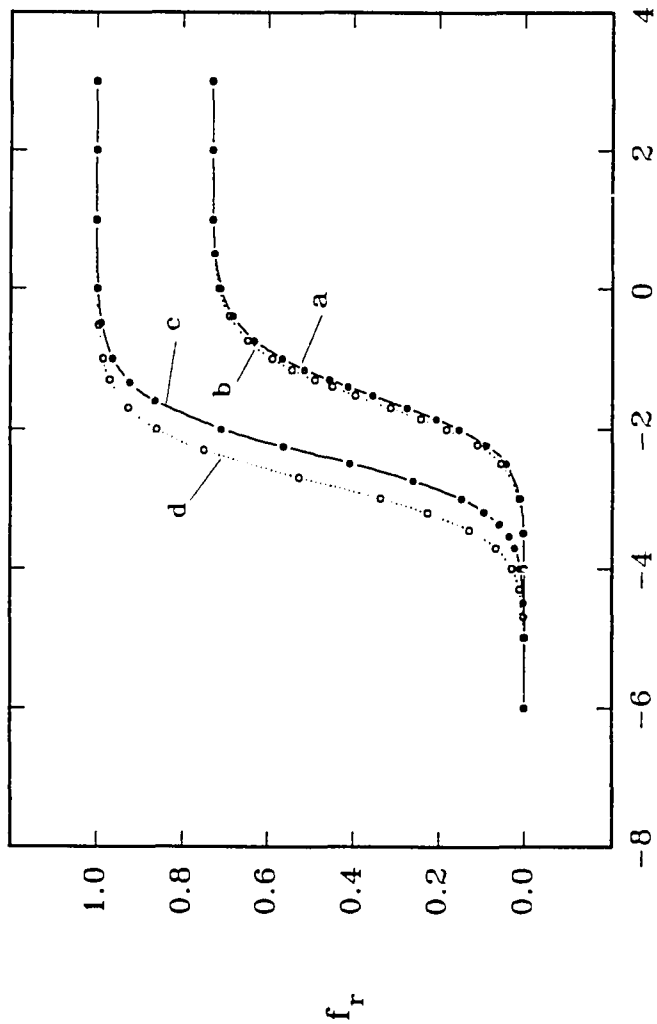

Fig. 7-3

Reproduced with permission of the copyright owner. Further reproduction prohibited without permission.

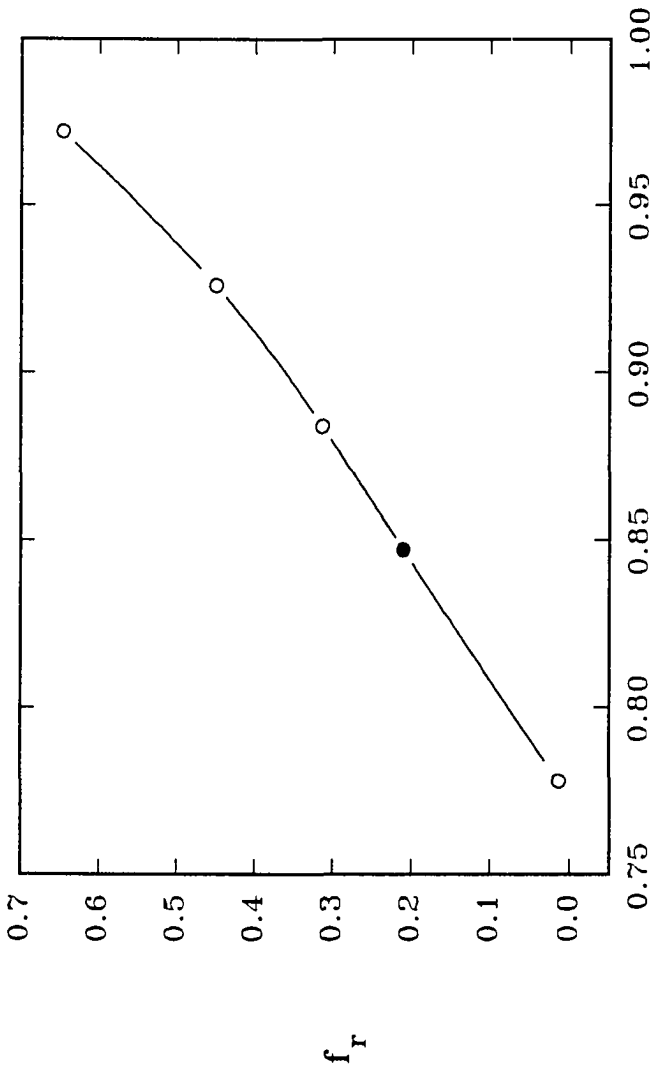

Fig. 7-4

Reproduced with permission of the copyright owner. Further reproduction prohibited without permission.

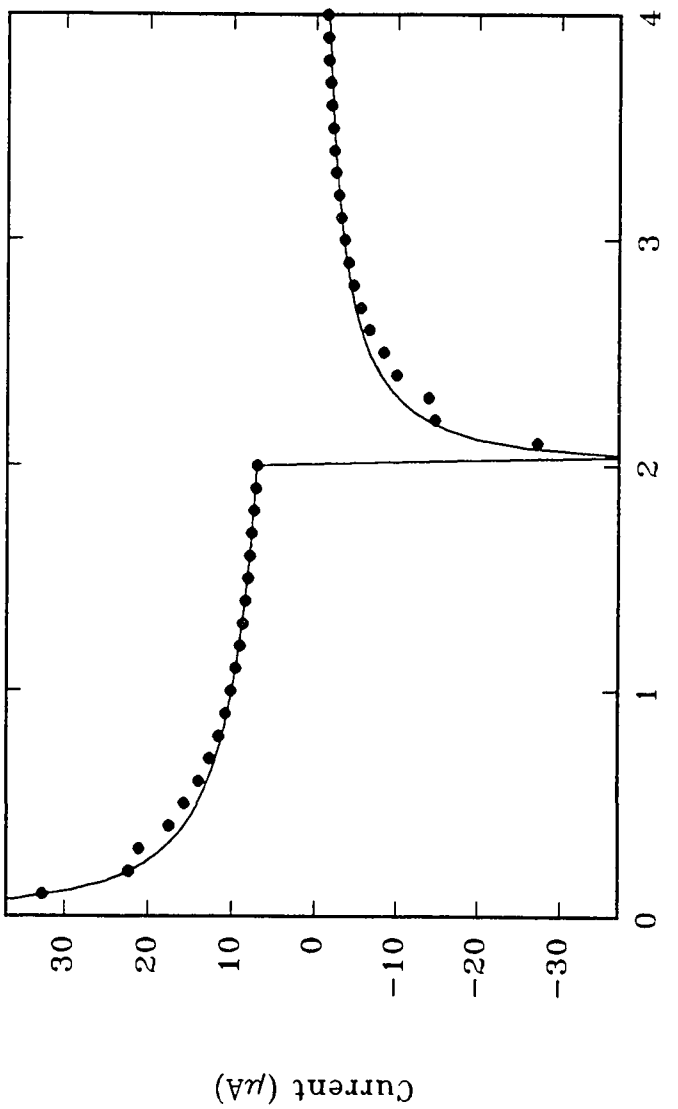

Fig. 8-1

Reproduced with permission of the copyright owner. Further reproduction prohibited without permission.

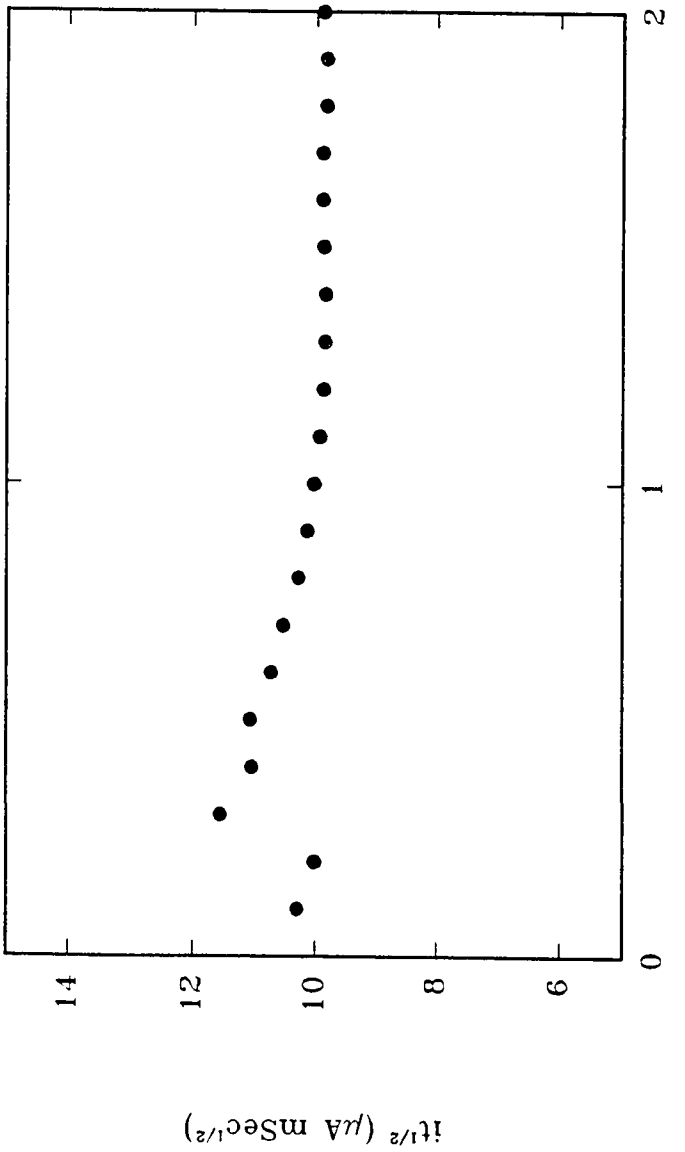

Fig. 8-2

Reproduced with permission of the copyright owner. Further reproduction prohibited without permission.

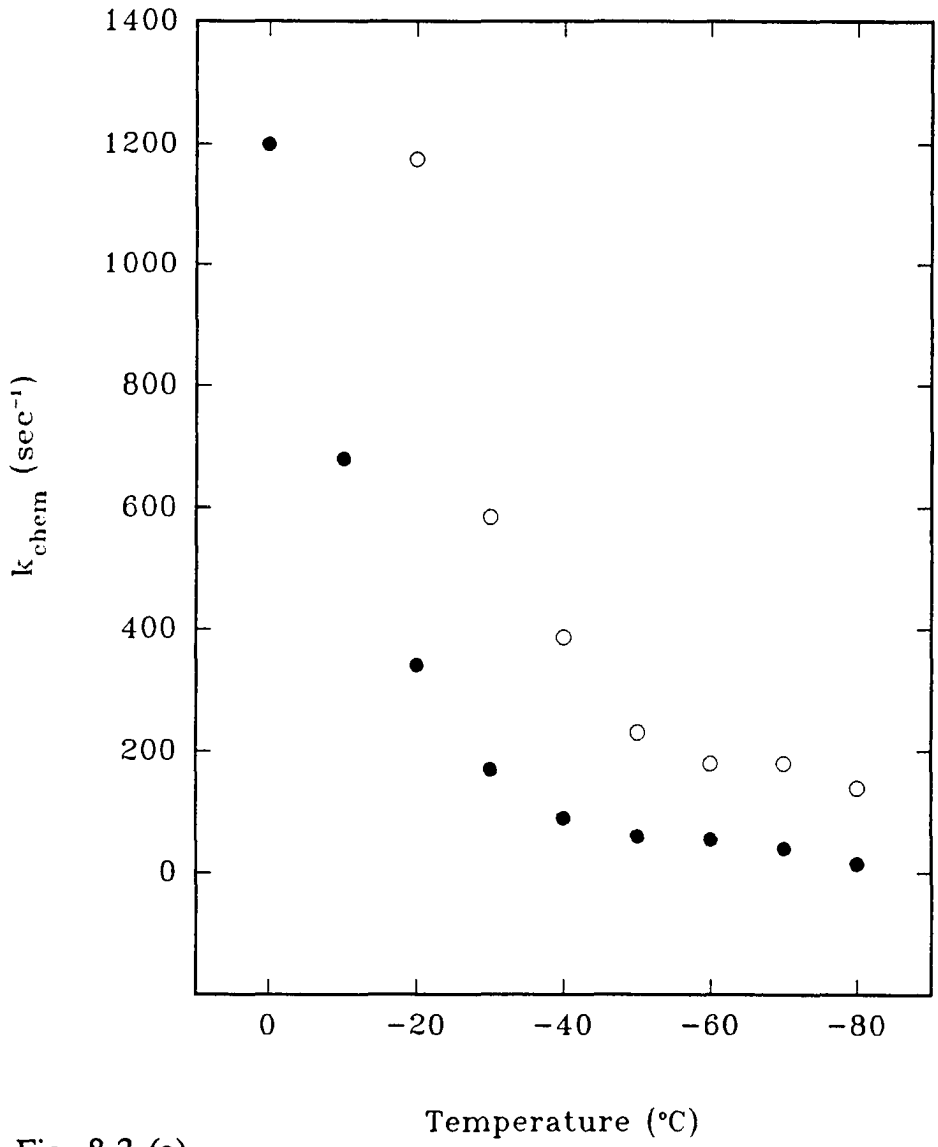

Fig. 8-3 (a)

Reproduced with permission of the copyright owner. Further reproduction prohibited without permission.

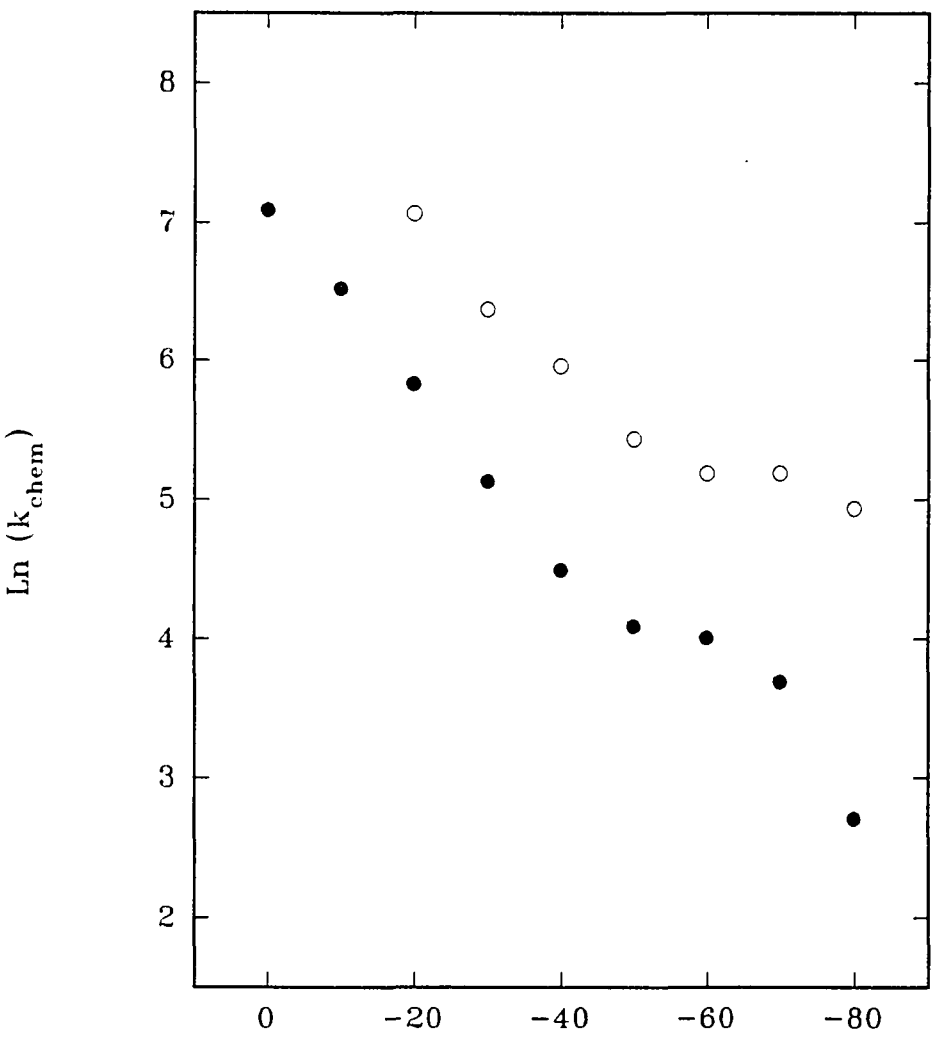

Fig. 8-3 (b)

Reproduced with permission of the copyright owner. Further reproduction prohibited without permission.

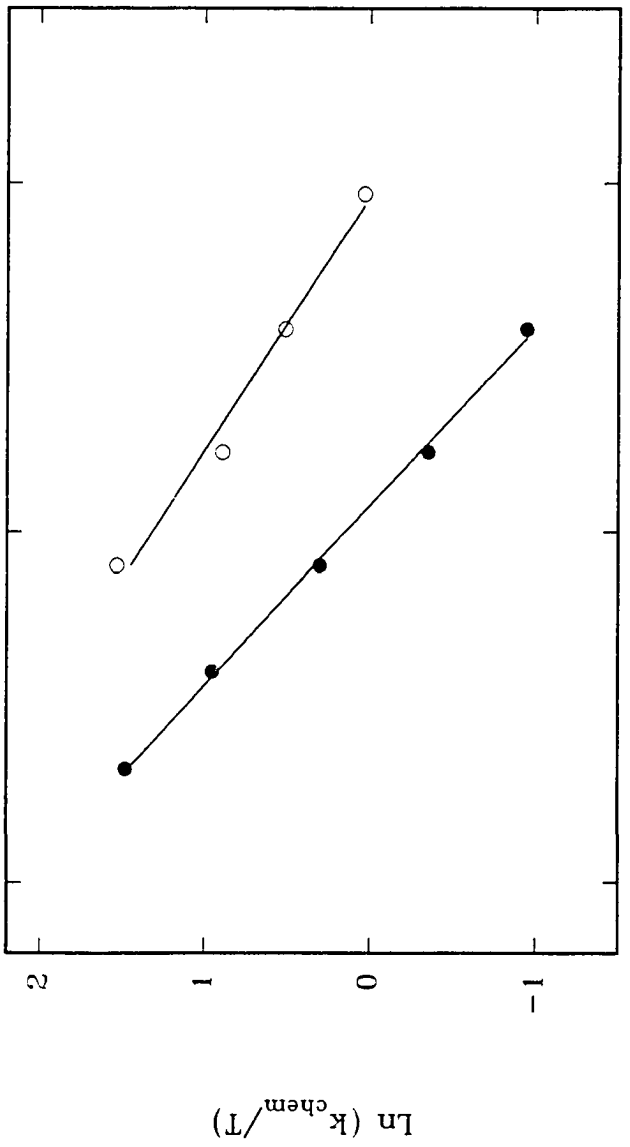

Fig. 8-4

Reproduced with permission of the copyright owner. Further reproduction prohibited without permission.

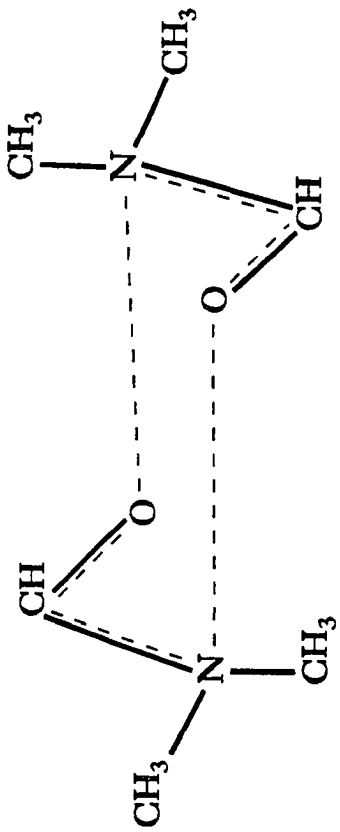

Fig. 8-5

Reproduced with permission of the copyright owner. Further reproduction prohibited without permission.

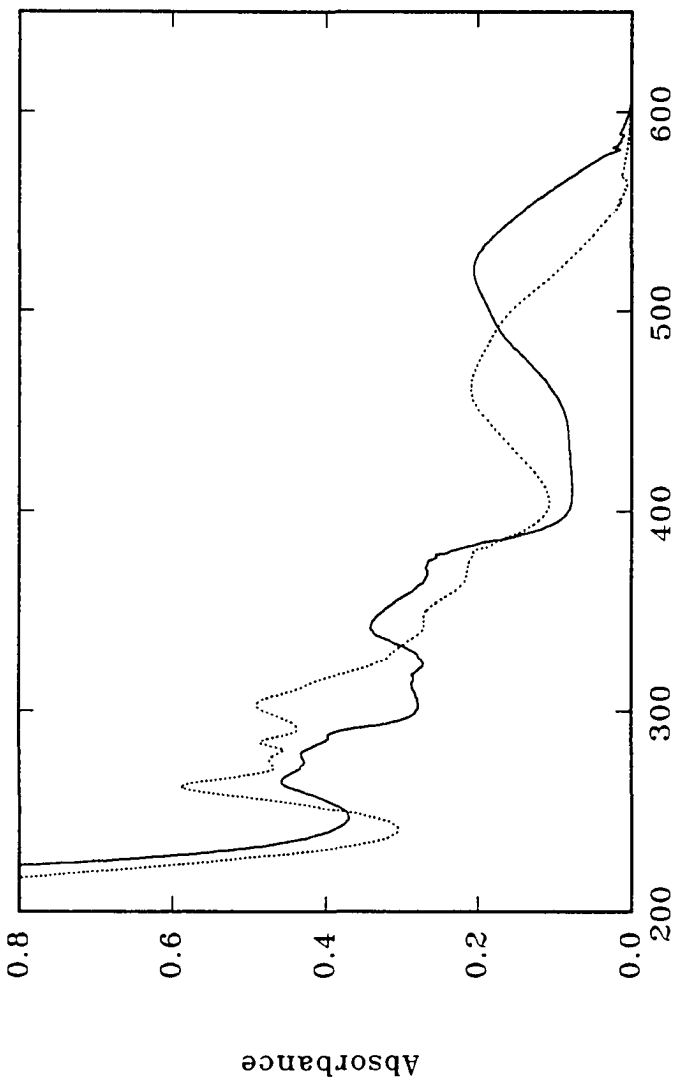

Fig. 9-1 (a)

Reproduced with permission of the copyright owner. Further reproduction prohibited without permission.

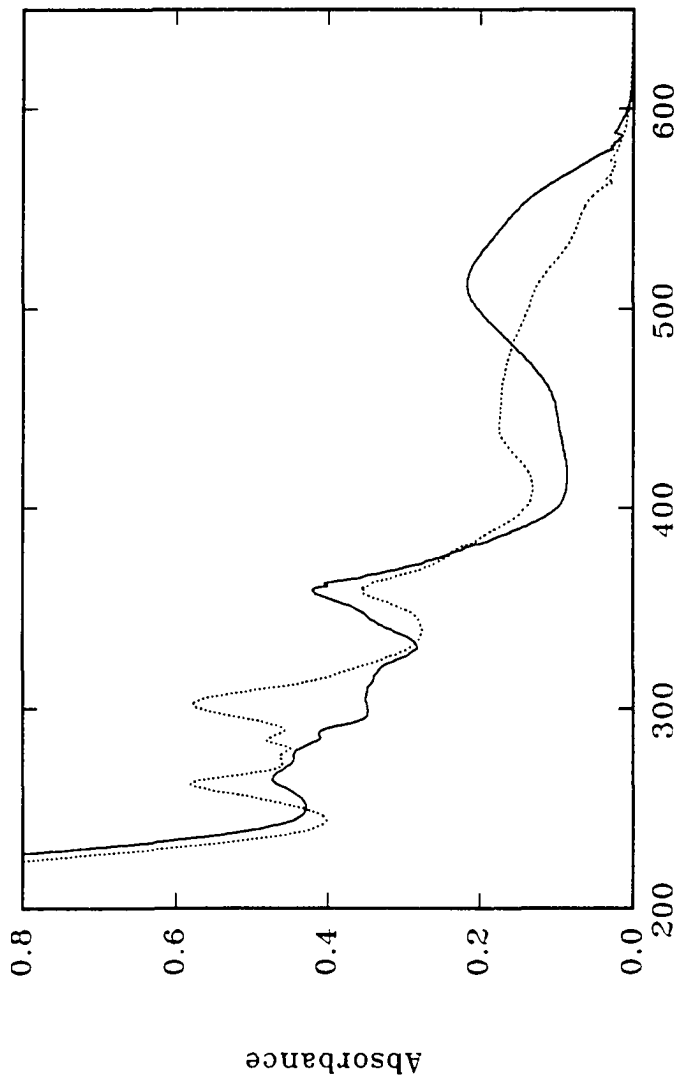

Fig. 9-1 (b)

Reproduced with permission of the copyright owner. Further reproduction prohibited without permission.

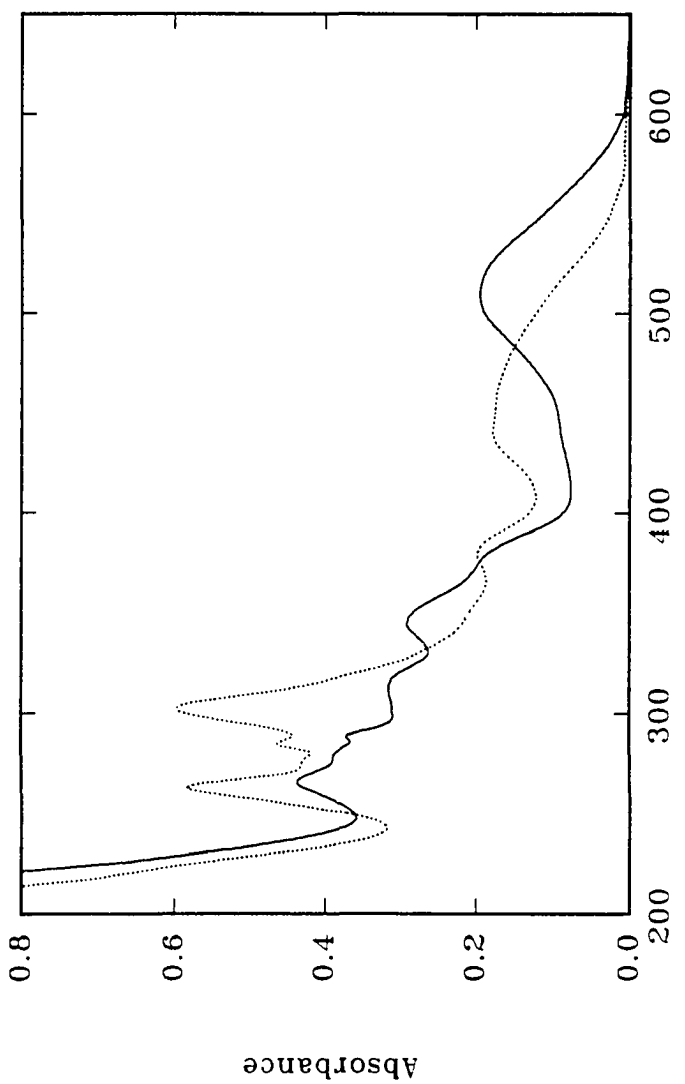

Fig. 9-1 (c)

Reproduced with permission of the copyright owner. Further reproduction prohibited without permission.

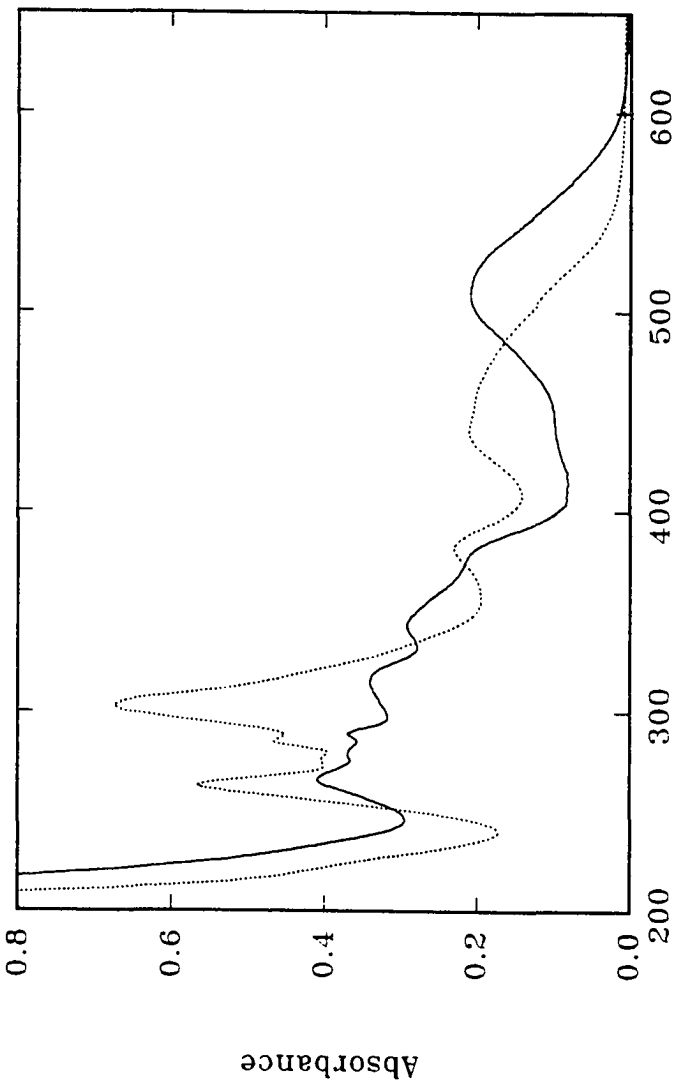

Fig. 9-1 (d)

Reproduced with permission of the copyright owner. Further reproduction prohibited without permission.

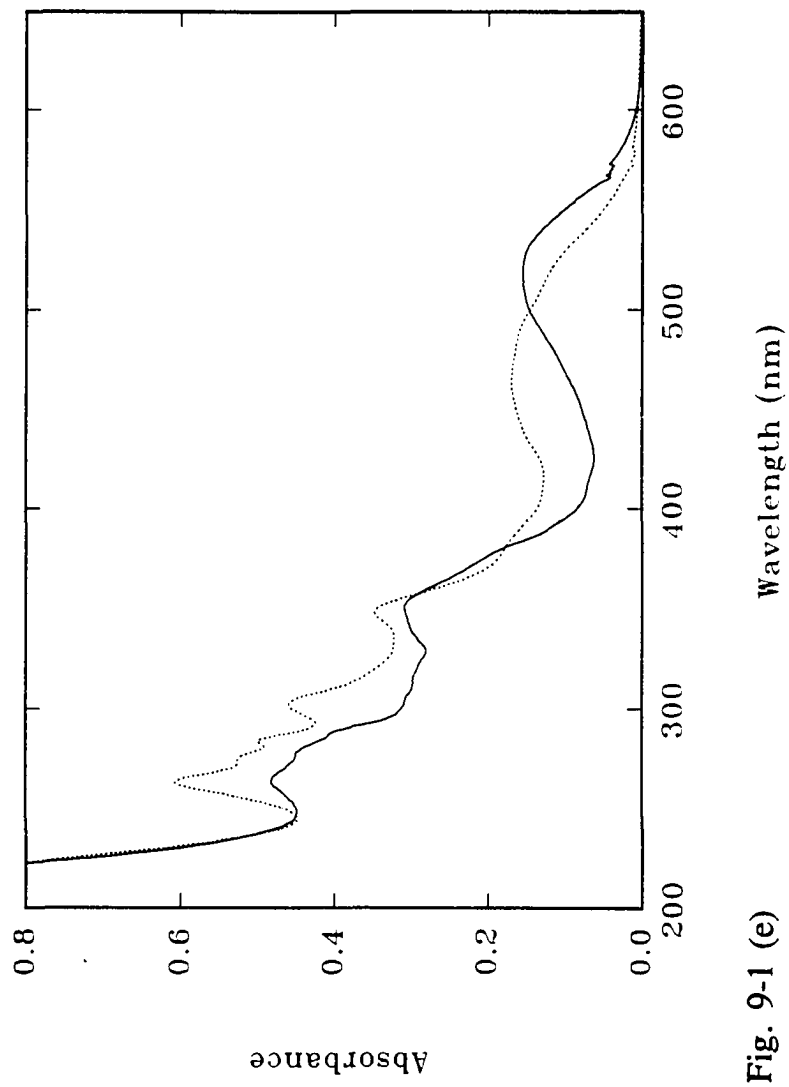

Fig. 9-1 (e)

Reproduced with permission of the copyright owner. Further reproduction prohibited without permission.

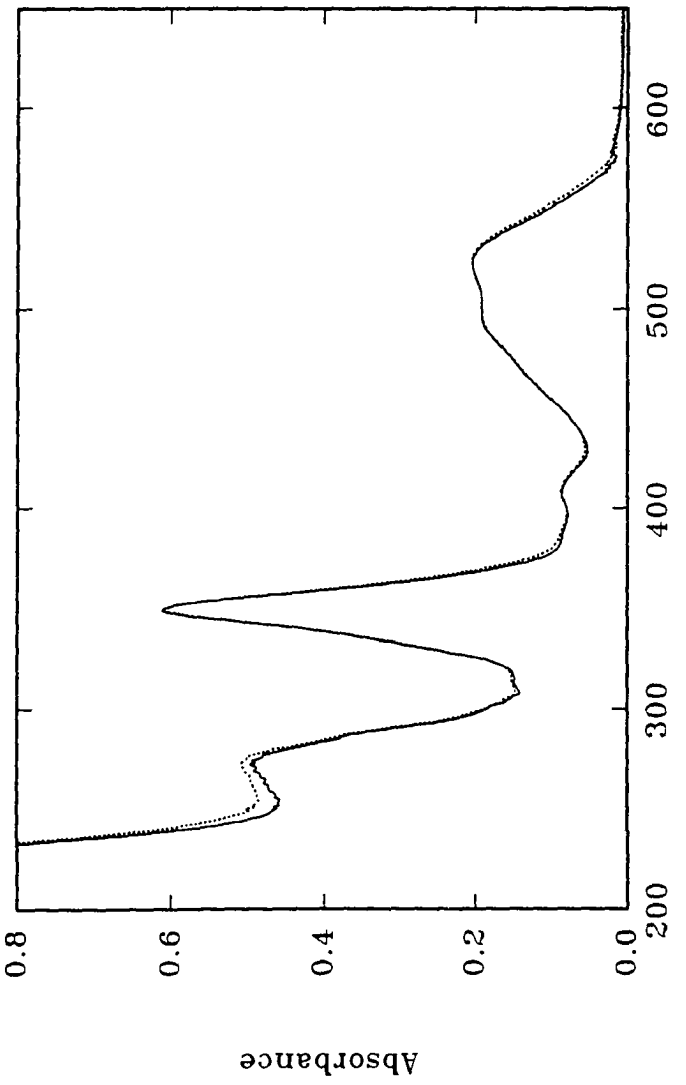

Fig. 9-2

Reproduced with permission of the copyright owner. Further reproduction prohibited without permission.

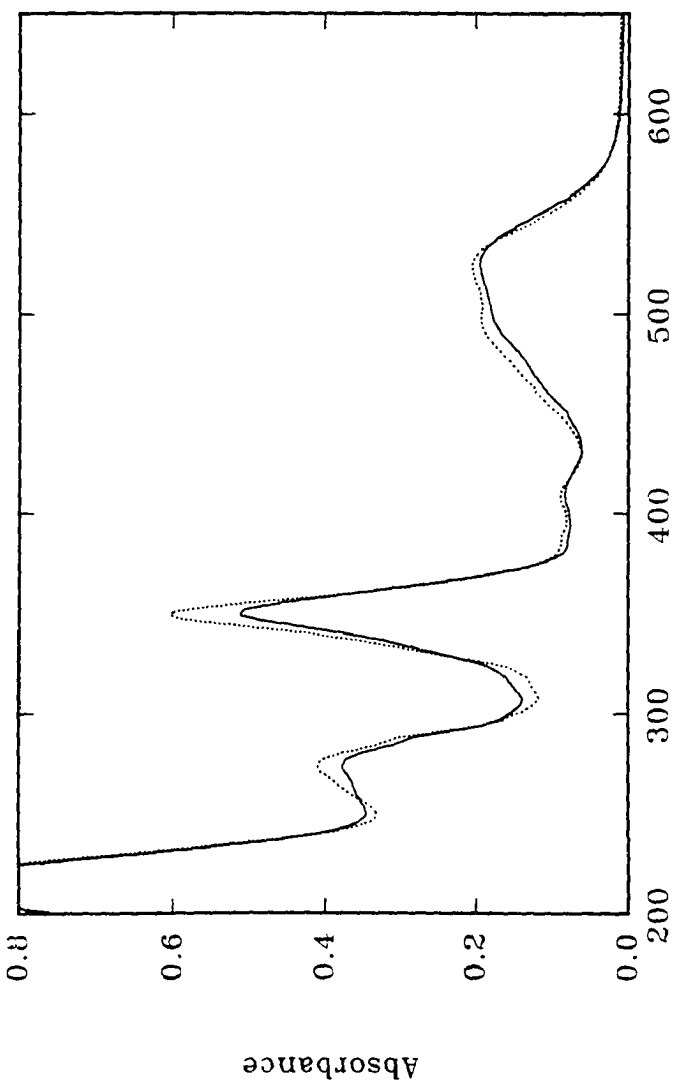

Fig. 9-3 (a)

Reproduced with permission of the copyright owner. Further reproduction prohibited without permission.

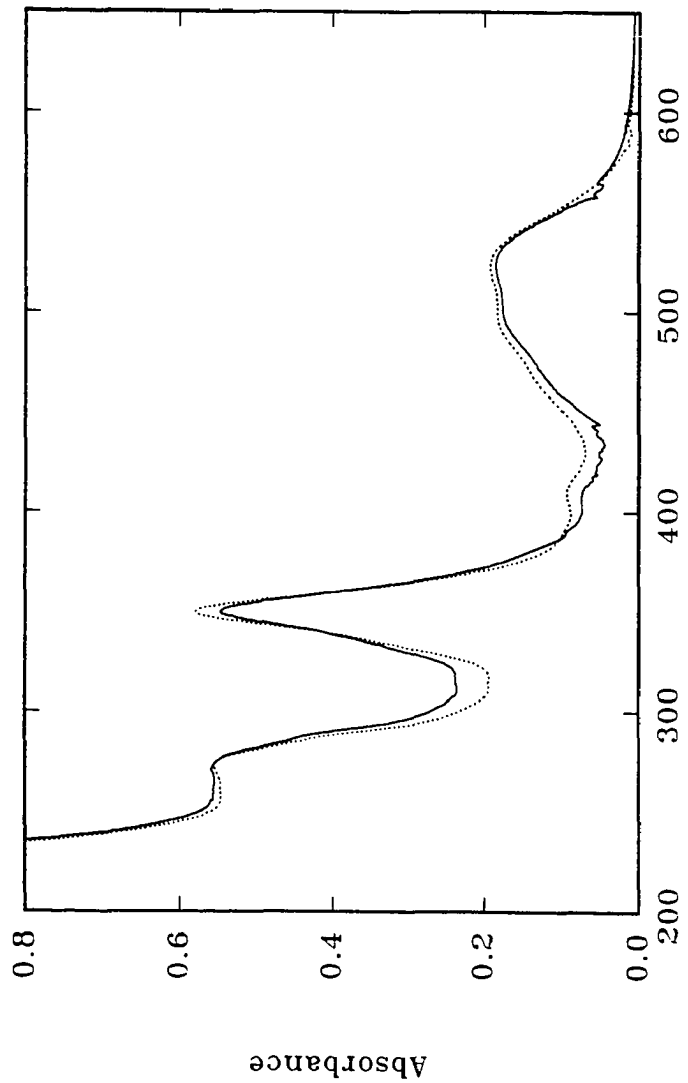

Fig. 9-3 (b)

Reproduced with permission of the copyright owner. Further reproduction prohibited without permission.

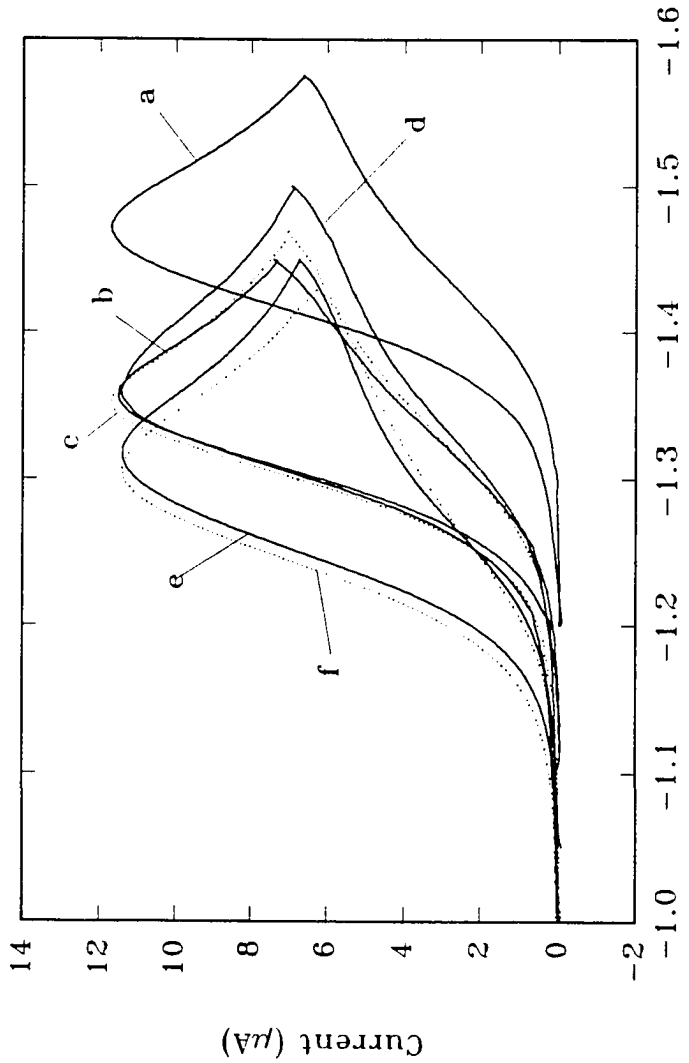

Fig. 9-4

Reproduced with permission of the copyright owner. Further reproduction prohibited without permission.

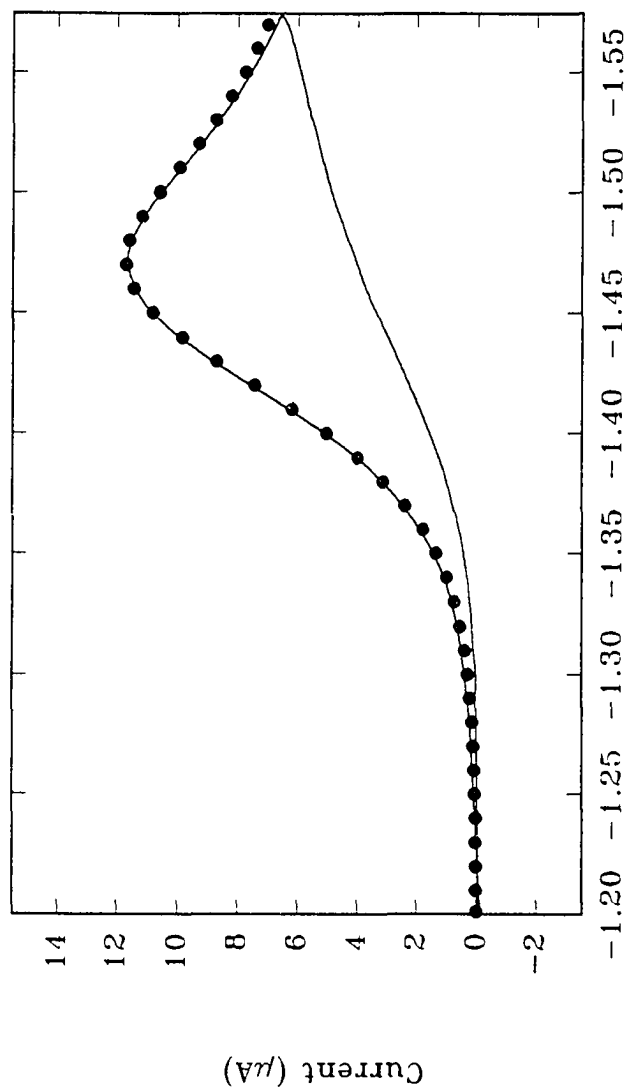

Fig. 9-5

Reproduced with permission of the copyright owner. Further reproduction prohibited without permission.

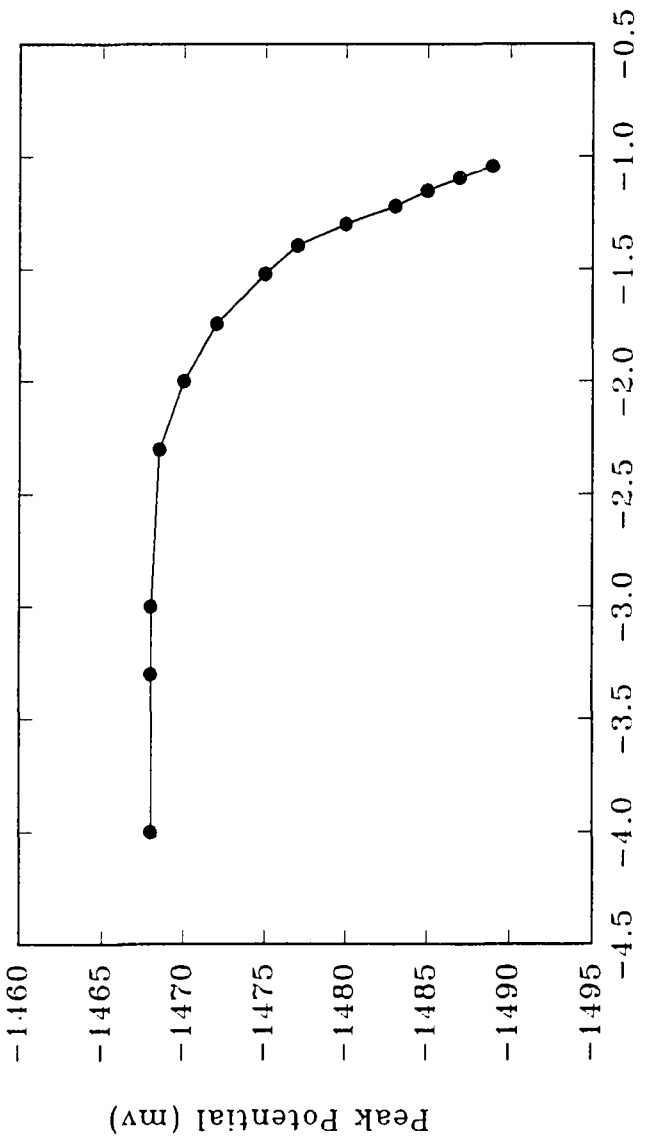

Fig. 9-6

Reproduced with permission of the copyright owner. Further reproduction prohibited without permission.

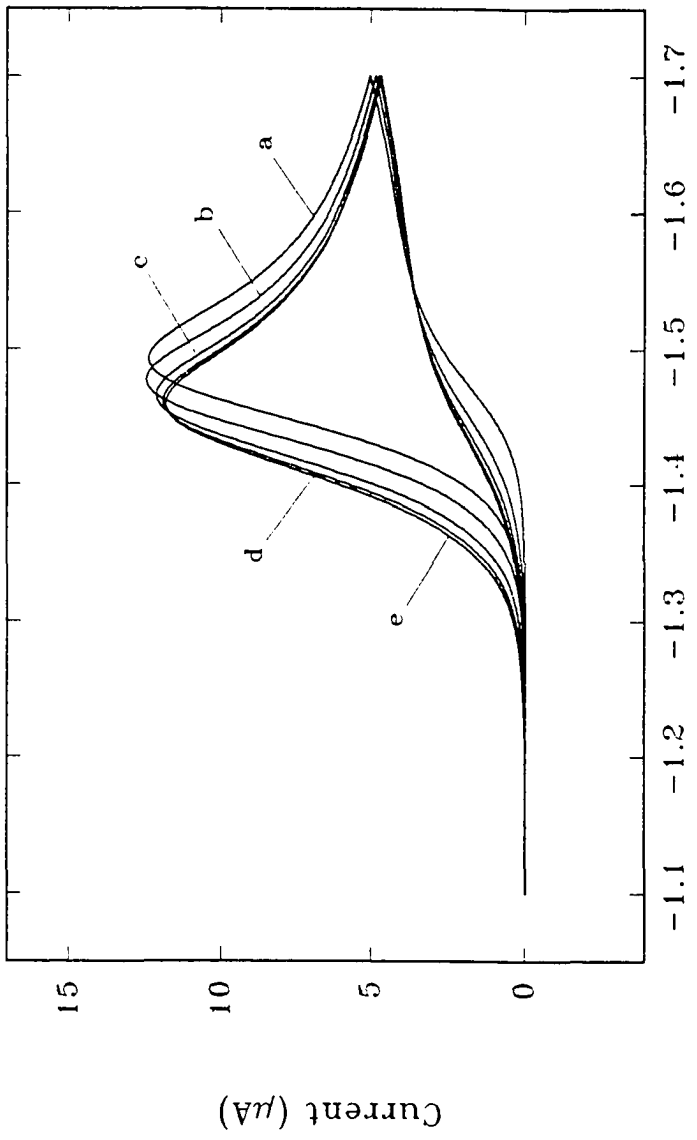

Fig. 9-7

Reproduced with permission of the copyright owner. Further reproduction prohibited without permission.

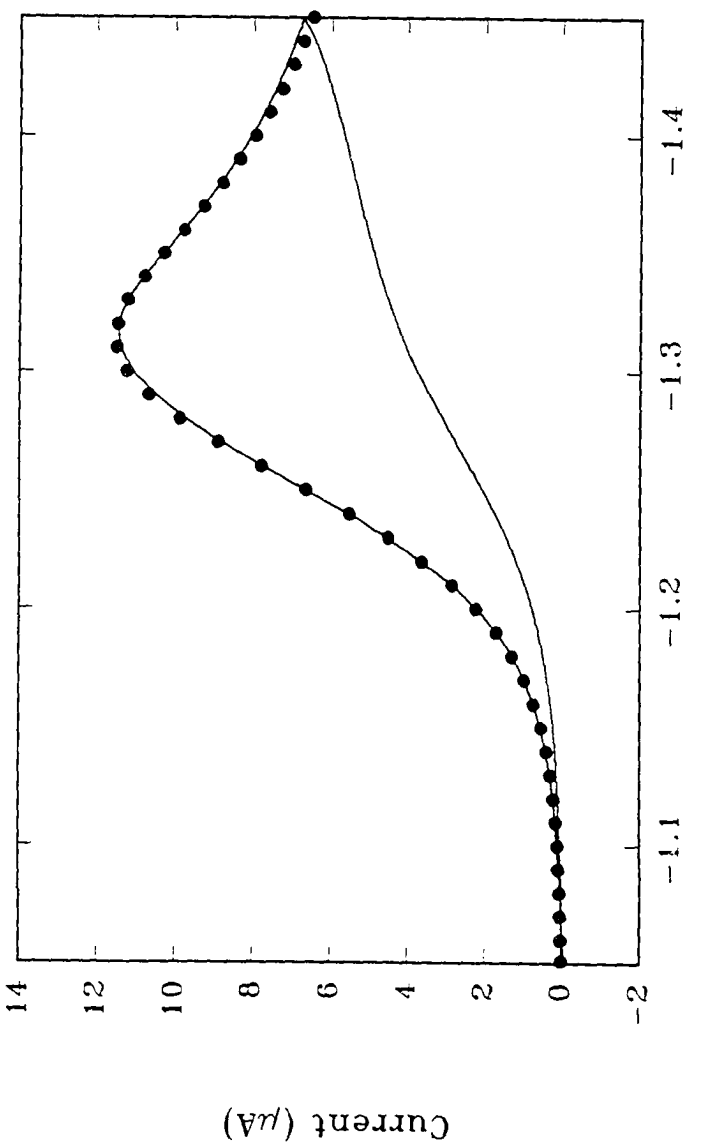

Fig. 9-8

Reproduced with permission of the copyright owner. Further reproduction prohibited without permission.

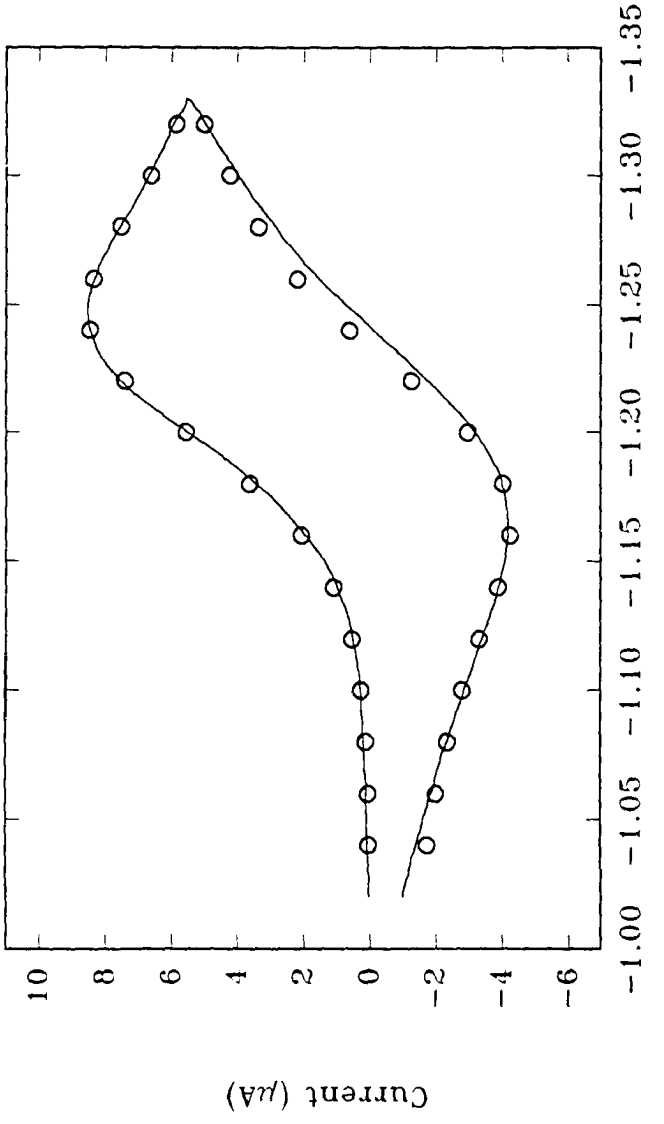

Fig. 9-9

Reproduced with permission of the copyright owner. Further reproduction prohibited without permission.

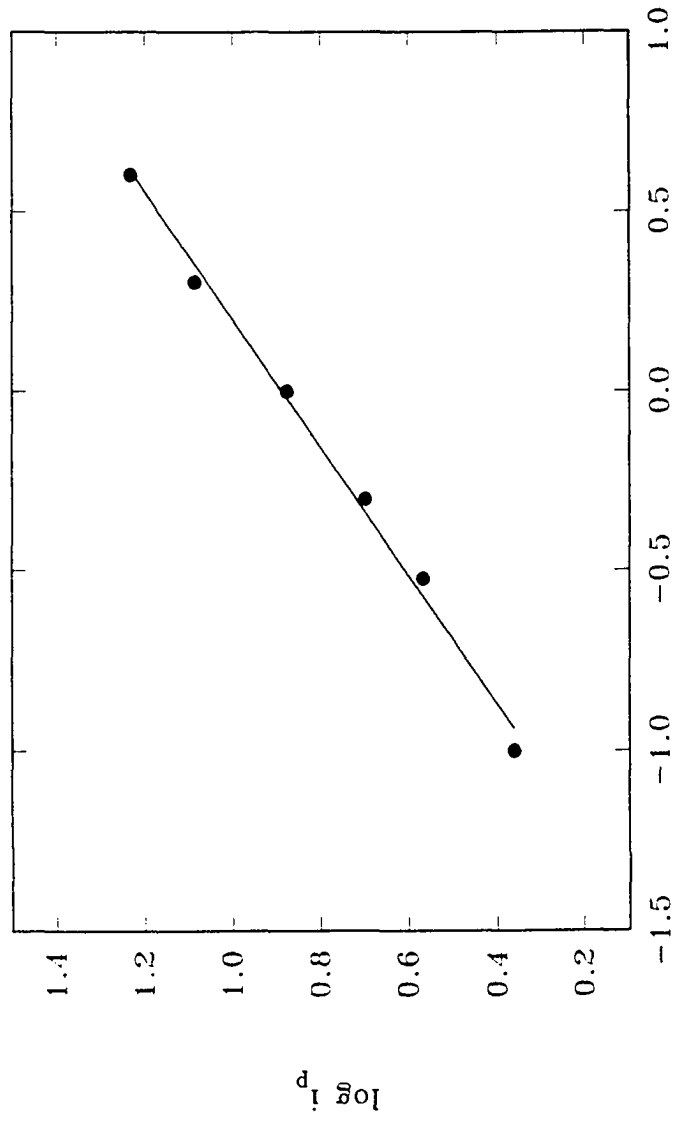

Fig. 9-10

Reproduced with permission of the copyright owner. Further reproduction prohibited without permission.

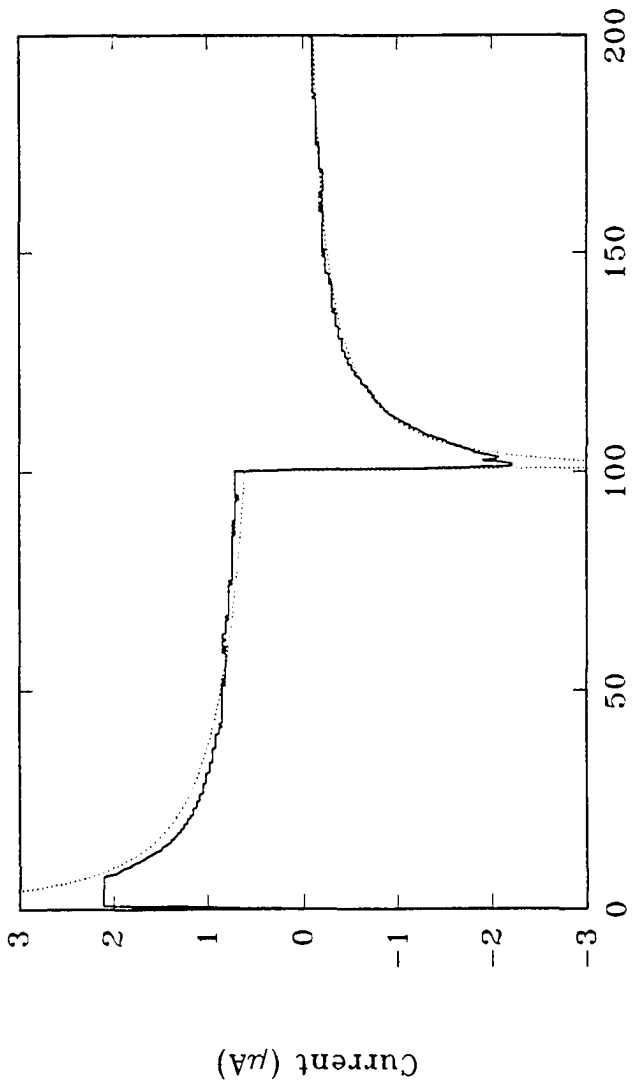

Fig. 9-11

Reproduced with permission of the copyright owner. Further reproduction prohibited without permission.

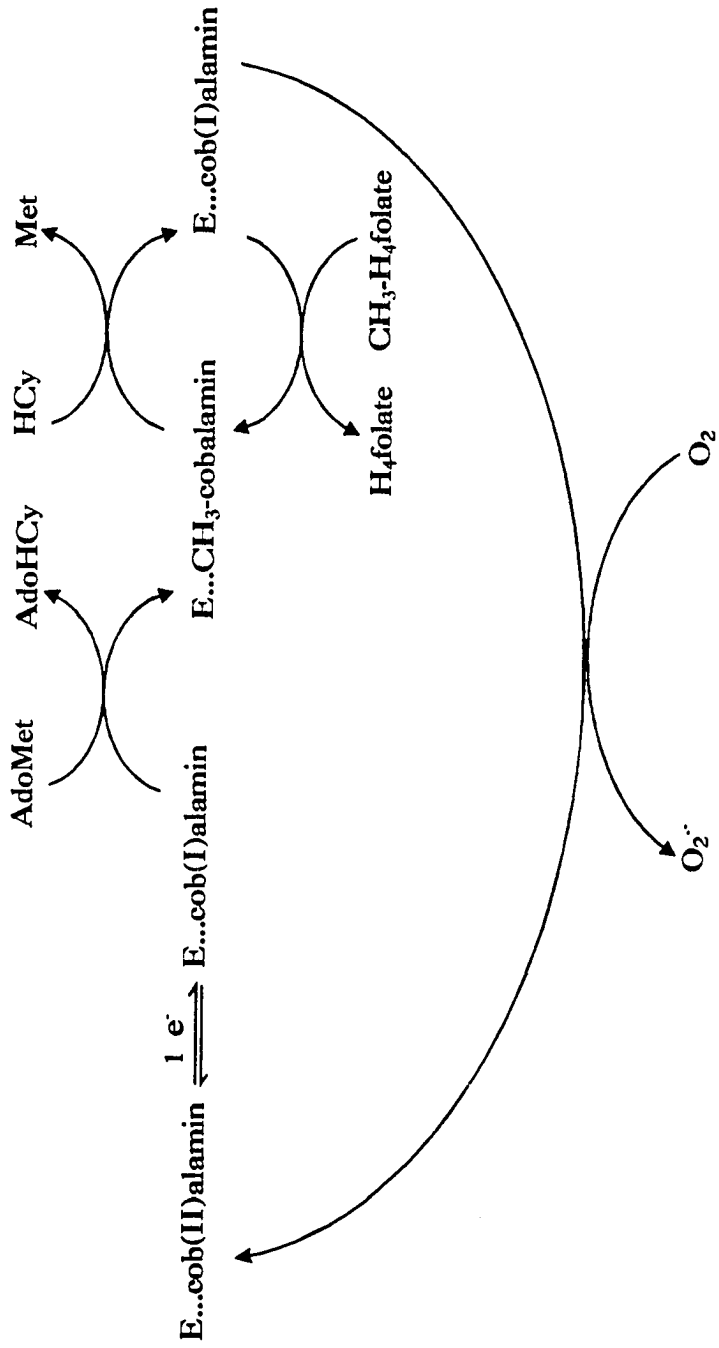

Scheme 6-1

Reproduced with permission of the copyright owner. Further reproduction prohibited without permission.

Scheme 7-1

Reproduced with permission of the copyright owner. Further reproduction prohibited without permission.

APPENDIX

Appendix 1.1 Data Communication Program

```
'+-------------------------------------------------------+
'|                                                       |
'|               Data Communication Program              |
'|     for BAS-100A/IBM PC-XT/AT Compatible Machine      |
'|                                                       |
'|                     Qingdong Huang                    |
'|                                                       |
'|                 Filename: BASCOM24.BAS                |
'|                    August 13, 1989                    |
'|                                                       |
'+-------------------------------------------------------+

starting:
  CLS
  INPUT "give the file name saved on the diskette: ", f$
  OPEN f$ FOR OUTPUT AS #2
  OPEN "com1:2400,n,8,1,cs,ds,cd" FOR RANDOM AS #1 LEN=3000
  PRINT
  PRINT "ask BAS-100A send file to the computer"
  PRINT
  PRINT "hit Esc to stop the communication"
  PRINT

  pause = 0: c$ = ""
  WHILE c$ <> CHR$(27)
     IF EOF(1) THEN GOTO OneMore
     b = LOC(1)
     IF b > 2000 THEN GOSUB ShakingOff
     IF b < 1001 AND pause = 1 THEN GOSUB ShakingOn
     ln$ = INPUT$(b, #1)
     PRINT #2, ln$;
     PRINT ln$;
OneMore:
     c$ = INKEY$
  WEND

CLOSE #1
CLOSE #2

PRINT f$; " was saved on the diskette, another try(y/n)?"
INPUT answer$
IF answer$ = "y" GOTO starting
END

ShakingOff:
   IF pause = 1 THEN GOTO ending
```

Reproduced with permission of the copyright owner. Further reproduction prohibited without permission.

```
   OUT &HF3FC, 0
   pause = 1

ending:
   RETURN

ShakingOn:
   OUT &HF3FC, 3
   pause = 0
   RETURN
```

Appendix 1.2 BAS-100A Data Conversion Program

```
'+-------------------------------------------------------+
'|                                                       |
'|            BAS-100A Data Conversion Program           |
'|  (convert CV data after line 13 in hexadecimal data file)
'|                                                       |
'|                      Qingdong Huang                   |
'|                                                       |
'|                  Filename: CVCONVT.BAS                |
'|                       May 19, 1989                    |
'|                                                       |
'+-------------------------------------------------------+

REP = 0
STARTING:
   CLS
   PRINT "Enter the file name to be converted:"
   INPUT FENTER$
   PRINT "Enter the new file name to be saved:"
   INPUT FSAVE$
   IF REP > 0 GOTO REPEATING
   PRINT "Enter  the initial potential in mVolt:"
   INPUT IV
   PRINT "Enter the switching potential in mVolt:"
   INPUT SV
   PRINT "Enter the final potential in mVolt:"
   INPUT FV
   PRINT "Enter the sensitivity index:"
   INPUT INDEX
   PRINT "Enter the steps in mVolt:"
   INPUT DELV

LOGVALUE = -INDEX * LOG(10)    'transfer index to decimal
SEN = EXP(LOGVALUE)

DIM GDATA$(8)
```

Reproduced with permission of the copyright owner. Further reproduction prohibited without permission.

```
DIM GDEC(8)

IF IV > SV THEN DELV = -DELV
DIM VX(2 * ABS(FV - SV) + 1)
FORWARD = FIX(ABS((IV - SV) / DELV) + .5)
BACKWARD = FIX(ABS((FV - SV) / DELV) + .5)
VX(0) = IV
VCHANGE = 0

FOR X = 1 TO FORWARD      'set 1st segment potential (mV)
   VCHANGE = VCHANGE + DELV
   VX(X) = IV + VCHANGE
NEXT X

VCHANGE = 0               'set 2nd segment potential (mV)
FOR X = (FORWARD + 1) TO (FORWARD + BACKWARD)
   VCHANGE = VCHANGE - DELV
   VX(X) = SV + VCHANGE
NEXT X

REPEATING:
   OPEN FENTER$ FOR INPUT AS #1
   OPEN FSAVE$ FOR OUTPUT AS #2

   U = 0
   VOL = 0
ReadGarbage:
   U = U + 1
   GARBAGE1$ = INPUT$(10, #1)  'count 1st 10 chars(garbage)

FOR I = 1 TO 8                 'read 8 groups in one line
   BS = 1
   TOTAL = 0
   GDATA$(I) = INPUT$(4, #1)   'one group for 4 hex decimal

   X$ = MID$(GDATA$(I), 2, 1)  'read 2nd hex in 1st group
   XH = VAL("&H" + X$) * BS
   BS = BS * 16
   TOTAL = TOTAL + XH

   X$ = MID$(GDATA$(I), 1, 1)  'read 1st hex in 1st group
   XH = VAL("&H" + X$) * BS
   BS = BS * 16
   TOTAL = TOTAL + XH

   X$ = MID$(GDATA$(I), 4, 1)  'read 2nd hex in 2nd group
   XH = VAL("&H" + X$) * BS
   BS = BS * 16
   TOTAL = TOTAL + XH

   X$ = MID$(GDATA$(I), 3, 1)  'read 1st hex in 2nd group
   XH = VAL("&H" + X$) * BS
```

Reproduced with permission of the copyright owner. Further reproduction prohibited without permission.

```
    TOTAL = TOTAL + XH
    GDEC(I) = TOTAL

    POINTS = GDEC(I) - 32768     'convert data to current
    CURRENT = -SEN * POINTS * 20 / 65537

    VOL = VOL + 1
    IF VOL = (FORWARD + BACKWARD + 2) THEN GOTO FINAL
    PRINT VX(VOL - 1), TAB(16); CURRENT
    PRINT #2, VX(VOL - 1), TAB(16); CURRENT
NEXT

GARBAGE2$ = INPUT$(4, #1)
GOTO ReadGarbage

FINAL:
    CLOSE #1
    CLOSE #2
    PRINT ("Convert another one with same parameters(y/n)?")
    INPUT ANSWER$
    REP = REP + 1
    IF ANSWER$ = "y" GOTO STARTING
    END
```

Appendix 2.1

The Cyclic Staircase (Cyclic Voltammetry) Waveform Generator Program

```
10 '*********************************************************
20 '*                                                       *
30 '*     Cyclic Staircase Waveform Generator Program       *
40 '*       (application program for CV experiments)        *
50 '*                                                       *
60 '*                    Qingdong Huang                     *
70 '*                   Filename: CV.BAS                    *
80 '*                    June 11, 1990                      *
90 '*                                                       *
100'*********************************************************
110 '
120 '
130 KEY OFF
140 CLS
150 DIM WDATA%(2048)
160 '
170 '
```

Reproduced with permission of the copyright owner. Further reproduction prohibited without permission.

```
180 '*****************************************************
190 '*                                                   *
200 '*                   WSB-10 PRESET                   *
210 '*                                                   *
220 '*****************************************************
230 '
240 'Define the offset of all the drivers
250 SETBAS= 7: DEFWAV=10: INTCLK=19: EXTCLK=22: REPEAT=25
260 SINGLE=28: SETDLY=31: WSTART=34: WRESET=37: WINIT =43
270 STATUS=46: INTRP =49: IRESET=52: VERNUM=55: WHOAMI=58
280 '
290 'Get the segment address of WSB1B.EXE, the WSB-10 BASIC
      driver
300 HOOK=&H180: DEF SEG=0: DEF SEG=PEEK(HOOK) + 256
      * PEEK(HOOK+1)
310 '
320 'Check if the driver has been installed
330 IF (PEEK(3) = &HAA) AND (PEEK(4) = &H55) THEN GOTO 430
340 BEEP:PRINT:PRINT "The WSB-10 driver is not installed!"
350 PRINT
360 PRINT "Before BASIC program controls WSB-10 waveform
      synthesizer,"
370 PRINT "the interface driver must be installed."
380 PRINT
390 PRINT "Exit BASIC, and execute WSB1B.EXE."
400 PRINT
410 END
420 '
430 PBASE% = &H330: CALL SETBAS( PBASE% )
440 '                                  'Set I/O port address
450 '
460 '*****************************************************
470 '*                                                   *
480 '*                SCREEN PARAMETERS                  *
490 '*                                                   *
500 '*****************************************************
510 '
520 LINE0 = 4: LINE1 = LINE0 + 3: LINE2 = LINE1 + 3
530 LINE3 = LINE2 + 3: LINE4 = LINE3 + 3: LINE5 = LINE4 + 4
540 COL1 = 1: COL2 = 26: COL3 = 52: COL4 = 41
550 '
560 '
570 '*****************************************************
580 '*                                                   *
590 '*         Initialize the Synthesizer Board          *
600 '*                                                   *
610 '*****************************************************
620 '
630 RATE0% = 1000: RATE1% = 1       'set default clock rate
640 NPOINTS1% = 10                  'set default data pts 10
650 NPOINTSP% = 10 -1               'set default preset pts 10
660 PRESETM = 1                     'set preset time 1 mSec
```

Reproduced with permission of the copyright owner. Further reproduction prohibited without permission.

```
670 DELAY% = 0: MODE$ = "R"          'set default delay/mode
680 PI = 0: PS = -1000: PF = 0       'set default range
690 SCAN = 1000                      'set default 1000 V/S
700 CALL WINIT
710 CALL SETDLY(DELAY%)
720 GOSUB 980                   'generate data points
730 GOSUB 2020                  'initialize screen
740 GOSUB 4110                  'display clock rate/frequency
750 CALL WSTART                 'start synthesizer
760 T% = 1                      'status variable
770 '
780 '
790 '*****************************************************
800 '*                                                   *
810 '*          Check Status and Update Display          *
820 '*                                                   *
830 '*****************************************************
840 '
850 LOCATE LINE4 + 1, COL3 + 5, 0
860 IF S% = 1 THEN PRINT "on " ELSE PRINT "off"
870 CALL STATUS(T%)                  'Read board status
880 A$ = INKEY$
890 IF T% <> S% THEN S% = T%: GOTO 850 ELSE GOTO 870
900 '
910 '
920'*****************************************************
930 '*                                                   *
940 '* Calculate Waveform Data Points and Program the Board *
950 '*                                                   *
960'*****************************************************
970 '
980 PERIOD = ABS(PI-PS)/(SCAN * 1000)
990 DELT = PERIOD/NPOINTS1%
1000 FIRST = NPOINTS1%
1010 IF PS = PF THEN NPOINTS2% = NPOINTS1%: GOTO 1040
1020 PERIOD2 = ABS(PS-PF)/(SCAN*1000)
1030 NPOINTS2% = PERIOD2/DELT
1040 SECOND = NPOINTS2%
1050 NPOINTS% = NPOINTS1% + NPOINTS2% + NPOINTSP% + 1
1060 DELV = ABS(PI-PS)/FIRST
1070 '
1080 IF DELT > .00655 THEN GOTO 1120  'generate clock rates
1090 RATE1% = 1
1100 RATE0% = 1000*10000*DELT
1110 GOTO 1150
1120 RATE0% = 10000!
1130 RATE1% = 1000 * DELT
1140 '
1150 CALL INTCLK(RATE0%, RATE1%)
1160 '
1170 FOR I = 0 TO NPOINTSP%          'generate preset points
1180 WDATA%(I) = PI/2.5
```

Reproduced with permission of the copyright owner. Further reproduction prohibited without permission.

```
1190 NEXT
1200 '
1210 IF (PI < PS) AND (PS > PF) THEN GOTO 1410
1220 IF (PI < PS) AND (PS < PF) THEN GOTO 1500
1230 IF (PI > PS) AND (PS < PF) THEN GOTO 1590
1240 IF (PI > PS) AND (PS > PF) THEN GOTO 1680
1250 IF (PI < PS) AND (PS = PF) THEN GOTO 1770
1260 IF (PI > PS) AND (PS = PF) THEN GOTO 1860
1270 '
1280 CALL STATUS(S%)
1290 CALL DEFWAV(NPOINTS%, WDATA%(0))
1300 RETURN
1310 '
1320 '
1330 '
1340 '*****************************************************
1350 '*                                                   *
1360 '*           Waveform Type Situations                *
1370 '*                                                   *
1380 '*****************************************************
1390 '
1400 'Situation 1
1410 FOR I = 1 TO FIRST
1420 WDATA%(I + NPOINTSP%) = WDATA%(0) + I * (DELV/2.5)
1430 NEXT I
1440 FOR I = (FIRST + 1) TO (FIRST + SECOND)
1450 WDATA%(I+NPOINTSP%) = WDATA%(FIRST+NPOINTSP%)
        - (I-FIRST)*(DELV/2.5)
1460 NEXT I
1470 GOTO 1280
1480 '
1490 'Situation 2
1500 FOR I = 1 TO FIRST
1510 WDATA%(I + NPOINTSP%) = WDATA%(0) + I * (DELV/2.5)
1520 NEXT I
1530 FOR I = (FIRST + 1) TO (FIRST + SECOND)
1540 WDATA%(I+NPOINTSP%) = WDATA%(FIRST+NPOINTSP%)
        + (I-FIRST)*(DELV/2.5)
1550 NEXT I
1560 GOTO 1280
1570 '
1580 'Situation 3
1590 FOR I = 1 TO FIRST
1600 WDATA%(I + NPOINTSP%) = WDATA%(0) - I * (DELV/2.5)
1610 NEXT I
1620 FOR I = (FIRST + 1) TO (FIRST + SECOND)
1630 WDATA%(I+NPOINTSP%) = WDATA%(FIRST+NPOINTSP%)
        + (I-FIRST)*(DELV/2.5)
1640 NEXT I
1650 GOTO 1280
1660 '
1670 'Situation 4
```

Reproduced with permission of the copyright owner. Further reproduction prohibited without permission.

```
1680 FOR I = 1 TO FIRST
1690 WDATA%(I + NPOINTSP%) = WDATA%(0) - I * (DELV/2.5)
1700 NEXT I
1710 FOR I = (FIRST + 1) TO (FIRST + SECOND)
1720 WDATA%(I+NPOINTSP%) = WDATA%(FIRST+NPOINTSP%)
         - (I-FIRST)*(DELV/2.5)
1730 NEXT I
1740 GOTO 1280
1750 '
1760 'Situation 5
1770 FOR I = 1 TO FIRST
1780 WDATA%(I + NPOINTSP%) = WDATA%(0) + I * (DELV/2.5)
1790 NEXT I
1800 FOR I = (FIRST + 1) TO (FIRST + SECOND)
1810 WDATA%(I + NPOINTSP%) = WDATA%(FIRST + NPOINTSP%)
1820 NEXT
1830 GOTO 1280
1840 '
1850 'Situation 6
1860 FOR I = 1 TO FIRST
1870 WDATA%(I + NPOINTSP%) = WDATA%(0) - I * (DELV/2.5)
1880 NEXT I
1890 FOR I = (FIRST + 1) TO (FIRST + SECOND)
1900 WDATA%(I + NPOINTSP%) = WDATA%(FIRST + NPOINTSP%)
1910 NEXT I
1920 GOTO 1280
1930 '
1940 '
1950 '
1960 '*****************************************************
1970 '*                                                   *
1980 '*                  Screen Message                   *
1990 '*                                                   *
2000 '*****************************************************
2010 ,
2020 LOCATE 2,18,0
2030 PRINT "CYCLIC STAIRCASE GENERATOR PROGRAM"
2040 LOCATE 3,18,0
2050 PRINT "**********************************"
2060 LOCATE LINE1, COL1, 0: PRINT "Initial E (mVolt)"
2070 LOCATE LINE1, COL2, 0: PRINT "Switching E (mVolt)"
2080 LOCATE LINE1, COL3, 0: PRINT "Final E (mVolt)"
2090 LOCATE LINE2, COL1, 0: PRINT "Scan Rate (Volt/Sec)"
2100 LOCATE LINE2, COL2, 0: PRINT "Point Number"
2110 LOCATE LINE2, COL3, 0: PRINT "Stepsize(mVolt)"
2120 LOCATE LINE3, COL1, 0: PRINT "Clock Rate0%"
2130 LOCATE LINE3, COL2, 0: PRINT "Clock Rate1%"
2140 LOCATE LINE3, COL3, 0: PRINT "Frequency (Hz)"
2150 LOCATE LINE4, COL1, 0: PRINT "Operation Mode"
2160 LOCATE LINE4, COL2, 0: PRINT "Preset Time (mSec)"
2170 LOCATE LINE4, COL3, 0: PRINT "Synthesizer"
2180 '
```

Reproduced with permission of the copyright owner. Further reproduction prohibited without permission.

```
2190 GOSUB 2840      'display default initial potential
2200 GOSUB 3040      'display default switching potential
2210 GOSUB 3230      'display default final potential
2220 GOSUB 3420      'display default scan rate
2230 GOSUB 3610      'display default point number
2240 GOSUB 3710      'display default operating mode
2250 GOSUB 3890      'display default delay time
2260 '
2270 LOCATE LINE5, COL1
2280 PRINT "F1 = initial potential (mVolt)";
2290 LOCATE LINE5+1, COL1
2300 PRINT "F2 = switching potential (mVolt)";
2310 LOCATE LINE5 + 2, COL1
2320 PRINT "F3 = final potential (mVolt)";
2330 LOCATE LINE5 + 3, COL1
2340 PRINT "F4 = scan rate (Volt/Sec)";
2350 LOCATE LINE5 + 4, COL1
2360 PRINT "F5 = point number";
2370 LOCATE LINE5, COL4
2380 PRINT "F6 = operation mode";
2390 LOCATE LINE5 + 1, COL4
2400 PRINT "F7 = preset time (mSec)";
2410 LOCATE LINE5 + 2, COL4
2420 PRINT "F8 = exit to system";
2430 LOCATE LINE5 + 3, COL4
2440 PRINT "F9 = start synthesizer"
2450 LOCATE LINE5 + 4, COL4
2460 PRINT "F10 = stop synthesizer";
2470 '
2480 ON KEY (1) GOSUB 2700    'reset initial potential
2490 ON KEY (2) GOSUB 2900    'reset switching potential
2500 ON KEY (3) GOSUB 3100    'reset final potential
2510 ON KEY (4) GOSUB 3290    'reset scan rate
2520 ON KEY (5) GOSUB 3480    'reset point number
2530 ON KEY (6) GOSUB 3670    'toggle operating mode
2540 ON KEY (7) GOSUB 3760    'reset preset time
2550 ON KEY (8) GOSUB 3930    'exit
2560 ON KEY (9) GOSUB 3970    'start synthesizer
2570 ON KEY (10) GOSUB 4010   'stop synthesizer
2580 '
2590 FOR J = 1 TO 10: KEY (J) ON: NEXT J
2600 RETURN
2610 '
2620 '
2630 '*****************************************************
2640 '*                                                   *
2650 '*          Setting Function Keys (F1-F10)           *
2660 '*                                                   *
2670 '*****************************************************
2680 '
2690 'Initial potential update (F1)
2700 FOR J = 1 TO 10: KEY(J) STOP: NEXT J
```

Reproduced with permission of the copyright owner. Further reproduction prohibited without permission.

```
2710 GOSUB 4460
2720 INPUT "Enter initial potential in Volt"; F1$
2730 GOSUB 4430
2740 IF F1$ = "" THEN GOTO 2860
2750 PI = VAL(F1$)
2760 IF (PI/1000<-5.12) OR (PI/1000>5.12) THEN GOTO 2710
2770 IF (ABS(PI-PS)< 100) THEN GOTO 2710
2780 GOSUB 4460
2790 PRINT "Calculating waveform data"
2800 GOSUB 980
2810 GOSUB 4100
2820 IF S% = 1 THEN CALL WSTART
2830 GOSUB 4430
2840 LOCATE LINE1 + 1,COL1 + 2,0:PRINT "                "
2850 LOCATE LINE1 + 1,COL1 + 2,0:PRINT USING "#####.#";PI
2860 FOR J = 1 TO 10: KEY(J) ON: NEXT J
2870 RETURN
2880 '
2890 'Switching potential update (F2)
2900 FOR J = 1 TO 10: KEY(J) STOP: NEXT J
2910 GOSUB 4460
2920 INPUT "Enter switching potential in Volt"; F2$
2930 GOSUB 4430
2940 IF F2$ = "" THEN GOTO 3060
2950 PS = VAL(F2$)
2960 IF (PS/1000<-5.12) OR (PS/1000>5.12) THEN GOTO 2910
2970 IF (ABS(PI-PS)<100) THEN GOTO 2910
2980 GOSUB 4460
2990 PRINT "Calculating waveform data"
3000 GOSUB 980
3010 GOSUB 4100
3020 IF S% = 1 THEN CALL WSTART
3030 GOSUB 4430
3040 LOCATE LINE1 + 1,COL2 + 4,0:PRINT "                "
3050 LOCATE LINE1 + 1,COL2 + 4,0:PRINT USING "#####.#"; PS
3060 FOR J = 1 TO 10: KEY(J) ON: NEXT J
3070 RETURN
3080 '
3090 'Final potential update (F3)
3100 FOR J = 1 TO 10: KEY(J) STOP: NEXT J
3110 GOSUB 4460
3120 INPUT "Enter final potential in Volt"; F3$
3130 GOSUB 4430
3140 IF F3$ = "" THEN GOTO 3250
3150 PF = VAL(F3$)
3160 IF (PF/1000<-5.12) OR (PF/1000>5.12) THEN GOTO 3110
3170 GOSUB 4460
3180 PRINT "Calculating waveform data"
3190 GOSUB 980
3200 GOSUB 4100
3210 IF S% = 1 THEN CALL WSTART
3220 GOSUB 4430
```

Reproduced with permission of the copyright owner. Further reproduction prohibited without permission.

```
3230 LOCATE LINE1 + 1,COL3 + 2,0:PRINT "                "
3240 LOCATE LINE1 + 1,COL3 + 2,0:PRINT USING "#####.#";PF
3250 FOR J = 1 TO 10: KEY(J) ON: NEXT J
3260 RETURN
3270 '
3280 'Scan rate update (F4)
3290 FOR J = 1 TO 10: KEY(J) STOP: NEXT J
3300 GOSUB 4460
3310 INPUT "Enter scan rate (Volt/Sec)"; SCAN$
3320 GOSUB 4430
3330 IF SCAN$ = "" THEN GOTO 3440
3340 SCAN = VAL(SCAN$)
3350 IF (SCAN < .005) OR (SCAN > 1000000!) THEN GOTO 3300
3360 GOSUB 4460
3370 PRINT "Calculating waveform data"
3380 GOSUB 980
3390 GOSUB 4100
3400 IF S% = 1 THEN CALL WSTART
3410 GOSUB 4430
3420 LOCATE LINE2 + 1,COL1,0:PRINT "                "
3430 LOCATE LINE2 + 1,COL1,0:PRINT USING "#######.###";SCAN
3440 FOR J = 1 TO 10: KEY(J) ON: NEXT J
3450 RETURN
3460 '
3470 'Point number update (F5)
3480 FOR J = 1 TO 10: KEY(J) STOP: NEXT J
3490 GOSUB 4460
3500 INPUT "Enter point number"; NPSA$
3510 GOSUB 4430
3520 IF NPSA$ = "" THEN GOTO 3630
3530 NPOINTS1% = VAL(NPSA$)
3540 IF (NPOINTS1%<2) OR (NPOINTS1%>2047) THEN GOTO 3490
3550 GOSUB 4460
3560 PRINT "Calculating waveform data"
3570 GOSUB 980
3580 GOSUB 4270
3590 IF S% = 1 THEN CALL WSTART
3600 GOSUB 4430
3610 LOCATE LINE2 + 1, COL2 + 3, 0: PRINT "                "
3620 LOCATE LINE2 + 1, COL2 + 3, 0: PRINT USING "####";
       NPOINTS1%
3630 FOR J = 1 TO 10: KEY(J) ON: NEXT J
3640 RETURN
3650 '
3660 'Define mode function (F6)
3670 IF MODE$ = "R" THEN MODE$ = "S" ELSE MODE$ = "R"
3680 IF MODE$ = "R" THEN CALL REPEAT
3690 IF MODE$ = "S" THEN CALL SINGLE
3700 GOSUB 980
3710 LOCATE LINE4 + 1, COL1 + 3
3720 IF MODE$ = "R" THEN PRINT "repeat" ELSE PRINT "single"
3730 RETURN
```

Reproduced with permission of the copyright owner. Further reproduction prohibited without permission.

```
3740 '
3750 'Preset time update (F7)
3760 GOSUB 4460
3770 INPUT "Enter preset time before waveform
          cycles (mSec)"; PRESETM$
3780 GOSUB 4430
3790 IF PRESETM$ = "" THEN GOTO 3910
3800 PRESETM = VAL(PRESETM$)
3810 PRESETS = PRESETM / 1000
3820 NPOINTSP% = INT(ABS(PRESETS / DELT) + .5)
3830 IF (NPOINTSP% < 0) OR (NPOINTSP% > 65535!) THEN GOTO 3770
3840 GOSUB 4460
3850 PRINT "Calculating waveform data"
3860 GOSUB 980
3870 IF S% = 1 THEN CALL WSTART
3880 GOSUB 4430
3890 LOCATE LINE4 + 1, COL2, 0: PRINT "                "
3900 LOCATE LINE4 + 1, COL2, 0: PRINT USING "#####.####";
          PRESETM
3910 RETURN
3920 '
3930 'Quit functions and exit (F8)
3940 KEY ON: CLS: END
3950 '
3960 'Start function (F9)
3970 CALL WSTART
3980 RETURN
3990 '
4000 'Stop function (F10)
4010 CALL WRESET
4020 RETURN
4030 '
4040 '
4050 '*****************************************************
4060 '*                                                   *
4070 '*              Clock Rate and Frequency             *
4080 '*                                                   *
4090 '*****************************************************
4100 '
4110 LOCATE LINE3 + 1, COL1 + 3, 0: PRINT "                "
4120 IF RATE0% < 2 THEN GOTO 4150
4130 LOCATE LINE3 + 1, COL1 + 3, 0: PRINT USING "######";
          RATE0%
4140 GOTO 4170
4150 LOCATE LINE3 + 1, COL1 + 3, 0:
          PRINT USING "######"; RATE0%; "(?)"
4160 '
4170 LOCATE LINE3 + 1, COL2 + 2, 0: PRINT "                "
4180 IF RATE1% < 1 THEN GOTO 4210
4190 LOCATE LINE3 + 1, COL2 + 2, 0: PRINT USING "######";
          RATE1%
4200 GOTO 4230
```

Reproduced with permission of the copyright owner. Further reproduction prohibited without permission.

```
4210 LOCATE LINE3 + 1, COL2 + 2, 0:
          PRINT USING "######"; RATE1%; "(?)"
4220 '
4230 HZ = (1000*10000)/(RATE0%*RATE1%)
4240 LOCATE LINE3 + 1, COL3 + 1, 0: PRINT "                "
4250 LOCATE LINE3 + 1, COL3 + 1, 0: PRINT USING
          "#######.#"; HZ
4260 '
4270 JUMPMV = (ABS(PS-PI))/NPOINTS1%
4280 IF JUMPMV < 2.5 THEN GOTO 4320
4290 LOCATE LINE2 + 1, COL3 + 2, 0: PRINT "                "
4300 LOCATE LINE2 + 1, COL3 + 2, 0: PRINT USING
          "#####.#"; JUMPMV
4310 GOTO 4340
4320 LOCATE LINE2 + 1, COL3 + 2, 0: PRINT "                "
4330 LOCATE LINE2 + 1, COL3 + 2, 0: PRINT "  < 2.5 (?)"
4340 RETURN
4350 '
4360 '
4370 '*****************************************************
4380 '*                                                   *
4390 '*       Clear Top Three Lines on the Screen         *
4400 '*                                                   *
4410 '*****************************************************
4420 '
4430 LOCATE LINE0, 1, 0
4440 PRINT "                                               "
4450 PRINT "                                               "
4460 LOCATE LINE0, 1, 0
4470 PRINT "                                               "
4480 RETURN
4490 '
```

Reproduced with permission of the copyright owner. Further reproduction prohibited without permission.

Appendix 2.2

The Potential Step Chronoamperometry Waveform Generator Program

```
10 '*********************************************************
20 '*                                                       *
30 '*           Potential Step Chronoamperometry            *
40 '*              Waveform Generator Program               *
50 '*                                                       *
60 '*                    Qingdong Huang                     *
70 '*                  Filename: STEPV.BAS                  *
80 '*                    June 13, 1990                      *
90 '*********************************************************
100 '
110 '
120 KEY OFF
130 CLS
140 DIM WDATA%(2048)
150 '
160 '
170 '*********************************************************
180 '*                                                       *
190 '*                   WSB-10 PRESET                       *
200 '*                                                       *
210 '*********************************************************
220 '
230 'Define the offset of all the drivers
240 SETBAS= 7: DEFWAV=10: INTCLK=19: EXTCLK=22: REPEAT=25
250 SINGLE=28: SETDLY=31: WSTART=34: WRESET=37: WINIT =43
260 STATUS=46: INTRP =49: IRESET=52: VERNUM=55: WHOAMI=58
270 '
280 'Get the segment address of WSB1B.EXE
290 HOOK=&H180: DEF SEG=0: DEF SEG=PEEK(HOOK) + 256
        * PEEK(HOOK+1)
300 '
310 'Check if the driver has been installed
320 IF (PEEK(3) = &HAA) AND (PEEK(4) = &H55) THEN GOTO 420
330 BEEP:PRINT:PRINT "The WSB-10 driver is not installed!"
340 PRINT
350 PRINT "Before BASIC program controls WSB-10 waveform
        synthesizer,"
360 PRINT "the interface driver must be installed."
370 PRINT
380 PRINT "Exit BASIC, and execute WSB1B.EXE."
390 PRINT
400 END
410 '
420 PBASE% = &H330: CALL SETBAS(PBASE%)
430 '                                   'Set I/O port address
440 '
```

Reproduced with permission of the copyright owner. Further reproduction prohibited without permission.

```
450 '*****************************************************
460 '*                                                   *
470 '*                  SCREEN PARAMETERS                *
480 '*                                                   *
490 '*****************************************************
500 '
510 LINE0 = 5: LINE1 = LINE0 + 3: LINE2 = LINE1 + 4
520 LINE3 = LINE2 + 4: LINE4 = LINE3 + 5
530 COL1 = 1: COL2 = 26: COL3 = 52: COL4 = 41
540 '
550 '
560 '*****************************************************
570 '*                                                   *
580 '*          Initialize the Synthesizer Board         *
590 '*                                                   *
600 '*****************************************************
610 '
620 INDEX = 10                  'set default index number 10
630 DELAY% = 0: MODE$ = "R"     'set default delay time/mode
640 IE = -100: FE = -1000       'set default potentials (mV)
650 DELTM = 1: DELT = DELTM/1000   'set default time 1 mSec
660 CALL WINIT
670 GOSUB 950                   'generate data points
680 GOSUB 1220                  'initialize screen
690 GOSUB 2870                  'display clock rate/frequency
700 CALL INTCLK(RATE0%, RATE1%)
710 CALL SETDLY(DELAY%)
720 CALL WSTART                 'start synthesizer
730 T% = 1                      'status variable
740 '
750 '
760 '*****************************************************
770 '*                                                   *
780 '*          CHECK STATUS AND UPDATE DISPLAY          *
790 '*                                                   *
800 '*****************************************************
810 '
820 LOCATE LINE2 + 1, COL3 + 5, 0
830 IF S% = 1 THEN PRINT "on " ELSE PRINT "off"
840 CALL STATUS(T%)                      'Read board status
850 A$ = INKEY$
860 IF T% <> S% THEN S% = T%: GOTO 820 ELSE GOTO 840
870 '
880 '
890 '*****************************************************
900 '*                                                   *
910 '*Calculate Waveform Data Points and Program the Board*
920 '*                                                   *
930 '*****************************************************
940 '
950 IF DELT > .00655 THEN GOTO 990
960 RATE1% = 1
```

Reproduced with permission of the copyright owner. Further reproduction prohibited without permission.

```
970 RATE0% = 1000 * 10000 * DELT
980 GOTO 1030
990 RATE0% = 10000
1000 RATE1% = 1000 * DELT
1010 '
1020 IF INDEX = 0 THEN GOTO 1070
1030 FOR I = 0 TO INDEX -1        'generate preset data pts
1040 WDATA%(I) = IE/2.5
1050 NEXT
1060 '
1070 WDATA%(INDEX) = FE/2.5       'generate final data pt
1080 WDATA%(INDEX + 1) = IE/2.5   'reset initial potential
1090 '
1100 NPOINTS% = INDEX + 2
1110 CALL STATUS(S%)
1120 CALL DEFWAV(NPOINTS%, WDATA%(0))
1130 RETURN
1140 '
1150 '
1160 '*****************************************************
1170 '*                                                   *
1180 '*                  Screen Message                   *
1190 '*                                                   *
1200 '*****************************************************
1210 ,
1220 LOCATE 2,8,0
1230 PRINT "STEP CHRONOAMPEROMETRY WAVEFORM GENERATOR PROGRAM"
1240 LOCATE 3,8,0
1250 PRINT "*************************************************"
1260 LOCATE LINE1, COL1, 0: PRINT "Initial E (mVolt)"
1270 LOCATE LINE1, COL2, 0: PRINT "Final E (mVolt)"
1280 LOCATE LINE1, COL3, 0: PRINT "Pulse Width (mSec)"
1290 LOCATE LINE2, COL1, 0: PRINT "Preset Index Number"
1300 LOCATE LINE2, COL2, 0: PRINT "Operation mode"
1310 LOCATE LINE2, COL3, 0: PRINT "Synthesizer"
1320 LOCATE LINE3, COL1, 0: PRINT "Clock Rate0%"
1330 LOCATE LINE3, COL2, 0: PRINT "Clock Rate1%"
1340 LOCATE LINE3, COL3, 0: PRINT "Frequency (Hz)"
1350 '
1360 GOSUB 1930     'display default initial potential
1370 GOSUB 2130     'display default switching potential
1380 GOSUB 2350     'display default pulse width in mSec
1390 GOSUB 2550     'display default index number
1400 GOSUB 2650     'display default operating mode
1410 '
1420 LOCATE LINE4, COL1
1430 PRINT "F1 = initial potential (mVolt)";
1440 LOCATE LINE4+1, COL1
1450 PRINT "F2 = final potential (mVolt)";
1460 LOCATE LINE4 + 2, COL1
1470 PRINT "F3 = pulse width (mSec)";
1480 LOCATE LINE4 + 3, COL1
```

Reproduced with permission of the copyright owner. Further reproduction prohibited without permission.

```
1490 PRINT "F4 = preset index number";
1500 LOCATE LINE4, COL4
1510 PRINT "F6 = operation mode";
1520 LOCATE LINE4 + 1, COL4
1530 PRINT "F8 = exit to system";
1540 LOCATE LINE4 + 2, COL4
1550 PRINT "F9 = start synthesizer"
1560 LOCATE LINE4 + 3, COL4
1570 PRINT "F10 = stop synthesizer";
1580 '
1590 ON KEY (1) GOSUB 1790    'reset initial potential
1600 ON KEY (2) GOSUB 1990    'reset final potential
1610 ON KEY (3) GOSUB 2190    'reset pulse width
1620 ON KEY (4) GOSUB 2410    'reset preset index number
1630 ON KEY (6) GOSUB 2610    'toggle operating mode
1640 ON KEY (8) GOSUB 2700    'exit
1650 ON KEY (9) GOSUB 2730    'start synthesizer
1660 ON KEY (10) GOSUB 2770   'stop synthesizer
1670 '
1680 FOR J = 1 TO 10: KEY (J) ON: NEXT J
1690 RETURN
1700 '
1710 '
1720 '*****************************************************
1730 '*                                                   *
1740 '*        Setting Function Keys (F1-F10)             *
1750 '*                                                   *
1760 '*****************************************************
1770 '
1780 'Initial potential update (F1)
1790 FOR J = 1 TO 10: KEY(J) STOP: NEXT J
1800 GOSUB 3140
1810 INPUT "Enter initial potential in mVolt"; F1$
1820 GOSUB 3110
1830 IF F1$ = "" THEN GOTO 1950
1840 IE = VAL(F1$)
1850 IF (IE/1000 < -5.1) OR (IE/1000 > 5.1) THEN GOTO 1800
1860 GOSUB 3140
1870 PRINT "Calculating waveform data"
1880 GOSUB 950
1890 CALL INTCLK(RATE0%,RATE1%)
1900 IF S% <> 1 THEN GOTO 1920
1910 CALL WSTART
1920 GOSUB 3110
1930 LOCATE LINE1 + 1,COL1 + 3,0:PRINT "                "
1940 LOCATE LINE1 + 1,COL1 + 3,0:PRINT USING "#####.#";IE
1950 FOR J = 1 TO 10: KEY(J) ON: NEXT J
1960 RETURN
1970 '
1980 'Final potential update (F2)
1990 FOR J = 1 TO 0: KEY(J) STOP: NEXT J
2000 GOSUB 3140
```

Reproduced with permission of the copyright owner. Further reproduction prohibited without permission.

```
2010 INPUT "Enter final potential in mVolt"; F2$
2020 GOSUB 3110
2030 IF F2$ = "" THEN GOTO 2150
2040 FE = VAL(F2$)
2050 IF (FE/1000 < -5.1) OR (FE/1000 > 5.1) THEN GOTO 2000
2060 GOSUB 3140
2070 PRINT "Calculating waveform data"
2080 GOSUB 950
2090 CALL INTCLK(RATE0%, RATE1%)
2100 IF S% <> 1 THEN GOTO 2120
2110 CALL WSTART
2120 GOSUB 3110
2130 LOCATE LINE1 + 1,COL2 + 3,0:PRINT "                "
2140 LOCATE LINE1 + 1,COL2 + 3,0:PRINT USING "#####.#";FE
2150 FOR J = 1 TO 10: KEY(J) ON: NEXT J
2160 RETURN
2170 '
2180 'Pulse width update (F3)
2190 FOR J = 1 TO 10: KEY(J) STOP: NEXT J
2200 GOSUB 3140
2210 INPUT "Enter pulse width in mSec"; F3$
2220 GOSUB 3110
2230 IF F3$ = "" THEN GOTO 2370
2240 DELTM = VAL(F3$)
2250 IF (DELTM < .0002) OR (DELTM > 20000) THEN GOTO 2200
2260 DELT = DELTM / 1000
2270 GOSUB 3140
2280 PRINT "Calculating waveform data"
2290 GOSUB 950
2300 GOSUB 2870
2310 CALL INTCLK(RATE0%, RATE1%)
2320 IF S% <> 1 THEN GOTO 2340
2330 CALL WSTART
2340 GOSUB 3110
2350 LOCATE LINE1 + 1,COL3,0:PRINT "                "
2360 LOCATE LINE1 + 1,COL3,0:PRINT USING "####.####";DELTM
2370 FOR J = 1 TO 10: KEY(J) ON: NEXT J
2380 RETURN
2390 '
2400 'Delay index number update (F4)
2410 FOR J = 1 TO 10: KEY(J) STOP: NEXT J
2420 GOSUB 3140
2430 INPUT "Enter preset index number"; INDEX$
2440 GOSUB 3110
2450 IF INDEX$ = "" THEN GOTO 2570
2460 INDEX = VAL(INDEX$)
2470 IF (INDEX < 0) OR (INDEX > 2046) THEN GOTO 2420
2480 GOSUB 3140
2490 PRINT "Calculating waveform data"
2500 GOSUB 950
2510 CALL INTCLK(RATE0%, RATE1%)
2520 IF S% <> 1 THEN GOTO 2540
```

Reproduced with permission of the copyright owner. Further reproduction prohibited without permission.

```
2530 CALL WSTART
2540 GOSUB 3110
2550 LOCATE LINE2 + 1,COL1 + 4,0:PRINT "                "
2560 LOCATE LINE2 + 1,COL1 + 4,0:PRINT USING "####";INDEX
2570 FOR J = 1 TO 10: KEY(J) ON: NEXT J
2580 RETURN
2590 '
2600 'Define mode function (F6)
2610 IF MODE$ = "R" THEN MODE$ = "S" ELSE MODE$ = "R"
2620 IF MODE$ = "R" THEN CALL REPEAT
2630 IF MODE$ = "S" THEN CALL SINGLE
2640 GOSUB 950
2650 LOCATE LINE2 + 1, COL2 + 4
2660 IF MODE$ = "R" THEN PRINT "repeat" ELSE PRINT "single"
2670 RETURN
2680 '
2690 'Quit functions and return to BASICA (F8)
2700 KEY ON: CLS: END
2710 '
2720 'Start function (F9)
2730 CALL WSTART
2740 RETURN
2750 '
2760 'Stop function (F10)
2770 CALL WRESET
2780 RETURN
2790 '
2800 '
2810 '*****************************************************
2820 '*                                                   *
2830 '*         Clock Rate and Frequency Display          *
2840 '*                                                   *
2850 '*****************************************************
2860 '
2870 LOCATE LINE3 + 1, COL1 + 4, 0: PRINT "               "
2880 IF RATE0% < 2 THEN GOTO 2910
2890 LOCATE LINE3+1,COL1+4,0:PRINT USING "#####";RATE0%
2900 GOTO 2930
2910 LOCATE LINE3+1,COL1+4,0:PRINT USING "#####";RATE0%; "(?)"
2920 '
2930 LOCATE LINE3 + 1, COL2 + 2, 0: PRINT "               "
2940 IF RATE1% < 1 THEN GOTO 2970
2950 LOCATE LINE3+1,COL2+2,0:PRINT USING "#####";RATE1%
2960 GOTO 2990
2970 LOCATE LINE3+1,COL2+2,0:PRINT USING "#####";RATE1%; "(?)"
2980 '
2990 HZ = (1000*10000)/(RATE0%*RATE1%)
3000 LOCATE LINE3 + 1,COL3,0:PRINT "                    "
3010 LOCATE LINE3 + 1,COL3,0:PRINT USING "########"; HZ
3020 RETURN
3030 '
3040 '
```

Reproduced with permission of the copyright owner. Further reproduction prohibited without permission.

```
3050 '*****************************************************
3060 '*                                                   *
3070 '*       Clear Top Three Lines on the Screen         *
3080 '*                                                   *
3090 '*****************************************************
3100 '
3110 LOCATE LINE0, 1, 0
3120 PRINT "                                               "
3130 PRINT "                                               "
3140 LOCATE LINE0, 1, 0
3150 PRINT "                                               "
3160 RETURN
3170 '
```

Appendix 2.3

Data Conversion Program for Waveform Analysis System

```
/*********************************************************/
/*                                                       */
/*    IS-2010 WAVEFORM ANALYSIS SYSTEM DATA CONVERTER    */
/* (convert and calibrate data point number by Turbo C++) */
/*                                                       */
/*                      Qingdong Huang                   */
/*                                                       */
/*                  Filename: COUNTNUM.C                 */
/*                    November 7, 1990                   */
/*                                                       */
/*********************************************************/

#include<stdio.h>
main()
{
   long words[20];
   int n, i, j, bytes[19], garbage[9];
   long int samples[2049];
   static float valuec;
   float timerate,gainfact[11],samptime[17],voltage[2049];
   float voltage1[2049], voltage2[2049], voltage3[2049];
   FILE *in, *out;
   char filein[13], fileout[13];

   gainfact[1] = 0.25;    gainfact[2] = 0.5 ;
   gainfact[3] = 1.0 ;    gainfact[4] = 2.5 ;
   gainfact[5] = 5.0 ;    gainfact[6] = 10.0;
   gainfact[7] = 25.0;    gainfact[8] = 50.0;
   gainfact[9] = 100.0;   gainfact[10] = 250.0;
```

Reproduced with permission of the copyright owner. Further reproduction prohibited without permission.

```
    samptime[7]=4.0e-8;  samptime[8]=8.0e-8;
    samptime[9]=1.6e-7;  samptime[10]=4.0e-7;
    samptime[11]=8.0e-7; samptime[12]=1.6e-6;
    samptime[13]=4.0e-6; samptime[14]=8.0e-6;
    samptime[15]=1.6e-5; samptime[16]=4.0e-5;
    samptime[17]=8.0e-5; samptime[18]=1.6e-4;
    samptime[19]=4.0e-4; samptime[20]=8.0e-4;
    samptime[21]=1.6e-3; samptime[22]=4.0e-3;

    printf("Enter the file name to be converted: ");
    scanf("%s", filein);
    printf("\nEnter the file name to be saved: ");
    scanf("%s", fileout);
    printf("\nEnter the vertical calibration value: ");
    scanf("%f", &valuec);

    in = fopen(filein, "rb");
    out = fopen(fileout, "w");
       {
       for (i=1; i<=19; i++)
          {
          words[i] = getc(in) + 256 * getc(in);
          if (words[i] > 32767) words[i] = words[i] - 65536;
          }

       for (i=1; i<=18; i++) bytes[i] = getc(in);
       for (i=1; i<=8; i++) garbage[i] = getc(in);

       i = 1;
       while((samples[i] = getc(in)) != EOF) i++;

       fclose(in);
       }

    j = i - 1;
    timerate = samptime[words[13]];
    printf("\ntotal data are %d\n", j);
    printf("\ncalibrating value = %5.4f\n", valuec);

    for (i = 1; i <= j; i++)
     {
     voltage1[i] = gainfact[words[14] + 1];
     voltage2[i]=82-((words[12]*samples[i]+words[9])/256.0);
     voltage3[i] = (words[15] - 8) * 20;
     voltage[i] = voltage1[i] * (voltage2[i] + voltage3[i])
           + valuec;
     fprintf(out, "%5d %11.4f\n", i * timerate, voltage[i]);
     }
    fclose(out);
}
```

Reproduced with permission of the copyright owner. Further reproduction prohibited without permission.

Reference Cited in Part 1

1. P.He, J.P.Avery and L.R.Faulkner, *Anal.Chem.*, **54** (1982) 1313A.

2. *BAS-100A Electrochemical Analyzer Manual*, Bioanalytical Systems, Inc., West Lafayette, Indiana, October 1989.

3. P.Norton, *Inside the IBM PC - Revised and Inlarged*, Brady Communications Company, Inc., 1986.

4. P.W.Gofton, Mastering Serial Communications, Sybex Inc., 1986.

5. L.R.Faulkner and P.He, *Memory Assignments and Data Storage Protocols for the BAS-100*, Bioanalytical Systems, Inc., West Lafayette, Indiana.

6. Model 270 Electrochemical Analysis Systems Manual, EG&G Princeton Applied Research, Princeton, New Jersey, 1991.

7. R.M.Wightman, *Science*, **240** (1988) 415.

8. C.P.Andrieux, P.Hapiot and J.M.Saveant, *J.Phys.Chem.*, **92** (1988) 5992.

9. R.M.Wightman and D.O.Wipf, *Acc.Chem.Res.*, **23** (1990) 64.

10. *WSB-10 Waveform Synthesizer Instruction Manual*, Version 2.00, Qua Tech, Inc., Akron, Ohio, 1987.

11. *IS-2010 Waveform Analysis System User's Manual*, Version 1.3, Integrated Systems Products, Inc., Camarillo, California, 1987.

12. A.Bard and L.R.Faulkner, *Electrochemical Methods - Fundamentals and Applications*, John Wiley & Sons, New York, 1980.

13. D.Britz, *J.Electroanal.Chem.*, **88** (1978) 309.

14. P.T.Kissinger and W.R.Heineman, *Laboratory Techniques in Electroanalytical Chemistry*, Marcel Dekker, Inc., New York, 1984.

15. *Semiconductor Reference Guide*, Radio Shack, Fort Worth, Texas, 1992.

16. J.O.Howell, W.G.Kuhr, R.E.Ensman and R.M.Wightman, *J.Electroanal.Chem.*, **209** (1986) 77.

17. *R.G.Irvine, Operational Amplifier Characteristics and Applications*, 2nd edition, Prentice-Hall, Inc., Englewood Cliffs, New Jersey, 1987.

Reproduced with permission of the copyright owner. Further reproduction prohibited without permission.

18. J.C.C.Nelson, *BASIC Operational Amplifiers*, Butterworths, London, 1986.

19. H.A.Strobel and W.T.Heineman, *Chemical Instrumentation - A Systematic Approach Their Edition*, Wiley & Son, New York, 1989.

20. J.C.Boyce, *Operational Amplifiers and Linear Integrated Circuits*, 2nd edition, PWS-Kent Publishing Company, Boston, 1988.

21. T.M.Frederiksen, *Intuitive Operational Amplifiers - From Basics to Useful Applications*, revised edition, McGraw-Hill Book Company, New York, 1989.

22. D.M.Morgan and S.G.Weber, *Anal.Chem.*, **56** (1984) 2560.

Reproduced with permission of the copyright owner. Further reproduction prohibited without permission.

Reference Cited in Part 2

1. R.P.Van Duyne and C.N.Reilley, *Anal.Chem.*, **44** (1972) 142.
2. R.P.Van Duyne and C.N.Reilley, *Anal.Chem.*, **44** (1972) 153.
3. R.P.Van Duyne and C.N.Reilley, *Anal.Chem.*, **44** (1972) 158.
4. N.R.Kestner, J.Logan and J.Jortner, *J.Phys.Chem.*, **78** (1974) 2148.
5. M.Cappadonia and U.Stimming, *J.Electroanal.Chem.*, **300** (1991) 235.
6. U.Frese, T.Iwasita, W.Schmickler and U.Stimming, *J.Phys.Chem.*, **89** (1985) 1059.
7. T.H.Huang, E.Davis, U.Frese and U.Stimming, *J.Phys.Chem.*, **92** (1988) 6874.
8. J.O.Bockris and J.Wass, *J.Electroanal.Chem.*, **267** (1989) 325.
9. J.O.Bockris and J.Wass, *J.Electroanal.Chem.*, **267** (1989) 329.
10. A.M.Bond and L.Zongpeng, *J.Electroanal.Chem.*, **259** (1989) 189.
11. A.M.Bond and M.Svestka, *J.Electroanal.Chem.*, **301** (1989) 139.
12. A.M.Bond and V.B.Pfund, *J.Electroanal.Chem.*, **335** (1992) 281.
13. A.M.Bond, M.Fleischmann and J.R.Robinson, *J.Electroanal.Chem.*, **180** (1984) 257.
14. G.B.Sergeev and V.A.Batyuk, *Cryochemistry*, Mir Publishers, Moscow, 1978.
15. J.M.Butler, *J.Electroanal.Chem.*, **14** (1967) 89.
16. D.K.Gosser Jr. and Q.Huang, *J.Electroanal.Chem.*, **267** (1989) 333.
17. D.K.Gosser Jr. and Q.Huang, *J.Electroanal.Chem.*, **278** (1990) 399.
18. D.K.Gosser Jr., Q.Huang and P.H.Rieger, *J.Electroanal.Chem.*, **286** (1990) 257.
19. Y.Q.Gosser, personal communication.
20. P. Mazur, *Cryobiology*, **14** (1977) 251.

Reproduced with permission of the copyright owner. Further reproduction prohibited without permission.

21. H.Bank, *Cryobiology*, **10** (1973) 157.

22. H.T.Meryman, *Science*, **124** (1956) 515.

23. D.E.Pegg, *J.Clin.Pathol.*, **29** (1976) 271.

24. H.T.Meryman, R.J.Williams and M.St.J.Douglas, *Cryobiology*, **14** (1977) 287.

25. P.Mazur, *Science*, **168** (1970) 939.

26. P.Mazur, *Am.J.Physiol.*, **247** (1984) c125.

27. H.T.Mariman, *Cryobiology*, **8** (1971) 489.

28. M.J.Ashwood-Smith, in *Low Temperature Preservation in Medicine and Biology*, M.J.Ashwood-Smith and J.Farrant (eds.), Pitman, Melbourne, 1980, p19.

29. V.Silani, A.Pizzuti, O.Strada, A.Falini, M.Buscaglia and G.Scarlato, *Brain Research*, **473** (1988) 169.

30. W.J.Tze and J.Tai, *Metabolism*, **39** (1990) 719.

31. G.M.Fahy, *Biophysical Journal*, **32** (1980) 837.

32. J.L.Roberts and D.T.Sawyer, *J.Electroanal.Chem.*, **9** (1965) 7.

33. C.G.Zoski, A.M.Bond, C.L.Colyer, J.C.Myland and K.B.Oldham, *J.Electroanal.Chem.*, **263** (1989) 1.

34. R.E.Pincock, *Acc.Chem.Res.*, **24** (1969) 97.

35. D.A.Skoog, *Principles of Instrumental Analysis*, 3rd edition, Saunders College Publishing, Philadelphia, 1985.

36. T.J.Stone, P.L.Buckman and H.M.McConnell, *Proc.Natl.Acad.Sci.*, **54** (1965) 1010.

37. J.H.Freed, in *Spin Labeling: Theory and Applications*, L.J.Berliner, (ed.), Academic Press, New York, 1976.

38. S.A.Goldman, G.V.Bruno, C.F.Polnaszek and J.H.Freed, *J.Chem.Phys.*, **56** (1972) 716.

39. A.M.Bobst, in *Spin Labeling II: Theory and Applications*, L.J.Berliner (ed.), Academic Press, New York, 1979.

Reproduced with permission of the copyright owner. Further reproduction prohibited without permission.

40. S.Ohnishi and H.M.McConnell, *J.Am.Chem.Soc.*, **87** (1965) 2293.

41. R.Briere and A.Rassat, *Tetrahedron*, **32** (1976) 2891.

42. L.H.Berliner (ed.), *Spin Labeling: Theory and Applications*, Academic Press, New York, 1976.

43. J.L.Holtzman (ed.), *Spin Labeling in Pharmacology*, Academic Press, Inc., Orlando, Fl, 1984.

44. A.Abragam, *Principles of Nuclear Magnetism*, Oxford University Press, Oxford, 1986.

45. B.S.Prabhananda, *Proc.Nucl.Phys. Solid State Phys.Symp.*, **24C** (1981) 431.

46. A.J.Bard and L.R.Faulkner, *Electrochemical Method - Fundamentals and Applications*, Wiley, New York, 1980, p218.

47. F.Franks, *Biophysics and biochemistry at low temperature*, Cambridge University Press, Cambridge, 1985.

48. T.Shedlowsky and R.L.Kay, *J.Phys.Chem.*, **60** (1956) 155.

49. G.H.B.Hoa and P.Douzou, *J.Biol.Chem.*, **248** (1973) 4649.

50. A.Buckley, *J.Chem.Educ.*, **42** (1965) 674.

51. A.L.Douzou, *Biochimie*, **53** (1971) 1580.

52. M.J.Ashwood-Smith, in *Low Temperature Preservation in Medicine and Biology*, M.J.Ashwood-Smith and J.Farrant (ed.), Tunbridge Wells, Pitman Medical Ltd., 1980.

53. G.M.Fahy, D.R.MacFarlane, C.A.Angell and H.T.Meryman, *Cryobiology*, **21** (1984) 407.

54. D.G.Whittingham, in *Principles of Embryo Preservation, Low Temperature Preservation in Medicine and Biology*, M.J.Ashwood-Smith and Farrant (eds.), pp65-84, Tunbridge Wells, Pitman Medical Ltd., 1980.

Reproduced with permission of the copyright owner. Further reproduction prohibited without permission.

Reference Cited in Part 3

1. D.O'Sullivan, *Chem. & Engineering News,* Feb. 4, 1991, p30.

2. B. Mishkin, *Complete Book of Vitamins & Minerals, Consumer Guide, Health Series,* **500** (1989) 127.

3. J.M.Pratt, *Inorganic Chemistry of Vitamin B_{12},* Academic Press, New York, 1972.

4. E.L.Rickes, N.G.Brink, F.R.Koniuszy, T.R.Wood and K.Folkers, *Science,* **107** (1948) 396.

5. E.L.Smith, *Nature,* **162** (1948) 144.

6. E.L.Smith and L.F.J.Parker, *J.Biochem.*, **43** (1948) viii.

7. B.Ellis, V.Petrow and G.F.Snook, *J.Pharm.Pharmacol.*, **1** (1949) 60.

8. H.A.Barker, H.Weissbach and R.D.Smith, *Proc.Nat.Acad.Sci.*, **44** (1958) 1093.

9. C.Brink, D.C.Hodgkin, J.Lindsey, J.Pickworth, J.H.Robertson and J.G.White, *Nature,* **174** (1954) 1169.

10. P.G.Lenhert and D.C.Hodgkin, *Nature,* **192** (1961) 937.

11. K.Folkers and D.E.Wolf, *Vitamins and Horm.*, **12** (1954) 1.

12. E.L.Smith, *Biochem.Soc.Symposia,* **13** (1955) 3.

13. A.W.John and A.Todd, *Vitamins and Horm.*, **15** (1957) 1.

14. K.Lindstrand, *Nature,* **204** (1964) 188.

15. E.Irion and L.Ljungdahl, *Biochem.*, **7** (1968) 2350.

16. L.Ljungdahl, E.Irion and H.G.Wood, *Biochem.* **4** (1965) 2772.

17. D.Lexa and J.M.Saveant, *Acc.Chem.Res.*, **16** (1983) 235.

18. B.A.Abd-El-Ney, *J.Electroanal.Chem.*, **53** (1974) 317.

19. T.H.Kenyhercz and H.B.Mark, *Anal.Lett.*, **7** (1974) 1.

20. H.P.C.Hogenkamp and S.Holmes, *Biochem.*, **9** (1970) 1886.

Reproduced with permission of the copyright owner. Further reproduction prohibited without permission.

21. J.Halpern, in B_{12} *Chemistry*, D.Dolphin (ed.), Vol. 1, Chapter 14, p513, Wiley-Interscience, New York, 1982.

22. P.G.Swetik and D.G.Brown, *J.Electroanal.Chem.*, **51** (1974) 433.

23. R.L.Birke, G.A.Brydon and M.F.Boyle, *J.Electroanal.Chem.*, **52** (1974) 237.

24. S.L.Tacket, J.W.Collat and J.C.Abott, *Biochemistry*, **2** (1963) 919.

25. S.L.Tacket, J.W.Collat and J.C.Abott, *J.Electroanal.Chem.*, **30** (1971) 510.

26. H.A.O.Hill, J.M.Pratt and R.P.J.Williams, *J.Chem.Soc.*, (1964) 5149.

27. P.K.Das, H.A.O.Hill, J.M.Pratt and R.P.J.Williams, *J.Biochem.Biophys.Acta*, **141** (1967) 644.

28. P.K.Das, H.A.O.Hill, J.M.Pratt and R.P.J.Williams, *J.Chem.Soc.*, (1968) A 1261.

29. D.Lexa and J.M.Saveant, *J.Am.Chem.Soc.*, **98** (1976) 2652.

30. D.Lexa, J.M.Saveant and J.Zickler, *J.Am.Chem.Soc.*, **99** (1977) 2786.

31. D.Lexa and J.M.Saveant, *J.Chem.Soc., Chem.Commun.*, (1975) 872.

32. D.Lexa and J.M.Saveant, *J.Am.Chem.Soc.*, **100** (1978) 3220.

33. N.R.De Tacconi, D.Lexa and J.M.Saveant, *J.Am.Chem.Soc.*, **101** (1979) 467.

34. D.Lexa, J.M.Saveant and J.Zickler, *J.Am.Chem.Soc.*, **102** (1980) 2654.

35. D.Lexa, J.M.Saveant and J.Zickler, *J.Am.Chem.Soc.*, **102** (1980) 4851.

36. D.Lexa, J.M.Saveant and J.P.Soufflet, *J.Electroanal.Chem.*, **100** (1979) 159.

37. C.Amatore, D.Lexa and J.M.Saveant, *J.Electroanal.Chem.*, **111** (1980) 81.

38. D.Faure, D.Lexa and J.M.Saveant, *J.Electroanal.Chem.*, **140** (1982) 269.

39. D.Faure, D.Lexa and J.M.Saveant, *J.Electroanal.Chem.*, **140** (1982) 285.

40. D.Faure, D.Lexa and J.M.Saveant, *J.Electroanal.Chem.*, **140** (1982) 295.

Reproduced with permission of the copyright owner. Further reproduction prohibited without permission.

41. C.L.Schmidt and H.S.Swofford, *Anal.Chem.*, **51** (1979) 2026.

42. C.L.Schmidt, C.F.Kolpin and H.S.Swofford, *Anal.Chem.*, **53** (1981) 41.

43. R.L.Birke and S.Venkatesan, *J.Electrochem.Soc.*, **128** (1981) 984.

44. H.A.O.Hill, J.M.Pratt, M.P.O'riordan, F.R.Williams and R.P.J.Williams, *Chem.Soc.*, **A** (1971) 1859.

45. R.G.Matthews and J.T.Drummond, *Chem.Rev.*, **90** (1990) 1275.

46. R.V.Banerjee, S.R.Harder, S.W.Ragsdale and R.G.Matthews, *Biochem.*, **29** (1990) 1129.

47. T.M.Zydowsky, L.F.Courtney, V.Frasca, K.Kobayashi, H.Shimizu, L.D.Yuen, R.G.Matthews, S.J.Benkovic and H.G.Floss, *J.Am.Chem.Soc.*, **108** (1986) 3152.

48. K.A.Rubinson, E.Itabashi and H.B.Mark, *Inorg.Chem.*, **21** (1982) 3571.

49. D.Lexa and J.M.Saveant, *J.Am.Chem.Soc.*, **100** (1978) 3220.

50. D.Lexa, J.M.Saveant and J.P.Soufflet, *J.Electroanal.Chem.*, **100** (1979) 159.

51. T.M.Kenyhercz, T.P.DeAngelis, B.J.Norris, W.R.Heineman and H.B.Mark, *J.Am.Chem.Soc.*, **98** (1976) 2469.

52. M.H.Kim and R.L.Birke, *J.Electroanal.Chem.*, **144** (1983) 331.

53. D.K.Gosser and F.Zhang, *Talanta,* **38** (1991) 715.

54. A.Bard and L.Faulkner, *Electrochemical Methods, Fundamentals and Applications,* John Wiley & Sons, New York, 1980.

55. D.K.Gosser and P.H.Reiger, *Anal.Chem.*, **60** (1988) 1159.

56. F.H.Walters, L.R.Parker,Jr., S.L.Morgan and S.N.Deming, *Sequential Simplex Optimization*, CRC Press, Inc., Boca Raton, Florida, 1991.

57. Q.Huang and D.K.Gosser, *Talanta,* **9** (1992) 1155.

58. Z.Stojek and Z.Kablik, *Electroanal. Chem. & Interfacial Electrochem.*, **60** (1975) 349.

59. P.He and L.R.Faulkner, *Anal.Chem.*, **58** (1986) 517.

60. W.M.Schwarz and I.Shain, *J.Phys.Chem.*, **69** (1965) 30.

Reproduced with permission of the copyright owner. Further reproduction prohibited without permission.

61. W.J.Bowyer, E.E.Engelman and D.H.Evans, *J.Electroanal.Chem.*, **262** (1989) 67.

62. V.D.Parker, K.L.Handoo, F.Roness and M.Tilset, *J.Am.Chem.Soc.*, **113** (1991) 7493.

63. R.J.Klingler and J.K.Kochi, *J.Phys.Chem.*, **85** (1981) 1731.

64. R.P.Duyne and C.N.Reilly, *Anal.Chem.*, **44** (1972) 142.

65. M.Rabbinovitz and A.Pines, *J.Am.Chem.Soc.*, **91** (1969) 1585.

66. J.M.Pratt, in *B_{12}: Chemistry*, D.Dolphin (ed.), p386, Wiley, New York, 1982.

67. B.D.Martin and R.G.Finke, *J.Am.Chem.Soc.*, **112** (1990) 2420.

68. B.P.Hay and R.G.Finke, *Inorg.Chem.*, **23** (1984) 3041.

69. B.P.Hay and R.G.Finke, *J.AM.Chem.Soc.*, **108** (1986) 4820.

70. J.Halpern, S.H.Kim and T.W.Leung, *J.Am.Chem.Soc.*, **106** (1984) 8317.

71. S.H.Kim, H.L.Chem, N.Feilchenfeld and J.Halpern, *J.Am.Chem.Soc.*, **110** (1988) 3120.

72. J.H.Grate and G.N.Schrauzer, *I.Am.Chem.Soc.*, **101** (1979) 4601.

73. G.N.Schrauzer and J.H.Grate, *J.Am.Chem.Soc.*, **103** (1981) 541.

74. D.Zhou, O.Tinembart, R.Scheffold and L.Walder, *Helvetica Chimica Acta*, **73** (1990) 2225.

75. D.Dolphin, in *Methods in Enzymology - Vitamins and Coenzymes*, Part C, Vol. XVIII, 1971.

76. O.Muller and G.Muller, *Biochem. Z.*, **336** (1962) 299.

77. H.P.C.Hogenkamp and T.G.Oikawa, *J.Biological.Chem.*, **239** (1964) 1911.

78. D.Dolphin, A.W.Johnson and R.Rodrigo, *Ann.N.Y.Acad.Sci.*, **112** (1964) 590.

79. G.N.Schrauzer, E.Deutsch and R.J.Windgassen, *J.Am.Chem.Soc.*, **90** (1968) 244.

80. A.W.Johnson, L.Mervyn, N.Shaw and E.L.Smith, *J.Chem.Soc.*, (1963) p4146.

81. R.L.Birke, *Vitamin B_{12} Research Proposal,* Sept. 1986.

Reproduced with permission of the copyright owner. Further reproduction prohibited without permission.

82. J.Hine, *Physical Organic Chemistry*, McGraw-Hill Book Co., New York, 1962.

83. G.N.Schrauzer and E.Deutsch, *J.Am.Chem.Soc.*, **91** (1969) 3341.

84. H.P.C.Hogenkamp, J.E.Rush and C.A.Swenson, *J.Biol.Chem.*, **240** (1965) 3641.

85. J.N.Ladd, H.P.C.Hogenkamp and H.A.Barker, *J.Biol.Chem.*, **236** (1961) 2114.

86. R.J.P.Williams, *Advances in the chemistry of Co-ordination Compounds*, 6th Internat. Congr. Co-ordination Chemistry, p65, Macmillan, New York, 1965.

87. J.A.Hill, J.M.Pratt and R.J.P.Williams, *J.Theor.Biol.*, **3** (1962) 423.

88. D.C.Hodgkin, J.Lindsey, R.A.Sparks, K.N.Trueblood and J.G.White, *Proc.Roy.Soc.*, **A266** (1962) 494.

89. P.G.Lenhert, *Proc.Roy.Soc.*, **A303** (1968) 45.

90. D.C.Hodgkin, J.Pickworth, J.H.Robertson, R.J.Prosen, R.A.Sparks and K.N.Trueblood, *Proc.Roy.Soc.*, **A251** (1959) 306.

91. C.Brink-Shoemaker, D.W.J.Cruikshank, D.C.Hodgkin, M.J.Kamper and D.Pilling, *Proc.Roy.Soc.*, **A278** (1964) 1.

92. J.D.Dunitz and E.F.Meyer, *Proc.Roy.Soc.*, **A288** (1965) 324.

93. F.M.Moore, B.T.M.Willis and D.C.Hodgkin, *Nature*, **214** (1967) 130.

94. V.Kumar and R.L.Birke, *Analytical Chemistry*, submitted.

95. R.A.Marcus, *Ann.Rev.Phys.Chem.*, **15** (1964) 155.

96. B.D.Martin and R.G.Finke, *J.Am.Chem.Soc.*, **114** (1992) 585.

97. C.Tavagnacco, G.Balducci, G.Costa, K.Taschler and W.V.Philipsborn, *Helv.Chim.Acta*, **73** (1990) 1469.

98. L.Zhaohui, J.Zhenbin and G.Dengping, *J.Electroanal.Chem.*, **259** (1989) 39.

99. R.L.Birke and Z.Huang, *Anal.Chem.*, **64** (1992) 1513.

100. X.Chen, J.Zhang and P.He, *J.Electroanal.Chem., Interfacial Electrochem.*, **271** (1989) 257.

101. K.R.Wehmeyer and R.M.Wightman, *Anal.Chem.*, **57** (1985) 1989.

Reproduced with permission of the copyright owner. Further reproduction prohibited without permission.

102. Z.Stojek and J.Osteryoung, *Anal.Chem.*, **57** (1989) 1305.

103. R.V.Banerjee, S.C.Harder, S.W.Ragsdale and R.G.Matthews, *Biochem.*, **29** (1990) 1129.

104. P.B.Armentrout and R.Georgiadis, *Polyhedron*, **7** (1988) 1573.

105. R.G.Finke and B.D.Martin, *J.Inorg.Biochem.*, **40** (1990) 19.

106. B.Krautler, *Helv.Chim.Acta*, **70** (1987) 1268.

107 J.F.Endicott, K.P.Balakrishnan and C.L.Wong, *J.Am.Chem.Soc.*, **102** (1980) 5519.

108. J.M.Pratt, *Chem.Soc.Rev.*, **14** (1985) 161.

109. J.Halpern, S.H.Kim and T.W.Leung, *J.Am.Chem.Soc.*, **112** (1990) 2419.

110. A.Pross and S.S.Shaik, *Acc.Chem.Res.*, **16** (1983) 363.

Reproduced with permission of the copyright owner. Further reproduction prohibited without permission.